Enzymatic Characterization of *N*-Acetyl-1-D-*myo*-inosityl-2-amino-2-deoxy-alpha-D-glucopyranoside Deacetylase (MshB)

Xinyi Huang

Dissertation submitted to the faculty of the Virginia Polytechnic Institute and State University in partial fulfillment of the requirements for the degree of

Doctor of Philosophy
In
Biochemistry

Marcy Hernick, Chair
Glenda Gillaspy
Michael Klemba
Jianyong Li

March 21, 2013
Blacksburg, VA

Keywords: metal-dependent deacetylase, metallohydrolase, mycothiol, enzyme mechanism, assay development, molecular binding

Enzymatic Characterization of *N*-Acetyl-1-D-*myo*-inosityl-2-amino-2-deoxy-alpha-D-glucopyranoside Deacetylase (MshB)

Xinyi Huang

ABSTRACT

Mycobacterium species, which contain the causative agent for human tuberculosis (TB), produce inositol derivatives including mycothiol (MSH). MSH is a unique and dominant cytosolic thiol that protects mycobacterial pathogens against the damaging effects of reactive oxygen species and is involved in antibiotic detoxification. Therefore, MSH is considered a potential drug target. The deacetylase MshB catalyzes the committed step in MSH biosynthesis by converting *N*-acetyl-1-D-*myo*-inosityl-2-amino-2-deoxy-alpha-D-glucopyranoside (GlcNAc-Ins) to 1-D-*myo*-inosityl-2-amino-2-deoxy-alpha-D-glucopyranoside (GlcN-Ins). In this dissertation, we present detailed functional analysis of MshB. Our work has shown that MshB is activated by divalent metal ions that can switch between Zn^{2+} and Fe^{2+} depending on environmental conditions, including metal ion availability and oxidative conditions. MshB employs a general acid-base catalyst mechanism wherein the Asp15 functions as a general base to activate the metal-bound water nucleophile for attack of the carbonyl carbon on substrate. Proton-transfer from a general acid catalyst facilitates breakdown of the tetrahedral intermediate and release of products. A dynamic tyrosine was identified that regulates access to the active site and participates in catalysis by stabilizing the oxyanion intermediate. Molecular docking simulations suggest that the GlcNAc moiety on GlcNAc-Ins is stabilized by hydrogen bonding interactions with active site residues, while a hydrophobic stacking interaction between the inositol ring and Met98 also appears to contribute to substrate affinity for MshB. Additional binding interactions with side chains in a hydrophobic cavity adjacent to the active site were suggested when the docking experiments were carried out with large amidase substrates. Together the results from this study provide groundwork for the rational design of specific inhibitors against MshB, which may circumvent current challenges with TB treatment.

ACKNOWLEDGEMENTS

I would like to thank the many people who have helped me as I pursued my Ph.D. First, I would like to thank my advisor, Dr. Marcy Hernick, who leads me into the great field of enzymology and provides excellent guidance in research. I am grateful for all I have learned during my time in her lab. Also, I would like to thank my committee members for their willingness to help: Dr. Glenda Gillaspy, Dr. Michael Klemba, and Dr. Jianyong Li. I also thank Dr. David Bevan for serving as the chair for my preliminary exam. I appreciate all their generous contributions of the time and effort.

Graduate school would not have been possible without the support of my family and friends. I am grateful for my parents, Fangmin Huang and Xiaomei Liu, who regularly provided encouragement and support for my aboard study in U.S. I am also thankful to numerous friends for all the support and inspiration for my life in Blacksburg, and there are simply too many of you to list by name.

TABLE OF CONTENTS

TABLE OF FIGURES

Chapter 2

Chapter 3

Chapter 4

Chapter 5

Chapter 6

Chapter 7

Appendix A

Appendix B

TABLE OF TABLES

LIST OF ABBREVIATIONS

ABC transporter	ATP-binding cassette transporter.
AcCoA	Acetyl coenzyme A
Act	Acetate
aMIPS	*myo*-inositol 1-P synthase from *Archaeoglobus fulgidus*
Ara*f*	D-arabinofuranose
AtMIPS	*myo*-inositol 1-P synthase from *Arabidopsis thaliana*
Bistris propane	1,3-bis(tris(hydroxymethyl)methylamino)propane
BOG	β-octyl-D-glucopyranoside
CSA	5'-O-[N-(L-cysteinyl) sulfamoyl]adenosine
Cys-GlcN-Ins	1-D-*myo*-inosityl-2-(L-cysteinyl)amido-2-deoxy-alpha-D-glucopyranoside
CySmB-GlcN-Ins	Monobromobimane S-conjugate of desacetylmycothiol
DAM	Desacetylmycothiol
DPA	Dipicolinic acid
EDTA	Ethylenediamine tetraacetic acid
EMB	Ethambutol
FAD	Flavin adenine dinucleotide
fCySmB-GlcN-Ins	Bimane S-conjugate of formyl-Cys-GlcN-Ins
FSA	Fluorescamine
GABC	General acid-base catalyst
GAC	General acid catalyst
GBC	General base catalyst
Glc-6P	Glucose-6-phosphate
GlcN-Ins	1-D-*myo*-inosityl-2-amino-2-deoxy-α-D-glucopyranoside
GlcNAc	*N*-acetyl-glucosamine
GlcNAc-Ins	*N*-acetyl-1-D-*myo*-inosityl-2-amino-2-deoxy-α-D-glucopyranoside
GlcNAc-Ins-P	1-*O*-(2-acetamido-2-deoxy--D-glucopyranosyl)-D-*myo*-inositol-3-phosphate
GOL	Glycerol
GSH	Glutathione

GT	Glycosyltransferase
HDAC8	Histone deacetylase 8
HEPES	2-[4-(2-hydroxyethyl)piperazin-1-yl]ethanesulfonic acid
IC	Ion Chromatography
IMAC	Immobilized Metal Ion Affinity Chromatography
IMPase	*myo*-inositol 1-phosphate phosphatase
Ins	*myo*-inositol
Ins-1P	L-*myo*-inositol 1-phosphate
IPTG	Isopropyl-β-D-thiogalactoside
LAM	Lipoarabinomannan
LM	Lipomannan
LpxC	UDP-3-*O*-(*R*-3-hydroxymyristoyl)-*N*-acetylglucosamine deacetylase
Man-LAM	Mannose capped LAM
Man*p*	α-D-mannopyranosyl
mBBr	monobromobimane
MBP	Maltose binding protein
MDR	Multi-drug resistant
MES	2-(*N*-morpholino)ethanesulfonic acid
MIPS	L-*myo*-inositol 1-phosphate synthase
MOPS	3-(*N*-morpholino)propanesulfonic acid
MS-acetamide	Iodoacetamide S-conjugate of mycothiol
MS-acetophenone	Bromoacetophenone S-conjugate of mycothiol
MS-conjugate	Mycothiol S-conjugate
MS-NEM	N-ethylmaleimide S-conjugate of mycothiol
MS-RifSV	Rifamycin S-conjugate of mycothiol
MSH	Mycothiol
MshB	*N*-acetyl-1-D-*myo*-inosityl-2-amino-2-deoxy-α-D-glucopyranoside deacetylase
MSmB	Monobromobimane S-conjugate of mycothiol
msMIPS	*myo*-inositol 1-P synthase from *Mycobacterium smegmatis*
MSNO	Nitrosomycothiol
MSSM	Mycothione

NAD^+	Nicotinamide adenine dinucleotide
NADH	Nicotinamide adenine dinucleotide reduced
NMR	Nuclear Magnetic Resonance
PCR	Polymerase Chain Reaction
PDB	Protein Data Bank
PI	Phosphatidylinositol
PI3P	Phosphatidylinositol 3-phosphate
PIMs	Phosphatidyl-*myo*-inositol mannosides
PPM	Polyprenol-phosphate-mannose
RNI	Reactive nitrogen intermediates
ROI	Reactive oxygen intermediates
SDS-PAGE	Sodium Dodecyl Polyacrylamide Gel Electrophoresis
TB	Tuberculosis
TCA	Tricholoroacetic acid
TCEP	Triscarboxyethylphosphine
TEV	Tobacco Etch Virus
tMIPS	*myo*-inositol 1-P synthase from *Mycobacterium tuberculosis*
UDP	Uridine diphosphate
UDP-GlcNAc	Uridine diphosphate *N*-acetylglucosamine
WT	Wild-type
XDR	Extensively-drug resistant
yMIPS	*myo*-inositol 1-P synthase from *Saccharomyces cerevisiae*

ATTRIBUTIONS

Several chapters of this dissertation were done in collaboration with others both in research and writing of the chapters. The contributing authors include graduate student Evren Kocabas and Assistant Professor Marcy Hernick from the Department of Biochemistry at Virginia Tech. Each chapter/appendix explains the specific contributions of each collaborator for that section. Each published chapter has the original work cited and is used with permission of the publishers. All works on this dissertation, unless noted, is my own.

Chapter 1

Introduction

Tuberculosis (TB) is caused by *Mycobacterium tuberculosis,* which infects one third of the population worldwide and causes 1.4 million deaths each year. (*1*) The current challenges in TB treatment include the persistence of the bacteria during latent infection and the emergence of multidrug resistant strains. (*1, 2*) *Mycobacterium* species produce a unique inositol-containing thiol, mycothiol (MSH), as the primary cellular reducing agent that has been considered a potential drug target. (*3*) The deacetylase MshB catalyzes the committed step in the overall biosynthesis of MSH, the hydrolysis of *N*-acetyl-1-D-*myo*-inosityl-2-amino-2-deoxy-α-D-glucopyranoside (GlcNAc-Ins) to generate 1-D-*myo*-inosityl-2-amino-2-deoxy-α-D-glucopyranoside (GlcN-Ins) and acetate. (*4*) MshB is one of the enzymes currently being targeted for MSH inhibition. The focus of this dissertation is on recent biochemical studies on the catalytic mechanism and molecular recognition properties of MshB.

Although inositol derivatives are ubiquitously found in eukaryotes and play essential roles in cellular signal transduction pathways, inositol metabolism is restricted to a certain class of prokaryotes including *Mycobacterium* species that incorporate *myo*-inositol in two unique pathways, namely, the production of phosphatidylinositol (PI) and the biosynthesis of mycothiol (MSH). (*5*) Chapter 2 reviews the recent progress on identification of mycobacterial genes involved in the biosynthesis of inositol and related derivatives, biochemical properties of inositol synthetic enzymes in mycobacteria, and their potential as TB drug targets.

MSH has become a focal point of drug discovery for TB treatment for the following reasons: 1) MSH is absent in eukaryotes; 2) MSH maintains the cellular redox state; 3) MSH enhances the survival of *M. tuberculosis* under an oxidative host environment; 4) synthesis and metabolism of MSH is active during the life-time of mycobacteria; and 5) MSH is involved in drug detoxification. Chapter 3 specifically reviews the literatures on the role of MSH in TB infection and persistence, as well as the enzymes involved in MSH biosynthesis and MSH-dependent detoxification.

MshB proteins from *Mycobacterium smegmatis* and *Mycobacterium bovis* Bacille Calmette–Guérin (*M. bovis* BCG) have been expressed and purified from *E. coli* as recombinant forms. MshB is a metalloenzyme whose activity is strictly dependent on the presence of a divalent metal ion (*6*) and a zinc ion has been observed in the active site of MshB crystal structures. (*7*) In Chapter 4, I describe a rapid fluorescamine (FSA)-based assay that we developed to measure the deacetylase activity of MshB. FSA itself is not fluorescent but reacts with primary amines to form a fluorescent product. This assay does not require separation of substrate and product, and was used to measure the rate of the MshB-catalyzed reaction at multiple substrate concentrations using a multi-well plate reader. (*8*)

This FSA-based assay was used to examine the metal cofactor preferences of MshB, as discussed in Chapter 5. Briefly, our work has shown that MshB is a cambialistic metalloenzyme that can be activated by Fe^{2+}, Co^{2+}, Zn^{2+}, Mn^{2+}, and Ni^{2+}. In addition, the cofactor utilized by MshB is dependent on environmental conditions. MshB prefers Fe^{2+} under anaerobic conditions regardless of the metal ion content of the medium and switches between Fe^{2+} and Zn^{2+} under aerobic conditions as the metal content of the

medium is altered. (*9*) The ability to switch cofactors in response to metal and oxygen availability may enable adaptation of *M. tuberculosis* during infection and persistence in host macrophage (*10*).

The three-dimensional structures of MshB lead to a hypothetical general-acid-base-catalysis mechanism. (*7, 11*) In Chapter 6, we probed the catalytic mechanism of MshB using a combination of site-directed mutagenesis and kinetics experiments. Results from these studies suggest that Asp15 functions as the general base to activate a metal-bound water, which serves as the nucleophile to attack the carbonyl carbon on GlcNAc. Solvent isotope effect experiments suggests a critical role of His144 in proton transfer steps, probably via acting as the general acid to protonate the leaving group. The ionization status of phenolic group on Tyr142 is also important for catalytic efficiency and the rotation of its side-chain is partially rate-limiting. (*12*) Structural data suggest that the dynamic movements of Tyr142 may regulate access to the active site and stabilize the oxyanion intermediate. (*12, 13*)

More recent studies have focused on examining the molecular recognition properties of MshB as described in Chapter 7. Automated docking of the native substrate GlcNAc-Ins as well as larger amidase substrates including CySmB-GlcN-Ins and fCySmB-GlcN-Ins to MshB (PDB 4EWL (*13*)) were performed in AutoDock4.2. Results from docking suggest that there is extensive hydrogen bonding interactions between the glucosamine hydroxyl groups and the side chains of Arg68, Asp95, and His144 that stabilize GlcNAc-Ins binding to the MshB active site. The importance of the Arg68, Asp95, and His144 side-chains in the recognition of GlcNAc substrate was confirmed with site-directed mutagenesis studies. The *myo*-inositol ring is accommodated at the

entrance of the active site by hydrophobic packing against Met98, a residue that is located on a mobile surface loop and blocks the entrance to the active site upon ligand binding. Moreover, a hydrophobic cavity adjacent to the active site has been identified and may contribute to the additional binding affinity of CySmB-GlcN-Ins through favorable interactions with the bimane moiety.

The work presented here is important for our understanding of the catalytic mechanism and molecular recognition properties of the deacetylase MshB. Findings from this work will aid in the development of drugs with high specificity and affinity for MshB, which may circumvent some of the current challenges in treatment of TB.

Reference

1. WHO. (2012) Global Tuberculosis Control.
2. Zhang, Y. (2005) The magic bullets and tuberculosis drug targets, *Annu Rev Pharmacol Toxicol 45*, 529-564.
3. Spies, H. S., and Steenkamp, D. J. (1994) Thiols of intracellular pathogens. Identification of ovothiol A in Leishmania donovani and structural analysis of a novel thiol from Mycobacterium bovis, *Eur J Biochem 224*, 203-213.
4. Newton, G. L., Av-Gay, Y., and Fahey, R. C. (2000) N-Acetyl-1-D-myo-inosityl-2-amino-2-deoxy-alpha-D-glucopyranoside deacetylase (MshB) is a key enzyme in mycothiol biosynthesis, *J Bacteriol 182*, 6958-6963.
5. Michell, R. H. (2008) Inositol derivatives: evolution and functions, *Nat Rev Mol Cell Biol 9*, 151-161.

6. Newton, G. L., Ko, M., Ta, P., Av-Gay, Y., and Fahey, R. C. (2006) Purification and characterization of Mycobacterium tuberculosis 1D-myo-inosityl-2-acetamido-2-deoxy-alpha-D-glucopyranoside deacetylase, MshB, a mycothiol biosynthetic enzyme, *Protein Expr Purif 47*, 542-550.

7. Maynes, J. T., Garen, C., Cherney, M. M., Newton, G., Arad, D., Av-Gay, Y., Fahey, R. C., and James, M. N. (2003) The crystal structure of 1-D-myo-inosityl 2-acetamido-2-deoxy-alpha-D-glucopyranoside deacetylase (MshB) from Mycobacterium tuberculosis reveals a zinc hydrolase with a lactate dehydrogenase fold, *J Biol Chem 278*, 47166-47170.

8. Huang, X., and Hernick, M. (2011) A fluorescence-based assay for measuring N-acetyl-1-D-myo-inosityl-2-amino-2-deoxy-alpha-D-glucopyranoside deacetylase activity, *Anal Biochem 414*, 278-281.

9. Huang, X., Kocabas, E., and Hernick, M. (2011) The activity and cofactor preferences of N-acetyl-1-D-myo-inosityl-2-amino-2-deoxy-alpha-D-glucopyranoside deacetylase (MshB) change depending on environmental conditions, *J Biol Chem 286*, 20275-20282.

10. Wagner, D., Maser, J., Lai, B., Cai, Z., Barry, C. E., 3rd, Honer Zu Bentrup, K., Russell, D. G., and Bermudez, L. E. (2005) Elemental analysis of Mycobacterium avium-, Mycobacterium tuberculosis-, and Mycobacterium smegmatis-containing phagosomes indicates pathogen-induced microenvironments within the host cell's endosomal system, *J Immunol 174*, 1491-1500.

11. McCarthy, A. A., Peterson, N. A., Knijff, R., and Baker, E. N. (2004) Crystal structure of MshB from Mycobacterium tuberculosis, a deacetylase involved in mycothiol biosynthesis, *J Mol Biol 335*, 1131-1141.

12. Huang, X., and Hernick, M. (2012) Examination of mechanism of N-acetyl-1-D-myo-inosityl-2-amino-2-deoxy-alpha-D-glucopyranoside deacetylase (MshB) reveals unexpected role for dynamic tyrosine, *J Biol Chem 287*, 10424-10434.

13. Broadley, S. G., Gumbart, J. C., Weber, B. W., Marakalala, M. J., Steenkamp, D. J., and Sewell, B. T. (2012) A new crystal form of MshB from Mycobacterium tuberculosis with glycerol and acetate in the active site suggests the catalytic mechanism, *Acta Crystallogr D Biol Crystallogr 68*, 1450-1459.

Chapter 2

Inositol derivatives in *Mycobacterium tuberculosis*: Function, Biosynthesis and Therapeutic Implications

Abstract

Inositol is a polyol used for the preparation of inositol derivatives that carry out essential functions in eukaryotes. Although rarely found in bacterial species, there are inositol derivatives that play critical roles in Actinomycetes, a group of Gram-positive bacteria that includes *Mycobacterium* species such as *M. tuberculosis*, the causative agent of tuberculosis (TB). Consequently, there is much interest in understanding the functions and biosynthesis of inositol derivatives in mycobacteria to gain insights that can be used for the development of therapeutic agents. Mycobacteria can either obtain inositol from the environment through inositol transporters or synthesize it *de novo* via a two-step enzymatic pathway. Cellular inositol is converted enzymatically into phosphatidyl-*myo*-inositol (PI), a precursor for more complex glycolipids, or incorporated as L-*myo*-inositol 1-phosphate (Ins-1P) into the small molecule mycothiol (MSH). These inositol derivatives carry out critical functions required for mycobacterial viability and virulence. The mycobacterial cell envelop contains an abundance of mannosyl-phosphatidyl-*myo*-inositol containing glycolipids and lipoglycans, including phosphatidylinositol mannosides (PIMs) lipoarabinomannan (LAM), and lipomannan (LM). Importantly, PIMs, LAM, and LM have been shown to function as immunomodulatory molecules, promote the entry of mycobacteria into phagocytic cells, and regulate phagosome maturation. Mycobacteria also produce the inositol derivative MSH, which is used by

mycobacteria as the primary reducing agent and in the detoxification of xenobiotics. Due to these important functions, mycobacterial inositol derivatives are of therapeutic interest as sources of potential targets for drug and vaccine development. This review summarizes mycobacterial uptake of inositol and biosynthesis of inositol derivatives, known functions of inositol derivatives in *M. tuberculosis*, and the progress to date on targeting inositol derivatives for drug development.

1. Introduction

Mycobacterium species are Actinobacteria, a group of Gram-positive bacteria with high G+C ratio. (*1*) Notably, *Mycobacterium tuberculosis* is the causative agent of human tuberculosis (TB), which infects one-third of the world's population with 8.7 million new cases and 1.4 million deaths worldwide each year. (*2*) Although the TB mortality rate has decreased by 41% since 1990, the global burden still remains enormous and TB is the second leading cause of deaths from an infectious disease worldwide. (*2*) The persistence of less active *M. tuberculosis* and the emergence of extensively drug-resistant strains remain significant challenges for current TB therapy. (*3*) Currently available antibiotics are ineffective against non-growing mycobacteria, and 10% of latent TB carriers develop active disease later in their lives due to immunodeficiency. (*3*) Moreover, about 4% of new cases and 20% of previously treated TB cases are estimated to have resistance to several first-line and second-line antibiotics. (*2*) Consequently, new therapeutic alternatives are needed.

Although inositol derivatives are ubiquitously found in eukaryotes and play an essential role in cellular signal transduction pathways, inositol metabolism in bacteria and

archea is limited. (*4*) Interestingly, *Mycobacteria* species do have the presence of inositol metabolism. Mycobacteria utilize inositol in two unique pathways, namely, in the production of PI lipids and the biosynthesis of MSH. (*5, 6*) (Fig. 1) Since mutations in the biosynthetic pathways of inositol derivatives severely impact the growth and pathogenesis of *M. tuberculosis*, these pathways may represent novel targets for drug development for treatment of TB. (*5-8*) Herein I review the current understanding of genes and proteins involved in inositol acquisition and biosynthesis in mycobacteria, the structure of inositol derivatives as well as their functions in the pathogenesis of this organism, and the therapeutic implication of inositol and relating compounds as drug targets for TB treatment.

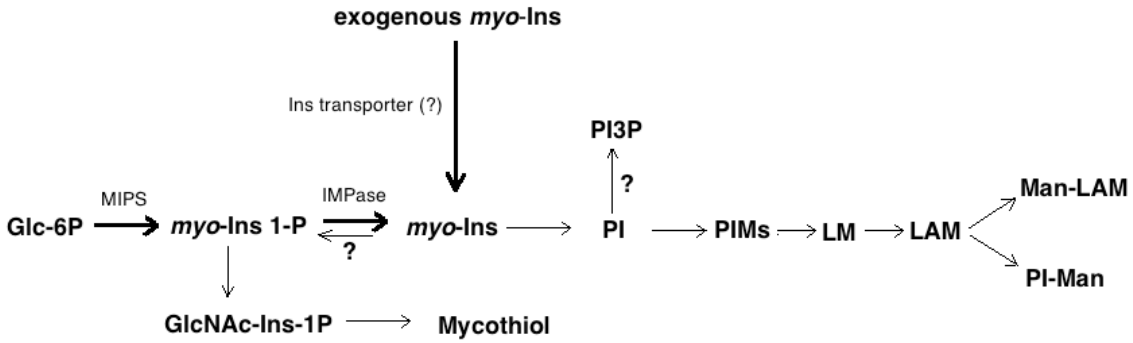

Figure 1. Metabolic pathways for the synthesis of inositol compounds in *Mycobacterium* species. The question marks indicate the existent routes that either the genes encoding the function have not been identified or that the activities of the gene products have not been examined.

2. Uptake of Inositol

It has been shown that inositol (Ins) can be taken up against a concentration gradient in mycobacteria, implicating the presence of an active transport system. (*5*) A cellular level of 1.2 mM in *Mycobacterium smegmatis* is observed after incubation with radiolabeled *myo*-inositol. (*9*) The majority of counts from [^{14}C]-Ins were associated

with the pellet fraction that contains the cell wall and incorporation of [^{3}H]-Ins was observed in PI and later in PIMs, presumably reflecting the incorporation into cell wall components. (*9, 10*) In the supernatant fraction, [^{14}C]-Ins was rapidly converted to [^{14}C]-Ins-1P and reached a steady level estimated as 0.2 mM, a value comparable with the apparent K_M (0.15 mM) of MshA, a glycosyltransferase that uses Ins-1P to produce the MSH precursor 1-*O*-(2-acetamido-2-deoxy--D-glucopyranosyl)-D-*myo*-inositol-3-phosphate (GlcNAc-Ins-1P) as described below. (*9*) Cellular [^{14}C]-MSH increased sharply during incubation, suggesting that the transported *myo*-inositol was converted to Ins-1P and utilized in the production of MSH in *M. smegmatis*. (*9*)

The *Rv3331* gene in *M. tuberculosis* encodes for a protein that shares 26% identity with the *Bacillus subtitlis* Ins transporter, and, therefore, is the most likely candidate for the Ins transporter in *M. tuberculosis*. (*11, 12*) There are at least six genes in the fast growing species *M. smegmatis* genome that encode for proteins homologous to the Na^{+}/inositol cotransporter, which are all absent in the *M. tuberculosis* genome. (*13*) Additionally, two genes downstream of the inositol synthase gene (*ino1*) in *M. smegmatis* that have been suggested to encode for two ABC transporters involved in inositol uptake are also missing from the *M. tuberculosis* genome, consistent with the observation that the inositol auxotroph mutant of *M. tuberculosis* requires extremely high concentration of exogenous inositol supplements (77mM) for growth. (*7*) Detailed study to confirm the *de novo* function of those genes are necessary to understand their roles in TB development.

3. Biosynthesis of Inositol

Inositol is synthesized through a two-step pathway that is conserved in all organisms. (*4*) The enzyme *myo*-inositol 1-phosphate synthase (MIPS) catalyzes the first and rate-limiting step in the pathway by converting D-glucose-6-phosphate (Glc-6P) to L-*myo*-inositol 1-phosphate (Ins-1P) (Fig. 2), which is also a substrate for MSH biosynthesis. (*6*) Dephosphorylation of Ins-1P by inositol monophosphatase (IMPase) yields *myo*-inositol (Fig. 2), which can further react with CDP-diacylglycerol to generate PI. (*14*) The virulence of *M. tuberculosis* mutants lacking functional inositol synthetic enzymes is severely attenuated, indicating their essential roles during TB development. The current understanding of the function and structure of MIPS and IMPase proteins are discussed below.

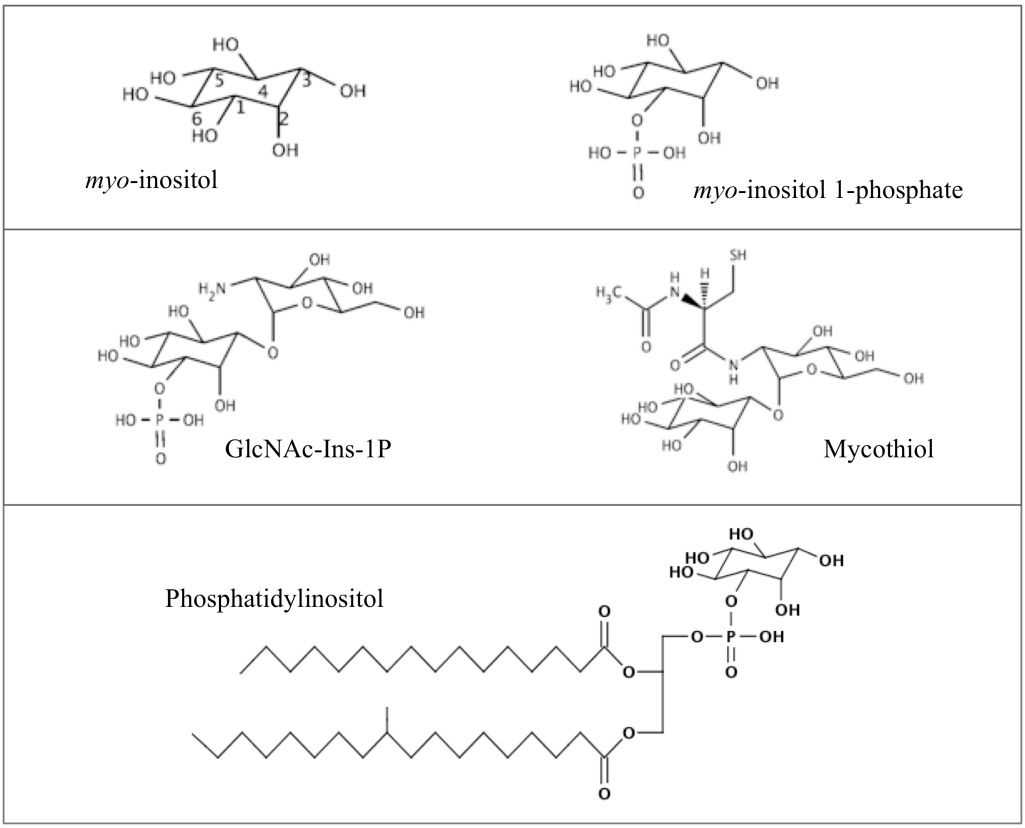

Figure 2. Structures of inositol derivatives found in *Mycobacterium* species

3.1 *myo*-inositol 1-phosphate synthase (MIPS)

The *Rv0046c* gene in *M. tuberculosis* encodes for *myo*-inositol 1-phosphate synthase (tMIPS), which was initially identified as a homolog of yeast MIPS. (*15*) (Fig. 3) Although the amino acid identity between yeast MIPS and tMIPS is <15%, *Rv0046c* was able to complement a *Saccharomyces cerevisiae ino1* mutant, confirming that this gene (*ino1*) encodes for tMIPS.(*16*) tMIPS is an essential enzyme for inositol synthesis in *M. tuberculosis*. Inhibition of tMIPS mRNA expression results in enhanced susceptibility of mycobacterial pathogens to antibiotics. (*17*) *M. tuberculosis* mutants lacking a functional *ino1* can only be isolated with media supplemented with 77 mM inositol, while the *M. smegmatis* mutant lacking a functional *ino1* grows normally in the presence of 0.1 mM inositol. (*7*) Additionally, it was found that MSH levels fell gradually over a four week period after the *ino1* mutant was transferred to inositol-free medium.(*7*) Interestingly, inositol taken up from the media must be converted to Ins-1P since inositol cannot be directly used as a substrate for MSH biosynthesis, which suggests the presence of a dedicated inositol kinase or reverse action of an IMPase, but no gene encoding these activities has been identified. (*5*) The virulence of *M. tuberculosis* is severely attenuated in the *ino1* mutants, as these mutants are cleared from macrophages while the CFU of the wild-type strain remains stable. (*18*) Additionally, the *M. tuberculosis ino1* mutant is incapable of developing disease in SCID mouse model. (*19*) The rapid killing of the *ino1* mutant may be attributed to the reduced MSH levels, which leave the bacteria susceptible to oxidative stress in macrophages. (*7*)

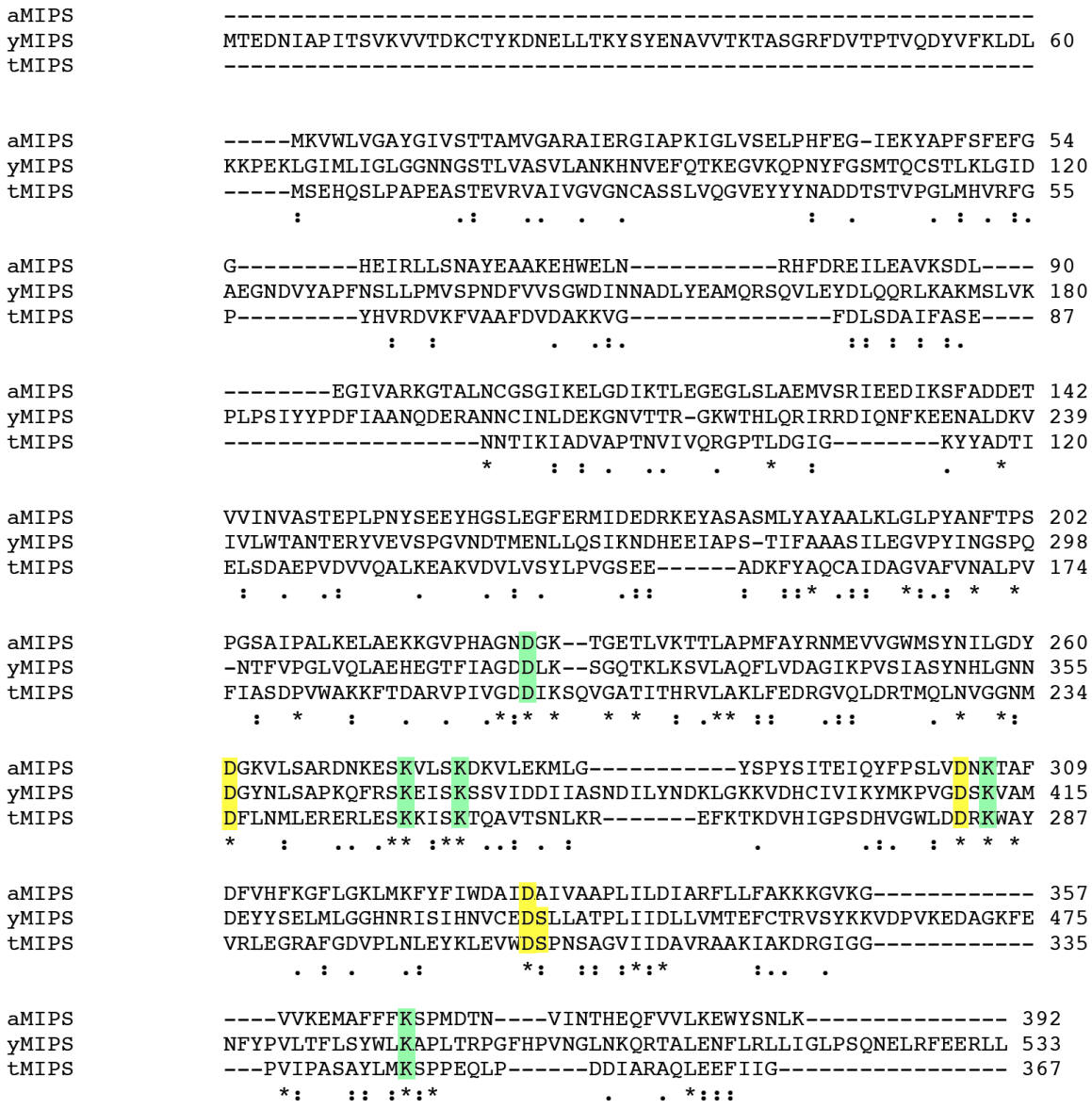

Figure 3. Sequence alignment of MIPS proteins from *A. fulgidus*, *M. tuberculosis,* and *S. cerevisiae* using ClustalW2. '*' identical residues in all sequences; ':' conserved substitutions; '.' semi-conserved substitutions. Conserved lysine residues involved in catalysis are marked with green. The second metal found in aMIPS is proposed to bind to Asp residues that are conserved in three MIPS and are labeled with yellow.

The crystal structure of tMIPS has been solved as a homotetramer with each unit comprised of two domains (PDB 1GR0). (*20*) The first domain is a Rossmann fold and contains the NAD^+ binding site. The second domain is composed of extensive β-sheets that form the dimer interface (Fig. 4), which is similar to the aMIPS (*Archaeoglobus fulgidus* MIPS) but much less shorter than yMIPS (*Saccharomyces cerevisiae* MIPS). (*20-22*) The active site is lined with highly conserved residues located at the cleft between two domains adjacent to the NAD^+ binding pocket. (*20, 21*) (Fig. 4) A tetrahedral zinc ion is coordinated in the structure with bonds of ~2.2 Å to NO7 and NO2 atoms on the NAD^+ nicotinamide moiety, the hydroxyl O atom on S310, and a water molecule that may mimic a hydroxyl group on the substrate. (*20*) (Fig. 5A) A metal ion is also observed in the same location in the crystal structure of yMIPS and aMIPS, which bridges the amide on the nicotinamide and the phosphodiester on NAD^+. (*21, 22*) (Fig. 3, Fig. 5B and 5C) This metal ion most likely has a structural role in stabilizing the NAD^+ cofactor and/or polarizing the nicotinamide ring for hydride transfer in the first catalytic step. (*21, 23*) In addition, only half of the subunits in the tetramer have a filled metal binding site and NAD^+ exhibits an altered conformation in the absence of bound metal, suggesting negative cooperativity of the tetramer. (*21, 22*) However, structural data indicate that this metal ion is too buried to carry a catalytic role. (*20, 22*) The activity of yMIPS is independent of the presence of EDTA, whereas aMIPS activity requires the presence of a divalent metal ion for catalysis. (*24-26*)

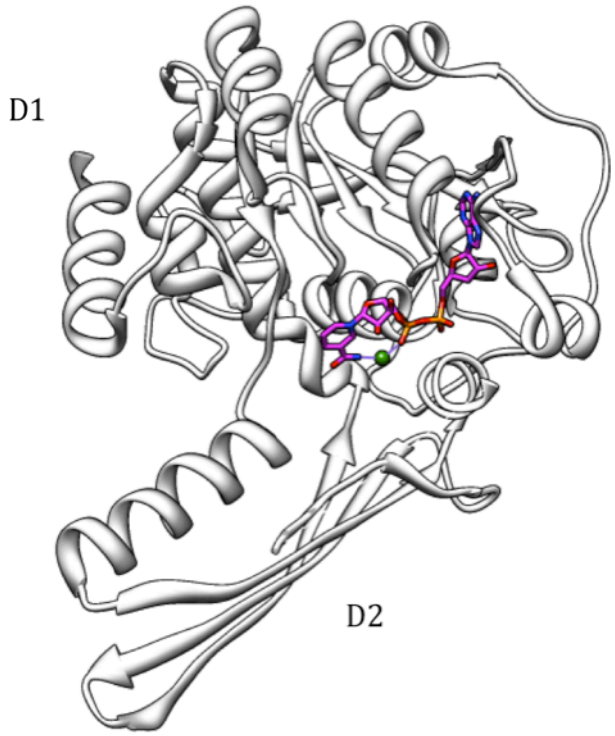

Figure 4. Structure of *M. tuberculosis* MIPS monomer. (PDB 1GR0) The structure contains two domains that D1 contains the NAD^+ (magenta stick) binding site and D2 forms the dimer interface. A zinc ion (green sphere) is found to bind at the cleft between two domains.

The *ino1* genes are clustered into two distinct phylogenetic branches, the bacterial and archaeal enzymes (~40 kDa) and the larger (~60 kDa) eukaryotic orthologs. (*27*) Sequence analyses suggest that the mycobacteria recruited the *ino1* gene from archaea through horizontal gene transfer. (*28*) While eukaryotic MIPSs are classified as type III aldolases that can be activated by ammonium ions, the aldol cyclization catalyzed by aMIPS follows the type II aldolase mechanism and uses a divalent cation, such as zinc or manganese, as a Lewis acid. (*24-26*) A second metal site that binds the catalytic divalent metal ion has been proposed in the active site of aMIPS that occupies the same position as the putative ammonium ion in yMIPS. (*21*) The putative divalent metal site contains five metal ligands including two hydroxyl O atoms (O1 and O2) from Glc-6P, two

carboxylate O atoms from D261 and D332, and one D304 bridged water molecule. (*21*) Interestingly, the three Asp residues are conserved in tMIPS (D235/D310/D282) and yMIPS (D356/D438/D410) (Fig. 3), leaving some ambiguity as to whether tMIPS catalyzes the reaction via a type II or type III aldolase mechanism. (*21*)

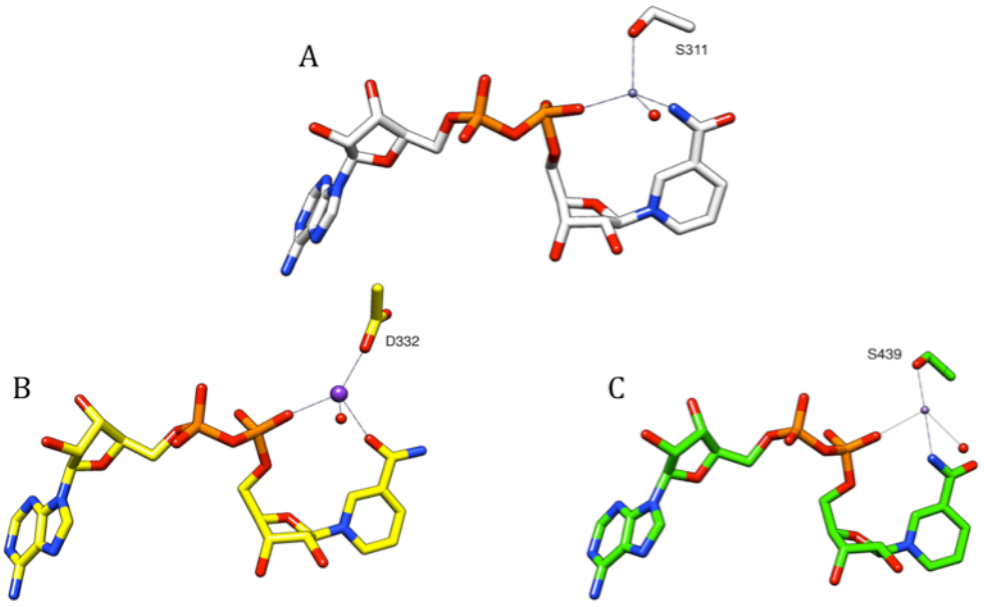

Figure 5. Metal ion observed in MIPS structures. (A) MIPS from *M. tuberculosis* binds a zinc ion with NAD^+, S311 and a water (PDB 1GR0). (B) MIPS from *A. fulgidus* coordinates a potassium ion through NAD^+, D332, and a water (PDB 1U1I). (C) MIPS from *S. cerevisiae* contains a manganese ion bound to NAD^+, S439, D410, and a water (PDB 1RM0).

A mechanism for tMIPS has been proposed based on the sequence homology with aMIPS and yMIPS (Fig. 3) using the conserved catalytic residues and NAD^+ (Fig. 5). The substrate Glc-6P is linearized before being captured by MIPS from solution. (*21-23*) The acyclic sugar binds in extended conformation with the C5 hydroxyl oriented toward NAD^+, which is held in the active conformation by the zinc ion. (*22*) Next, a proton from 5-OH of Glc-6P is held by the K248-D197 relay (K274-D225 in aMIPS and K369-D320 in yMIPS) and a hydride is transferred from C5 of Glc-6-P to the reactive C4 of the nicotinamide ring on NAD^+ to generate the keto-Glc-6P intermediate. (*21, 22*) A subsequent enolization at the C5-C6 bond is catalyzed by K346 (K367 in aMIPS and K489 in yMIPS) that acts as a base to withdraw a *pro*-R proton from the C6. (*21*) The aldol condensation step can only occur if C1 is brought in close proximity to C6, probably through a large conformational change of the active site. (*22, 23*) The negative charged O1 is stabilized by the conserved K284/K252 (K306/K278 in aMIPS and K369/K373 in yMIPS) and a cation, which is either a divalent metal ion (aMIPS) or an ammonium ion (yMIPS). (*21, 24-26*) In the last step, a direct hydride transfer from NADH reduces C5 in the inosose intermediate to generate L-*myo*-inositol 1-phosphate. (*22*) (Fig. 6) Site-directed mutagenesis of D197, K284, D310 or K346, respectively, to Ala resulted in a complete loss of MIPS activity in *M. tuberculosis* (*7*), which is consistent with both mechanisms. It remains to be seen whether tMIPS uses a divalent metal ion or ammonium ion to stabilize the intermediate in aldol condensation.

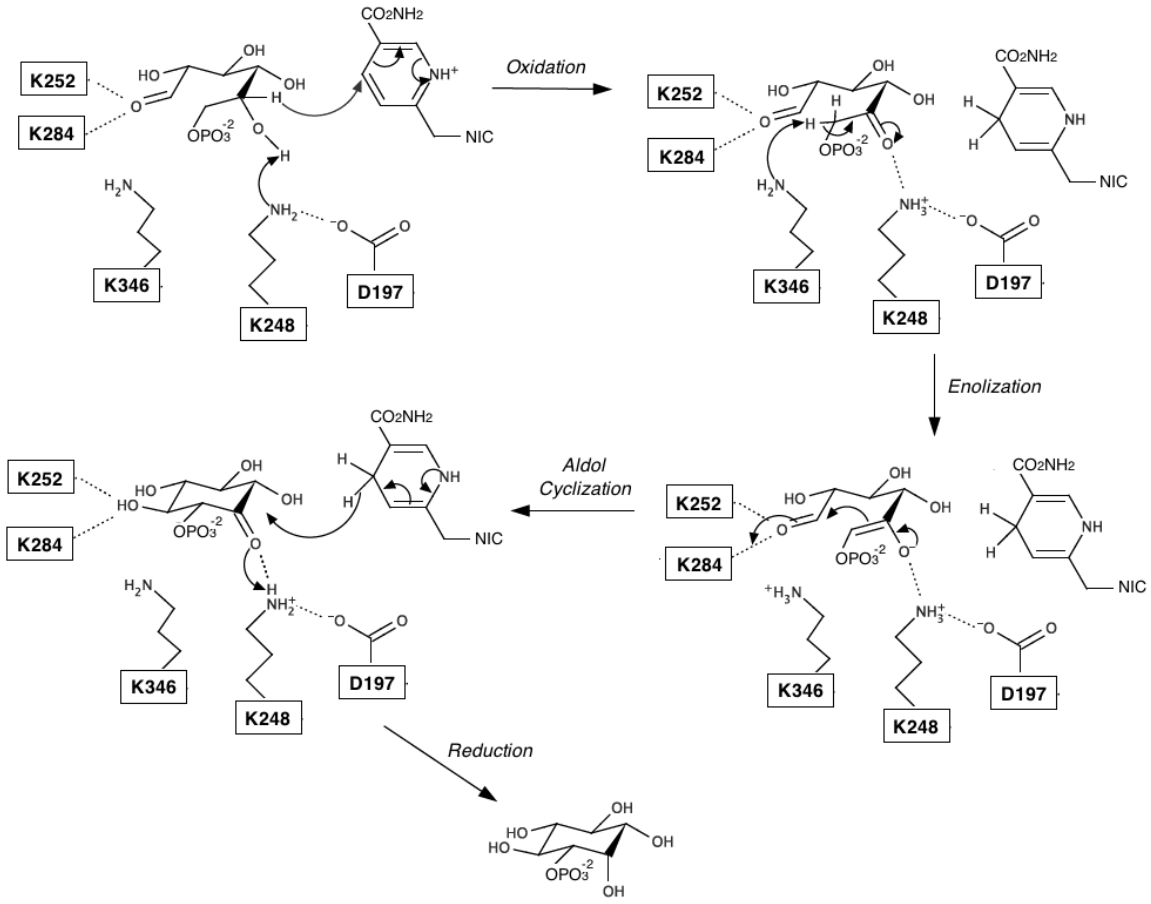

Figure 6. A Proposed mechanism of *M. tuberculosis* MIPS based on sequence and structure alignment with *A. fulgidus* MIPS and *S. cerevisiae* MIPS. Glc-6P binds in tMIPS as acyclic form with the C5 hydroxyl orienting toward NAD^+. The proton on 5-OH of Glc-6P is held by the K248-D197 relay, followed by hydride transfer from C5 of G-6-P to C4 of nicotinamide ring on NAD^+ to generate keto-Glc-6P. K346 acts as a base to withdraw a *pro*-R proton from the C6 to enolize the C5-C6 bond. The aldol condensation step occurs with negative charged O1 stabilized by conserved K284/K252. In the last step, a direct hydride transfer from NADH reduces C5 in inosose intermediate to generate Ins-1P.

3.2 Inositol monophosphatase (IMPase)

There are four inositol monophosphatase (IMPase) homologues in *M. tuberculosis* genomic DNA, namely *impA* (*Rv1604*), *suhB* (*Rv2701c*), *cysQ* (*Rv2131c*), and *impC* (*Rv3137*), which share modest identity to each other (27-32%) and to human IMPase homology (22-30%). (*8, 29, 30*) (Fig. 7) The mRNA levels of *impA*, *suhB*, *cysQ*, and

impC were shown to be 0.4, 0.11, 0.95, and 0.36 to the control gene *sigA* in *M. tuberculosis*. (*8*) Sequence alignment indicates a highly conserved active site among all four mycobacterial IMPase homologs, which is composed of two conserved motifs: one located at the N-terminus that contains the residues involving in binding of catalytic metal ions and the phosphate moiety on Ins-1P, and the other near the C-terminus that composes the rest of the metal binding site. (*8*) (Fig.7) Mutants in *impA*, *suhB*, or *cysQ* have been isolated respectively with no significant changes in the phosphatase activity of cell lysates and cellular levels of PIMs, LAM, LM and MSH, indicating that these IMPase either have redundant functions or are not involved in inositol biosynthesis in *M. tuberculosis*. (*8*) Failure to isolate an *impC* mutant in the presence of inositol suggests that this gene may encode for a function unrelated to inositol biosynthesis. (*8*)

3.2.1 ImpA

The *impA* genes from *M. smegmatis* (*MSMEG_3210*) and *M. tuberculosis* (*Rv1604*) are 70% identical to each other. (*30*) ImpA has been shown to be critical for cell wall synthesis in *M. smegmatis*, as altered cell envelope morphology and permeability is observed with the *impA* mutant. (*30*) This is likely a consequence resulting from decreased levels of PI and PIM_2. Without a functional copy of *impA*, only 50% of hydrophobic lipophilic molecules were accumulated in cell compared to the parent strain, consistent with enhanced resistance to hydrophobic antibiotics including chloramphenicol and erythromycin. (*30*) On the other hand, the function of *impA* gene remains unclear in *M. tuberculosis*, as the *impA* mutant did not exhibit any differences in cell wall morphology compared to the wild-type strain.(*8*) One possible explanation for

this finding could be the slower growth rate of *M. tuberculosis* which could allow for other IMPases to complement for ImpA activity in cell-wall synthesis. Functional study on mycobacterial ImpA, especially the substrate specificity, will shed light on its role in growth and virulence of mycobacterial pathogens.

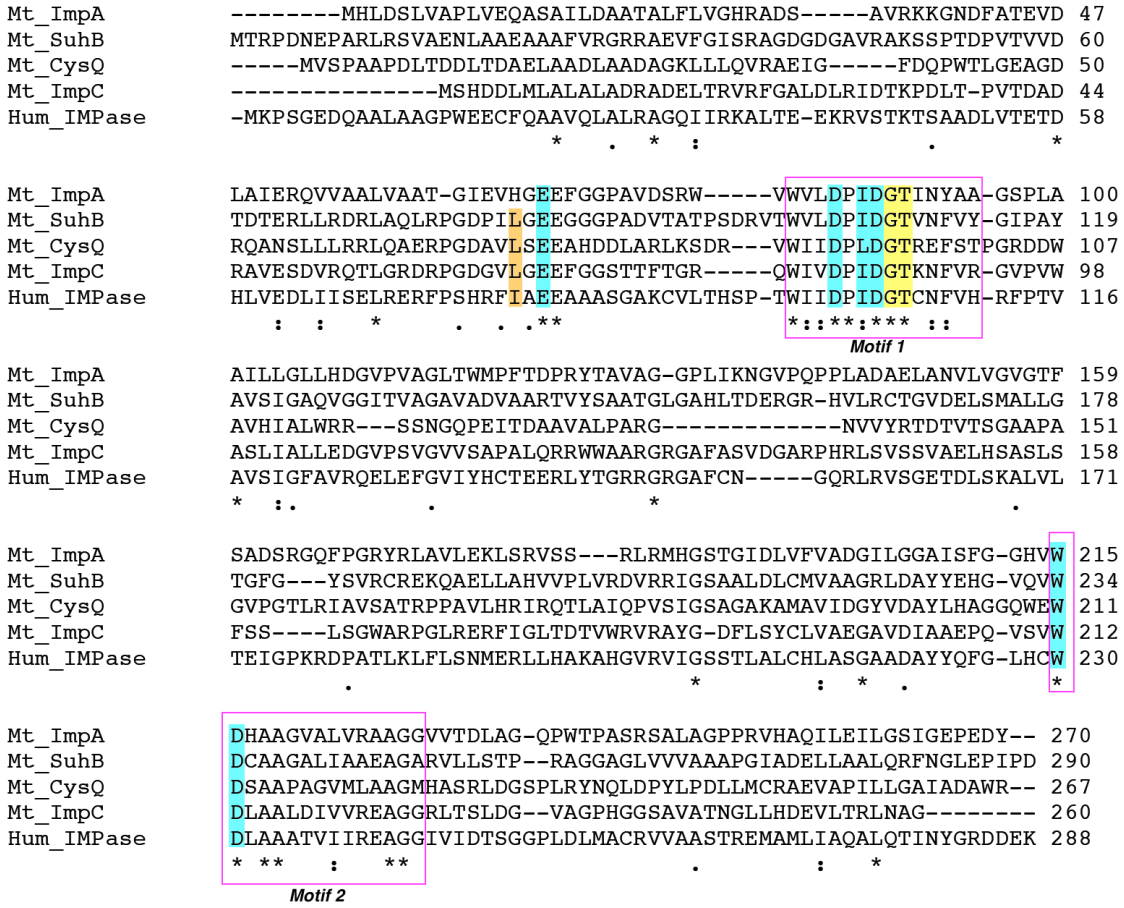

Figure 7. Sequence alignment of *M. tuberculosis* IMP homologs with human IMPase using ClustalW2. '*' identical residues in all sequences; ':' conserved substitutions; '.' semi-conserved substitutions. The conserved residues that coordinate the catalytic magnesium and that accommodate phosphate moiety on Ins-1P are marked with cyan and yellow, respectively. Conserved residues that mediate the Li^+ inhibition are marked with orange.

3.2.2 SuhB

Mycobacterial *suhB* is named after the *E. coli suhB* gene due to the high similarity in sequence shared by the genes (53%). (*15*) Although the function of *suhB* in *E. coli* remains unclear since there is no detectable inositol compounds found in this species, recombinant SuhB from *M. tuberculosis* has been biochemically characterized and confirmed to have IMPase activity. (*8, 29*) However, the *in vivo* function of SuhB in mycobacteria still remains unclear and no obvious differences on phenotype have been observed for *suhB* mutant derived from *M. tuberculosis*. (*8*) SuhB exhibits broad substrate specificity with the highest activity on D-Ins-1-P (activity with L-Ins-1-P has not been tested), followed by inositol-2-phosphate and Glc-6P, which have 40% and 70% the reactivity compared to Ins-1P, respectively. Mannitol-1-phosphate, glycerol-2-phosphate, and 2'-AMP have ~10-20% the reactivity compared to Ins-1P. (*29*)

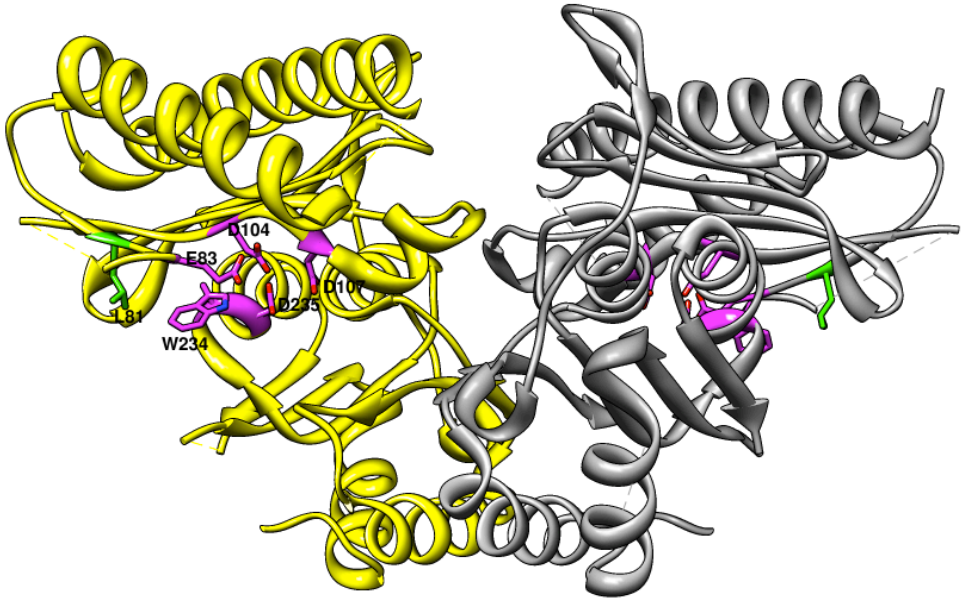

Figure 8. Structure of *M. tuberculosis* SuhB dimer. The dimer is formed by two identical subunits (yellow and grey) that each contains a conserved metal site that binds three magnesium ions. Side-chains involved in magnesium binding are labeled and shown in magenta sticks. L81 that mediates the Li^{+}-sensitivity is shown in green stick.

SuhB activity is stimulated by divalent metal ions and exhibits a maximum activity in the presence of 6 mM Mg^{2+}, a concentration much higher than its mammalian homologs that require 1mM Mg^{2+}. (*29*) A conserved metal site that binds three magnesium ions (Mg^{2+}) has been identified in the crystal structure and is composed of E83, D104, D107, W234 and D235. (*31*) (Fig. 8) Binding of Mg^{2+} to SuhB triggers dimerization of the protein, with the dimerized form becomes dominant in solution when the concentration of Mg^{2+} is increased from 1 mM to 5 mM. (*31*) Correlation of Mg^{2+} dependence of SuhB activity with dimerization suggests that catalytic activity is linked to dimerization of the protein. (*31*) The conserved active site is situated in a cavity at the N-terminal end of the protein that binds Ins-1-P with the inositol moiety stabilized by D107 and D235 and the phosphate moiety is ligated to G108 and T109 through hydrogen bonding interactions. (*31*) Similar to other IMPases, the activity of SuhB is inhibited by Li^{+} with IC_{50} value of 0.9 mM. (*29*) Structural analysis indicates that the Li^{+} competes for one of three catalytic Mg^{2+} sites in the active site. (*31*) 10-fold increase in resistance to Li^{+} was observed in L81A mutant (*29*), indicating that L81 mediates the Li^{+}-sensitivity probably via hydrophobic contact with the metal ligand W234. This residue is also conserved in ImpC, CysQ, and human IMPase, but is absent in ImpA (Fig. 7). (*29, 31*) The present structure of SuhB may serve as a template for future study on other mycobacterial IMPase.

3.2.3 CysQ

M. tuberculosis CysQ shares 30% identity with its homolog in *E. coli*, and a copy of *Rv2131c* (*cysQ*) can reverse the cysteine auxotroph in an *E. coli cysQ* mutant. (*15, 32*)

CysQ is unlikely to be involved in inositol biosynthesis in mycobacteria since isolation of the *M. tuberculosis cysQ* mutant was unsuccessful even with the presence of 77 mM inositol in the medium, a concentration that was sufficient to support the normal growth of the *ino1* mutant. (*8*) Instead, CysQ has been proposed to function as a 3'-phosphoadenosine-5'-phosphatase (PAPase) in sulfur metabolism *in vivo*. Recombinant CysQ from *M. tuberculosis* catalyzes the dephosphotation of PAP with a 1,000-fold lower K_M value and 16,000-fold higher k_{cat}/K_M value than those observed with Ins-1P substrate. (*32*) The role of CysQ in sulfur assimilation of *M. tuberculosis* has been suggested by Hatzios, *et al*. (*33*) In their study, a *cysQ* mutant with a 340 internal bases-deletion showed decreased levels of Sulfolipid-1, a unique lipid that is exclusively found on the outer envelope of *M. tuberculosis*.

3.2.4 ImpC

The expression level of *impC* increases 3-fold in a *M. tuberculosis ino1* mutant when transferred to inositol free medium, indicating that *impC* is regulated in response to changes in inositol levels. (*8*) However, mutation of *impC* is lethal in *M. tuberculosis* even when the media is supplemented with high concentrations of exogenous inositol. (*8*) The inability to isolate an *impC* mutant is not due to the toxicity of accumulated Ins-1P since an *ino1* mutant background is not sufficient to isolate an *impC* mutant (*8*), suggesting that the effects of the *impC* mutation are unrelated to inositol production, but involving in another essential pathway in *M. tuberculosis.* One possible explanation is that the *impC* gene encodes for the MshA2 activity in the MSH biosynthesis. (*8*) MshA2 is an unidentified protein that removes phosphate from the inositol ring of GlcNAc-Ins-P

to generate 1-*O*-(2-acetamido-2-deoxy-α-D-glucopyranosyl)-D-*myo*-inositol (GlcNAc-Ins). (*6*) However, since it is currently unable to obtain an *impC* mutant or to purify ImpC for *in vitro* analysis (*8*), there is no biochemical evidence about the function of ImpC in mycobacteria. Further biochemical and structural studies on the protein encoded by *impC* are necessary to illuminate its physiological function.

4. Inositol lipids

One distinctive feature of *Mycobacterium* species is the presence of abundant and various inositol-lipid derivatives in the cell wall, which are rarely observed in other bacteria. The structures and functions of mycobacterial derivatives exhibit unique properties different from the membrane inositol-lipids extensively found in eukaryotic cells, making them attractive drug targets for TB treatment. Inositol lipid metabolism in mycobacteria has been clarified in detail over the past several years and described in several recent reviews (*5, 14, 34*). Herein I summarize the biosynthesis of inositol lipids and roles of mycobacterial inositol-lipid glycans in TB adaptation in the host, including their interference in macrophage maturation.

4.1 Structure

Inositol is the building block for PI (Fig. 9), a glycerophospholipid with a glycerol backbone that carries two non-polar fatty acyl residues with carboxylic ester bonds and a molecule of Ins-1P with phosphoester bond. (*4*) In mycobacteria, PI serves as the membrane anchor for glycolipids that play key roles in host-pathogen interaction. (*35*) PI can be further elaborated to form unique cell wall-associated lipids, including PIMs, LM,

and LAM. (*36*) A recent study suggests that phosphatidylinositol 3-phosphate (PI3P), the membrane-trafficking lipid widely found in eukaryotic cells, is also a down-stream product of PI synthesis in *M. smegmatis*. (*37*)

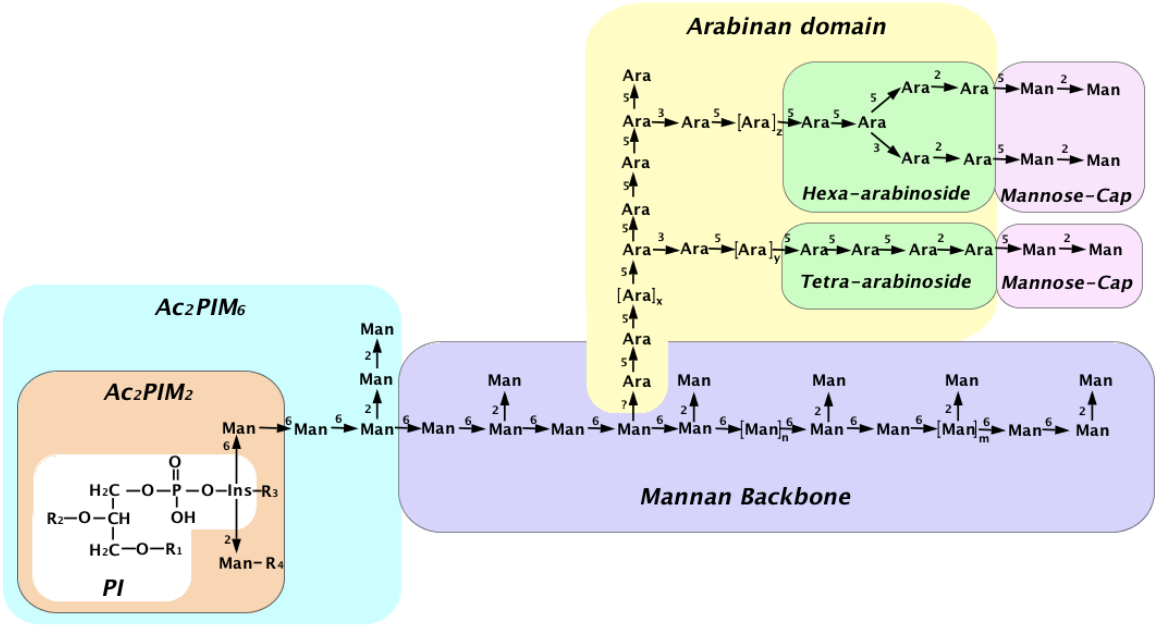

Figure 9. Schematic structures of phosphatidylinositol (PI) and related glycoconjugates. PI is glycosylated at the 2-OH and 6-OH of *myo*-inositol by Man*p* (inset in white), and acylated at 3-OH of inositol and 6-OH of the Man*p* linked at O-2 of inositol in Ac_2PIM_2 (inset in light brown). Man*p* at the 6-OH of inositol is linked to further three and two residues of α(1→6)-Man*p* and α(1→2)-Man*p*, respectively, in Ac_2PIM_6 (inset in cyan). In the mannan backbone of LM, PIM_6 is linked to additional 17–19 residues of α(1→6)-Man*p* and 7–9 singular branched α(1→2)-Man*p* (purple). LM is further linked via an unknown linkage to an arabinan domain containing approximately 70 Ara*f* residues (yellow) branched with α(3→5)-Ara*f* towards its nonreducing end resulting in a linear tetra-arabinoside or/and branched hexa-arabinoside domain (green), which in turn is terminated by β(1→2)-Ara*f* and capped by α(1→2)-Man*p* units (pink). R1, R2, R3 and R4 show different acyl groups in Ac_2PIM_2; n, m, x, y and z represent different degrees of species-specific glycosylation in LM and LAM.

PIMs are the mannosylated PI species that contains two or six α-D-mannopyranosyl (Man*p*) attached to *myo*-inositol ring. (*38*) (Fig. 9) Substitution of the 2-OH and 6-OH of inositol with Man*p* units generates PIM_2, the mannosyl phosphate inositol (MIP) anchor (*39*). The heterogenous nature of MIP results from variations occurring on the nature of fatty acids acylated at 1-OH and 2-OH of the glycerol unit, 3-OH of *myo*-inositol and the 6-OH of the Man*p* residue linked at the O-2 of inositol (see R1, R2, R3 and R4 in Fig. 9) (*38, 40*). Acylated forms of PIM_2 (Ac_1/Ac_2PIM_2) are both metabolic end products and intermediates in the biosynthesis of high-order PIMs, such as Ac_1/Ac_2PIM_6 (*38, 41*).

The core structure of LM is composed of 21–34 residues of α (1→6)-Man*p* attached to Ac_1/Ac_2PIM_2 (*42*) and the mannose backbone is elaborated by 8-9 units of α(1→2)-Man*p* monomer branches, making this oligomannose polymer highly variable (*43*). (Fig. 9) LAM is built from LM with the mannan core further elaborated by the addition of 55–70 α(1→5)D-arabinofuranose (Ara*f*) residues to the backbone. (*43, 44*) (Fig. 9) The arabinan domain is highly branched with two conserved chain arrangements: linear tetra-arabinoside of the structure β-D-Ara*f* (1→2)-α-D-Ara*f* (1→5)-α-D-Ara*f* (1→5)-α-D-Ara*f* and branched hexa-arabinoside motifs with the structure [β-D-Ara*f* (1→2)-α-D-Ara*f*] 2-3,5-α-D-Ara*f* (1→5)-α-D-Ara*f*. (*45*) (Fig. 9) In pathogenic mycobacteria, such as *M. tuberculosis* and *M. marinum*, the arabinan termini of LAM is further capped with mono, di- and tri-α(1→2)-D-Man*p* units to form Man-LAM (*45*), and the number of mannose caps is species specific (*40, 46*). (Fig. 9) This mannose cap structure is not present in avirulent species, which either contain a phosphatidylinositol capping motif as identified from *M. smegmatis* (PI-LAM) (*46*) or are absent of a capping

motif as observed in *Mycobacterium chelonae* (*47*).

4.2 Biosynthesis

4.2.1 PI

In actinobacteria, PI accounts for up to one quarter of total phospholipids (*48*), which is both a bulk membrane phospholipid and a precursor for the synthesis of PIMs, LM, and LAM. Constant turned over of PI has been suggested by Haites, *et al*: the [^{3}H]-Ins labeled PI was chased out over 7 hours and a *M. smegmatis* inositol auxotroph depleted the entire pool of PI in 3–5 h. (*10*) The first step in the production of PI is phosphorylation of diacylglycerol (DAG) by a DAG kinase (*Rv2252*) to form phosphatidic acid (*49*). Phosphatidic acid is then activated by CTP through the activity of a CDP-DAG synthase (*Rv2881c*) to form CDP-DAG, a key branch point in lipid biosynthetic pathways (*50*), which further reacts with *myo*-inositol in a reaction catalyzed by the PI synthetase (*51*). The *pgsA* gene that encodes PI synthetase is essential for *M. smegmatis* (*MSMEG_2933*) and *M. tuberculosis* (*Rv2612c*) (*48*), suggesting that PI and/or more complex glycosylated PI are required for normal growth.

4.2.2 PI3P

In a recent study**,** PI3P has been identified in *M. smegmatis* (*37*). PI3P is an important inositol-lipid in signal transduction that is extensively found in eukaryotic cells, but rarely observed in prokaryotes (*52*). The concentration of mycobacterial PI3P is estimated to be 2.3 μM, corresponding ~1.6% of total PI in the plasma membrane. Because of its transient production (*37*), PI3P was initially considered to be an

intermediate for PI synthesis through an alternative pathway, in which Ins-1P reacts with CDP-DAG to form PI3P, which is further dephosphorylated to form PI (*53*). However, mass spectrometric analysis of *M. smegmatis* crude lysates showed that PI3P contained predominantly C18:1/C19:0 fatty acids, in contrast to bulk PI that contains mainly C16:0/C19:0 (*37*). Therefore, PI3P is not an intermediate for PI synthesis. In addition, inhibition of dephosphorylation on PI3P resulted in increased levels of both PI3P and PI (*37*), which are more consistent with PI3P being a down-stream product of PI synthesis.

4.2.3 PIMs

Mycobacterial PIM biosynthesis follows a linear pathway: PI → PIM_2→ PIM_4→ PIM_6. Glycosylation of PI by different α-mannopyranosyltransferases and acetylation by acyltransferases results in the synthesis of Ac_1/Ac_2PIMs (*38, 54-60*). The committed step in PIM biosynthesis is catalyzed by PimA (*Rv2610c*), an α-mannopyranosyl-transferase that transfers a mannose from GDP-Man*p* to the 2-OH of inositol moiety on PI (*54*). The downstream *Rv2611c* encodes an acyltransferase (AcylT) that acylates the 6-OH of Man*p* residue linked to the 2-OH of *myo*-inositol in PIM_1 to generate Ac_1PIM_1 (*55*). PimB' (*Rv2188c*) is an α-D-mannose-α(1→6)-phosphatidylinositol-mannopyranosyltransferase that catalyzes the second mannosylation step to form Ac_1PIM_2. (*58-60*) PimC is an Ac_1PIM_2:α-D-mannose-α(1→6)-phosphatidylinositol-mannopyranosyltransferase, which transfer a Man*p* from GDP-Man*p* to the 6-OH of mannose at Ac_1/Ac_2PIM_2, and bioinformatical analysis suggested the existence of redundant genes for PimC (*56*). Ac_1/Ac_2PIM_3 is further α(1→6) mannosylated by an unidentified α(1→6)-mannopyranosyltransferase (PimD) to generate Ac_1/Ac_2PIM_4, a key regulatory product

involved in Ac_1/Ac_2PIM_6 and/or LM biosynthesis (*36, 57, 61*). An α(1→2)-mannopyranosyltransferase PimE (*Rv1159*) utilizes polyprenol-phosphate-mannose (PPM) as a donor to add an α(1→2)-Man*p* to Ac_1/Ac_2PIM_4, resulting in the product Ac_1/Ac_2PIM_5 (*57*). It remains unclear whether PimE is solely responsible for the synthesis of both Ac_1/Ac_2PIM_5 and Ac_1/Ac_2PIM_6. In addition, a putative acyl transferase (*Rv1565c*) was suggested in the acylation of higher-order PIMs, LM and LAM, and a *Rv1565c* deletion mutant of *Mycobacterium marinum* showed reduced incorporation of 1,2-[^{14}C]-acetate. (*62*)

4.2.4 LM

Two α(1→6)-mannopyranosyltransferases use PPM as the mannose donor to extend Ac_1/Ac_2PIM_2 for LM biosynthesis. (*61, 63, 64*) MptB **(***Rv1459c***)** is shown to be involved in synthesis of the proximal end of the mannan backbone and speculated to extend an Ac_1/Ac_2PIM_4 acceptor with 12–17 Man*p* units (*61*), while MptA (*Rv2174*) further elongates the short LM intermediate by synthesizing the distal end of the α(1→6)-Man*p* backbone (*63, 64*). The α(1→6)-Man*p* core is further decorated with single α(1→2)-Man*p* branches by a PPM-dependent glycosyltransferases, MptC (*Rv2181*) (*14, 43, 65*). In addition, a recent study suggests a branching-dependent chain termination mechanism that the elongation of α(1→6)-Man*p* core is controlled by α(1→2) branching (*65*).

4.2.5 LAM

Mature LM has been considered as the precursor of LAM by serving as the

anchor for arabinan assembly (*41*). LM is primed by a few Ara*f* units in a similar fashion as arabinogalactan synthesis in mycobacteria (*66*), but the enzyme responsible for this activity is not known. The primed Ara*f*-LM is then further extended by EmbC (*Rv3793*) (*67, 68*) with 12–16 α(1→5)-Ara*f* residues (*44*). Several polytopic membrane proteins are also involved in arabinan biosynthesis. AftC (*Rv2673*) introduces the α(1→3)-Ara*f* branch points (*44*) to generate $[Ara f]_{12–16}$-LM. A second branching α(1→3)-arabinofuranosyltransferase, AftD (*Rv0236c*) (*69*), is likely involved in the synthesis of LAM arabinan. The possibility of AftD functioning as an α(1→5)-arabinofuranosyltransferase and involving in α(1→5)-Ara*f* extension of the nonreducing termini of the arabinan domain has also been suggested (*69*). The final enzyme in arabinan domain biosynthesis is AftB (*Rv3805c*), a β(1→2)-arabinofuranosyltransferase that generates a terminal tetra- and hexa-arabinofuranoside structure on LAM (*44, 70*).

4.2.6 Man-LAM

Man-LAM is found in all pathogenic species of *Mycobacterium* and is responsible for some immunomodulatory properties (*71*). *Rv1635c* encodes an α(1→5)-mannopyranosyltransferase, CapA, that is involving in Man-LAM capping by adding the first Man*p* residue on the nonreducing arabinan termini of LAM (*72*). The gene ortholog of *Rv1635c* is absent in the *M. smegmatis* genome (*5*), consistent with its role in Man*p*-capping in pathogenic species. The second and possibly the third Man*p* are added by MptC, an α(1→2) mannopyranosyltransferase that is also responsible for branching of LM/LAM (*63*).

Table 1. Genes involved in the biosynthesis of inositol lipids in *Mycobacterium tuberculosis*

ORF	Activity	Function	References
Rv2252	Kinase	Phosphorylates DAG	(*49*)
Rv2281c	CDP-DAG synthase	Activates DAG by CTP	(*50*)
Rv2612c (PsgA)	PI synthaase (PI3P synthase?)	Adds *myo*-inositol to CDP-DAG to generate PI	(*48*)
Rv2610c (PimA)	α(1→2)-Mannopyranosyl-transferase	Adds α(1→2)-Man*p* on inositol moiety of PI to generate PIM_1	(*54*)
Rv2611c	Acyltransferase	Synthesis of Ac_1/Ac_2PIM_1	(*55*)
Rv2188c (PimB')	α(1→6)-Mannopyranosyl-transferase	Synthesis of Ac_1/Ac_2PIM_2	(*58-60*)
PimC	α(1→6)-Mannopyranosyl-transferase	Synthesis of Ac_1/Ac_2PIM_3	(*56*)
PimD	α(1→6)-Mannopyranosyl-transferase	Synthesis of Ac_1/Ac_2PIM_4	(*36, 57, 61*)
Rv1565c (PimE)	α(1→2)-Mannopyranosyl-transferase	Synthesis of Ac_1/Ac_2PIM_5 (and Ac_1/Ac_2PIM_6?)	(*57*)
Rv1565c	Acyltransferase	Acylates high order PIMs, LM, and LAM	(*62*)
Rv1459c (MptB)	α(1→6)-Mannopyranosyl-transferase	Synthesis of proximal mannan backbone	(*61*)
Rv2174 (MptA)	α(1→6)-Mannopyranosyl-transferase	Synthesis of distal mannan backbone	(*63, 64*)
Rv2181 (MptC)	α(1→2)-Mannopyranosyl-transferase	Adds α(1→2)-Man*p* on the mannan backbone and adds a second mannose cap on ManLAM	(*14, 43, 65*)
Rv3793 (EmbC)	α(1→5)-arabinofuranosyl-transferase	Synthesis of α(1→5) arabinan backbone	(*67, 68*)
Rv2673 (AftC)	α(1→3)-arabinofuranosyl-transferase	Adds Ara*f* branch points in α(3→5) direction on arabinan backbone	(*44*)
Rv0236c (AftD)	α(1→5)-arabinofuranosyl-transferase	Adds α(1→5)-Ara*f* branch on the nonreducing termini of arabinan domain	(*69*)
Rv3805c (AftB)	β(1→2)-arabinofuranosyl-transferase	Generates terminal tetra- and hexa-Ara*f* structure on LAM	(*44, 70*)
Rv1635c (CapA)	α(1→5)-mannopyranosyl-transferase	Capping of LAM by adding the first Man*p* on the nonreducing arabinan termini	(*72*)

4.3 Function in TB development

The ability of adaptation in the host results in latent-TB infections and about 90% of TB carriers don't develop active disease.(*3*) The cell wall-associated lipids play key roles in modulating the host immune response during infection and their activity depends on the degree of acylation and mannosylation. (*36*) PIMs, LM and LAM all display several immunomodulatory properties by interacting with different receptors in the immune system during host-pathogen interaction, resulting in less inflammatory immune responses (*35*). The specific interactions between the immune system of host and each type of inositol-lipid on the mycobacterial cells has been reviewed recently by Mishra, *et al* (*14*). This chapter shortly summarizes the role of inositol lipids in blockade of phagosome maturation in pathogenic *Mycobacterium,* a critical process for their intracellular survival and adaptation to host.

In *M. tuberculosis,* Man-LAM interferes with the phagosome maturation process, inhibiting the fusion of the phagosome with late endosomal and lysosomal organelles, a process that normally leads to killing and digestion of pathogens in an acid environment (*73*). Normally, the phagosome–lysosome fusion process starts after a cytosolic Ca^{2+} increase. (*74*) A Ca^{2+} /calmodulin-dependent mechanism sequentially induces the recruitment of a membrane tethering protein early endosome autoantigen 1 (EEA1) to the phagosome (*75*), and EEA1 induces the delivery of lysosomal hydrolases and H^{+}-ATPase from the trans-Golgi network to the phagosome. (*76*) The evasion strategy of blocking phagosome maturation can be mediated by Man-LAM. (*77*) During mycobacterial uptake, the normal cytosolic Ca^{2+} increase upon an infection is absent (*78*). In macrophages infected with *M. tuberculosis*, EEA1 is excluded from the early endosome,

thereby inhibiting phagosome maturation. (*76*) A role for macrophage phosphatase SHP-1 to be activated by Man-LAM and impair Ca^{2+} signaling has been suggested. (*74*)

Man-LAM and related lipoglycans contribute to the MMR-mediated phagocytosis of mycobacteria. (*79*) MMR (CD206) is a type I transmembrane monomeric C-type lectin with eight carbohydrate recognition domains. (*80*) MMR signaling may induce an anti-inflammatory response and uptake via the MMR may lead to a latent infection instead of active disease. (*79*) MMR only recognizes the mannose-capped Man-LAM that appears to be restricted to the more virulent *Mycobacterium* species (*81*), but shows low affinity to avirulent mycobacteria as *M. smegmatis* and *M. phlei* that bear LAM without a mannose cap. (*82*) A *M. marinum* mutant that produces LAM devoid of mannose caps showed a significant increase in colocalization with phagolysosomes in murine macrophages compared to the parent strain. (*72*) Furthermore, MMR recognizes virulent *M. tuberculosis* strains Erdman and H37Rv, but not avirulent H37Ra, which has subtle structural differences in Man-LAM. (*83*)

PIMs are also recognized by MMR and play important roles in phagosome maturation, although via a distinct mechanism from Man-LAM. (*84*) MMR binds higher-order PIMs and the interactions stimulate fusion phagosme with early endosomes by evading acidification. (*85*) The fusion triggered by PIMs allows mycobacterial pathogens to retrieve nutrients necessary for residing in phagosomal compartments. (*85, 86*) This indicates a balance between Man-LAM preventing maturation into the phagolysosome on one hand and PIMs stimulating early endosomal fusion to retrieve nutrients on the other. (*86*)

The pathway of *de novo* synthesis and physical functions of PI3P in *Mycobacterium* species are currently unclear. Transient and simulated production of PIP3 in *M. smegmatis* as a response to elevated salt concentrations, but not non-ionic solutes (*37*), implies that PIP3 possibly serves as a mediator of signaling in mycobacteria similar as observed with eukaryotic cells. It has been shown that *M. tuberculosis* can modulate PI levels and membrane trafficking steps in their mammalian hosts during infection (*75, 87*), probably through secretion of the mycobacterial enzymes for PI3P synthesis in hosts (*5*). Further studies on the presence and synthesis of PI3P in mycobacteria could shed light on the function of PI3P in pathogen-host interaction.

5. Mycothiol

Mycobacterium species produce MSH, a unique low molecular mass thiol that is often present in millimolar amounts, as a surrogate of glutathione (GSH) found in other organisms. (*88*) Failure in isolating *M. tuberculosis* mutants with abolished MSH synthesis implies the essential role of MSH in cell growth (*89, 90*). Mutants that produce decreased level of MSH (*91*) or alternate thiol analogs (*92*) exhibit enhanced sensitivity to antibiotics and reduced infectivity to macrophages, indicating MSH as a potential target for treatment of latent TB infections. Several reviews (*6, 93, 94*) has summarized the current progress on the biochemical properties of the MSH enzymes and suggested the potential of MSH synthetic pathways in drug development. This chapter shortly describes the general steps in MSH synthesis, functions of MSH in TB development, and enzymes involving in MSH pathways.

Table 2. Genes involved in the mycothiol pathways in *Mycobacterium tuberculosis*

ORF	Activity	Function	References
Rv0046 (MIPS)	Ins-1P synthase	Converts Glc-6P to Ins-1P	(*7*)
Rv0486 (MshA)	Glycosyltransferase	Generates GlcNAc-Ins-1P by transferring glucosamine group to Ins-1P	(*89, 100*)
MshA2	Phosphatase	Removes the phosphate group from GlcNAc-Ins-P	(*9*)
Rv1170 (MshB)	Deacetylase	Removes the acetyl group from GlcNAc-Ins	(*91*)
Rv2130c (MshC)	Ligase	Ligation of cysteine with GlcN-Ins	(*90*)
Rv0819 (MshD)	MSH synthase	Acetylates cysteine moiety on Cys-GlcN-Ins	(*99*)
Rv0443 (MST)	Mycothiol S-transferase	Transfers the electrophiles xenobiotics to the thiol group on MSH	(*98*)
Rv1082 (Mca)	MS-conjugate amidase	Cleaves an amide bond in mycothiol S-conjugates	(*97*)
Rv2259 (MscR)	Dehydrogenase	Detoxifies formaldehyde or nitrite	(*96*)
Rv0274	Glyoxylase I homolog	Detoxifies methylglyoxal	(*95*)

5.1 Structure and Biosynthesis

MSH contains a cysteine core with the amino group acetylated and the carboxyl group *N*-linked to D-glucosamine, which is in turn α(1→1) linked to *myo*-inositol (Fig. 2), resulting in a unique thiol that is 30-fold and 7-fold more stable than cysteine and glutathione (GSH), respectively, against heavy metal-catalyzed autoxidation (*88*).

The biosynthesis of MSH starts with the conversion of Glc-6P to Ins-1P by MIPS (*Rv0046c*) (*15, 16*). The glycosyltransferase MshA (*Rv0486*) (*89, 100*) transfers the glucosamine group from UDP-GlcNAc to Ins-1P to form GlcNAc-Ins-P. Dephosphorylation by a putative phosphatase, MshA2, yields GlcNAc-Ins (*9*), the substrate of a metal dependent deacetylase MshB (*Rv1170*) (*101*). The product of MshB is 1-*O*-(2-amino-2-deoxy-α-D-glucopyranosyl)-D-*myo*-inositol (GlcN-Ins), the major intermediate found in mycobacteria extracts. Ligation of cysteine with GlcN-Ins by MshC (*Rv2130c*) (*102*) produces 1-*O*-[2-[[(2R)-2-amino-3-mercapto-1-oxopropyl]amino]-2-deoxy-α-D-glucopyranosyl]-D-*myo*-inositol (Cys-GlcN-Ins). The final step is the acetylation of cysteine by MshD (*Rv0819*) to yield MSH. (Fig. 10)

The functions of all MSH synthetic enzymes except MshA2 have been genetically conformed *in vivo* by mutagenesis studies. (*7, 89, 90, 95, 99, 103, 104*) In addition, MIPS, MshB, MshC, and MshD from *M. tuberculosis* have been purified and mechanically examined in *vitro* and the three-dimensional structures for these four enzymes have been solved (*20, 101, 102, 105-107*). Although the structure of mycobacterial MshA is not yet available, the structure of MshA from *Corynebacterium glutamicum* has been solved, which provides valuable information about the biochemical

properties of mycobacterial MshA. (*108*) As mentioned above, the gene encoding the MshA2 activity is unidentified.

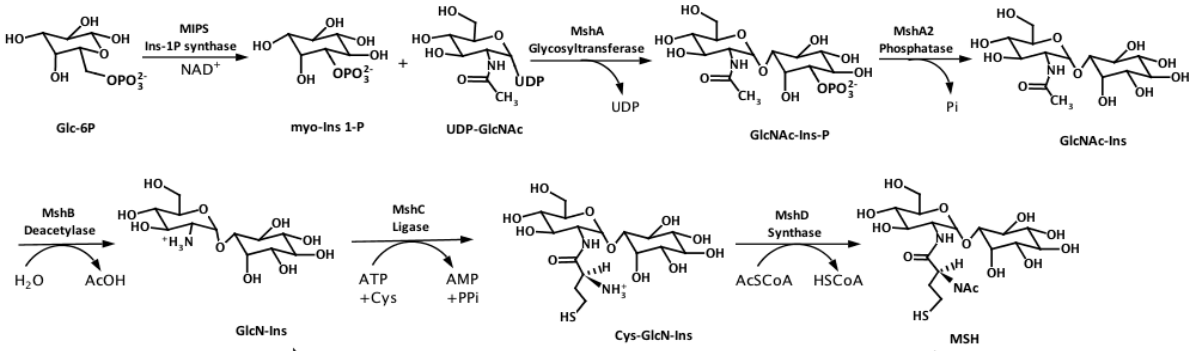

Figure 10. Mycothiol biosynthetic pathway. Synthesis of MSH starts from converting Glc-6P to Ins-1P by MIPS. The MshA transfers the glucosamine group from UDP-GlcNAc to Ins-1P to form GlcNAc-Ins-P. Dephosphorylation by MshA2 yields GlcNAc-Ins, which is further hydrolyzed by MshB to produce GlcN-Ins. Ligation of cysteine with GlcN-Ins by MshC in an ATP-dependent manner produces Cys-GlcN-Ins. In the final step, MshD acetylates Cys-GlcN-Ins to generate MSH.

5.2 Function in TB development

MSH is essential for the growth for *M. tuberculosis* and plays a critical role for survival in the hostile environment inside macrophage and adaptation in the host. As the dominant thiol in mycobacterial cytosol, MSH is present in concentrations of ~5 mM in *M. tuberculosis* during the exponential growth phase and 20 mM in the stationary phase. (*6*) The major function of MSH is to maintain intracellular redox homeostasis by serving as the cellular thiol buffer. Mycobacterial MSH mutants exhibit enhanced sensitivity to hydrogen peroxide, redox cycling agents as menadione, plumbagin, and gaseous nitric oxide. (*95, 109, 110*) This ability to protect against damaging effects from reactive oxygen species, a natural by-product of aerobic life, is critical for proper functions of biological processes, including enzyme activation, cell-cycle regulation, and DNA synthesis. (*6, 88, 96*) MSH also provides some protection during adaptation to growth in

an oxygen-rich environment in host, and *M. tuberculosis* mutants with decreased levels of MSH fail to grow in primary murine macrophages. (*111, 112*)

The constant metabolism of MSH during latent infection is necessary to support mycobacteria survival in the hostile host environment. In *M. smegmatis*, the half-life for loss of MSH is 50 hours during the stationary phase, indicating the MSH metabolism is constant during the bacterial lifetime. (*113*) About 10% of the cellular MSH has been found associated with proteins through mycothiolation, which produces the protein-SSM disulfides in a similar manner as protein glutathionylation, a process that is important for the dormancy of fungal spores. (*113, 114*)

MSH also plays a role in xenobiotic detoxification. MSH mutants exhibit enhanced sensitivities to antibiotics including rifamycin, streptomycin, erythromycin, and azithromycin, and alkylating agents (*95, 110*), suggesting that either MSH or MSH-dependent enzymes are involved in protecting mycobacteria from oxidants and toxins. (*95*) The primary mechanism of MSH-dependent detoxification is to produce less toxic S-conjugates with electrophiles xenobiotics by MST (*Rv0443*), a mycothiol S-transferase. (*98*) The S-conjugates can either accumulate within the cell without adverse consequence (*115*) or be cleaved by Mca (*Rv1082*), a MS-conjugate amidase, to generate mercapturic acids (AcCysR) that is exported from the cell, and the resulting GlcN-Ins is used to regenerate MSH. (*97*)

MSH can function as the cofactor for several enzymes, such as MscR (*Rv2259*), a NAD^+-dependent dehydrogenase that detoxifies either formaldehyde or nitrite through two distinctive mechanisms. (*96*) Enhanced sensitivity to peroxides in MSH-deficient *M. smegmatis* and *M. tuberculosis* suggests the presence of an MSH-dependent peroxidase in

which the MSH acts as an electron donor for peroxiredoxins. (*96*) MSH has also been associated with the detoxification of methylglyoxal by a glyoxylase I-type activity, and sequence analysis indicates that *Rv0274* encodes a GSH-glyoxylase I homolog. (*95*)

6. Therapeutic Implications

Mycobacterium species contain a variety of inositol compounds including PI, the membrane anchor for cell wall lipoglycans, and MSH, a glutathione analogue. (*5, 6, 14*) These inositol-containing molecules play critical roles in the TB infection and disease development, and therefore are considered as attractive drug targets.

6.1 Inositol synthetic pathway

The essentiality of inositol for the survival of *M. tuberculosis* indicates that the inositol synthetic pathway may provide a source for drug targets. *M. tuberculosis* mutants lacking the functional *ino1* can only be isolated when the media is supplemented with 77 mM inositol, while the equivalent *S. cerevisiae* and *M. smegmatis* mutants only require supplementation with 27 μM and 100 μM, respectively, for normal growth, indicating that inositol synthesis or acquisition is essential for the viability of *M. tuberculosis*. (*7*) The phosphorothioate-modified antisense oligodeoxyribonucleotides (PS-ODNs) against the mRNA of *ino1* have been considered potential lipophilic drugs that can pass through the cell wall to enter the cytoplasm of *M. tuberculosis*. Treatment with μM level of antisense PS-ODNs successfully inhibited the expression of tMIPS and the proliferation of *M. tuberculosis*. (*17*) Detailed characterization of the catalytic process and cofactor preference of tMIPS is necessary to differentiate the type II or type

III aldolase mechanism utilized by the mycobacterial enzyme, which could shed light on the rational design of inhibitors against tMIPS. (*20, 21*) Although four genes have been found to be homologous to human IMPase and presence of redundant IMPase activities has been implied, failure to isolate the *impC* mutant indicates the potential of ImpC as a target for killing *M. tuberculosis*. (*8*)

6.2 Inositol-lipid pathways

Cell wall components are often the targets of effective chemotherapeutic agents against bacterial infection (*116-118*). Ethambutol (EMB), a front-line drug for TB treatment (*119*), is proposed to specifically target the inhibition biosynthesis of arabinan core of LAM (*120*). The EMB-resistant mutant derived from *M. smegmatis* makes a truncated LAM, suggesting an effect on arabinosyltransferases. (*120*) A three-gene operon, termed *embCAB*, in *M. tuberculosis* has been identified as the putative target of EMB. (*121*) EmbC is required for synthesis of LAM (*67*), while *embAB* genes encode Ara*f*T involved in the polymerization of arabinose (*122*). Overproduction or structural mutations in Emb protein(s) might cause the high-level resistance to EMB (*121*). Furthermore, one EMB derivatives, SQ109, has been identified as a novel antibiotic with very efficient antimycobacterial activity (*123, 124*). Interestingly, SQ109 shows no cross-resistance to EMB or multidrug resistant strains of *M. tuberculosis*. Other novel and highly potent anti-TB compounds targeting on arabinan synthesis for LAM assembly include benzothiazinones (BTZ) (*125*) and dinitrobenzamides (DNB) (*126*).

Rapid emergence of drug-resistant TB indicates the urgency for the development of more effective drugs that act on novel drug targets with no cross-resistance to existing

drugs. The availability of complete genome sequences of *M. tuberculosis* (*15*) allows identification of enzymes and genes involved in the biosynthesis of inositol-containing glycolipids. Majority of these enzymes that play critical roles in the growth and infection of *M. tuberculosis* lack homologs in mammalian systems, thus make them attractive drug targets. For example, PI synthetase is critical for the normal growth of *M. smegmatis* and *M. tuberculosis* (*48*). The inability to isolate a *pimA* mutant (*54*) suggests that mannosylated PI species are potential targets against mycobacterial pathogens. Additional targets may be enzymes that are not required for growth, but are critical during TB infection. One example is MptA that mutation of this enzyme resulted in altered cell wall phenotype with accumulation of a truncated lipoglycan deficient in α(1→6)Man*p* units (*63*). Also, given the importance of the mannose capping structure on Man-LAM in the inhibition of phagosome maturation (*72*), enzymes such as CapA (*72*) and MptC (*43*) are possible targets against TB disease development.

6.3 Mycothiol pathways

The MSH pathways have become a focal point of drug discovery for TB treatment in recent years. Efforts and progress in development of inhibitors against MSH pathways have been summarized recently by Hernick (*93*) and are briefly described here. UDP-(5F)-GlcNAc has been identified as a slow, tight-binding inhibitor for MshA, which exhibits competitive inhibition with respect to the substrate UDP-GlcNAc (K_i of ~1.4 μM). (*127*) Inhibitor libraries for MshB that were designed to incorporate features of substrate GlcNAc-Ins, and compounds that inhibit MshB with IC_{50} values low to μM have been identified (*128, 129*). A rapid fluorescence-based assay for measuring MshB

activity has been recently developed in our lab and described in Appendix A. This new assay would facilitate inhibitor screening and characterization (*130*).

Intensive efforts have been made to develop MshC inhibitors. 5'-*O*-[*N*-(L-cysteinyl) sulfamoyl]adenosine (CSA) is a bisubstrate analog to MshC that exhibit the inhibition with IC_{50} of ~50 nM (*131*). Dequalinium, an ATP-competitive inhibitor that binds to MshC (K_D of ~0.22 μM), inhibits the growth of *M. tuberculosis* under aerobic and anaerobic conditions (*132*). NTF1836 (IC_{50} of ~100 μM) is a potent inhibitor against MshC identified in cell-based assays (*133*). Treatment with NTF1836 leads to killing nonreplicating *M. tuberculosis* cells and loss of MSH production (*133*), validating MSH biosynthesis as drug target for latent TB.

Bromotyrosine containing natural products and analogs inhibit Mca with IC_{50} values in low μM range and show *in vitro* activity against *M. tuberculosis* and *M. bovis*. (*134-137*) In addition, Mca inhibitors designed as substrate analogs have been reported to exhibit IC_{50} in mid μM range (*138*).

7. Conclusions

The current challenges in TB therapy remain in the difficulty to eradicate latent and multi-drug resistant pathogens. Exploring novel drug targets involved in TB latency is an alternative means to shorten treatment time and decrease the possibility of the emergence of resistant mutants. Inositol-containing derivatives found in *M. tuberculosis* are critical for pathogenesis. The availability of complete genome sequences of *M. tuberculosis* has allowed for the identification of enzymes and genes involved in the biosynthesis of inositol and related derivatives as attractive drug targets for TB treatment.

Inositol can be obtained either from exogenous sources through Ins transporters or from *de novo* synthesis. An active transport system has been suggested to import inositol from growth medium against a concentration gradient to maintain stable cellular levels of inositol in mycobacteria. Moreover, the fast growing species *M. smegmatis* contains additional genes encoding for a Na^+/inositol cotransporter and ABC transporters that are absent from the genome of *M. tuberculosis*.

The enzymatic synthesis of *myo*-inositol in mycobacteria follows a conversed pathway involving two enzymes, MIPS and IMPase. MIPS is important for the normal growth of *M. tuberculosis* and the MIPS-deficient mutant can only be isolated with the presence of inositol supplement. A structural zinc ion is observed in the crystal structure of MIPS from *M. tuberculosis*, which is most likely to stabilize and polarize the cofactor NAD^+ for catalysis. Sequence analyses suggest mycobacteria recruited the *ino1* gene from archaea. However, it remains unclear whether mycobacterial MIPS follows the mechanism of type II aldolase as archeal MIPS that using a divalent metal ion to complete the reaction, or is a type III aldolase as eukaryotic MIPS that is activated by ammonium ion.

Dephosphorylation of Ins-1P by Inositol monophosphatase (IMPase) produces the *myo*-inositol. Four IMPase homologs (ImpA, SuhB, CysQ, and ImpC) have been identified in the genome of *M. tuberculosis*, which are probably involved in cell wall lipid synthesis, sulfur metabolism, and MSH production. In addition, the *impC* gene may play an essential role in the growth of *M. tuberculosis* since no mutant with a deficient *impC* could be generated so far. Thus ImpC is most likely involved in an important pathway in *M. tuberculosis* that could be targeted for TB treatment. Further studies on

the biochemical and structural characteristics of MIPS and IMPase enzymes are necessary to explore their potential as drug targets.

Inositol is the building block for PI, the precursor for the synthesis of mycobacteria specific cell wall-associated inositol-lipids, including PIMs, LM, and LAM. Interestingly, production of PI3P, a membrane-trafficking lipid widely found in the signal transduction in eukaryotic cells, has also been found as a down-stream production of PI synthesis in *M. smegmatis*, although its function is still unknown. The unique mannosylated PI lipids play key roles in host-pathogen interaction, resulting in less inflammatory response and delay of phagosome maturation. The majority of enzymes in the biosynthesis of inositol-lipids lack homologs in mammalian systems, making them attractive drug targets.

Inositol is also incorporated into MSH in mycobacteria, which is a unique low molecular mass thiol that maintains the mycobacterial cellular redox status during infection and persistence in hostile host environments, and is also involved in xenobiotic detoxification. MSH provides protection against damaging effects from the reactive oxygen species, a natural by-product of aerobic life. MSH-deficient *M. tuberculosis* mutants exhibit increased sensitivity to oxidative stress as well as antibiotics such as streptomycin, ethionamide, and rifampin. Therefore enzymes in MSH pathways have become focus for drug discovery and significant progress has been made over the last several years to develop and screen inhibitors targeting on MSH pathways.

References

1. Ventura, M., Canchaya, C., Tauch, A., Chandra, G., Fitzgerald, G. F., Chater, K. F., and van Sinderen, D. (2007) Genomics of Actinobacteria: tracing the evolutionary history of an ancient phylum, *Microbiol Mol Biol Rev 71*, 495-548.
2. WHO. (2012) Global Tuberculosis Control.
3. Zhang, Y. (2005) The magic bullets and tuberculosis drug targets, *Annu Rev Pharmacol Toxicol 45*, 529-564.
4. Michell, R. H. (2008) Inositol derivatives: evolution and functions, *Nat Rev Mol Cell Biol 9*, 151-161.
5. Morita, Y. S., Fukuda, T., Sena, C. B., Yamaryo-Botte, Y., McConville, M. J., and Kinoshita, T. (2011) Inositol lipid metabolism in mycobacteria: biosynthesis and regulatory mechanisms, *Biochim Biophys Acta 1810*, 630-641.
6. Newton, G. L., Buchmeier, N., and Fahey, R. C. (2008) Biosynthesis and functions of mycothiol, the unique protective thiol of Actinobacteria, *Microbiol Mol Biol Rev 72*, 471-494.
7. Movahedzadeh, F., Smith, D. A., Norman, R. A., Dinadayala, P., Murray-Rust, J., Russell, D. G., Kendall, S. L., Rison, S. C., McAlister, M. S., Bancroft, G. J., McDonald, N. Q., Daffe, M., Av-Gay, Y., and Stoker, N. G. (2004) The Mycobacterium tuberculosis ino1 gene is essential for growth and virulence, *Mol Microbiol 51*, 1003-1014.
8. Movahedzadeh, F., Wheeler, P. R., Dinadayala, P., Av-Gay, Y., Parish, T., Daffe, M., and Stoker, N. G. (2010) Inositol monophosphate phosphatase genes of Mycobacterium tuberculosis, *BMC Microbiol 10*, 50.

9. Newton, G. L., Ta, P., Bzymek, K. P., and Fahey, R. C. (2006) Biochemistry of the initial steps of mycothiol biosynthesis, *J Biol Chem 281*, 33910-33920.

10. Haites, R. E., Morita, Y. S., McConville, M. J., and Billman-Jacobe, H. (2005) Function of phosphatidylinositol in mycobacteria, *J Biol Chem 280*, 10981-10987.

11. Yoshida, K., Yamamoto, Y., Omae, K., Yamamoto, M., and Fujita, Y. (2002) Identification of two myo-inositol transporter genes of Bacillus subtilis, *J Bacteriol 184*, 983-991.

12. Bettaney, K. E., Sukumar, P., Hussain, R., Siligardi, G., Henderson, P. J., and Patching, S. G. (2012) A systematic approach to the amplified expression, functional characterization and purification of inositol transporters from Bacillus subtilis, *Mol Membr Biol*.

13. Titgemeyer, F., Amon, J., Parche, S., Mahfoud, M., Bail, J., Schlicht, M., Rehm, N., Hillmann, D., Stephan, J., Walter, B., Burkovski, A., and Niederweis, M. (2007) A genomic view of sugar transport in Mycobacterium smegmatis and Mycobacterium tuberculosis, *J Bacteriol 189*, 5903-5915.

14. Mishra, A. K., Driessen, N. N., Appelmelk, B. J., and Besra, G. S. (2011) Lipoarabinomannan and related glycoconjugates: structure, biogenesis and role in Mycobacterium tuberculosis physiology and host-pathogen interaction, *FEMS Microbiol Rev 35*, 1126-1157.

15. Cole, S. T., Brosch, R., Parkhill, J., Garnier, T., Churcher, C., Harris, D., Gordon, S. V., Eiglmeier, K., Gas, S., Barry, C. E., 3rd, Tekaia, F., Badcock, K., Basham, D., Brown, D., Chillingworth, T., Connor, R., Davies, R., Devlin, K., Feltwell, T., Gentles, S., Hamlin, N., Holroyd, S., Hornsby, T., Jagels, K., Krogh, A., McLean,

J., Moule, S., Murphy, L., Oliver, K., Osborne, J., Quail, M. A., Rajandream, M. A., Rogers, J., Rutter, S., Seeger, K., Skelton, J., Squares, R., Squares, S., Sulston, J. E., Taylor, K., Whitehead, S., and Barrell, B. G. (1998) Deciphering the biology of Mycobacterium tuberculosis from the complete genome sequence, *Nature 393*, 537-544.

16. Bachhawat, N., and Mande, S. C. (1999) Identification of the INO1 gene of Mycobacterium tuberculosis H37Rv reveals a novel class of inositol-1-phosphate synthase enzyme, *J Mol Biol 291*, 531-536.

17. Li, Y., Chen, Z., Li, X., Zhang, H., Huang, Q., Zhang, Y., and Xu, S. (2007) Inositol-1-phosphate synthetase mRNA as a new target for antisense inhibition of Mycobacterium tuberculosis, *J Biotechnol 128*, 726-734.

18. Smith, D., Hansch, H., Bancroft, G., and Ehlers, S. (1997) T-cell-independent granuloma formation in response to Mycobacterium avium: role of tumour necrosis factor-alpha and interferon-gamma, *Immunology 92*, 413-421.

19. Hansch, H. C., Smith, D. A., Mielke, M. E., Hahn, H., Bancroft, G. J., and Ehlers, S. (1996) Mechanisms of granuloma formation in murine Mycobacterium avium infection: the contribution of CD4+ T cells, *Int Immunol 8*, 1299-1310.

20. Norman, R. A., McAlister, M. S., Murray-Rust, J., Movahedzadeh, F., Stoker, N. G., and McDonald, N. Q. (2002) Crystal structure of inositol 1-phosphate synthase from Mycobacterium tuberculosis, a key enzyme in phosphatidylinositol synthesis, *Structure 10*, 393-402.

21. Stieglitz, K. A., Yang, H., Roberts, M. F., and Stec, B. (2005) Reaching for mechanistic consensus across life kingdoms: structure and insights into catalysis

of the myo-inositol-1-phosphate synthase (mIPS) from Archaeoglobus fulgidus, *Biochemistry 44*, 213-224.

22. Jin, X., and Geiger, J. H. (2003) Structures of NAD(+)- and NADH-bound 1-l-myo-inositol 1-phosphate synthase, *Acta Crystallogr D Biol Crystallogr 59*, 1154-1164.

23. Jin, X., Foley, K. M., and Geiger, J. H. (2004) The structure of the 1L-myo-inositol-1-phosphate synthase-NAD+-2-deoxy-D-glucitol 6-(E)-vinylhomophosphonate complex demands a revision of the enzyme mechanism, *J Biol Chem 279*, 13889-13895.

24. Chen, L., Zhou, C., Yang, H., and Roberts, M. F. (2000) Inositol-1-phosphate synthase from Archaeoglobus fulgidus is a class II aldolase, *Biochemistry 39*, 12415-12423.

25. Escamilla, J. E., Contreras, M., Martinez, A., and Zentella-Pina, M. (1982) L-myoinositol-1-phosphate synthase from Neurospora crassa: purification to homogeneity and partial characterization, *Arch Biochem Biophys 218*, 275-285.

26. Neelon, K., Wang, Y., Stec, B., and Roberts, M. F. (2005) Probing the mechanism of the Archaeoglobus fulgidus inositol-1-phosphate synthase, *J Biol Chem 280*, 11475-11482.

27. Bachhawat, N., and Mande, S. C. (2000) Complex evolution of the inositol-1-phosphate synthase gene among archaea and eubacteria, *Trends Genet 16*, 111-113.

28. Majumder, A. L., Chatterjee, A., Ghosh Dastidar, K., and Majee, M. (2003) Diversification and evolution of L-myo-inositol 1-phosphate synthase, *FEBS Lett 553*, 3-10.

29. Nigou, J., Dover, L. G., and Besra, G. S. (2002) Purification and biochemical characterization of Mycobacterium tuberculosis SuhB, an inositol monophosphatase involved in inositol biosynthesis, *Biochemistry 41*, 4392-4398.

30. Parish, T., Liu, J., Nikaido, H., and Stoker, N. G. (1997) A Mycobacterium smegmatis mutant with a defective inositol monophosphate phosphatase gene homolog has altered cell envelope permeability, *J Bacteriol 179*, 7827-7833.

31. Brown, A. K., Meng, G., Ghadbane, H., Scott, D. J., Dover, L. G., Nigou, J., Besra, G. S., and Futterer, K. (2007) Dimerization of inositol monophosphatase Mycobacterium tuberculosis SuhB is not constitutive, but induced by binding of the activator Mg2+, *BMC Struct Biol 7*, 55.

32. Hatzios, S. K., Iavarone, A. T., and Bertozzi, C. R. (2008) Rv2131c from Mycobacterium tuberculosis is a CysQ 3'-phosphoadenosine-5'-phosphatase, *Biochemistry 47*, 5823-5831.

33. Hatzios, S. K., Schelle, M. W., Newton, G. L., Sogi, K. M., Holsclaw, C. M., Fahey, R. C., and Bertozzi, C. R. (2011) The Mycobacterium tuberculosis CysQ phosphatase modulates the biosynthesis of sulfated glycolipids and bacterial growth, *Bioorg Med Chem Lett 21*, 4956-4959.

34. Guerin, M. E., Kordulakova, J., Alzari, P. M., Brennan, P. J., and Jackson, M. (2010) Molecular basis of phosphatidyl-myo-inositol mannoside biosynthesis and regulation in mycobacteria, *J Biol Chem 285*, 33577-33583.

35. Torrelles, J. B., and Schlesinger, L. S. (2010) Diversity in Mycobacterium tuberculosis mannosylated cell wall determinants impacts adaptation to the host, *Tuberculosis (Edinb) 90*, 84-93.

36. Morita, Y. S., Patterson, J. H., Billman-Jacobe, H., and McConville, M. J. (2004) Biosynthesis of mycobacterial phosphatidylinositol mannosides, *Biochem J 378*, 589-597.

37. Morita, Y. S., Yamaryo-Botte, Y., Miyanagi, K., Callaghan, J. M., Patterson, J. H., Crellin, P. K., Coppel, R. L., Billman-Jacobe, H., Kinoshita, T., and McConville, M. J. (2010) Stress-induced synthesis of phosphatidylinositol 3-phosphate in mycobacteria, *J Biol Chem 285*, 16643-16650.

38. Khoo, K. H., Dell, A., Morris, H. R., Brennan, P. J., and Chatterjee, D. (1995) Structural definition of acylated phosphatidylinositol mannosides from Mycobacterium tuberculosis: definition of a common anchor for lipomannan and lipoarabinomannan, *Glycobiology 5*, 117-127.

39. Severn, W. B., Furneaux, R. H., Falshaw, R., and Atkinson, P. H. (1998) Chemical and spectroscopic characterisation of the phosphatidylinositol manno-oligosaccharides from Mycobacterium bovis AN5 and WAg201 and Mycobacterium smegmatis mc2 155, *Carbohydr Res 308*, 397-408.

40. Nigou, J., Gilleron, M., and Puzo, G. (2003) Lipoarabinomannans: from structure to biosynthesis, *Biochimie 85*, 153-166.

41. Besra, G. S., Morehouse, C. B., Rittner, C. M., Waechter, C. J., and Brennan, P. J. (1997) Biosynthesis of mycobacterial lipoarabinomannan, *J Biol Chem 272*, 18460-18466.

42. Hunter, S. W., and Brennan, P. J. (1990) Evidence for the presence of a phosphatidylinositol anchor on the lipoarabinomannan and lipomannan of Mycobacterium tuberculosis, *J Biol Chem 265*, 9272-9279.

43. Kaur, D., Obregon-Henao, A., Pham, H., Chatterjee, D., Brennan, P. J., and Jackson, M. (2008) Lipoarabinomannan of Mycobacterium: mannose capping by a multifunctional terminal mannosyltransferase, *Proc Natl Acad Sci U S A 105*, 17973-17977.

44. Birch, H. L., Alderwick, L. J., Appelmelk, B. J., Maaskant, J., Bhatt, A., Singh, A., Nigou, J., Eggeling, L., Geurtsen, J., and Besra, G. S. (2010) A truncated lipoglycan from mycobacteria with altered immunological properties, *Proc Natl Acad Sci U S A 107*, 2634-2639.

45. Chatterjee, D., Khoo, K. H., McNeil, M. R., Dell, A., Morris, H. R., and Brennan, P. J. (1993) Structural definition of the non-reducing termini of mannose-capped LAM from Mycobacterium tuberculosis through selective enzymatic degradation and fast atom bombardment-mass spectrometry, *Glycobiology 3*, 497-506.

46. Khoo, K. H., Dell, A., Morris, H. R., Brennan, P. J., and Chatterjee, D. (1995) Inositol phosphate capping of the nonreducing termini of lipoarabinomannan from rapidly growing strains of Mycobacterium, *J Biol Chem 270*, 12380-12389.

47. Guerardel, Y., Maes, E., Briken, V., Chirat, F., Leroy, Y., Locht, C., Strecker, G., and Kremer, L. (2003) Lipomannan and lipoarabinomannan from a clinical isolate of Mycobacterium kansasii: novel structural features and apoptosis-inducing properties, *J Biol Chem 278*, 36637-36651.

48. Jackson, M., Crick, D. C., and Brennan, P. J. (2000) Phosphatidylinositol is an essential phospholipid of mycobacteria, *J Biol Chem 275*, 30092-30099.

49. Owens, R. M., Hsu, F. F., VanderVen, B. C., Purdy, G. E., Hesteande, E., Giannakas, P., Sacchettini, J. C., McKinney, J. D., Hill, P. J., Belisle, J. T., Butcher, B. A., Pethe, K., and Russell, D. G. (2006) M. tuberculosis Rv2252 encodes a diacylglycerol kinase involved in the biosynthesis of phosphatidylinositol mannosides (PIMs), *Mol Microbiol 60*, 1152-1163.

50. Nigou, J., and Besra, G. S. (2002) Cytidine diphosphate-diacylglycerol synthesis in Mycobacterium smegmatis, *Biochem J 367*, 157-162.

51. Salman, M., Lonsdale, J. T., Besra, G. S., and Brennan, P. J. (1999) Phosphatidylinositol synthesis in mycobacteria, *Biochim Biophys Acta 1436*, 437-450.

52. Cockcroft, S. (1999) Mammalian phosphatidylinositol transfer proteins: emerging roles in signal transduction and vesicular traffic, *Chem Phys Lipids 98*, 23-33.

53. Morii, H., Ogawa, M., Fukuda, K., Taniguchi, H., and Koga, Y. (2010) A revised biosynthetic pathway for phosphatidylinositol in Mycobacteria, *J Biochem 148*, 593-602.

54. Kordulakova, J., Gilleron, M., Mikusova, K., Puzo, G., Brennan, P. J., Gicquel, B., and Jackson, M. (2002) Definition of the first mannosylation step in phosphatidylinositol mannoside synthesis. PimA is essential for growth of mycobacteria, *J Biol Chem 277*, 31335-31344.

55. Kordulakova, J., Gilleron, M., Puzo, G., Brennan, P. J., Gicquel, B., Mikusova, K., and Jackson, M. (2003) Identification of the required acyltransferase step in

the biosynthesis of the phosphatidylinositol mannosides of mycobacterium species, *J Biol Chem 278*, 36285-36295.

56. Kremer, L., Gurcha, S. S., Bifani, P., Hitchen, P. G., Baulard, A., Morris, H. R., Dell, A., Brennan, P. J., and Besra, G. S. (2002) Characterization of a putative alpha-mannosyltransferase involved in phosphatidylinositol trimannoside biosynthesis in Mycobacterium tuberculosis, *Biochem J 363*, 437-447.

57. Morita, Y. S., Sena, C. B., Waller, R. F., Kurokawa, K., Sernee, M. F., Nakatani, F., Haites, R. E., Billman-Jacobe, H., McConville, M. J., Maeda, Y., and Kinoshita, T. (2006) PimE is a polyprenol-phosphate-mannose-dependent mannosyltransferase that transfers the fifth mannose of phosphatidylinositol mannoside in mycobacteria, *J Biol Chem 281*, 25143-25155.

58. Lea-Smith, D. J., Martin, K. L., Pyke, J. S., Tull, D., McConville, M. J., Coppel, R. L., and Crellin, P. K. (2008) Analysis of a new mannosyltransferase required for the synthesis of phosphatidylinositol mannosides and lipoarbinomannan reveals two lipomannan pools in corynebacterineae, *J Biol Chem 283*, 6773-6782.

59. Guerin, M. E., Kaur, D., Somashekar, B. S., Gibbs, S., Gest, P., Chatterjee, D., Brennan, P. J., and Jackson, M. (2009) New insights into the early steps of phosphatidylinositol mannoside biosynthesis in mycobacteria: PimB' is an essential enzyme of Mycobacterium smegmatis, *J Biol Chem 284*, 25687-25696.

60. Mishra, A. K., Batt, S., Krumbach, K., Eggeling, L., and Besra, G. S. (2009) Characterization of the Corynebacterium glutamicum deltapimB' deltamgtA double deletion mutant and the role of Mycobacterium tuberculosis orthologues Rv2188c and Rv0557 in glycolipid biosynthesis, *J Bacteriol 191*, 4465-4472.

61. Mishra, A. K., Alderwick, L. J., Rittmann, D., Wang, C., Bhatt, A., Jacobs, W. R., Jr., Takayama, K., Eggeling, L., and Besra, G. S. (2008) Identification of a novel alpha(1-->6) mannopyranosyltransferase MptB from Corynebacterium glutamicum by deletion of a conserved gene, NCgl1505, affords a lipomannan- and lipoarabinomannan-deficient mutant, *Mol Microbiol 68*, 1595-1613.

62. Driessen, N. N., Stoop, E. J., Ummels, R., Gurcha, S. S., Mishra, A. K., Larrouy-Maumus, G., Nigou, J., Gilleron, M., Puzo, G., Maaskant, J. J., Sparrius, M., Besra, G. S., Bitter, W., Vandenbroucke-Grauls, C. M., and Appelmelk, B. J. (2010) Mycobacterium marinum MMAR_2380, a predicted transmembrane acyltransferase, is essential for the presence of the mannose cap on lipoarabinomannan, *Microbiology 156*, 3492-3502.

63. Kaur, D., McNeil, M. R., Khoo, K. H., Chatterjee, D., Crick, D. C., Jackson, M., and Brennan, P. J. (2007) New insights into the biosynthesis of mycobacterial lipomannan arising from deletion of a conserved gene, *J Biol Chem 282*, 27133-27140.

64. Mishra, A. K., Alderwick, L. J., Rittmann, D., Tatituri, R. V., Nigou, J., Gilleron, M., Eggeling, L., and Besra, G. S. (2007) Identification of an alpha(1-->6) mannopyranosyltransferase (MptA), involved in Corynebacterium glutamicum lipomanann biosynthesis, and identification of its orthologue in Mycobacterium tuberculosis, *Mol Microbiol 65*, 1503-1517.

65. Sena, C. B., Fukuda, T., Miyanagi, K., Matsumoto, S., Kobayashi, K., Murakami, Y., Maeda, Y., Kinoshita, T., and Morita, Y. S. (2010) Controlled expression of

branch-forming mannosyltransferase is critical for mycobacterial lipoarabinomannan biosynthesis, *J Biol Chem 285*, 13326-13336.

66. Alderwick, L. J., Seidel, M., Sahm, H., Besra, G. S., and Eggeling, L. (2006) Identification of a novel arabinofuranosyltransferase (AftA) involved in cell wall arabinan biosynthesis in Mycobacterium tuberculosis, *J Biol Chem 281*, 15653-15661.

67. Zhang, N., Torrelles, J. B., McNeil, M. R., Escuyer, V. E., Khoo, K. H., Brennan, P. J., and Chatterjee, D. (2003) The Emb proteins of mycobacteria direct arabinosylation of lipoarabinomannan and arabinogalactan via an N-terminal recognition region and a C-terminal synthetic region, *Mol Microbiol 50*, 69-76.

68. Alderwick, L. J., Lloyd, G. S., Ghadbane, H., May, J. W., Bhatt, A., Eggeling, L., Futterer, K., and Besra, G. S. (2011) The C-terminal domain of the Arabinosyltransferase Mycobacterium tuberculosis EmbC is a lectin-like carbohydrate binding module, *PLoS Pathog 7*, e1001299.

69. Skovierova, H., Larrouy-Maumus, G., Pham, H., Belanova, M., Barilone, N., Dasgupta, A., Mikusova, K., Gicquel, B., Gilleron, M., Brennan, P. J., Puzo, G., Nigou, J., and Jackson, M. (2010) Biosynthetic origin of the galactosamine substituent of Arabinogalactan in Mycobacterium tuberculosis, *J Biol Chem 285*, 41348-41355.

70. Seidel, M., Alderwick, L. J., Birch, H. L., Sahm, H., Eggeling, L., and Besra, G. S. (2007) Identification of a novel arabinofuranosyltransferase AftB involved in a terminal step of cell wall arabinan biosynthesis in Corynebacterianeae, such as

Corynebacterium glutamicum and Mycobacterium tuberculosis, *J Biol Chem 282*, 14729-14740.

71. Briken, V., Porcelli, S. A., Besra, G. S., and Kremer, L. (2004) Mycobacterial lipoarabinomannan and related lipoglycans: from biogenesis to modulation of the immune response, *Mol Microbiol 53*, 391-403.

72. Appelmelk, B. J., den Dunnen, J., Driessen, N. N., Ummels, R., Pak, M., Nigou, J., Larrouy-Maumus, G., Gurcha, S. S., Movahedzadeh, F., Geurtsen, J., Brown, E. J., Eysink Smeets, M. M., Besra, G. S., Willemsen, P. T., Lowary, T. L., van Kooyk, Y., Maaskant, J. J., Stoker, N. G., van der Ley, P., Puzo, G., Vandenbroucke-Grauls, C. M., Wieland, C. W., van der Poll, T., Geijtenbeek, T. B., van der Sar, A. M., and Bitter, W. (2008) The mannose cap of mycobacterial lipoarabinomannan does not dominate the Mycobacterium-host interaction, *Cell Microbiol 10*, 930-944.

73. Nguyen, L., and Pieters, J. (2005) The Trojan horse: survival tactics of pathogenic mycobacteria in macrophages, *Trends Cell Biol 15*, 269-276.

74. Vergne, I., Chua, J., Singh, S. B., and Deretic, V. (2004) Cell biology of mycobacterium tuberculosis phagosome, *Annu Rev Cell Dev Biol 20*, 367-394.

75. Vergne, I., Chua, J., and Deretic, V. (2003) Mycobacterium tuberculosis phagosome maturation arrest: selective targeting of PI3P-dependent membrane trafficking, *Traffic 4*, 600-606.

76. Fratti, R. A., Backer, J. M., Gruenberg, J., Corvera, S., and Deretic, V. (2001) Role of phosphatidylinositol 3-kinase and Rab5 effectors in phagosomal

biogenesis and mycobacterial phagosome maturation arrest, *J Cell Biol 154*, 631-644.

77. Vergne, I., Chua, J., and Deretic, V. (2003) Tuberculosis toxin blocking phagosome maturation inhibits a novel Ca2+/calmodulin-PI3K hVPS34 cascade, *J Exp Med 198*, 653-659.

78. Malik, Z. A., Iyer, S. S., and Kusner, D. J. (2001) Mycobacterium tuberculosis phagosomes exhibit altered calmodulin-dependent signal transduction: contribution to inhibition of phagosome-lysosome fusion and intracellular survival in human macrophages, *J Immunol 166*, 3392-3401.

79. Torrelles, J. B., Knaup, R., Kolareth, A., Slepushkina, T., Kaufman, T. M., Kang, P., Hill, P. J., Brennan, P. J., Chatterjee, D., Belisle, J. T., Musser, J. M., and Schlesinger, L. S. (2008) Identification of Mycobacterium tuberculosis clinical isolates with altered phagocytosis by human macrophages due to a truncated lipoarabinomannan, *J Biol Chem 283*, 31417-31428.

80. Sweet, L., Singh, P. P., Azad, A. K., Rajaram, M. V., Schlesinger, L. S., and Schorey, J. S. (2010) Mannose receptor-dependent delay in phagosome maturation by Mycobacterium avium glycopeptidolipids, *Infect Immun 78*, 518-526.

81. Schlesinger, L. S., Hull, S. R., and Kaufman, T. M. (1994) Binding of the terminal mannosyl units of lipoarabinomannan from a virulent strain of Mycobacterium tuberculosis to human macrophages, *J Immunol 152*, 4070-4079.

82. Astarie-Dequeker, C., N'Diaye, E. N., Le Cabec, V., Rittig, M. G., Prandi, J., and Maridonneau-Parini, I. (1999) The mannose receptor mediates uptake of

pathogenic and nonpathogenic mycobacteria and bypasses bactericidal responses in human macrophages, *Infect Immun 67*, 469-477.

83. Schlesinger, L. S. (1993) Macrophage phagocytosis of virulent but not attenuated strains of Mycobacterium tuberculosis is mediated by mannose receptors in addition to complement receptors, *J Immunol 150*, 2920-2930.

84. Kang, P. B., Azad, A. K., Torrelles, J. B., Kaufman, T. M., Beharka, A., Tibesar, E., DesJardin, L. E., and Schlesinger, L. S. (2005) The human macrophage mannose receptor directs Mycobacterium tuberculosis lipoarabinomannan-mediated phagosome biogenesis, *J Exp Med 202*, 987-999.

85. Torrelles, J. B., Azad, A. K., and Schlesinger, L. S. (2006) Fine discrimination in the recognition of individual species of phosphatidyl-myo-inositol mannosides from Mycobacterium tuberculosis by C-type lectin pattern recognition receptors, *J Immunol 177*, 1805-1816.

86. Vergne, I., Fratti, R. A., Hill, P. J., Chua, J., Belisle, J., and Deretic, V. (2004) Mycobacterium tuberculosis phagosome maturation arrest: mycobacterial phosphatidylinositol analog phosphatidylinositol mannoside stimulates early endosomal fusion, *Mol Biol Cell 15*, 751-760.

87. Deretic, V., Singh, S., Master, S., Kyei, G., Davis, A., Naylor, J., de Haro, S., Harris, J., Delgado, M., Roberts, E., and Vergne, I. (2007) Phosphoinositides in phagolysosome and autophagosome biogenesis, *Biochem Soc Symp*, 141-148.

88. Spies, H. S., and Steenkamp, D. J. (1994) Thiols of intracellular pathogens. Identification of ovothiol A in Leishmania donovani and structural analysis of a novel thiol from Mycobacterium bovis, *Eur J Biochem 224*, 203-213.

89. Buchmeier, N., and Fahey, R. C. (2006) The mshA gene encoding the glycosyltransferase of mycothiol biosynthesis is essential in Mycobacterium tuberculosis Erdman, *FEMS Microbiol Lett 264*, 74-79.

90. Sareen, D., Newton, G. L., Fahey, R. C., and Buchmeier, N. A. (2003) Mycothiol is essential for growth of Mycobacterium tuberculosis Erdman, *J Bacteriol 185*, 6736-6740.

91. Buchmeier, N. A., Newton, G. L., Koledin, T., and Fahey, R. C. (2003) Association of mycothiol with protection of Mycobacterium tuberculosis from toxic oxidants and antibiotics, *Mol Microbiol 47*, 1723-1732.

92. Newton, G. L., Ta, P., and Fahey, R. C. (2005) A mycothiol synthase mutant of Mycobacterium smegmatis produces novel thiols and has an altered thiol redox status, *J Bacteriol 187*, 7309-7316.

93. Hernick, M. (2013) Mycothiol: a target for potentiation of rifampin and other antibiotics against Mycobacterium tuberculosis, *Expert Review of Anti-infective Therapy 11*, 49-67.

94. Fan, F., Vetting, M. W., Frantom, P. A., and Blanchard, J. S. (2009) Structures and mechanisms of the mycothiol biosynthetic enzymes, *Curr Opin Chem Biol 13*, 451-459.

95. Rawat, M., Newton, G. L., Ko, M., Martinez, G. J., Fahey, R. C., and Av-Gay, Y. (2002) Mycothiol-deficient Mycobacterium smegmatis mutants are hypersensitive to alkylating agents, free radicals, and antibiotics, *Antimicrob Agents Chemother 46*, 3348-3355.

96. Rawat, M., and Av-Gay, Y. (2007) Mycothiol-dependent proteins in actinomycetes, *FEMS Microbiol Rev 31*, 278-292.

97. Newton, G. L., Av-Gay, Y., and Fahey, R. C. (2000) A novel mycothiol-dependent detoxification pathway in mycobacteria involving mycothiol S-conjugate amidase, *Biochemistry 39*, 10739-10746.

98. Newton, G. L., Leung, S. S., Wakabayashi, J. I., Rawat, M., and Fahey, R. C. (2011) The DinB superfamily includes novel mycothiol, bacillithiol, and glutathione S-transferases, *Biochemistry 50*, 10751-10760.

99. Buchmeier, N. A., Newton, G. L., and Fahey, R. C. (2006) A mycothiol synthase mutant of Mycobacterium tuberculosis has an altered thiol-disulfide content and limited tolerance to stress, *J Bacteriol 188*, 6245-6252.

100. Bhave, D. P., Muse, W. B., 3rd, and Carroll, K. S. (2007) Drug targets in mycobacterial sulfur metabolism, *Infect Disord Drug Targets 7*, 140-158.

101. Huang, X., Kocabas, E., and Hernick, M. (2011) The activity and cofactor preferences of N-acetyl-1-D-myo-inosityl-2-amino-2-deoxy-alpha-D-glucopyranoside deacetylase (MshB) change depending on environmental conditions, *J Biol Chem 286*, 20275-20282.

102. Fan, F., Luxenburger, A., Painter, G. F., and Blanchard, J. S. (2007) Steady-state and pre-steady-state kinetic analysis of Mycobacterium smegmatis cysteine ligase (MshC), *Biochemistry 46*, 11421-11429.

103. Rawat, M., Kovacevic, S., Billman-Jacobe, H., and Av-Gay, Y. (2003) Inactivation of mshB, a key gene in the mycothiol biosynthesis pathway in Mycobacterium smegmatis, *Microbiology 149*, 1341-1349.

104. Newton, G. L., Koledin, T., Gorovitz, B., Rawat, M., Fahey, R. C., and Av-Gay, Y. (2003) The glycosyltransferase gene encoding the enzyme catalyzing the first step of mycothiol biosynthesis (mshA), *J Bacteriol 185*, 3476-3479.

105. Huang, X., and Hernick, M. (2012) Examination of mechanism of N-acetyl-1-D-myo-inosityl-2-amino-2-deoxy-alpha-D-glucopyranoside deacetylase (MshB) reveals unexpected role for dynamic tyrosine, *J Biol Chem 287*, 10424-10434.

106. Fan, F., and Blanchard, J. S. (2009) Toward the catalytic mechanism of a cysteine ligase (MshC) from Mycobacterium smegmatis: an enzyme involved in the biosynthetic pathway of mycothiol, *Biochemistry 48*, 7150-7159.

107. Vetting, M. W., Yu, M., Rendle, P. M., and Blanchard, J. S. (2006) The substrate-induced conformational change of Mycobacterium tuberculosis mycothiol synthase, *J Biol Chem 281*, 2795-2802.

108. Vetting, M. W., Frantom, P. A., and Blanchard, J. S. (2008) Structural and enzymatic analysis of MshA from Corynebacterium glutamicum: substrate-assisted catalysis, *J Biol Chem 283*, 15834-15844.

109. Miller, C. C., Rawat, M., Johnson, T., and Av-Gay, Y. (2007) Innate protection of Mycobacterium smegmatis against the antimicrobial activity of nitric oxide is provided by mycothiol, *Antimicrob Agents Chemother 51*, 3364-3366.

110. Rawat, M., Johnson, C., Cadiz, V., and Av-Gay, Y. (2007) Comparative analysis of mutants in the mycothiol biosynthesis pathway in Mycobacterium smegmatis, *Biochem Biophys Res Commun 363*, 71-76.

111. Rengarajan, J., Bloom, B. R., and Rubin, E. J. (2005) Genome-wide requirements for Mycobacterium tuberculosis adaptation and survival in macrophages, *Proc Natl Acad Sci U S A 102*, 8327-8332.

112. Zhang, Y. (2004) Persistent and dormant tubercle bacilli and latent tuberculosis, *Front Biosci 9*, 1136-1156.

113. Bzymek, K. P., Newton, G. L., Ta, P., and Fahey, R. C. (2007) Mycothiol import by Mycobacterium smegmatis and function as a resource for metabolic precursors and energy production, *J Bacteriol 189*, 6796-6805.

114. Dalle-Donne, I., Rossi, R., Giustarini, D., Colombo, R., and Milzani, A. (2007) S-glutathionylation in protein redox regulation, *Free Radic Biol Med 43*, 883-898.

115. Rawat, M., Uppal, M., Newton, G., Steffek, M., Fahey, R. C., and Av-Gay, Y. (2004) Targeted mutagenesis of the Mycobacterium smegmatis mca gene, encoding a mycothiol-dependent detoxification protein, *J Bacteriol 186*, 6050-6058.

116. Schneider, T., and Sahl, H. G. (2010) Lipid II and other bactoprenol-bound cell wall precursors as drug targets, *Curr Opin Investig Drugs 11*, 157-164.

117. Barkan, D., Liu, Z., Sacchettini, J. C., and Glickman, M. S. (2009) Mycolic acid cyclopropanation is essential for viability, drug resistance, and cell wall integrity of Mycobacterium tuberculosis, *Chem Biol 16*, 499-509.

118. Saravanan, P., Avinash, H., Dubey, V. K., and Patra, S. (2012) Targeting essential cell wall lipase Rv3802c for potential therapeutics against tuberculosis, *J Mol Graph Model 38*, 235-242.

119. Wolucka, B. A., McNeil, M. R., de Hoffmann, E., Chojnacki, T., and Brennan, P. J. (1994) Recognition of the lipid intermediate for arabinogalactan/arabinomannan biosynthesis and its relation to the mode of action of ethambutol on mycobacteria, *J Biol Chem 269*, 23328-23335.

120. Mikusova, K., Huang, H., Yagi, T., Holsters, M., Vereecke, D., D'Haeze, W., Scherman, M. S., Brennan, P. J., McNeil, M. R., and Crick, D. C. (2005) Decaprenylphosphoryl arabinofuranose, the donor of the D-arabinofuranosyl residues of mycobacterial arabinan, is formed via a two-step epimerization of decaprenylphosphoryl ribose, *J Bacteriol 187*, 8020-8025.

121. Telenti, A., Philipp, W. J., Sreevatsan, S., Bernasconi, C., Stockbauer, K. E., Wieles, B., Musser, J. M., and Jacobs, W. R., Jr. (1997) The emb operon, a gene cluster of Mycobacterium tuberculosis involved in resistance to ethambutol, *Nat Med 3*, 567-570.

122. Belanger, A. E., Besra, G. S., Ford, M. E., Mikusova, K., Belisle, J. T., Brennan, P. J., and Inamine, J. M. (1996) The embAB genes of Mycobacterium avium encode an arabinosyl transferase involved in cell wall arabinan biosynthesis that is the target for the antimycobacterial drug ethambutol, *Proc Natl Acad Sci U S A 93*, 11919-11924.

123. Protopopova, M., Hanrahan, C., Nikonenko, B., Samala, R., Chen, P., Gearhart, J., Einck, L., and Nacy, C. A. (2005) Identification of a new antitubercular drug candidate, SQ109, from a combinatorial library of 1,2-ethylenediamines, *J Antimicrob Chemother 56*, 968-974.

124. Tahlan, K., Wilson, R., Kastrinsky, D. B., Arora, K., Nair, V., Fischer, E., Barnes, S. W., Walker, J. R., Alland, D., Barry, C. E., 3rd, and Boshoff, H. I. (2012) SQ109 targets MmpL3, a membrane transporter of trehalose monomycolate involved in mycolic acid donation to the cell wall core of Mycobacterium tuberculosis, *Antimicrob Agents Chemother 56*, 1797-1809.

125. Makarov, V., Riabova, O. B., Yuschenko, A., Urlyapova, N., Daudova, A., Zipfel, P. F., and Mollmann, U. (2006) Synthesis and antileprosy activity of some dialkyldithiocarbamates, *J Antimicrob Chemother 57*, 1134-1138.

126. Christophe, T., Jackson, M., Jeon, H. K., Fenistein, D., Contreras-Dominguez, M., Kim, J., Genovesio, A., Carralot, J. P., Ewann, F., Kim, E. H., Lee, S. Y., Kang, S., Seo, M. J., Park, E. J., Skovierova, H., Pham, H., Riccardi, G., Nam, J. Y., Marsollier, L., Kempf, M., Joly-Guillou, M. L., Oh, T., Shin, W. K., No, Z., Nehrbass, U., Brosch, R., Cole, S. T., and Brodin, P. (2009) High content screening identifies decaprenyl-phosphoribose 2' epimerase as a target for intracellular antimycobacterial inhibitors, *PLoS Pathog 5*, e1000645.

127. Frantom, P. A., Coward, J. K., and Blanchard, J. S. (2010) UDP-(5F)-GlcNAc acts as a slow-binding inhibitor of MshA, a retaining glycosyltransferase, *J Am Chem Soc 132*, 6626-6627.

128. Metaferia, B. B., Fetterolf, B. J., Shazad-Ul-Hussan, S., Moravec, M., Smith, J. A., Ray, S., Gutierrez-Lugo, M. T., and Bewley, C. A. (2007) Synthesis of natural product-inspired inhibitors of Mycobacterium tuberculosis mycothiol-associated enzymes: the first inhibitors of GlcNAc-Ins deacetylase, *J Med Chem 50*, 6326-6336.

129. Gammon, D. W., Steenkamp, D. J., Mavumengwana, V., Marakalala, M. J., Mudzunga, T. T., Hunter, R., and Munyololo, M. (2010) Conjugates of plumbagin and phenyl-2-amino-1-thioglucoside inhibit MshB, a deacetylase involved in the biosynthesis of mycothiol, *Bioorg Med Chem 18*, 2501-2514.

130. Huang, X., and Hernick, M. (2011) A fluorescence-based assay for measuring N-acetyl-1-D-myo-inosityl-2-amino-2-deoxy-alpha-D-glucopyranoside deacetylase activity, *Anal Biochem 414*, 278-281.

131. Gutierrez-Lugo, M. T., and Bewley, C. A. (2011) Susceptibility and mode of binding of the Mycobacterium tuberculosis cysteinyl transferase mycothiol ligase to tRNA synthetase inhibitors, *Bioorg Med Chem Lett 21*, 2480-2483.

132. Gutierrez-Lugo, M. T., Baker, H., Shiloach, J., Boshoff, H., and Bewley, C. A. (2009) Dequalinium, a new inhibitor of Mycobacterium tuberculosis mycothiol ligase identified by high-throughput screening, *J Biomol Screen 14*, 643-652.

133. Newton, G. L., Buchmeier, N., La Clair, J. J., and Fahey, R. C. (2011) Evaluation of NTF1836 as an inhibitor of the mycothiol biosynthetic enzyme MshC in growing and non-replicating Mycobacterium tuberculosis, *Bioorg Med Chem 19*, 3956-3964.

134. Nicholas, G. M., Newton, G. L., Fahey, R. C., and Bewley, C. A. (2001) Novel bromotyrosine alkaloids: inhibitors of mycothiol S-conjugate amidase, *Org Lett 3*, 1543-1545.

135. Nicholas, G. M., Eckman, L. L., Ray, S., Hughes, R. O., Pfefferkorn, J. A., Barluenga, S., Nicolaou, K. C., and Bewley, C. A. (2002) Bromotyrosine-derived

natural and synthetic products as inhibitors of mycothiol-S-conjugate amidase, *Bioorg Med Chem Lett 12*, 2487-2490.

136. Kottakota, S. K., Evangelopoulos, D., Alnimr, A., Bhakta, S., McHugh, T. D., Gray, M., Groundwater, P. W., Marrs, E. C., Perry, J. D., Spilling, C. D., and Harburn, J. J. (2012) Synthesis and biological evaluation of purpurealidin E-derived marine sponge metabolites: aplysamine-2, aplyzanzine A, and suberedamines A and B, *J Nat Prod 75*, 1090-1101.

137. Fetterolf, B., and Bewley, C. A. (2004) Synthesis of a bromotyrosine-derived natural product inhibitor of mycothiol-S-conjugate amidase, *Bioorg Med Chem Lett 14*, 3785-3788.

138. Metaferia, B. B., Ray, S., Smith, J. A., and Bewley, C. A. (2007) Design and synthesis of substrate-mimic inhibitors of mycothiol-S-conjugate amidase from Mycobacterium tuberculosis, *Bioorg Med Chem Lett 17*, 444-447.

Chapter 3.

Mycothiol as Potential Drug Target for Tuberculosis

Abstract

Mycobacterium tuberculosis, a member of actinobacteria, is the causative agent of tuberculosis (TB). The difficulty in eradicating latent and drug-resistant bacilli remains the major challenge in current TB therapies. Mycothiol (MSH) is a unique thiol exclusively produced by Actinobacteria as a surrogate of glutathione found in other organisms. MSH is essential in maintaining the cellular redox environment and, as a result, is important for the survival of mycobacterial pathogens in hostile host environment. In addition, due to the presence of a thiol group on its structure, MSH also participates in detoxification of xenobiotic toxins. Therefore, MSH has been considered as an attractive source of targets for TB drug development. This Chapter reviews the pathogenic properties of *M. tuberculosis* that causes the complexities in TB therapy, the essential role of MSH in mycobacterial viability and virulence, and the potential of enzymes involved in MSH biosynthesis and MSH-dependent detoxification as drug targets.

1. *Mycobacterium tuberculosis* and TB

Mycobacterium species belong to Actinobacteria, a group of Gram-positive bacteria with high G+C ratio. (*1*) *Mycobacterium tuberculosis* is the causative agent of human tuberculosis, which infects one-third of the world's population with 8.7 million new cases and 1.4 million deaths world-wild each year. (*2*) The persistence of less active

M. tuberculosis and the emergence of extensively drug-resistant TB remain as significant obstructions for TB therapy. (*3*) The current antibiotics are ineffective against non-growing mycobacteria and ~10% of latent TB carriers develop active disease later in life due to immunodeficiency. (*3*) Moreover, about 3.7% of new cases and 20% of previously treated cases of TB are estimated to have multidrug resistant strains of *M. tuberculosis*. (*2*) Therefore, the development of novel drugs is necessary to eradicate the persistent bacteria and to circumvent the current drug resistance.

1.1 Latent TB

The extraordinarily high numbers of morbidity and mortality attributed to TB are due to the ability of *M. tuberculosis* to evade immune responses and persist within the host organism for long periods of time without developing disease, known as a "latent state". (*4, 5*) Approximately 90% of TB carriers are latently infected with TB that is often life-long and can reactivate to infectious TB due to an immunodeficiency. (*3*) During latency, a dynamic balance between the host immune response and *M. tuberculosis* persistence is maintained. (*6*) Immune response forms the first line of defense against TB infection. Alveolar macrophages, epithelioid cells or Langhans giant cells harbor intracellular mycobacteria and present antigens to activate T cells to produce a variety of cytokines and chemokines. (*5*) Chemokines recruit additional cells from circulating blood to the site of primary infection to encapsulate the granuloma, within which the mycobacertia reside and persist with the absence of cell division. (*7, 8*) IFN-γ activates macrophages to kill the intracellular bacteria via reactive oxygen intermediates (ROI) or reactive nitrogen intermediates (RNI). (*9, 10*)

In an attempt to avoid direct confrontation with the host immune defense, *M. tuberculosis* retards its replication rate and transforms into a latent state. (*11*) Those mycobacteria residing within granulomas lack a change in metabolism and thereby are unsusceptible to conventional antibiotic treatment. (*12*) Moreover, rapid adaption allows *M. tuberculosis* to persist for long periods of time. The dormant *M. tuberculosis* adapts to the low oxygen tension by activating alternative pathways in the citrate cycle to utilize lipids in the granulomas (*13, 14*) Oxygen-deprived *M. tuberculosis* up-regulates a metabolic pathway called the "glyoxylate shunt" that converts fatty acids into acetyl-CoA, by employing an anaerobic nitrate reductase and using nitrate as an electron acceptor. (*13, 15*) An adaptation has also been observed at the transcriptional level. One of the *M. tuberculosis* sigma factors SigF, a homolog to a sigma factor of *Bacillus subtilis* that is involved in stress responses and sporulation, is highly expressed during persistence, but is undetectable under active growth condition. (*16, 17*)

1. 2 Drug-resistant TB

TB therapy is difficult since the bacillary persistence requires a long period of chemotherapy (6-9 months) and a complicated regiment of antibiotics to eradicate the mycobacteria. (*3*) Typical treatment of active TB requires a cocktail of four first-line antibiotics, each targeting on different bacterial subpopulations: isoniazid (INH), kills those that are actively growing; ethambutol (EMB), inhibits bacterial growth; rifampin (RIF), kills bacteria with spurts of metabolism; pyrazinamide (PZA), kills bacteria with low metabolic activity and that reside in acid pH environment. (*3*) Failure to complete the entire course of treatment could result in the emergence of drug-resistant TB strains.

In case of resistance to any of the first-line drugs, one or more second-line agents (ethionamide (ETA); streptomycin (SM); amikacin/kanamycin; *p*-aminosalicyclic acid; fluoroquinolones (FQ); cycloserine) are used. However, multi-drug resistant (MDR) and extensively-drug resistant (XDR) strains with resistance to several first-line and second-line antibiotics have been widely diagnosed. (*2*) Therefore, the inability to eradicate latent bacilli with current antibiotics remains a major challenge in TB therapy. The development of novel antibiotics that can circumvent existing mechanisms of drug resistance is urgently needed for TB treatment.

2. Mycothiol

One unique feature of *Mycobacterium tuberculosis* is the production of MSH, a low molecular mass thiol that is often present in millimolar amounts. (*18*) MSH carries out similar functions to GSH in protecting against damaging effects from reactive oxygen species, a natural by-product of aerobic life, and electrophilic toxins. (*19*). (Fig. 1) MSH mutants display increased sensitivity to oxidative stress and antibiotics such as streptomycin, ethionamide, rifampin, and alkylating toxins. In addition, MSH provides some protection during adaptation to grow in an oxygen-rich environment and *M. tuberculosis* mutants with decreased level of MSH fail to survive in primary murine macrophages. (*20*) The importance of MSH for TB infection and persistence, as well as the absence of MSH in humans, makes MSH an attractive source of targets for drug development for TB treatment.

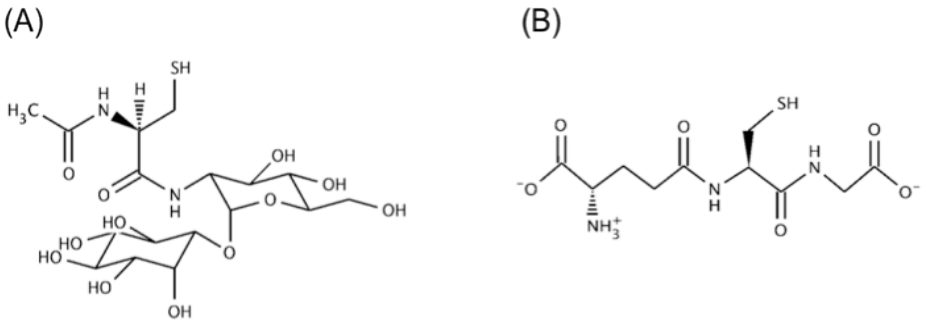

Figure 1. Structure of (A) mycothiol and (B) glutathione.

2.1 Redox cellular buffer

Intracellular redox homeostasis is critical for the proper function of biological processes, including enzyme activation, cell-cycle regulation, and DNA synthesis. (*21*) MSH is the dominant thiol in the mycobacterial cytosol, with a concentration of ~ 5 mM in *M. tuberculosis* at exponential growth phase and ~ 20 mM at stationary phase. (*22*) Cysteine undergoes heavy metal-catalyzed autoxidation rapidly, a property attributable to the ability of cysteine to provide three metal ligands ($-S^-$, $-NH_2$, and $-COO^-$) in a favorable geometric arrangement. (*23*) In MSH, the cysteine moiety is blocked with an acetylated amino group and the carboxyl group is *N*-linked to D-glucosamine, which is in turn α(1→1) linked to *myo*-inositol (*18*), resulting in a stable thiol that undergoes Cu-catalyzed autoxidation 30-fold slower than cysteine and 7-fold slower than GSH (*24*). (Fig. 1) MSH mutants that produce alternative thiols lacking the acetylated amino group showed a 10-fold decrease in thiol-to-disulfide ratio. (*25*) Therefore, MSH is efficient in maintaining the intracellular reducing environment in mycobacteria.

2.2 MSH-dependent Detoxification

Mutants deficient in MSH production exhibit enhanced sensitivity to redox cycling agents such as menadione and plumbagin, and become more susceptible to antibiotics including rifamycin, streptomycin, erythromycin, and azithromycin, and alkylating agents. (*26, 27*) These findings suggest that either MSH or MSH-dependent enzymes are involved in protecting mycobacteria from oxidants and toxins. (*26*) The primary role of MSH in detoxification is to react with electrophilic antibiotics, such as cerulenin and lincomycin, to produce less toxic S-conjugates that can accumulate within the cell without adverse consequence. (*28*) An enzyme with MSH S-transferase activity has been proposed to complete this step. (*29*) (Fig. 2) If the S-conjugates are still toxic to cell, a MS-conjugate amidase cleaves the amide bond to generate the AcCysR, a mercapuric acid that is pumped out of the cell, and the GlcN-Ins that is used to recycle the MSH. (*30*) (Fig. 2) In addition, MSH is involved in detoxifying formaldehyde by functioning as the cofactor for a NAD^+-dependent dehydrogenase**.** (*21*)

2.3 MSH in TB infection

To infect the host, mycobacterial pathogens need to endure the oxidizing environment of host macrophage during phagocytosis. (*12*) Generally, ROIs are generated in the macrophage through a pathway that NADPH oxidase transfers electrons to molecular oxygen to produce $O_2\cdot^-$, followed by reduction to hydrogen peroxide (H_2O_2) and further conversion into the highly damaging hydroxyl radical (OH·). (*31, 32*) Nitric oxide synthase can generate RNIs by oxidizing the guanidino nitrogen of arginine to yield ·NO. (*9*) The combination of the two systems can exert a synergistic effect in

macrophages to generate the "oxidative burst" that kills bacteria via oxidative damage to a range of protein and DNA targets. (*33, 34*) One strategy of mycobacterial survival inside the oxygen-rich host is to use MSH to maintain the cellular redox balance. The thiol/ disulfide status may also impact the activity of the cell through DosS, a heme-containing protein that functions as a redox sensor in *M. tuberculosis*. (*35*) Moreover, enzymes such as peroxidases and catalases might employ MSH as a cofactor to detoxify the ROI/RNI and therefore promote intracellular survival and persistence in host. (*22*)

2.4 MSH during latency

The constant metabolism of MSH should be maintained during the lifetime, including latent phase for the purpose of supporting mycobacterial survival within the hostile host environment. In *M. smegmatis*, the half-life for loss of MSH is 50 hours at the stationary phase, indicating that MSH metabolism is constant during the lifetime. (*36*) About 10% of the cellular MSH has been found associated with protein through mycothiolation, which produces the protein-SSM disulfides in a process similar to protein glutathionylation. (*36*) Glutathionylation of proteins is important in the dormancy of fungal spores and is regulated under oxidative stress (*37, 38*). Therefore, MSH most likely functions in a similar way for protein mycothiolation during persistence in host. Moreover, genes involved in sulfur metabolism have been reported to be consistently up-regulated in response to oxidative stress and nutrient starvation, as well as during macrophage infection and dormancy adaptation within the granuloma. (*20, 39-41*) Therefore it is likely that the biosynthesis and metabolism of MSH is active during the latency, and the active turnover of MSH in non-growing mycobacteria makes it an

attractive target for killing latent TB.

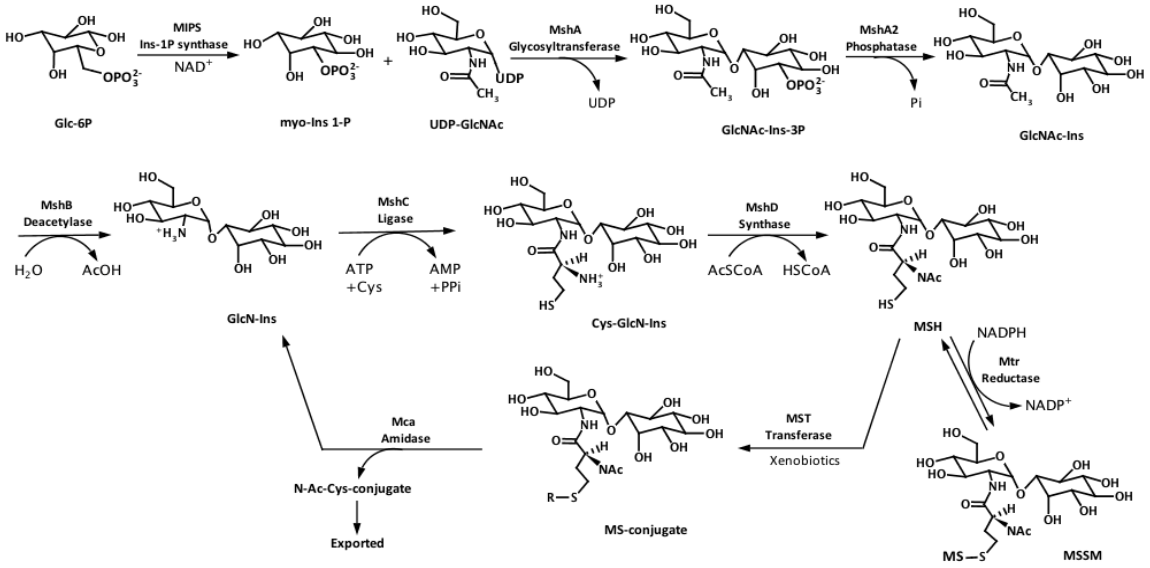

Figure 2. Mycothiol biosynthetic and MSH-dependent detoxification pathways.

3. MSH biosynthetic enzymes

Given the important role of MSH in TB development and persistence, enzymes involved in MSH biosynthesis are potential targets for TB treatment. Synthesis of MSH starts with the conversion of Glucose-6-phosphate (Glc-6P) to *L-myo*-inositol 1-phosphate (Ins-1P), a step catalyzed by *myo*-inositol 1-phosphate synthase (MIPS). The glycosyltransferase MshA transfers the glucosamine group from UDP-GlcNAc to Ins-1P to form 1-*O*-(2-acetamido-2-deoxy-α-D-glucopyranosyl)-D-*myo*-inositol-3-phosphate (GlcNAc-Ins-P). Dephosphorylation by MshA2 yields 1-*O*-(2-acetamido-2-deoxy-α-D-glucopyranosyl)-D-*myo*-inositol (GlcNAc-Ins), the major intermediate found in mycobacteria extracts and the substrate of deacetylase MshB. The product of MshB is 1-*O*-(2-amino-2-deoxy-α-D-glucopyranosyl)-D-*myo*-inositol (GlcN-Ins). Ligation of

cysteine with GlcN-Ins by MshC produces 1-*O*-[2-[[(2R)-2-amino-3-mercapto-1-oxopropyl]amino]-2-deoxy-α-D-glucopyranosyl]-D-*myo*-inositol (Cys-GlcN-Ins). The final step is acetylation of cysteine by MshD, yielding MSH. (*22*) (Fig. 2) MIPS, MshB, MshC, and MshD from *M. tuberculosis* have been recombinantly expressed and significant effort on structural and kinetic studies have been made by several different research groups, while the crystal structure of *Corynebacterium glutamicum* MshA has been determined and provides valuable information about the biochemical properties of mycobacterial MshA. The gene encoding for the MshA2 activity remains unidentified at this time. Current and future studies on the biochemical properties of the MSH biosynthetic enzymes are important for the development of potent and specific inhibitors.

3.1 MIPS

Rv0046c (*ino1*) from the genome of *M. tuberculosis* has been genetically confirmed to encode a MIPS (tMIPS) and the mycobacterial gene successfully complemented a *Saccharomyces cerevisiae ino1* mutant. (*42, 43*) Inhibiting mRNA expression of tMIPS results in enhanced susceptibility of mycobacterial pathogens to antibiotics. (*44*) *M. tuberculosis* mutants without a functional *ino1* can only be isolated in the presence of 77 mM inositol in the medium, indicating that tMIPS is an essential enzyme for inositol synthesis. (*45*) The virulence of the *ino1* mutant is severely attenuated such that the *M. tuberculosis* mutants are cleared from the macrophage while the CFU of the wild-type strain is stable. (*46*) The rapid killing of the *ino1* mutant may result from a reduction in MSH levels which fall gradually over a four week period after

transferring into inositol-free medium, thus leaving the bacteria susceptible to oxidative stress in macrophage. (*45*) The mycobacterial MIPS is discussed in detail in Chapter 2.

3.2 MshA

MshA is a glycosyltransferases and belongs to the GT-B superfamily. (*47, 48*) MshA activity was first detected in cellular extracts of *M. smegmatis,* which transferred GlcNAc from UDP-GlcNAc to Ins-1P to form GlcNAc-Ins-P. (*49*) The gene encoding MshA has been identified in a *M. smegmatis* transposon mutant that displays a complete loss in synthesis of GlcNAc-Ins, GlcN-Ins, and MSH. (*47*) The *M. tuberculosis mshA* ortholog, *Rv0486,* can complement the phenotype in the *M. smegmatis* mutant. (*50, 51*) However, *M. smegmatis* mutants with transposon mutations in *mshA* are viable, while in *M. tuberculosis mshA* is essential for growth. (*47, 50*) Interestingly, the *M. smegmatis* MshA mutants dramatically overproduce a 15-kDa organic hydroperoxide resistance protein (Ohr), which functions in destroying organic hydroperoxides in the cell and conferring increased resistance to CuOOH. (*52*) Overexpression of Ohr may partially compensate for the loss of MSH, and, as a consequence, contributes to the viability of *M. smegmatis* in the absence of a functional *mshA* gene.

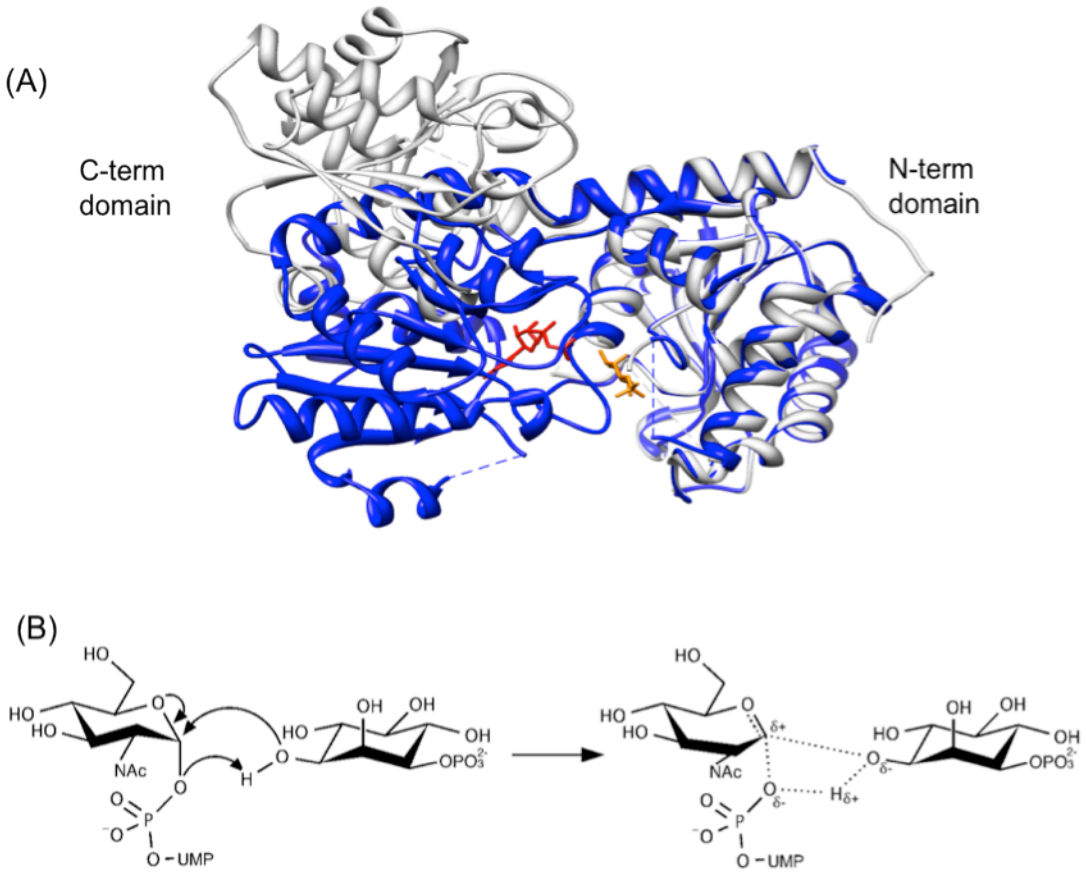

Figure 3. MshA (A) Structure of *Corynebacterium glutamicum* MshA. The overlay of apo-MshA (gray, PDB 3C48) and MshA-UDP-Ins1P complex (blue, PDB 3C4V) reveals a rotation of the C-terminal domain relative to the N-terminal domain upon UDP binding (red), a process that generates the binding site for Ins-1P (orange). (B) Proposed mechanism for MshA.

The crystal structure of MshA from *Corynebacterium glutamicum* has been solved and, based on this structure a sequential mechanism has been proposed. (*53*) A portion of the N-terminal domain is disordered in the apo state and becomes ordered in the binary MshA-UDP complex, suggesting a substantial conformational change occurs upon UDP binding. (*53*) (Fig. 3A) Rotation of the C-terminal domain relative to the N-terminal domain generates the binding site for Ins-1P and brings the substrates into close proximity. (Fig. 3A) Kinetic studies on CgMshA are consistent with the structural data,

suggesting that MshA follows a sequential mechanism with UDP-GlcNAc binding first followed by Ins-1P. (*53*) Moreover, a model of the ternary complex with UDP-GlcNAc and Ins-1-P binding in the active site of MshA is consistent with a S_{Ni} mechanism. (*53*) (Fig. 3) In this mechanism, breakage of phospho-sugar bond and formation of glycosidic bond occur in a concerted, but asynchronous, manner on the same face of the sugar moiety. The β-phosphate of the UDP-GlcNAc acts as the general base to promote the nucleophilic attack of the 3-OH group on Ins-1P. (*53*) (Fig. 3B)

3.3 MshA2

The third step of MSH biosynthesis is the dephosphorylation of the GlcNAc-Ins-P, the product of MshA, to generate GlcNAc-Ins, the substrate for MshB (Fig. 2). A hypothetical MshA2 phosphatase has been proposed to catalyze this step. (*49*) However, gene encoding for the MshA2 activity remains unknown, leaving MshA2 the only enzyme uncharacterized in MSH biosynthesis. A recently study suggested that *impC* (*Rv3137*) may encode the MshA2 activity (*54*), which is discussed in Chapter 2.

3.4 MshB

Rv1170 in *M. tuberculosis* encodes a metallohydrolase, MshB, that catalyzes the fourth step in MSH biosynthesis (Fig. 2). (*55*) A zinc ion observed in the crystal structure of *M. tuberculosis* MshB is coordinated by three protein ligands (H13, D16, and H147) and molecule of acetate, the product of deacetylation reaction. (Fig. 4A) (*56*) A general acid-base catalyst mechanism has been proposed for MshB (Fig. 4B) and is discussed in detail in Chapters 5-7. Abolishing MshB activity results in a dramatic

impact on the ratio of GlcNAc-Ins to GlcN-Ins, which rises from 0.15 in wild-type cells to 100 in mutants, with a total of 30-fold reduction of GlcN-Ins and a 50-fold increase in GlcNAc-Ins. (*57*) GlcNAc-Ins accumulates with almost twice the MSH level in *M. smegmatis*, and the cellular levels of the MshB product, GlcN-Ins, and the MshC product, Cys-GlcN-Ins, are 60-fold and 6000-fold lower than that of GlcNAc-Ins, respectively. (*58*) Moreover, among all MSH enzymes that have been tested *in vitro*, the lowest value of k_{cat}/K_M with corresponding native substrates is observed for MshB, suggesting that MshB activity is a control point for MSH production.

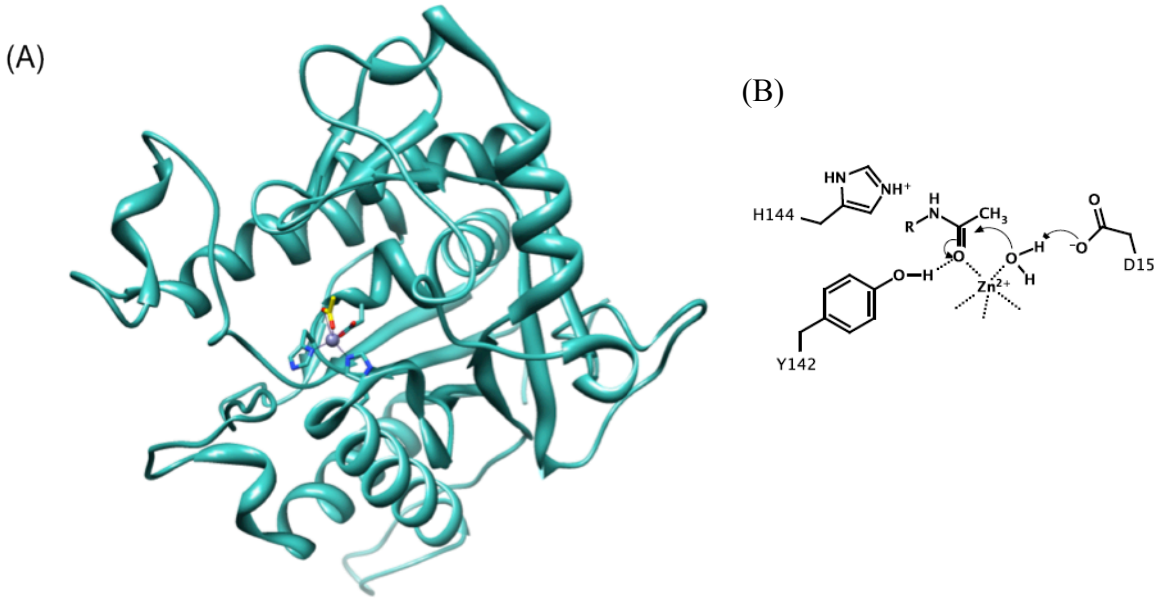

Figure 4. MshB (A) Structure of *Mycobacterium tuberculosis* MshB (PDB 4EWL) containing two homologous domains, with the active site located at the interface. A zinc ion (grey sphere) is bound in the active site through three protein ligands (H13, D16, and H147) and a molecule of acetate (yellow). (B) Proposed mechanism for MshB

The MSH levels of MshB mutants decrease to 5-10% and 20% of the parental level in *M. smegmatis* and *M. tuberculosis*, respectively, indicating the presence of alternative deacetylases to compensate for the loss of MshB in MSH biosynthesis. (*57,*

58) A likely candidate is the MS-conjugate amidase Mca. Mca from *M. tuberculosis* can use GlcNAc-Ins as substrate, but the specific activity is 4000-fold lower than MshB. (*57*) The minor deacetylase activity of Mca is likely not important except in MshB mutants that accumulates high level of cellular GlcNAc-Ins. (*57*) The concentration of GlcN-Ins is estimated to reach 3 nmol/10^9 cells during stationary phase if GlcNAc-Ins is solely deacetylated by Mca, close to that found in MshB mutants. (*57*) In addition, the *mshB /Mca* double null deletion mutant derived from *M. smegmatis* produces no detectable MSH, while complementation with *mshB* gene restores MSH biosynthesis. (*59*) However, overexpression of Mca is unable to increase MSH levels in MshB mutant probably because even a small amount of MSH can down-regulate or block Mca activity on GlcNAc-Ins. (*58*) Thus, the overlapping function of MshB and Mca is critical for maintaining the MSH level, and inhibitors targeting on both enzymes are required to block MSH biosynthesis. (*60*)

3.5 MshC

MshC is an ATP-dependent ligase that catalyzes the conjugation of GlcN-Ins with cysteine to form Cys-GlcN-Ins, the fifth step in MSH biosynthesis (Fig. 2). (*61*) The MshC activity was initially identified in the chemical mutant I64 of *Mycobacterium smegmatis*, which lacked the Cys-GlcN-Ins ligase activity and MSH production. (*26*) When *M. tuberculosis Rv2130c* (*mshC*) is introduced epichromatically into *M. smegmatis* I64, the production of MSH increases to 150% of the parental level, while the targeted disruption of *mshC* in *M. tuberculosis* produces no viable clones. (*62*) These results indicate that the *mshC* gene is required for MSH production and is essential for the

growth of *M. tuberculosis*. In *M. tuberculosis*, *mshC* evolved from *cysS* (*Rv3580c*), which encodes cysteinyl-tRNA synthetase, via gene duplication. (*63*) The three-dimensional structural of MshC shares a similar overall fold to CysS, with the exception that MshC lacks the conserved anti-codon recognition site at the C-terminal sequence observed in CysS. (*63*)

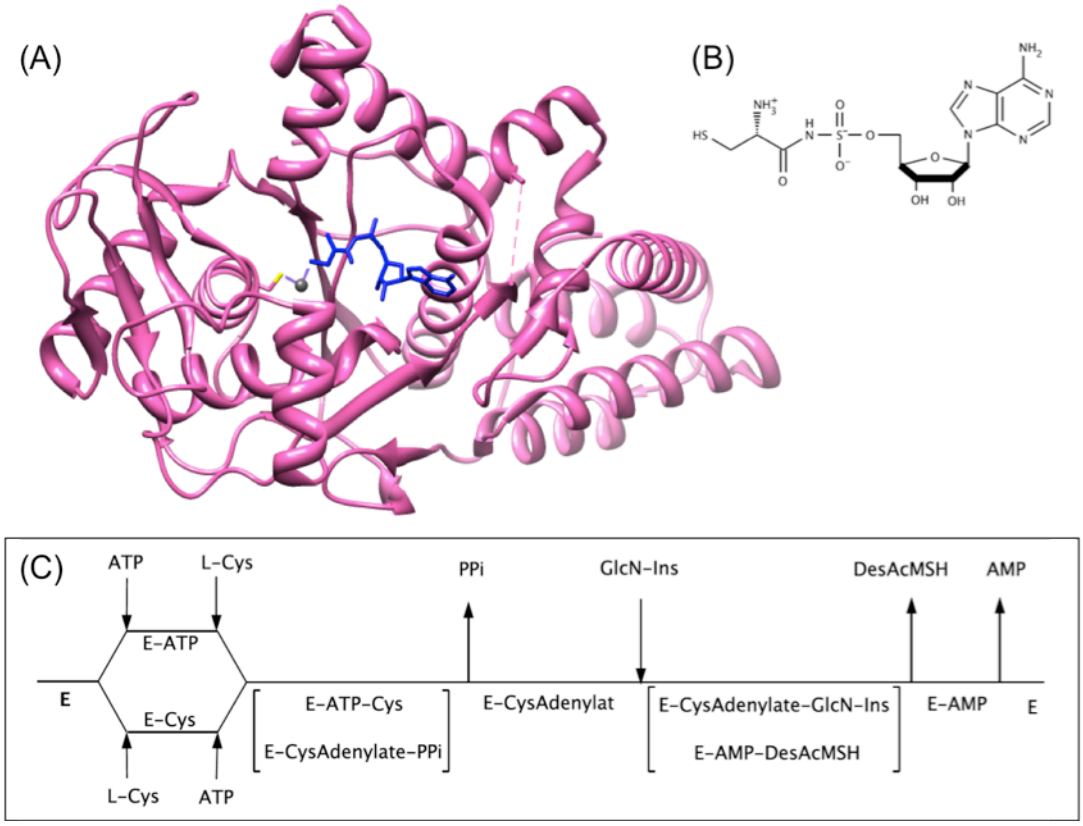

Figure 5. MshC (A) Structure of *Mycobacterium smegmatis* MshC (PDB 3C8Z). The bi-substrate analog CSA (blue) is co-crystallized in the active site with the thiol group bonded to the catalytic zinc ion (grey sphere). (B) The structure of CSA. (C) Ping Pong mechanism of MshC.

The bi-substrate structural analog 5'-*O*-[*N*-(L-cysteinyl) sulfamoyl]adenosine (CSA) is a potent inhibitor of MshC with inhibition constant of 304 nM and 50 nM for MshC from *M. smegmatis* and *M. tuberculosis*, respectively. (*61*) (Fig. 5B) CSA competes with the binding of substrates through its high affinity to the active site zinc.

Co-crystallization with CSA provides insight into the catalytic mechanism (Fig. 5A). (*61*) MshC proceeds via a Bi Uni Uni Bi Ping Pong mechanism. (Fig. 5C) In the first half reaction (cysteine activation by ATP), MshC follows a similar mechanism as that described for CysS. ATP and L-cysteine bind to free enzyme in a random order to form the ternary E-ATP-cysteine complex. (*61*) Pyrophosphate is then released, leaving cysteinyl-AMP intermediate in the active site. (*64*) In the second half reaction (cysteine ligation), the amine of GlcN-Ins carries out nucleophilic attack on cysteinyl-AMP, and an amide bond is formed along with the cleavage of the adenylate anhydride to generate Cys-GlcN-Ins. (*61*)

3.6 MshD

MshD is the final enzyme in the MSH biosynthetic pathway and catalyzes acetylation of the amino group on Cys-GlcN-Ins to form acetyl-Cys-GlcN-Ins (MSH). (*65*) The rate of Cys-GlcN-Ins auto-oxidization is 11-fold faster than MSH, most likely due to the close proximity of the reactive amino group to the thiol. (*66*) Therefore, acetylation protects the primary amine from side reactions during MSH reduction or conjugation. The MshD activity is encoded by *Rv0819* in *M. tuberculosis*. (*25*) Disruption of *Rv0819* results in 1% of normal MSH levels, and high levels of Cys-GlcN-Ins along with two novel thiols: *N*-formyl-Cys-GlcN-Ins (fCys-GlcN-Ins) and *N*-succinyl-Cys-GlcN-Ins. (*66*) However, the presence of the MSH-analogs is not sufficient to compensate for the loss of MSH synthesis in *M. tuberculosis*. In MshD mutants, the thiol content is consistently low, ranging from 27% to 48% of wild-type levels, and the total thiol-to-disulfide ratio is 10-fold lower than that observed for the wild-type strain,

resulting in limited growth of *M. tuberculosis* under oxidative stress and acidic conditions. (*25, 66, 67*) In addition, the novel thiols act as poor substitutes in MSH-dependent enzymatic processes. For example, a 10 to 100-fold decrease in activity is observed for Mca and Mtr using fCys-GlcN-Ins as an alternative substrate for MSH. (*51*)

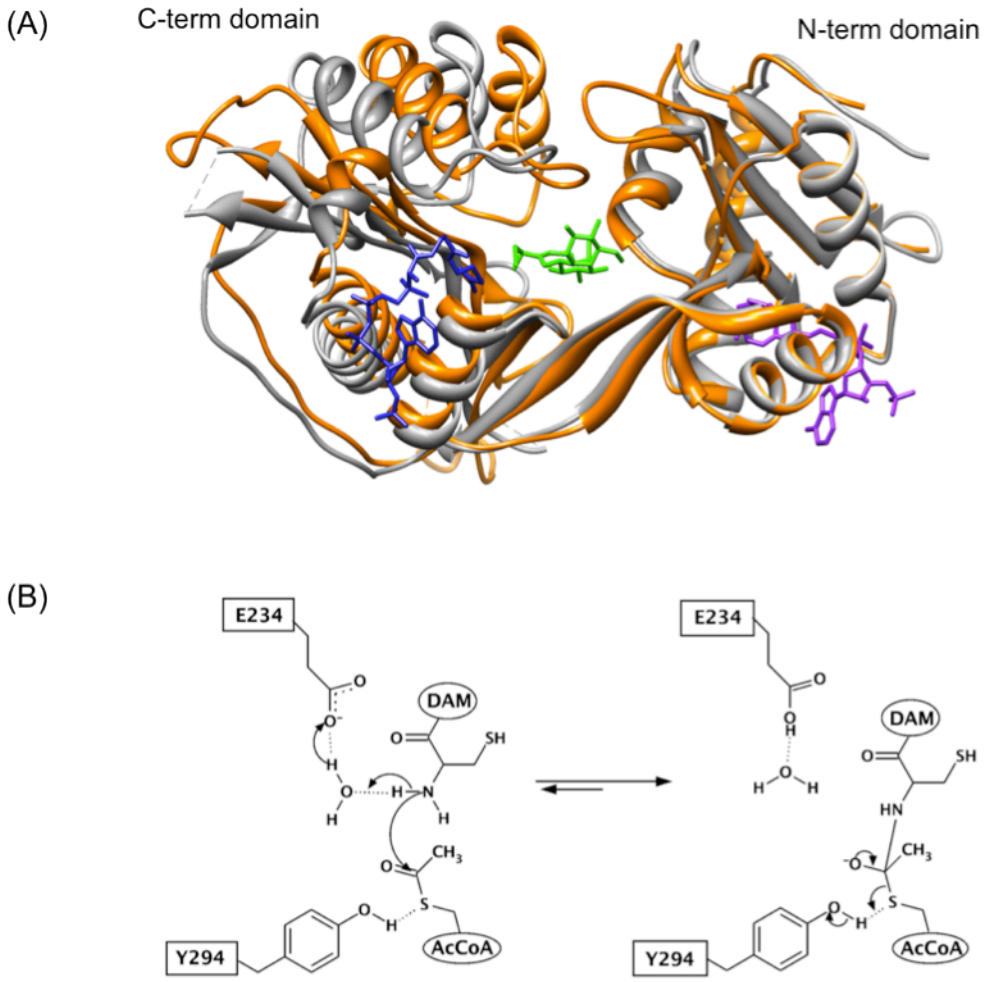

Figure 6. MshD (A) Structure of *Mycobacterium tuberculosis* MshD contains two GNAT domains each of which contains an acetyl-CoA binding site. Overlay of MshD-AcCoA complex (gray, PDB 1OZP) and MshD-AcCoA-DAM complex (orange, PDB 2C27) reveals a conformational change in C-terminal domain that contracts two domains around the substrate DAM (green). AcCoA binds in C-term domain and N-term domain in MshD-AcCoA-DAM complex is colored with blue and purple, respectively. (B) Proposed mechanism for MshD.

The crystal structure of MshD from *M. tuberculosis* has been solved as part of a binary complex with acetyl-CoA (AcCoA) and as a ternary complex with CoA and Cys-GlcN-Ins (desacetylmycothiol, DAM). (*68, 69*) MshD is a structural homolog of *N*-acetyl-transferases in the GNAT family and contains two GNAT domains as a result of gene duplication. (*65, 68, 70*) Although both domains are capable of binding AcCoA, only the C-terminal GNAT domain is functional. (*69*) It is unlikely that the N-terminal domain exhibits any acetyltransferase activity, since the acetyl group of AcCoA is completely buried inside a hydrophobic pocket and the acid and base residues that participate in chemistry are absent. (*68, 69*) (Fig. 6A) Structural studies indicate a large conformational change upon substrate binding. In the ternary complex, two GNAT domains are brought together through shared interactions with DAM, and the conformational movement narrows the central groove down, shielding the reaction coordinate from bulk solvents. (*69*) (Fig. 6A) MshD proceeds through a mechanism in which the acceptor amine nucleophilically attacks the AcCoA. (*68*) E234 acts as a general base to abstract a proton from the cysteine, and CoA-SH is then released after accepting a proton from the conserved Y294. (*69*) (Fig. 6B)

4. MSH-dependent detoxification enzymes

MSH is involved in many enzymatic processes in mycobacteria, including reductions, detoxification of electrophiles, and inactivation of ROI and RNI. Some MSH-dependent enzymes, including MSH S-transferase (MST), MS-conjugate amidase (Mca), MSH-disulfide reductase (Mtr), and MscR, have been characterized and are summarized below.

4.1 MSH S-transferase

MSH S-transferase (MST) catalyzes the thiol-dependent detoxification of antibiotic, electrophiles, and oxidants through the production of thiol S-conjugates. (Fig. 2) In GSH-producing organisms, thiol-reactive xenobiotic toxins are conjugated to GSH by GSH S-transferases (GSTs), followed by the stepwise cleavage of the glutamate and glycine moieties, resulting in cysteine S-conjugates that are acetylated later for excretion. (*71*) MST functions in a similar manner as GST by catalyzing the conjugation of MSH with a wide range of electrophiles. (*21, 29*) MST activity was first detected in cell extracts of *M. smegmatis,* in which the MSH-monobimane conjugate (MSmB) was produced from monobromobimane (mBBr) in a MSH-dependent and protein-dependent manner.(*29*) (Fig. 7) The protein with MST activity has been isolated and identified from the crude lysates of *M. smegmatis*, and the gene encoding the MST in *M. tuberculosis* has been identified as *Rv0443* based on sequence homology. (*29*) MST belongs to the DinB_2 superfamily, which also contains bacillithiol S-transferase (BST) from *Bacillus subtilis.* (*29, 72*) The crystal structure of BST (PDB 1RXQ) contains a zinc-binding site that is surrounded by conserved hydrophobic amino acids that may define a pocket for hydrophobic substrates such as mBCl, CDNB, CuOOH, and cerulenin (*29, 73*), and may serve as a template for structural and functional studies on MST.

4.2 MS-conjugate amidase

MS-conjugate amidase (Mca) is a metalloenzyme encoded by *Rv1082* in *M. tuberculosis* and plays a role in MSH-dependent detoxification of antibiotics,

electrophiles, and oxidants. (*30, 74*) (Fig. 2) Mca cleaves an amide bond in mycothiol S-conjugates to release the mercapturic acid that is rapidly lost from the cell, and GlcN-Ins that is retained to regenerate MSH. (*28*) (Fig. 2)

Mca shows substantial activity to a wide range of MSH conjugates. For example, rifamycin S has been found to form complex conjugate with MSH (MS-RifSV) and is converted to the mercapturic acid AcCyS-RifSV. (*74*) (Fig. 7) Other antibiotics, including granaticin A and naphthomycin A, can also form MSH-derived adducts that serve as substrates for Mca. (*22*) Moreover, streptomycin, which is capable of forming a thiohemiacetal adduct through the thiol-reactive aldehyde with MSH, is also a target for Mca dependent detoxification and the *Mca* mutant has shown enhanced sensitivity to streptomycin. (*28*) Detoxification of oxidants, such as menadione and plumbagin, may also require Mca. A similar finding has been observed in yeast, as incubation with menadione results in decreased levels of GSH and reduced exportation of corresponding mercapturic acid. (*75*) Indeed, the disruption of *Mca* results in increased sensitivity to oxidants. (*26*)

The substrate specificity of Mca with a various amidase and deacetylase substrates has been examined, and the results indicate that its activity is critically dependent upon the integrity of the MSH moiety. Removal of the inositol residue or the acetyl group from MSmB reduces the value of k_{cat}/K_M 900-fold. (*74*)

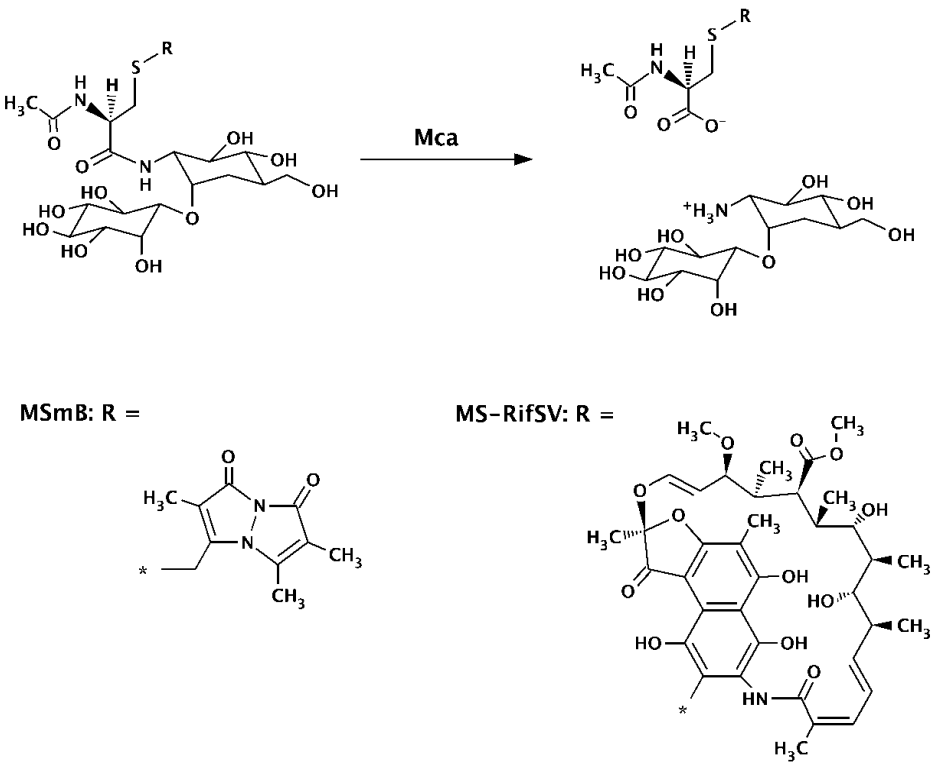

Figure 7. Top, Reaction catalyzed by Mca. Bottom, Structures of MSmB and MS-RifSV. Mycothiol S-conjugates with monobromobimane (mBBr) and rifamycin S, respectively.

4.3 MSH disulfide reductase

One of the key enzymes involved in mediating the cellular redox homeostasis is MSH disulfide reductase (Mtr). (*76*) When subjected to oxidative stress, MSH is oxidized to mycothione (MSSM), the disulfide form of MSH. To maintain the high thiol/disulfide ratios within the cell, Mtr cleaves the disulfide bond with concomitant oxidation of NADPH. (*76*) The gene (*Rv2855*) encoding Mtr in *M. tuberculosis* has been identified as a homolog to GSH reductase and trypanothione reductase. (*76*) Mtr is required only under oxidative stress. No significant difference is observed in the average MSH levels between wild type and *mtr* mutant of *M. smegmatis* when grown under standard condition. (*77*) After treatment with peroxide, a 50% decrease in MSH levels is

found in the *mtr* mutant, while MSH level is constant in wild type. (*77*)

Mtr belongs to the pyridine nucleotide-disulfide reductase superfamily that requires FAD as a cofactor. (*21*) A bi-bi ping-pong mechanism has been proposed for Mtr and probed kinetically. (*76*) (Fig. 8) In the oxidative half-reaction, NADPH rapidly binds to the oxidized enzyme, which transfers a hydride to FAD to generate the reduced enzyme. The side-chains of redox-active cysteines (Cys39 and Cys44) form a charge-transfer complex with the FAD. (*76*) In the reductive half-reaction, Mtr reduces the disulfide in MSSM via dithiol-disulfide interchange and releases the $NADP^+$, yielding two molecules of MSH and an oxidized enzyme. (*76*) The catalytically essential H444-E449 ion pair likely functions as a GAC to release the second MSH. (*76*) Moreover, Mtr exhibits a substantial degree of substrate specificity. Removal of the GlcN group or substitution of acetyl residue on AcCys moiety on MSH results in a significant loss of Mtr activity. (*76*) However, only a minor loss of activity is observed if the inositol group is replaced by a benzyl ring. (*78*)

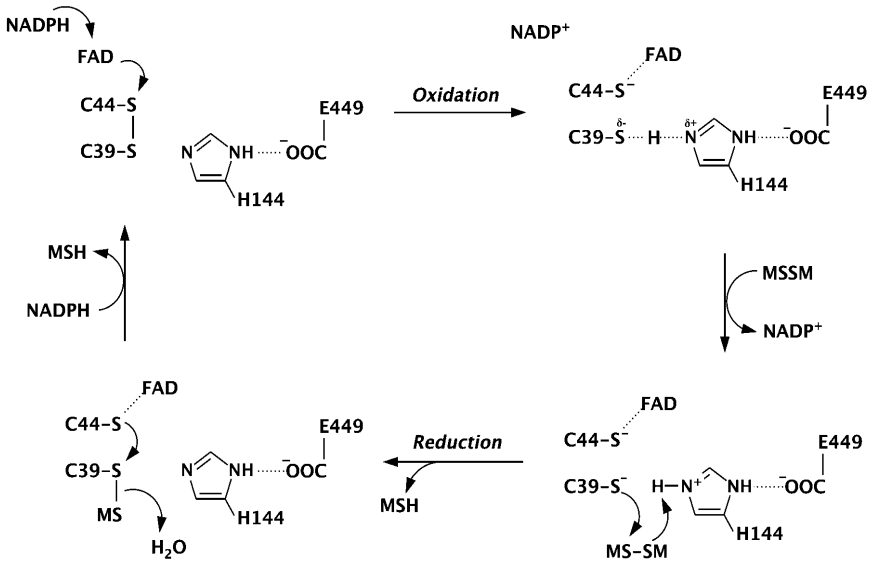

Figure 8. Proposed mechanism for reduction of mycothione (MSSM) by *Mycobacterium tuberculosis* Mtr.

4.4 MscR

Rv2259 is an essential gene for the growth of *M. tuberculosis* and has been shown to encode a MSH-dependent detoxification enzyme MscR. (*67*) MscR is involved in detoxifying either formaldehyde or nitrite via different mechanisms. (*79*) The formaldehyde is generated from biological degradation of natural C1 compounds such as methylated amines and sulfur compounds. (*21*) MSH reacts spontaneously with formaldehyde to form S-hydroxymethyl MSH, a hemithioacetal substrate that is converted to MSH formate ester by MscR, followed by rapid hydrolysis to regenerate MSH. (*21, 80*) (Fig. 9A) MscR detoxifies nitrite through its nitrosothiol reductase activity. (*80*) Nitrite can react with MSH to form nitrosomycothiol (MSNO), and MscR reduces MSNO to MSSM and nitrate. (Fig. 9B) In addtion, the reductase activity of *M. smegmatis* MscR has shown to be 80 times higher than that of the formaldehyde dehydrogenase activity. (*80*)

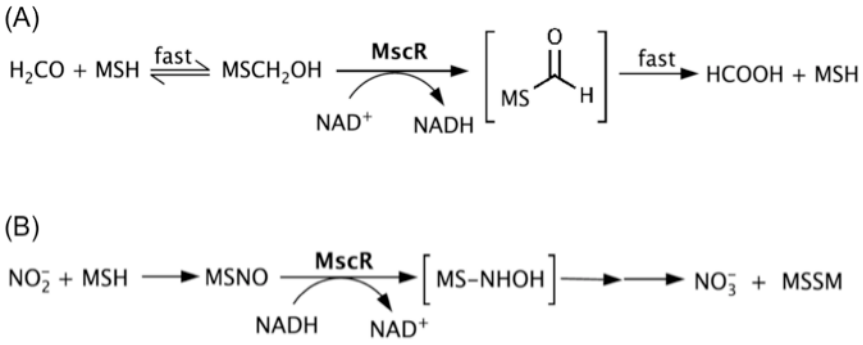

Figure 9. Two known activities of MscR. (A) MSH-dependent formaldehyde dehydrogenase reaction. (B) Nitrosothiol reductase reaction, with MSNO eventually converted to nitrate *in vivo*.

4.4 Other MSH-dependent enzymes

More enzymes involved in MSH-dependent detoxification remain to be identified. Examples include MSH-dependent peroxidase and Glyoxylase-I type enzymes. (*21*)

Treatment of *M. bovis* BCG with hydrogen peroxide results in an increased level of oxidized MSH. (*81*) Enhanced sensitivity to peroxides in MSH-deficient *M. smegmatis* and *M. tuberculosis* suggests the presence of an MSH-dependent peroxidase, in which the MSH is possibly acting as an electron donor to peroxiredoxins. (*21*) MSH has also been associated with the detoxification of methylglyoxal via a glyoxylase I-type activity, and sequence analysis indicates that *Rv0274* encodes a GSH-glyoxylase I homolog. (*21, 26*)

5. Conclusion

The major challenges in TB therapy remain in the difficulty to eradicate the latent and multi-drug resistant strains of *M. tuberculosis*. Thus, exploring novel drug targets involved in TB latency are alternative ways to shorten the treatment time and decrease the possibility of the emergence of resistant mutants. MSH has been considered a potential target for TB treatment with the following reasons: 1) MSH is exclusively produced in mycobacteria and is absent in eukaryotes; 2) MSH is essential to maintain the cellular redox state; 3) MSH enhances the survival of *M. tuberculosis* in oxidative host environment; 4) synthesis and metabolism of MSH is active during the life-time of mycobacteria; 5) MSH is involved in drug detoxification. In addition, enzymes involved in MSH biosynthesis and MSH-dependent detoxification have been shown to be critical for the survival and virulence of *M. tuberculosis*. Significant progress on detailed genetic, catalytic and structural studies on those enzymes has been made over the last several years, and provides valuable information to elucidate their potential as drug targets. Future studies on mechanistic and molecular recognition will be helpful in identifying and designing inhibitors with high affinity.

References

1. Ventura, M., Canchaya, C., Tauch, A., Chandra, G., Fitzgerald, G. F., Chater, K. F., and van Sinderen, D. (2007) Genomics of Actinobacteria: tracing the evolutionary history of an ancient phylum, *Microbiol Mol Biol Rev 71*, 495-548.
2. WHO. (2012) Global Tuberculosis Control.
3. Zhang, Y. (2005) The magic bullets and tuberculosis drug targets, *Annu Rev Pharmacol Toxicol 45*, 529-564.
4. Kaufmann, S. H. (2001) How can immunology contribute to the control of tuberculosis?, *Nat Rev Immunol 1*, 20-30.
5. Mariano, M. (1995) The experimental granuloma. A hypothesis to explain the persistence of the lesion, *Rev Inst Med Trop Sao Paulo 37*, 161-176.
6. Stewart, G. R., Robertson, B. D., and Young, D. B. (2003) Tuberculosis: a problem with persistence, *Nat Rev Microbiol 1*, 97-105.
7. Ulrichs, T., and Kaufmann, S. H. (2006) New insights into the function of granulomas in human tuberculosis, *J Pathol 208*, 261-269.
8. Lukacs, N. W., Chensue, S. W., Strieter, R. M., Warmington, K., and Kunkel, S. L. (1994) Inflammatory granuloma formation is mediated by TNF-alpha-inducible intercellular adhesion molecule-1, *J Immunol 152*, 5883-5889.
9. MacMicking, J., Xie, Q. W., and Nathan, C. (1997) Nitric oxide and macrophage function, *Annu Rev Immunol 15*, 323-350.
10. Shiloh, M. U., and Nathan, C. F. (2000) Reactive nitrogen intermediates and the pathogenesis of Salmonella and mycobacteria, *Curr Opin Microbiol 3*, 35-42.

11. Ulrichs, T., and Kaufmann, S. H. (2002) Mycobacterial persistence and immunity, *Front Biosci 7*, d458-469.

12. Zhang, Y. (2004) Persistent and dormant tubercle bacilli and latent tuberculosis, *Front Biosci 9*, 1136-1156.

13. McKinney, J. D., Honer zu Bentrup, K., Munoz-Elias, E. J., Miczak, A., Chen, B., Chan, W. T., Swenson, D., Sacchettini, J. C., Jacobs, W. R., Jr., and Russell, D. G. (2000) Persistence of Mycobacterium tuberculosis in macrophages and mice requires the glyoxylate shunt enzyme isocitrate lyase, *Nature 406*, 735-738.

14. Glickman, M. S., Cox, J. S., and Jacobs, W. R., Jr. (2000) A novel mycolic acid cyclopropane synthetase is required for cording, persistence, and virulence of Mycobacterium tuberculosis, *Mol Cell 5*, 717-727.

15. Escoto, M. L., and de Kantor, I. N. (1978) Nitrate reductase activity of Mycobacterium tuberculosis and Mycobacterium bovis in the presence of electron donors, *J Clin Microbiol 7*, 601-602.

16. DeMaio, J., Zhang, Y., Ko, C., and Bishai, W. R. (1997) Mycobacterium tuberculosis sigF is part of a gene cluster with similarities to the Bacillus subtilis sigF and sigB operons, *Tuber Lung Dis 78*, 3-12.

17. DeMaio, J., Zhang, Y., Ko, C., Young, D. B., and Bishai, W. R. (1996) A stationary-phase stress-response sigma factor from Mycobacterium tuberculosis, *Proc Natl Acad Sci U S A 93*, 2790-2794.

18. Spies, H. S., and Steenkamp, D. J. (1994) Thiols of intracellular pathogens. Identification of ovothiol A in Leishmania donovani and structural analysis of a novel thiol from Mycobacterium bovis, *Eur J Biochem 224*, 203-213.

19. McCarthy, A. A., Peterson, N. A., Knijff, R., and Baker, E. N. (2004) Crystal structure of MshB from Mycobacterium tuberculosis, a deacetylase involved in mycothiol biosynthesis, *J Mol Biol 335*, 1131-1141.

20. Rengarajan, J., Bloom, B. R., and Rubin, E. J. (2005) Genome-wide requirements for Mycobacterium tuberculosis adaptation and survival in macrophages, *Proc Natl Acad Sci U S A 102*, 8327-8332.

21. Rawat, M., and Av-Gay, Y. (2007) Mycothiol-dependent proteins in actinomycetes, *FEMS Microbiol Rev 31*, 278-292.

22. Newton, G. L., Buchmeier, N., and Fahey, R. C. (2008) Biosynthesis and functions of mycothiol, the unique protective thiol of Actinobacteria, *Microbiol Mol Biol Rev 72*, 471-494.

23. Held, K. D., and Biaglow, J. E. (1994) Mechanisms for the oxygen radical-mediated toxicity of various thiol-containing compounds in cultured mammalian cells, *Radiat Res 139*, 15-23.

24. Newton, G. L., Bewley, C. A., Dwyer, T. J., Horn, R., Aharonowitz, Y., Cohen, G., Davies, J., Faulkner, D. J., and Fahey, R. C. (1995) The structure of U17 isolated from Streptomyces clavuligerus and its properties as an antioxidant thiol, *Eur J Biochem 230*, 821-825.

25. Buchmeier, N. A., Newton, G. L., and Fahey, R. C. (2006) A mycothiol synthase mutant of Mycobacterium tuberculosis has an altered thiol-disulfide content and limited tolerance to stress, *J Bacteriol 188*, 6245-6252.

26. Rawat, M., Newton, G. L., Ko, M., Martinez, G. J., Fahey, R. C., and Av-Gay, Y. (2002) Mycothiol-deficient Mycobacterium smegmatis mutants are hypersensitive

to alkylating agents, free radicals, and antibiotics, *Antimicrob Agents Chemother 46*, 3348-3355.

27. Rawat, M., Johnson, C., Cadiz, V., and Av-Gay, Y. (2007) Comparative analysis of mutants in the mycothiol biosynthesis pathway in Mycobacterium smegmatis, *Biochem Biophys Res Commun 363*, 71-76.

28. Rawat, M., Uppal, M., Newton, G., Steffek, M., Fahey, R. C., and Av-Gay, Y. (2004) Targeted mutagenesis of the Mycobacterium smegmatis mca gene, encoding a mycothiol-dependent detoxification protein, *J Bacteriol 186*, 6050-6058.

29. Newton, G. L., Leung, S. S., Wakabayashi, J. I., Rawat, M., and Fahey, R. C. (2011) The DinB superfamily includes novel mycothiol, bacillithiol, and glutathione S-transferases, *Biochemistry 50*, 10751-10760.

30. Newton, G. L., Av-Gay, Y., and Fahey, R. C. (2000) A novel mycothiol-dependent detoxification pathway in mycobacteria involving mycothiol S-conjugate amidase, *Biochemistry 39*, 10739-10746.

31. Ushio-Fukai, M. (2006) Localizing NADPH oxidase-derived ROS, *Sci STKE 2006*, re8.

32. Hampton, M. B., Kettle, A. J., and Winterbourn, C. C. (1998) Inside the neutrophil phagosome: oxidants, myeloperoxidase, and bacterial killing, *Blood 92*, 3007-3017.

33. Beckman, J. S., Beckman, T. W., Chen, J., Marshall, P. A., and Freeman, B. A. (1990) Apparent hydroxyl radical production by peroxynitrite: implications for

endothelial injury from nitric oxide and superoxide, *Proc Natl Acad Sci U S A 87*, 1620-1624.

34. Assreuy, J., Cunha, F. Q., Epperlein, M., Noronha-Dutra, A., O'Donnell, C. A., Liew, F. Y., and Moncada, S. (1994) Production of nitric oxide and superoxide by activated macrophages and killing of Leishmania major, *Eur J Immunol 24*, 672-676.

35. Kumar, A., Toledo, J. C., Patel, R. P., Lancaster, J. R., Jr., and Steyn, A. J. (2007) Mycobacterium tuberculosis DosS is a redox sensor and DosT is a hypoxia sensor, *Proc Natl Acad Sci U S A 104*, 11568-11573.

36. Bzymek, K. P., Newton, G. L., Ta, P., and Fahey, R. C. (2007) Mycothiol import by Mycobacterium smegmatis and function as a resource for metabolic precursors and energy production, *J Bacteriol 189*, 6796-6805.

37. Dalle-Donne, I., Rossi, R., Giustarini, D., Colombo, R., and Milzani, A. (2007) S-glutathionylation in protein redox regulation, *Free Radic Biol Med 43*, 883-898.

38. Fahey, R. C., Brody, S., and Mikolajczyk, S. D. (1975) Changes in the glutathione thiol-disulfide status of Neurospora crassa conidia during germination and aging, *J Bacteriol 121*, 144-151.

39. Hampshire, T., Soneji, S., Bacon, J., James, B. W., Hinds, J., Laing, K., Stabler, R. A., Marsh, P. D., and Butcher, P. D. (2004) Stationary phase gene expression of Mycobacterium tuberculosis following a progressive nutrient depletion: a model for persistent organisms?, *Tuberculosis (Edinb) 84*, 228-238.

40. Dubnau, E., Fontan, P., Manganelli, R., Soares-Appel, S., and Smith, I. (2002) Mycobacterium tuberculosis genes induced during infection of human macrophages, *Infect Immun 70*, 2787-2795.

41. Ohno, H., Zhu, G., Mohan, V. P., Chu, D., Kohno, S., Jacobs, W. R., Jr., and Chan, J. (2003) The effects of reactive nitrogen intermediates on gene expression in Mycobacterium tuberculosis, *Cell Microbiol 5*, 637-648.

42. Bachhawat, N., and Mande, S. C. (1999) Identification of the INO1 gene of Mycobacterium tuberculosis H37Rv reveals a novel class of inositol-1-phosphate synthase enzyme, *J Mol Biol 291*, 531-536.

43. Cole, S. T., Brosch, R., Parkhill, J., Garnier, T., Churcher, C., Harris, D., Gordon, S. V., Eiglmeier, K., Gas, S., Barry, C. E., 3rd, Tekaia, F., Badcock, K., Basham, D., Brown, D., Chillingworth, T., Connor, R., Davies, R., Devlin, K., Feltwell, T., Gentles, S., Hamlin, N., Holroyd, S., Hornsby, T., Jagels, K., Krogh, A., McLean, J., Moule, S., Murphy, L., Oliver, K., Osborne, J., Quail, M. A., Rajandream, M. A., Rogers, J., Rutter, S., Seeger, K., Skelton, J., Squares, R., Squares, S., Sulston, J. E., Taylor, K., Whitehead, S., and Barrell, B. G. (1998) Deciphering the biology of Mycobacterium tuberculosis from the complete genome sequence, *Nature 393*, 537-544.

44. Li, Y., Chen, Z., Li, X., Zhang, H., Huang, Q., Zhang, Y., and Xu, S. (2007) Inositol-1-phosphate synthetase mRNA as a new target for antisense inhibition of Mycobacterium tuberculosis, *J Biotechnol 128*, 726-734.

45. Movahedzadeh, F., Smith, D. A., Norman, R. A., Dinadayala, P., Murray-Rust, J., Russell, D. G., Kendall, S. L., Rison, S. C., McAlister, M. S., Bancroft, G. J.,

McDonald, N. Q., Daffe, M., Av-Gay, Y., and Stoker, N. G. (2004) The Mycobacterium tuberculosis ino1 gene is essential for growth and virulence, *Mol Microbiol 51*, 1003-1014.

46. Smith, D., Hansch, H., Bancroft, G., and Ehlers, S. (1997) T-cell-independent granuloma formation in response to Mycobacterium avium: role of tumour necrosis factor-alpha and interferon-gamma, *Immunology 92*, 413-421.

47. Newton, G. L., Koledin, T., Gorovitz, B., Rawat, M., Fahey, R. C., and Av-Gay, Y. (2003) The glycosyltransferase gene encoding the enzyme catalyzing the first step of mycothiol biosynthesis (mshA), *J Bacteriol 185*, 3476-3479.

48. Campbell, J. A., Davies, G. J., Bulone, V., and Henrissat, B. (1997) A classification of nucleotide-diphospho-sugar glycosyltransferases based on amino acid sequence similarities, *Biochem J 326 (Pt 3)*, 929-939.

49. Newton, G. L., Ta, P., Bzymek, K. P., and Fahey, R. C. (2006) Biochemistry of the initial steps of mycothiol biosynthesis, *J Biol Chem 281*, 33910-33920.

50. Buchmeier, N., and Fahey, R. C. (2006) The mshA gene encoding the glycosyltransferase of mycothiol biosynthesis is essential in Mycobacterium tuberculosis Erdman, *FEMS Microbiol Lett 264*, 74-79.

51. Bhave, D. P., Muse, W. B., 3rd, and Carroll, K. S. (2007) Drug targets in mycobacterial sulfur metabolism, *Infect Disord Drug Targets 7*, 140-158.

52. Ta, P., Buchmeier, N., Newton, G. L., Rawat, M., and Fahey, R. C. (2011) Organic hydroperoxide resistance protein and ergothioneine compensate for loss of mycothiol in Mycobacterium smegmatis mutants, *J Bacteriol 193*, 1981-1990.

53. Vetting, M. W., Frantom, P. A., and Blanchard, J. S. (2008) Structural and enzymatic analysis of MshA from Corynebacterium glutamicum: substrate-assisted catalysis, *J Biol Chem 283*, 15834-15844.

54. Movahedzadeh, F., Wheeler, P. R., Dinadayala, P., Av-Gay, Y., Parish, T., Daffe, M., and Stoker, N. G. (2010) Inositol monophosphate phosphatase genes of Mycobacterium tuberculosis, *BMC Microbiol 10*, 50.

55. Newton, G. L., Av-Gay, Y., and Fahey, R. C. (2000) N-Acetyl-1-D-myo-inosityl-2-amino-2-deoxy-alpha-D-glucopyranoside deacetylase (MshB) is a key enzyme in mycothiol biosynthesis, *J Bacteriol 182*, 6958-6963.

56. Broadley, S. G., Gumbart, J. C., Weber, B. W., Marakalala, M. J., Steenkamp, D. J., and Sewell, B. T. (2012) A new crystal form of MshB from Mycobacterium tuberculosis with glycerol and acetate in the active site suggests the catalytic mechanism, *Acta Crystallogr D Biol Crystallogr 68*, 1450-1459.

57. Buchmeier, N. A., Newton, G. L., Koledin, T., and Fahey, R. C. (2003) Association of mycothiol with protection of Mycobacterium tuberculosis from toxic oxidants and antibiotics, *Mol Microbiol 47*, 1723-1732.

58. Rawat, M., Kovacevic, S., Billman-Jacobe, H., and Av-Gay, Y. (2003) Inactivation of mshB, a key gene in the mycothiol biosynthesis pathway in Mycobacterium smegmatis, *Microbiology 149*, 1341-1349.

59. Xu, X., Vilcheze, C., Av-Gay, Y., Gomez-Velasco, A., and Jacobs, W. R., Jr. (2011) Precise null deletion mutations of the mycothiol synthesis genes reveal their role in isoniazid and ethionamide resistance in Mycobacterium smegmatis, *Antimicrob Agents Chemother 55*, 3133-3139.

60. Metaferia, B. B., Fetterolf, B. J., Shazad-Ul-Hussan, S., Moravec, M., Smith, J. A., Ray, S., Gutierrez-Lugo, M. T., and Bewley, C. A. (2007) Synthesis of natural product-inspired inhibitors of Mycobacterium tuberculosis mycothiol-associated enzymes: the first inhibitors of GlcNAc-Ins deacetylase, *J Med Chem 50*, 6326-6336.

61. Fan, F., Luxenburger, A., Painter, G. F., and Blanchard, J. S. (2007) Steady-state and pre-steady-state kinetic analysis of Mycobacterium smegmatis cysteine ligase (MshC), *Biochemistry 46*, 11421-11429.

62. Sareen, D., Newton, G. L., Fahey, R. C., and Buchmeier, N. A. (2003) Mycothiol is essential for growth of Mycobacterium tuberculosis Erdman, *J Bacteriol 185*, 6736-6740.

63. Sareen, D., Steffek, M., Newton, G. L., and Fahey, R. C. (2002) ATP-dependent L-cysteine:1D-myo-inosityl 2-amino-2-deoxy-alpha-D-glucopyranoside ligase, mycothiol biosynthesis enzyme MshC, is related to class I cysteinyl-tRNA synthetases, *Biochemistry 41*, 6885-6890.

64. Fan, F., and Blanchard, J. S. (2009) Toward the catalytic mechanism of a cysteine ligase (MshC) from Mycobacterium smegmatis: an enzyme involved in the biosynthetic pathway of mycothiol, *Biochemistry 48*, 7150-7159.

65. Koledin, T., Newton, G. L., and Fahey, R. C. (2002) Identification of the mycothiol synthase gene (mshD) encoding the acetyltransferase producing mycothiol in actinomycetes, *Arch Microbiol 178*, 331-337.

66. Newton, G. L., Ta, P., and Fahey, R. C. (2005) A mycothiol synthase mutant of Mycobacterium smegmatis produces novel thiols and has an altered thiol redox status, *J Bacteriol 187*, 7309-7316.

67. Sassetti, C. M., Boyd, D. H., and Rubin, E. J. (2003) Genes required for mycobacterial growth defined by high density mutagenesis, *Mol Microbiol 48*, 77-84.

68. Vetting, M. W., Roderick, S. L., Yu, M., and Blanchard, J. S. (2003) Crystal structure of mycothiol synthase (Rv0819) from Mycobacterium tuberculosis shows structural homology to the GNAT family of N-acetyltransferases, *Protein Sci 12*, 1954-1959.

69. Vetting, M. W., Yu, M., Rendle, P. M., and Blanchard, J. S. (2006) The substrate-induced conformational change of Mycobacterium tuberculosis mycothiol synthase, *J Biol Chem 281*, 2795-2802.

70. Dyda, F., Klein, D. C., and Hickman, A. B. (2000) GCN5-related N-acetyltransferases: a structural overview, *Annu Rev Biophys Biomol Struct 29*, 81-103.

71. Hinchman, C. A., and Ballatori, N. (1994) Glutathione conjugation and conversion to mercapturic acids can occur as an intrahepatic process, *J Toxicol Environ Health 41*, 387-409.

72. Newton, G. L., Rawat, M., La Clair, J. J., Jothivasan, V. K., Budiarto, T., Hamilton, C. J., Claiborne, A., Helmann, J. D., and Fahey, R. C. (2009) Bacillithiol is an antioxidant thiol produced in Bacilli, *Nat Chem Biol 5*, 625-627.

73. Rajan, S. S., Yang, X., Shuvalova, L., Collart, F., and Anderson, W. F. (2004) YfiT from Bacillus subtilis is a probable metal-dependent hydrolase with an unusual four-helix bundle topology, *Biochemistry 43*, 15472-15479.

74. Steffek, M., Newton, G. L., Av-Gay, Y., and Fahey, R. C. (2003) Characterization of Mycobacterium tuberculosis mycothiol S-conjugate amidase, *Biochemistry 42*, 12067-12076.

75. Zadzinski, R., Fortuniak, A., Bilinski, T., Grey, M., and Bartosz, G. (1998) Menadione toxicity in Saccharomyces cerevisiae cells: activation by conjugation with glutathione, *Biochem Mol Biol Int 44*, 747-759.

76. Patel, M. P., and Blanchard, J. S. (1999) Expression, purification, and characterization of Mycobacterium tuberculosis mycothione reductase, *Biochemistry 38*, 11827-11833.

77. Holsclaw, C. M., Muse, W. B., 3rd, Carroll, K. S., and Leary, J. A. (2011) Mass Spectrometric Analysis of Mycothiol levels in Wild-Type and Mycothiol Disulfide Reductase Mutant Mycobacterium smegmatis, *Int J Mass Spectrom 305*, 151-156.

78. Stewart, M. J., Jothivasan, V. K., Rowan, A. S., Wagg, J., and Hamilton, C. J. (2008) Mycothiol disulfide reductase: solid phase synthesis and evaluation of alternative substrate analogues, *Org Biomol Chem 6*, 385-390.

79. Misset-Smits, M., van Ophem, P. W., Sakuda, S., and Duine, J. A. (1997) Mycothiol, 1-O-(2'-[N-acetyl-L-cysteinyl]amido-2'-deoxy-alpha-D-glucopyranosyl)-D- myo-inositol, is the factor of NAD/factor-dependent formaldehyde dehydrogenase, *FEBS Lett 409*, 221-222.

80. Vogt, R. N., Steenkamp, D. J., Zheng, R., and Blanchard, J. S. (2003) The metabolism of nitrosothiols in the Mycobacteria: identification and characterization of S-nitrosomycothiol reductase, *Biochem J 374*, 657-666.

81. Ung, K. S., and Av-Gay, Y. (2006) Mycothiol-dependent mycobacterial response to oxidative stress, *FEBS Lett 580*, 2712-2716.

Chapter 4

A fluorescence-based assay for measuring MshB activity

Reproduced with permission from: Huang, X. and Hernick, M. "A fluorescence-based assay for measuring *N*-acetyl-1-D-*myo*-inosityl-2-amino-2-deoxy-alpha-D-glucopyranoside deacetylase activity." Anal Biochem, 2011. 414(2): p. 278-81.

Author Contributions
Xinyi Huang performed all the experiments and wrote the article
Marcy Hernick directed the research and wrote the article

Abstract

Here we report a new fluorescence-based assay for measuring MshB (*N*-acetyl-1-D-*myo*-inosityl-2- amino-2-deoxy-α-D-glucopyranoside deacetylase) activity. The current assay for measuring MshB activity requires the fluorescent labeling of reaction mixtures and subsequent analysis using high-performance liquid chromatography (HPLC), resulting in a significant amount of processing time per sample. Here we describe a more rapid fluorescence-based assay for the measurement of MshB activity that does not require HPLC analysis and can be carried out in multiwell plates. This fluorescamine (FSA)-based assay was used to determine the steady-state parameters for the deacetylation of *N*-acetyl-glucosamine (GlcNAc) by MshB, and the results from these experiments support the hypothesis that the inositol moiety primarily contributes to the affinity of GlcNAc-Ins (*N*-acetyl-1-D-*myo*-inosityl-2-amino-2-deoxy-α-D-glucopyranoside) for MshB. The rapid nature of this assay will aid efforts toward a more detailed biochemical characterization of MshB. Furthermore, because this assay relies on the formation of a primary amine, it could be adapted to measure the activity of

mycothiol-S-conjugate amidase, a metal-dependent amidase that is a potential drug target involved in the mycothiol detoxification pathway.

1. Introduction

Mycobacteria are a class of gram-positive organisms known as *Actinomycetes* and include a number of pathogenic organisms such as *Mycobacterium tuberculosis*, *Mycobacterium leprae*, *Mycobacterium bovis*, and *Mycobacterium avium*. Mycobacteria do not produce glutathione and instead use a small thiol known as mycothiol (MSH) (Fig. 1A) to serve similar protective roles, functioning as the primary antioxidant for these organisms and as a nucleophile in the detoxification of drugs and other toxins. (*1-4*) As a result of the important role that MSH plays in mycobacterial survival, the enzymes involved in MSH biosynthesis and detoxification are targets for the development of inhibitors with the potential to function as antibiotics in the treatment of infections such as tuberculosis. (*5-10*) The metalloenzyme MshB (*N*-acetyl-1-D-*myo*-inosityl-2-amino-2-deoxy-α-D-glucopyranoside deacetylase) catalyzes the rate-limiting step (*11*), the fourth step overall, in MSH biosynthesis (Fig. 1B) and is one of the enzymes currently being targeted for MSH inhibitors. (*6-10*) The development of potent and specific MshB inhibitors will be facilitated by a detailed biochemical characterization of MshB, including information regarding the chemical mechanisms of the enzyme and its molecular recognition properties.

There is currently one assay that is used to measure MshB activity. (*12, 13*) In this assay, quenched MshB reaction mixtures are derivatized with AccQ-fluor and then analyzed using high-performance liquid chromatography (HPLC). Although this method

has been used successfully for the initial biochemical characterization of MshB (*12-14*), studies designed to probe the chemical mechanism and molecular recognition properties of MshB in greater detail would benefit tremendously from an activity-based assay that does not rely on HPLC analysis, which adds approximately an additional 30 min of processing time for each sample. This means that the measurement of the observed rate of MshB deacetylation at one given substrate concentration would require approximately 3 h of HPLC processing time assuming 6 time points per rate. In contrast, an alternative fluorescence-based assay that does not require HPLC separation of substrate and product could measure the rate of the MshB-catalyzed reaction at multiple substrate concentrations in minutes using a multi-well plate reader.

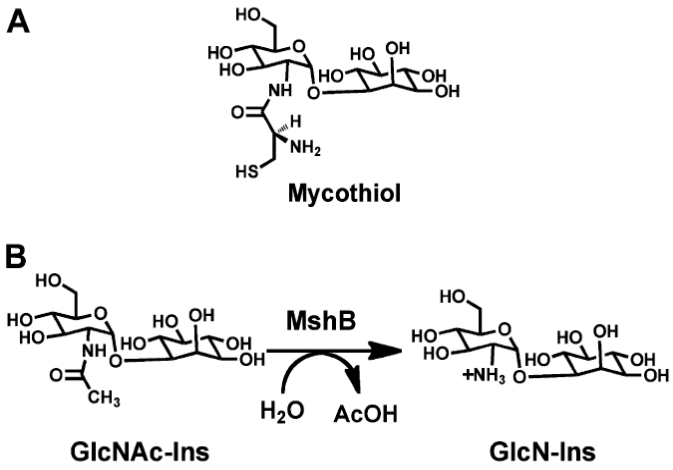

Figure 1. (A) Structure of mycothiol. (B) Reaction catalyzed by MshB.

Here we describe a method to measure MshB deacetylase activity using a fluorescamine (FSA)-based assay with the substrate N- acetyl-glucosamine (GlcNAc) and recombinant *Mycobacterium smegmatis* MshB (reconstituted with stoichiometric Zn^{2+}). FSA- based assays have been successfully used in the past to measure the activity of the metal-dependent deacetylase LpxC (UDP-3-*O*-(R-3-hydroxymyristoyl)-*N*-

acetylglucosamine deacetylase). (*15, 16*) FSA itself is not fluorescent but reacts with primary amines to form a fluorescent product. Consequently, following incubation with FSA, there is no increase in fluorescence (excitation 395 nm, emission 485 nm) observed for the substrate GlcNAc, whereas there is a concentration-dependent increase in fluorescence observed for the product GlcN (Fig. 2A). Although GlcNAc is not the natural substrate for MshB and has a weakened affinity for MshB due to loss of the inositol moiety (*12*), it has the advantage of being commercially available. Importantly, the GlcNAc moiety is the portion of GlcNAc–Ins (*N*-acetyl-1-D-*myo*-inosityl-2-amino-2-deoxy-α-D-glucopyranoside) that undergoes the chemical transformation by MshB in MSH biosynthesis. We have used this FSA-based assay to determine the steady-state parameters of MshB for the substrate GlcNAc. Results from these experiments are consistent with the hypothesis that the inositol moiety primarily contributes to the affinity of GlcNAc-Ins for MshB.

2. Materials and Methods

2.1 Materials

All solutions were prepared using MilliQ water. Primers were purchased from Integrated DNA Technologies (IDT). *M. smegmatis* genomic DNA was purchased from American Type Culture Collection (ATCC). Restriction enzymes were purchased from Promega and New England Biolabs. DNA sequencing was performed at the Virginia Bioinformatics Institute DNA Sequencing Facility (Virginia Tech). Plasmids and polymerase chain reaction (PCR) products were purified using the Wizard Plus SV Minipreps DNA Purification System and Wizard SV Gel and PCR Cleanup Kit

(Promega), respectively. All chemicals were purchased from ThermoFisher Scientific, Sigma-Aldrich, and Gold Biotechnology.

2.2 Protein expression and purification

The gene for MshB from *M. smegmatis* was cloned into the pVP55A (His tag) vector using the Flexi technology (Promega). (*17*) BL21(DE3) cells transformed with the pHis–MshB plasmid were grown in Luria-Bertani (LB) medium supplemented with ampicillin (100 μg/ml) at 37 °C with shaking (250 rpm) until an OD_{600} of approximately 0.6 was reached. Protein expression was induced with the addition of 1 mM isopropyl-β-D-thiogalactoside, the temperature was decreased to 25 °C, and the cells were incubated with shaking. After 4-14 h, cells were harvested by centrifugation, resuspended in buffer A (30mM HEPES, 150 mM NaCl, and 0.5 mM imidazole, pH 7.5), and stored at -80°C. Cells were lysed using a high-pressure homogenizer (Avestin), and the cell lysate was clarified by centrifugation (18,000 rpm, 4 °C, 1 h). Cleared cell lysate was loaded onto a pre-equilibrated (buffer A) Co-IMAC (immobilized metal affinity chromatography) column. His-MshB was purified at 4 °C using a 0.5-300-mM imidazole step gradient (His-MshB elutes with buffer A + 300 mM imidazole). Fractions containing His–MshB were combined and dialyzed overnight against 2 × 4 L of buffer A in the presence of His–TEV (tobacco etch virus) protease (300 μg/ml) to remove the His tag. The resulting TEV cleaved protein was loaded onto a pre-equilibrated (buffer A + 25 mM imidazole) Co-IMAC column. The His tag and His-TEV remain bound to the Co-IMAC column, whereas MshB elutes in the flow-through. Fractions containing MshB (via 12% SDS-PAGE) were combined, concentrated, and dialyzed versus 2 × 4 L of 25 mM HEPES and

1.5 mM tris(2-carboxyethyl)phosphine (TCEP) (pH 7.5) (Slide-a-Lyzer molecular weight cutoff [MWCO] = 10,000, Pierce). Protein concentration was determined using the Bradford assay (Pierce). Protein aliquots were flash-frozen in liquid nitrogen and stored at -80 °C.

2.3 Enzyme activity

Assay mixtures containing 50 mM HEPES, 50 mM NaCl, and 1 mM TCEP (pH 7.5) and 5.6 mM GlcNAc were pre-equilibrated at 30 °C prior to the addition of enzyme (1 μM) to initiate the reaction. After various times, reaction aliquots (30 μl) were quenched by the addition of 20% trichloroacetic acid (TCA, 10 μl), which precipitates the protein. After centrifugation (15,000 rpm, 10 min), the supernatant (25 μl) was transferred into a 96-well plate, diluted with 1 M borate (pH 9.0, 75 μl), and reacted with 10 mM FSA (30 μl in CH_3CN, Invitrogen). After 10 min (note that the fluorescence signal is stable for up to 1 h), the resulting fluorescence was measured (excitation 395nm, emission 485 nm) using a SpectraMax M5 plate reader (Molecular Devices). The observed increase in fluorescence (fluorescence units [FU]/min) was converted into μM/min using a glucosamine (GlcN) standard curve (Fig. 2B). Initial rates of product formation (< 10%) were determined from these data. For determination of the steady-state parameters, activity was measured at six different concentrations of GlcNAc (0-150 mM), and the parameters k_{cat}, K_M, and k_{cat}/K_M were obtained by fitting the Michaelis–Menten equation to the initial linear velocities using the curve-fitting program Kaleidagraph (Synergy Software), which also calculates the asymptotic standard errors.

3. Results and Discussion

We examined the steady-state turnover of GlcNAc as a function of substrate concentration using the FSA-based assay. A sample plot showing the initial rate of GlcNAc deacetylation by MshB using the FSA-based assay is shown in Fig. 2C. In this example, the observed rate of deacetyation at 5.6 mM GlcNAc is 6.1 ± 0.4 μM/min. For determination of the steady-state parameters, activity was measured at six different concentrations of GlcNAc (0–150 mM), and the results from these experiments are shown in Fig. 2D. The fit of the Michaelis–Menten equation to these data yields the following steady-state parameters: K_M = 38 ± 4 mM, k_{cat} = 46 ± 2.2 min^{-1}, and k_{cat}/K_M = 1.2 ± 0.08 mM^{-1} min^{-1} for the substrate GlcNAc. This is the first report of the steady-state parameters for the deacetylation of GlcNAc. The observed K_M value of 38 mM is significantly larger (~110-fold) than the K_M of GlcNAc–Ins (340 ± 80 μM) (*12*), consistent with the proposed weakened affinity of GlcNAc for MshB compared with GlcNAc-Ins. In contrast, we see that there is less than a 2-fold change in k_{cat} for GlcNAc versus GlcNAc–Ins (0.49 ± 0.04 s^{-1}) (*12*). These results are consistent with the hypothesis that the inositol moiety primarily contributes to the affinity of GlcNAc-Ins for MshB and may suggest that the steady-state parameter k_{cat} reflects the rate of chemistry given that product release would be expected to be significantly faster for GlcN compared with GlcNAc-Ins (1-D-*myo*-inosityl-2-amino-2-deoxy-α-D-glucopyranoside) due to the weakened affinity on loss of the inositol moiety. These data for the Michaelis–Menten plot were obtained in approximately 2 min compared with approximately 18 h that would have been required using HPLC, a great improvement in the overall efficiency of measuring MshB activity.

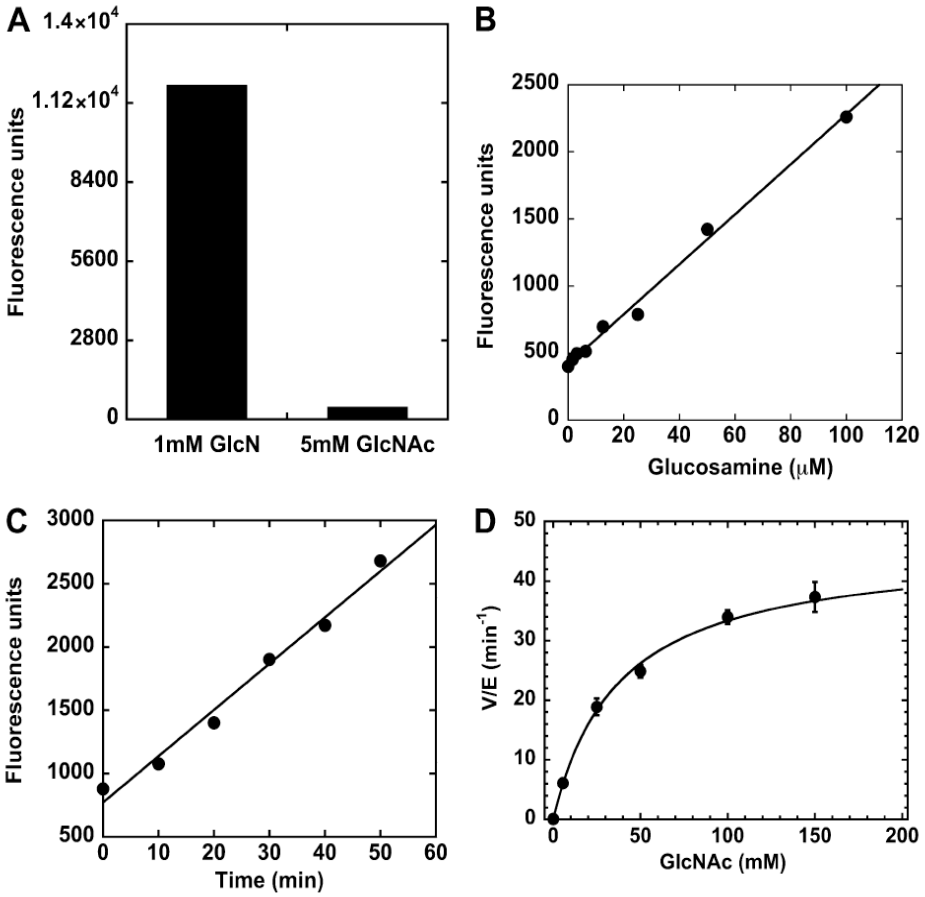

Figure 2. Catalytic activity of MshB. (A) Fluorescence observed following reaction of glucosamine (GlcN) and GlcNAc with FSA. Solutions of GlcN (1 mM) or GlcNAc (5 mM) in buffer (50 mM HEPES, 50 mM NaCl, 1 mM TCEP pH 7.5) were diluted (4-fold) with 1 M borate (pH 9.0) and mixed with FSA (2.3 mM final), and the resulting fluorescence was measured (Ex. 395 nm, Em. 485 nm). (B) Glucosamine standard curve. Solutions of glucosamine (0-100 /μM). The resulting increase in fluorescence was plotted against glucosamine concentration to yield the standard curve. A linear equation was fit to these data. (C) MshB-catalyzed reaction. GlcNAc (5.6 mM) was pre-equilibrated at 30 °C and the reaction was initiated by the addition of MshB (1 μM) to this mixture. The observed rate of 6.1 ± 0.4 μM/min. (D) Michaelis-Menten plot of Zn^{2+}-MshB. The initial rates for the deacetylation of GlcNAc (0-150 mM) were measured at 30 °C. The steady-state parameters k_{cat}, K_M, and k_{cat}/K_M were obtained by fitting the Michaelis-Menten equation to the initial rates: k_{cat} = 46 ± 2.2 min^{-1}, K_M = 38 ± 4 mM, and k_{cat}/K_M = 1.2 ± 0.08 mM^{-1} min^{-1}.

In conclusion, a new fluorescence-based assay for measuring MshB activity has been developed. This assay does not require HPLC analysis and, therefore, is more rapid than the traditionally used method. In addition, the FSA-based assay has the potential to be used for the measurement of mycothiol-S-conjugate amidase (Mca) activity. Mca is a metal-dependent amidase that is a potential drug target involved in the mycothiol detoxification pathway and shares overlapping substrate specificities with MshB. (*18*) The new FSA-based assay has been used to determine the steady-state parameters of MshB with the substrate GlcNAc. The results from these experiments are consistent with the proposal that the inositol moiety on GlcNAc-Ins is primarily responsible for enhancing the binding affinity of substrate for MshB and suggest that the parameter k_{cat} may reflect the chemical step of the reaction. The development of this new assay for measuring MshB activity will facilitate a more rapid examination of the chemical mechanism and molecular recognition properties of this enzyme.

Acknowledgement

This work was supported by Jeffress Memorial Trust grant J960 (to M.H.).

References

1. Newton, G. L., Buchmeier, N., and Fahey, R. C. (2008) Biosynthesis and functions of mycothiol, the unique protective thiol of Actinobacteria, *Microbiol Mol Biol Rev 72*, 471-494.

2. Jothivasan, V. K., and Hamilton, C. J. (2008) Mycothiol: synthesis, biosynthesis and biological functions of the major low molecular weight thiol in actinomycetes, *Nat Prod Rep 25*, 1091-1117.

3. Rawat, M., and Av-Gay, Y. (2007) Mycothiol-dependent proteins in actinomycetes, *FEMS Microbiol Rev 31*, 278-292.

4. Fan, F., Vetting, M. W., Frantom, P. A., and Blanchard, J. S. (2009) Structures and mechanisms of the mycothiol biosynthetic enzymes, *Curr Opin Chem Biol 13*, 451-459.

5. Gutierrez-Lugo, M. T., Baker, H., Shiloach, J., Boshoff, H., and Bewley, C. A. (2009) Dequalinium, a new inhibitor of Mycobacterium tuberculosis mycothiol ligase identified by high-throughput screening, *J Biomol Screen 14*, 643-652.

6. Gammon, D. W., Steenkamp, D. J., Mavumengwana, V., Marakalala, M. J., Mudzunga, T. T., Hunter, R., and Munyololo, M. (2010) Conjugates of plumbagin and phenyl-2-amino-1-thioglucoside inhibit MshB, a deacetylase involved in the biosynthesis of mycothiol, *Bioorg Med Chem 18*, 2501-2514.

7. Gutierrez-Lugo, M. T., and Bewley, C. A. (2008) Natural products, small molecules, and genetics in tuberculosis drug development, *J Med Chem 51*, 2606-2612.

8. Metaferia, B. B., Fetterolf, B. J., Shazad-Ul-Hussan, S., Moravec, M., Smith, J. A., Ray, S., Gutierrez-Lugo, M. T., and Bewley, C. A. (2007) Synthesis of natural product-inspired inhibitors of Mycobacterium tuberculosis mycothiol-associated enzymes: the first inhibitors of GlcNAc-Ins deacetylase, *J Med Chem 50*, 6326-6336.

9. Nicholas, G. M., Eckman, L. L., Newton, G. L., Fahey, R. C., Ray, S., and Bewley, C. A. (2003) Inhibition and kinetics of mycobacterium tuberculosis and mycobacterium smegmatis mycothiol-S-conjugate amidase by natural product inhibitors, *Bioorg Med Chem 11*, 601-608.

10. Bhave, D. P., Muse, W. B., 3rd, and Carroll, K. S. (2007) Drug targets in mycobacterial sulfur metabolism, *Infect Disord Drug Targets 7*, 140-158.

11. Newton, G. L., Av-Gay, Y., and Fahey, R. C. (2000) N-Acetyl-1-D-myo-inosityl-2-amino-2-deoxy-alpha-D-glucopyranoside deacetylase (MshB) is a key enzyme in mycothiol biosynthesis, *J Bacteriol 182*, 6958-6963.

12. Newton, G. L., Ko, M., Ta, P., Av-Gay, Y., and Fahey, R. C. (2006) Purification and characterization of Mycobacterium tuberculosis 1D-myo-inosityl-2-acetamido-2-deoxy-alpha-D-glucopyranoside deacetylase, MshB, a mycothiol biosynthetic enzyme, *Protein Expr Purif 47*, 542-550.

13. Anderberg, S. J., Newton, G. L., and Fahey, R. C. (1998) Mycothiol biosynthesis and metabolism. Cellular levels of potential intermediates in the biosynthesis and degradation of mycothiol in mycobacterium smegmatis, *J Biol Chem 273*, 30391-30397.

14. Nicholas, G. M., Eckman, L. L., Kovac, P., Otero-Quintero, S., and Bewley, C. A. (2003) Synthesis of 1-D- and 1-L-myo-inosityl 2-N-acetamido-2-deoxy-alpha-D-glucopyranoside establishes substrate specificity of the Mycobacterium tuberculosis enzyme AcGI deacetylase, *Bioorg Med Chem 11*, 2641-2647.

15. Wang, W., Maniar, M., Jain, R., Jacobs, J., Trias, J., and Yuan, Z. (2001) A fluorescence-based homogeneous assay for measuring activity of UDP-3-O-(R-3-

hydroxymyristoyl)-N-acetylglucosamine deacetylase, *Anal Biochem 290*, 338-346.

16. Pirrung, M. C., Tumey, L. N., Raetz, C. R., Jackman, J. E., Snehalatha, K., McClerren, A. L., Fierke, C. A., Gantt, S. L., and Rusche, K. M. (2002) Inhibition of the antibacterial target UDP-(3-O-acyl)-N-acetylglucosamine deacetylase (LpxC): isoxazoline zinc amidase inhibitors bearing diverse metal binding groups, *J Med Chem 45*, 4359-4370.

17. Sobrado, P., Goren, M. A., James, D., Amundson, C. K., and Fox, B. G. (2008) A Protein Structure Initiative approach to expression, purification, and in situ delivery of human cytochrome b5 to membrane vesicles, *Protein Expr Purif 58*, 229-241.

18. Steffek, M., Newton, G. L., Av-Gay, Y., and Fahey, R. C. (2003) Characterization of Mycobacterium tuberculosis mycothiol S-conjugate amidase, *Biochemistry 42*, 12067-12076.

Chapter 5

The Activity and Cofactor Preferences of MshB change depending on environmental conditions.

Reproduced with permission from: Huang, X., Kocabas, E. and Hernick, M. "The activity and cofactor preferences of *N*-acetyl-1-D-*myo*-inosityl-2-amino-2-deoxy-alpha-D-glucopyranoside deacetylase (MshB) change depending on environmental conditions." J Biol Chem, 2011. 286(23): p. 20275-82.

Author Contributions
Xinyi Huang performed all the experiments except mentioned below and wrote the article.
Evren Kocabas performed the HaloTag pull-down experiments and metal ion affinity experiments.
Marcy Hernick directed the research and wrote the article.

Abstract

Actinomycetes, such as *Mycobacterium* species, are Gram-positive bacteria that utilize the small molecule mycothiol (MSH) as their primary reducing agent. Consequently, the enzymes involved in MSH biosynthesis are targets for drug development. The metal-dependent enzyme *N*-acetyl-1-D-*myo*-inosityl-2-amino-2-deoxy-α-D-glucopyranoside deacetylase (MshB) catalyzes the hydrolysis of *N*-acetyl-1-D-*myo*-inosityl-2-amino-2-deoxy-α-D-glucopyranoside to form 1-D-*myo*-inosityl-2-amino-2-deoxy-α-D-glucopyranoside and acetate, the fourth overall step in MSH biosynthesis. Inhibitors of metalloenzymes typically contain a group that binds to the active site metal ion; thus, a comprehensive understanding of the native cofactor(s) of metalloenzymes is critical for the development of biologically effective inhibitors. Herein, we examined the effect of metal ions on the overall activity of MshB and probed the identity of the native cofactor. We found that the activity of MshB follows the trend

$Fe^{2+} > Co^{2+} > Zn^{2+} > Mn^{2+}$ and Ni^{2+}. Additionally, our results show that the identity of the cofactor bound to purified MshB is highly dependent on the purification conditions used (aerobic versus anaerobic), as well as the metal ion content of the medium during protein expression. MshB prefers Fe^{2+} under anaerobic conditions regardless of the metal ion content of the medium and switches between Fe^{2+} and Zn^{2+} under aerobic conditions as the metal content of the medium is altered. These results indicate that the cofactor bound to MshB under biological conditions is dependent on environmental conditions, suggesting that MshB may be a cambialistic metallohydrolase that contains a dynamic cofactor. Consequently, biologically effective inhibitors will likely need to dually target Fe^{2+}-MshB and Zn^{2+}-MshB.

1. Introduction

Actinomycetes, such as *Mycobacterium* species, do not have glutathione. Instead, these organisms use the small molecule mycothiol (MSH) as their primary reducing agent and in xenobiotic metabolism for the detoxification of drugs and other toxins. (*1-4*) MSH is likely to be critical for the survival of mycobacteria inside activated macrophages, where the mycobacteria are subjected to oxidative bursts. Consequently, the enzymes involved in MSH biosynthesis and detoxification (Fig. 1A), including the metalloenzymes *N*-acetyl-1-D-*myo*-inosityl-2-amino-2-deoxy-α-D-glucopyranoside deacetylase (MshB) and MSH-conjugate amidase, are targets for the development of antibiotics for the treatment of diseases such as tuberculosis. (*5-10*)

The enzyme MshB catalyzes the hydrolysis of *N*-acetyl-1-D-*myo*-inosityl-2-amino-2-deoxy-α-D-glucopyranoside (GlcNAc- Ins) to form 1-D-*myo*-inosityl-2-amino-

2-deoxy-α-D-glucopyranoside (GlcN-Ins) and acetate, the fourth overall step in MSH biosynthesis (rate-limiting step). (*11*) MshB is an attractive drug target because it is a metalloenzyme; there are past successes in targeting metalloenzymes, including inhibitors of carbonic anhydrase, matrix metalloproteases, and angiotensin-converting enzyme. (*12-15*) Inhibitors of metalloenzymes typically contain a group that binds to the catalytic metal ion. Consequently, a comprehensive understanding of metalloenzyme cofactor preferences is necessary for the development of potent and specific metalloenzyme inhibitors.

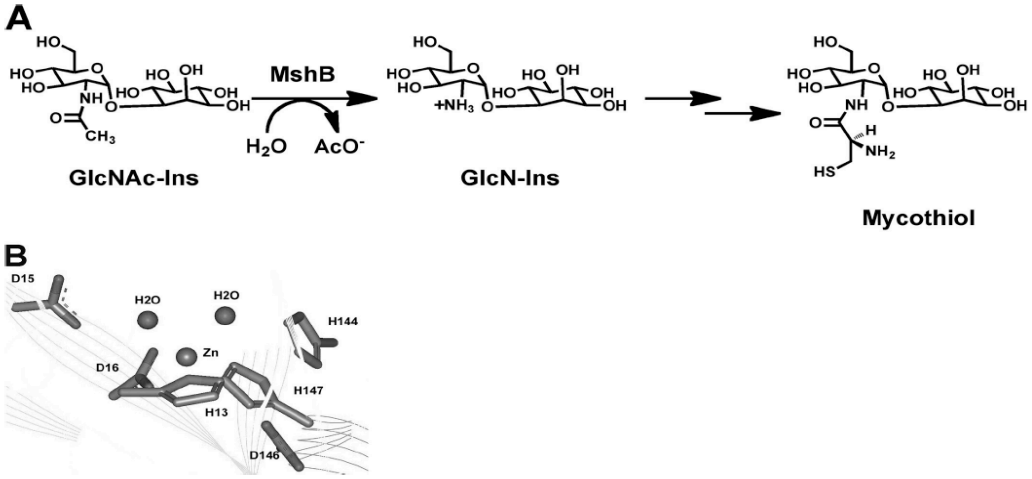

Figure 1. A, reaction catalyzed by MshB. B, active site of MshB (Protein Data Bank code 1Q74) containing a catalytic zinc ion.

MshB was previously identified as a Zn^{2+}-dependent enzyme based on the observations that the enzyme copurifies with Zn^{2+} (Fig. 1B) and that the enzyme activity is reversibly inhibited by treatment with 1,10-phenanthroline. (*16-18*) On the basis of the structure of the enzyme active site, MshB is thought to catalyze the hydrolysis of GlcNAc-Ins via one of two potential chemical mechanisms using general acid-base catalysts (GABC). (*19*) One possible mechanism uses a single bifunctional GABC to

facilitate the hydrolysis of GlcNAc-Ins, whereas the other uses a GABC pair to carry out this reaction. However, Fe^{2+} was not examined as a potential cofactor in these experiments. Furthermore, MshB was purified using zinc immobilized metal ion affinity chromatography (IMAC) under aerobic conditions, which is biased toward zinc incorporation into metalloenzymes. (*16*) Purified MshB contains nickel (0.82 eq) when purified using nickel-IMAC (aerobic conditions). (*16*) There have been several examples over the last decade of Fe^{2+}-enzymes being misidentified as exclusive Zn^{2+}-enzymes, including peptide deformylase, S-ribosyl-homocysteinase (LuxS), UDP-3-*O*-(R-3-hydroxymyristoyl)-*N*-acetylglucosamine deacetylase (LpxC), and possibly histone deacetylase-8 (HDAC8). (*20-27*) In all these enzymes, the Fe^{2+} cofactor is either exclusively preferred or is preferred over Zn^{2+} under certain environmental conditions. The incorporation of Zn^{2+} into these enzymes that led to the initial characterizations as zinc-enzymes is attributed to purification of the enzymes under aerobic conditions, which leads to oxidation of Fe^{2+}, dissociation of Fe^{3+} from the enzyme, and replacement with Zn^{2+}. The finding that the zinc ion observed in the crystal structure of MshB is a 5-coordinate metal ion (*28*) suggests that Fe^{2+} could also possibly serve as a cofactor for MshB because Fe^{2+} prefers coordination numbers of 5- 6. (*19*) Consequently, we have examined whether Fe^{2+} can serve as an efficient cofactor for MshB.

Herein, we demonstrate that the activity of MshB is 3-fold higher with Fe^{2+} as a cofactor compared with Zn^{2+}. The activity of Fe^{2+}-MshB is air-sensitive, whereas the activity of Zn^{2+}-MshB is stable under aerobic conditions. Additionally, we demonstrate that MshB preferentially binds Fe^{2+} over Zn^{2+} when purified under anaerobic conditions and when purified under aerobic conditions in the absence of added Zn^{2+}. Although

MshB exhibits a higher affinity for Zn^{2+} over Fe^{2+}, it is likely that higher free [Fe^{2+}] accounts for the cofactor preferences that are observed in these experiments. These results suggest that MshB likely uses Fe^{2+} and Zn^{2+} as biological cofactors under different environmental conditions. These results may have important biological implications in light of the dynamic changes in zinc and iron concentrations that occur during the course of infection and suggest that biologically effective inhibitors will need to dually target Fe^{2+}-MshB and Zn^{2+}-MshB.

2. Materials and Methods

2.1 General Procedures

All solutions were prepared using Milli-Q water. Primers were purchased from Integrated DNA Technologies. Genomic DNA was purchased from American Type Culture Collection. DNA sequencing was performed at the Virginia Bioinformatics Institute DNA Sequencing Facility (Virginia Tech). Plasmids and PCR products were purified using the Wizard Plus SV Minipreps DNA purification system and Wizard SV Gel and PCR Clean-up kits (Promega), respectively. All chemicals were purchased from Thermo Fisher Scientific, Sigma, and Gold Biotechnology. For all kinetic and thermodynamic experiments, solutions were prepared with reagents that did not contain extraneous metal ions and/or were treated with Chelex (Bio-Rad), and solutions were stored in "metal-free" plasticware. For Fe^{2+} experiments, a 400 mM $FeCl_2$ stock was prepared in 10 mM dithionite and diluted to 100 mM with 1× assay buffer prior to incubation with apo-MshB. Similarly, a 100 mM $ZnSO_4$ solution was prepared in 50 mM HEPES (pH 7.5) and diluted to 100 mM with 1× assay buffer prior to incubation with

apo-MshB. To maintain anaerobic conditions, experiments were carried out either in an anaerobic chamber (Coy Laboratory Products, Grass Lake, MI) and/or using assay buffers containing 10 mM tris(2-carboxyethyl)- phosphine (TCEP) and completed in < 2 h to ensure that MshB was maximally active during the course of the assays. The concentrations of metal ions were measured by ion chromatography on a Dionex ICS-3000 system.

2.2 Cloning

The mshB genes from *Mycobacterium smegmatis* (Ms) and *Mycobacterium bovis* BCG (Mt) were cloned into expression vectors using Flexi® technology (Promega). The expression plasmids used in these studies yield recombinant proteins containing an N-terminal affinity tag linked to MshB via a tobacco etch virus (TEV) protease site: pVP55A (His tag) (*29*), pVP56K (His-maltose-binding protein (MBP) tag) (*30*), and pFN18K (HaloTag, Promega). The mshB genes were amplified from genomic DNA with PmeI and SgfI restriction sites at the 5'- and 3'-ends, respectively. PCR products were digested with Flexi enzyme blend (PmeI and SgfI) and ligated into Flexi- digested expression plasmids with T4 ligase (New England Biolabs). For MtMshB, which contains an internal SgfI site, the PCR product was first ligated into a pZeroBlunt vector (Stratagene), the internal restriction site was removed by introducing a silent mutation using the QuikChange Lightning site-directed mutagenesis kit (Stratagene), and the mshB gene was liberated by Flexi digest prior to ligation into the Flexi-digested pVP55A, pVP56K, and pFN18K vectors. The plasmid sequences were verified by DNA sequencing.

2.3 Protein Expression and Purification

For large-scale production of recombinant proteins, the pHis-MsMshB or pHisMBP-MtMshB plasmids were transformed into BL21(DE3) cells. Cells were grown in LB medium supplemented with ampicillin (100 μg/ml) or kanamycin (50 μg/ml) at 37 °C with shaking (250 rpm) until an OD_{600} of ~0.6 was reached. Protein expression was induced with the addition of 1 mM isopropyl β-D-thioga-lactopyranoside, the temperature was decreased to 25 °C, and the cells were incubated with shaking overnight. After 4 –14 h, cells were harvested by centrifugation, resuspended in Buffer A (30 mM HEPES, 150 mM NaCl, and 0.5 mM imidazole (pH 7.5)), and stored at -80 °C.

Cells were lysed using an EmulsiFlex-C3 high-pressure homogenizer (Avestin). The cell lysate was clarified by centrifugation (18,000 rpm, 4 °C) and loaded onto a pre-equilibrated (Buffer A) cobalt or nickel IMAC column (50 ml of chelating Sepharose (GE Healthcare) charged with $NiCl_2$ or $CoCl_2$). MshB was purified at 4 °C. The column was washed with 150 ml of Buffer A, and His-MshB or His-MBP-MshB was eluted using an imidazole step gradient (200 ml each of Buffer A + 10 mM imidazole, Buffer A + 25 mM imidazole, and Buffer A + 300 mM imidazole). Fractions containing His-MshB or His-MBP-MshB (via SDS-PAGE) were combined, concentrated (Amicon Ultra-15 centrifugal devices, Millipore), and dialyzed (SnakeSkin tubing, M_r cutoff of 10,000, Pierce) versus 2 × 4 liters of Buffer A overnight in the presence of His-TEV protease (300 μg/ml) to remove the His or His-MBP tag. The resulting TEV-cleaved protein was loaded onto a pre-equilibrated (Buffer A + 25 mM imidazole) cobalt or nickel IMAC column. His-MBP and His-TEV remain bound to the cobalt IMAC column, whereas

MshB eluted in the flow-through fraction. Fractions containing MshB (via 12% SDS-PAGE) were combined, concentrated, and dialyzed versus 2 × 4 liters of 25 mM HEPES and 1.5 mM TCEP (pH 7.5) (Slide-A-Lyzer, M_r cutoff of 10,000, Pierce). Protein concentration was determined using the Bradford Assay (Pierce or Sigma). Protein aliquots were flash-frozen in liquid nitrogen and stored at -80 °C. Protein identity was confirmed via mass spectroscopy (by Keith Ray and Rich Helm, Virginia Tech) following digest with trypsin and peptide sequencing (MALDI-TOF/ TOF). The resulting peptide sequences were analyzed using Matrix Science Mascot and confirmed the identity of MshB from *M. smegmatis* and *M. tuberculosis*, respectively, with peptide sequence coverage of 33% (MsMshB) and 44% (MtMshB).

2.4 Molecular Weight Determination

The solution molecular weight of MshB was examined using size exclusion chromatography (Fig. 2). (*31*) Purified enzyme was loaded onto a Superdex 200 10/300 GL column (GE Healthcare) pre-equilibrated with 50 mM sodium phosphate and 150 mM NaCl (pH 7.5). The elution volumes were used to calculate the K_{av} values ($K_{av} = (V_e - V_0)/(V_t - V_0)$, where V_0 is the void volume of the column, V_t is the total volume of the column, and V_e is the elution volume of the protein). A standard curve was prepared by plotting log M_r versus K_{av} using the following protein standards (GE Healthcare): aprotinin (6.5 kDa), ribonuclease A (13.7 kDa), carbonic anhydrase (29 kDa), ovalbumin (44 kDa), and conalbumin (75 kDa).

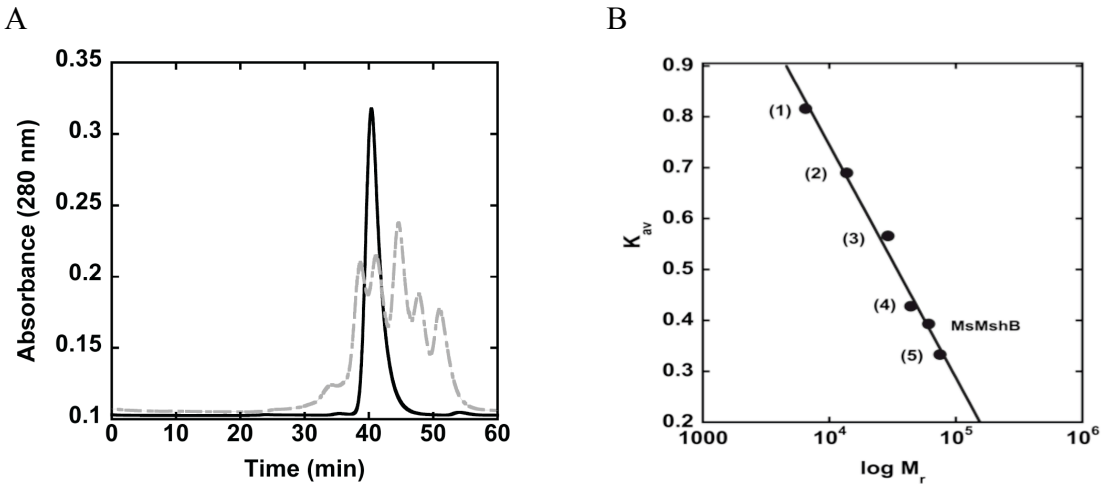

Figure 2: Solution molecular weight of MshB. (A) Chromatogram for apo-MshB (black line) elution. Chromatogram for standards represented by gray line. (B) The elution volume for aprotinin (1), ribonuclease A (2), carbonic anhydrase (3), ovalbumin (4), and conalbumin (5) were used to calculate the K_{av} values ($K_{av} = (V_e-V_0)/(V_t-V_0)$, where V_0 is the void volume of the column, V_t is the total volume of the column, and V_e is the elution volume of the protein.) The K_{av} value for MsMshB is also shown. These results suggest that MshB is a dimer in solution, consistent with previous reports *(16)*.

2.4 Preparation of Apo-MshB and Metal Reconstitution

As purified, MshB contains bound metal ions, and the metal ion content of purified MshB varies depending on the nature of the purification used. Consequently, for our studies, we prepared apo-MshB and then selectively reconstituted the enzyme with the desired metal ions. For the preparation of apo-MshB, purified protein (≤100 μM) was incubated with 10 mM HEPES, 20 mM dipicolinic acid, and 250 μM EDTA (pH 7.5) on ice. After 1 h, the protein solution was concentrated, washed (diluted with buffer and then concentrated) with 3 × 15 ml of 25 mM HEPES and 1.5 mM TCEP (pH 7.5), and run over a desalting column to remove residual dipicolinic acid/EDTA. Metal ion concentrations were determined using the ICS-3000 system. Apo-MshB samples contained ≤ 10% metal/protein (Table 1).

Table 1. Metal substitution of MshB

Metal Ion	$[Me^{2+}]/[MshB]$
Apo (after Co IMAC)	<0.01
Zn^{2+}	0.96 ± 0.02[1]
Co^{2+}	0.87 ± 0.12[1]
Mn^{2+}	0.94 ± 0.08[1]
Ni^{2+}	1.2 ± 0.1[1]
Cu^{2+}	0.29 ± 0.03[2]
Apo (after Ni IMAC)	0.2 ± 0.02

[1] Apo-MshB was incubated with 1 equiv. Me^{2+}
[2] Apo-MshB was incubated with 3 equiv. Cu^{2+}

Prior to activity measurements, apo-MshB (≤ 10 μM) was incubated with a stoichiometric concentration of the desired metal ion ($CoCl_2$, $FeCl_2$, $FeCl_3$, $MnCl_2$, $NiCl_2$, or $ZnSO_4$) and incubated on ice for 30 min. For experiments examining the optimal metal/protein ratio, apo-MshB was incubated with various concentrations of the desired metal ion (0 –20 μM) for 30 min on ice prior to activity assay.

2.5 MshB Deacetylase Activity

MshB deacetylase activity was measured with the substrate GlcNAc (Sigma) using a fluorescamine-based assay. (*32*) In general, assay mixtures containing 50 mM HEPES, 50 mM NaCl (pH 7.5), and 0 –150 mM GlcNAc were pre-equilibrated at 30 °C, and the reactions were initiated by the addition of enzyme (1 μM). For pH dependence experiments, the following buffers (all 50 mM containing 1 mM TCEP) were used: MES (pH 6 – 6.8), MOPS (pH 6.5–7.5), HEPES (pH 7.3–8.8), *N,N*-bis(2-hydroxyethyl)-glycine (pH 8–9), borate (pH 9–10), and carbonate (pH 10–11). After incubation for various times, reactions aliquots (30 μl) were quenched by the addition of 20% TCA (10 μl), and the cleared supernatant (25 μl) was transferred into a 96-well plate, diluted with

75 µl of 1 M borate (pH 9), and reacted with fluorescamine (30 µl in CH_3CN, Invitrogen). After 10 min, the fluorescence was measured (excitation, 395 nm; emission, 485 nm) using a SpectraMax M5^e plate reader (Molecular Devices). The initial rates of product formation (< 10%) were determined from these data. Equation 1 was fit to the pH-rate profile, where k_1 represents V/K at the pH optimum, and K_{a1} and K_{a2} represent the dissociation constants describing the two ionizations.

For determination of the steady-state parameters, deacetylase activity was measured at six to eight different concentrations of GlcNAc (0–150 mM), and the parameters k_{cat}, K_M, and k_{cat}/K_M were obtained by fitting the Michaelis-Menten equation to the initial linear velocities using the curve-fitting program KaleidaGraph (Synergy Software), which also calculates the asymptotic standard errors.

Equation. 1: $$V/K_{obs} = \frac{k_1}{\left(1 + \frac{[H^+]}{K_{a1}} + \frac{K_{a2}}{[H^+]}\right)}$$

2.5 UV-visible Spectrophotometry

Apo-MsMshB (1 µM) was incubated with 1 µM $FeCl_2$ or $ZnSO_4$ in an anaerobic glove box in 50 mM HEPES and 10 mM TCEP (pH7.5) for 30 min on ice to reconstitute the holoenzyme. The enzyme solutions were transferred to sealed anaerobic cuvettes (Precision Cells), and the UV-visible spectrum was recorded on an Agilent 8453 UV-visible spectrophotometer. The spectrum of the Zn^{2+}-MshB sample was subtracted from Fe^{2+}-MshB to account for background absorbance attributed to the protein. The absorbance difference spectrum for Fe^{2+}-MshB is shown in Fig. 4B.

2.6 HaloTag Pulldown Experiments

BL21(DE3) cells were transformed with pHalo-MshB and grown in chemically defined medium (100 ml) supplemented with kanamycin (50 μg/ml) at 37 °C with shaking (250 rpm) until an A600 of ~0.6 was reached. (*27*) Protein expression was induced by the addition of 1 mM isopropyl β-D-thiogalactopyranoside along with the addition of no added metals, 20 μM $ZnSO_4$, 20 μM ferric ammonium citrate, or both metal supplements, and the cells were incubated overnight (12–14 h) with shaking (250 rpm) at 25 °C. Cells were harvested by centrifugation and washed with 1 × 10 ml of 5 mM $CaCl_2$ and 2 × 10 ml of 10 mM MOPS (pH 7). Cell pellets were resuspended in 3 ml of pulldown buffer (40 mM MOPS, 150 mM NaCl, and 10 mM TCEP (pH 7.5)) and lysed by incubation with lysozyme (1 mg/ml) at room temperature for 15–30 min. For anaerobic experiments, washed cell pellets were transferred into an anaerobic chamber prior to resuspension in pulldown buffer. The cell lysate was cleared by centrifugation (15,000 rpm, 25–30 min) and then incubated with 150 μl of HaloLink™ resin (pre-equilibrated in pulldown buffer, Promega) for 30 min. HaloLink™ resin was washed with pulldown buffer (5 × 500 μl), resuspended in 250 μl of pulldown buffer containing TEV protease (5 units/μl), and incubated at 37 °C for 45-60 min. The TEV protease expressed and purified in our laboratory was dialyzed against an EDTA-containing buffer and therefore has a low metal content (< 0.001 metal ion/protein). Cleaved MshB was separated from the resin by centrifugation (13,200 rpm, 2 min). The concentrations of metal ions were determined using the ICS-3000 system, and the concentration of MshB was determined using the Bradford assay.

2.7 Metal Ion Affinity Experiments

The affinity of MshB for Zn(II) was determined using ultrafiltration as described for LpxC deacetylase. (*33*) Briefly, apo-MshB (1 μM) was incubated in a metal ion and pH buffer containing 1 mM nitrilotriacetic acid, 5 mM MOPS (pH 7), and 0-0.5 mM total zinc (0-3.3 nM free zinc) at 30 °C for ≥ 25 min. Free and bound metal ions were separated by centrifugation (1500 relative centrifugal force, 5 min), and the concentration of metal ions (filtrate and retentate) was determined using ion chromatography. The $K_D^{Zn(II)}$ value was determined by fitting a binding isotherm to these data.

The affinity of MshB for Fe(II) was determined by measuring the catalytic activity of MshB in the presence of varying concentrations of free Fe(II). Apo-MshB (1 μM) was incubated in a metal ion and pH buffer containing 1 mM nitrilotriacetic acid, 5 mM MOPS (pH 7), and 0 –950 μM total Fe(II) (0 –2.6 μM free Fe(II)) at 30 °C for ≥ 30 min in an anaerobic chamber. Activity assays were carried out as described above using 50 mM GlcNAc and 1 μM MshB. The $K_D^{Fe(II)}$ value was determined by fitting a binding isotherm to these data.

2.8 Metal Ion Dissociation Rate Constants

The first-order rate constant for metal ion dissociation from MshB was measured by determining the time-dependent loss of activity upon incubation of MshB with the chelator EDTA. Zn^{2+}-MshB or Fe^{2+}-MshB (50 μM) was diluted into assay buffer (50 mM HEPES, 50 mM NaCl, and 1 mM TCEP (pH 7.5)) containing 1 mM EDTA and incubated at 30 °C. After various times (0 -200 min), an aliquot of enzyme was diluted 100-fold into assay buffer containing 20 mM GlcNAc, and the activity was measured as

described above. A single exponential decay was fit to the initial rates as a function of time to obtain the k_{off} value.

3. Results

3.1 MshB is a Mononuclear Metalloenzyme

MshB was previously shown to undergo reversible inhibition by treatment with 1,10-phenanthroline, demonstrating that MshB is a metalloenzyme. (*16, 28*) However, determination of whether MshB is a mononuclear or binuclear metalloenzyme was not examined. Because Zn^{2+} is proposed to be the native cofactor for MshB, we examined the effect of varying the Zn^{2+} / MshB ratio on catalytic activity (Fig. 3A). The results from these experiments demonstrate that MshB was maximally active with ~1 Zn^{2+} ion/MshB, indicating that MshB is a mononuclear metalloenzyme. This finding is consistent with the crystal structure of MshB that reveals a single bound zinc ion in the active site (Fig. 1B). (*28*) Experiments on the titration of Fe^{2+} and Co^{2+} with MshB are also consistent with a mononuclear metalloenzyme (Fig. 4A).

3.2 The pH Dependent activity is Bell-shaped

The MshB-catalyzed reaction (*V/K* conditions) exhibits a bell-shaped dependence on pH, indicating that there are two ionizations that are important for maximal catalytic activity (Fig. 3B) with observed pK_a values of 7.3 and 10.4 for Zn^{2+}-MshB. These results are consistent with MshB proceeding through either a single bifunctional GABC or a GABC pair mechanism, as observed for other metal-dependent deacetylases. (*19*)

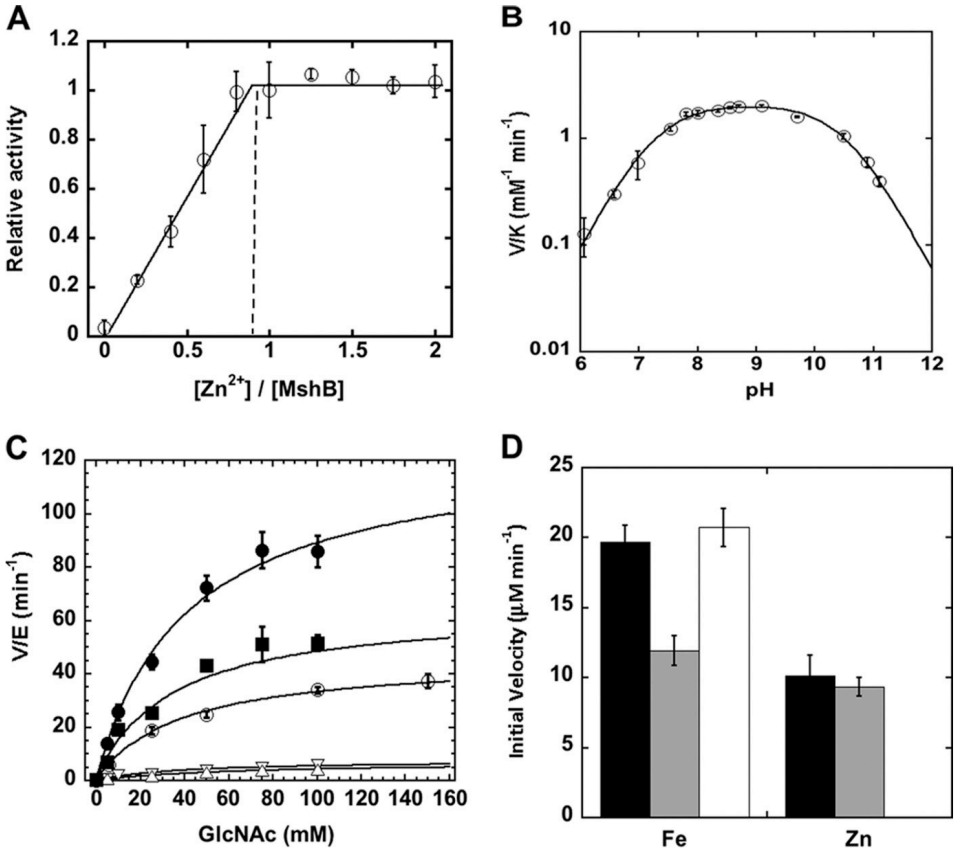

Figure 3. Catalytic activity of MshB. (A), activation of apo-MshB with (○) Zn^{2+}. Deacetylase activity was measured as a function of zinc/MshB stoichiometry. Apo-MshB was incubated with 0–2 eq of Zn^{2+}. After 30 min, the enzyme was diluted into assay buffer containing the substrate GlcNAc (50 mM), and the resulting deacetylase activity was measured at 30 °C. (B), pH dependence of the Zn^{2+}-MshB catalyzed reaction. The *V/K* values were measured at 30 °C using subsaturating concentrations of GlcNAc (5mM). (C), steady-state turnover catalyzed by metal-substituted MshB: (▽) apo-MshB, (■) Co^{2+}, (○) Zn^{2+}, (●) Fe^{2+}, (△) Fe^{3+}. Apo-MshB was incubated with stoichiometric amounts of metal ions. The initial rates for the deacetylation of GlcNAc (0–150 mM) were measured at 30 °C. The steady-state parameters k_{cat}, K_M, and k_{cat}/K_M (Table 1) were obtained by fitting the Michaelis-Menten equation to the initial rates. (D), Fe^{2+}-MshB activity is air-sensitive. Apo-MshB was reconstituted with Fe^{2+} or Zn^{2+}, and the resulting deacetylase activity was measured at 30 °C at t = 0 (anaerobic; black bars). The enzyme was then either exposed to aerobic conditions for 3 h (gray bars) or kept under anaerobic conditions for 3 h (white bars), and the resulting deacetylase activity was measured using the substrate GlcNAc (50 mM).

3.3 Fe^{2+}-MshB Exhibits the Highest Activity

In previous experiments, the steady-state parameters for Zn^{2+}-MshB were determined using the substrates GlcNAc-Ins, monobromobimane S-conjugated MSH, and bimane S-conjugated Cys-GlcN-Ins. (*16*) Although it was stated that the activity of apo-MshB could be restored with Zn^{2+}, Ni^{2+}, Mn^{2+}, or Co^{2+}, no specific values for the rate enhancements observed were reported, and the steady-state parameters for MshB activity were provided only for Zn^{2+}-MshB. Because information about the chemical mechanism can be gained from the relative changes in activity upon reconstitution with different metal ions and Fe^{2+} had not been previously examined as a potential cofactor, we determined the steady-state parameters for MshB substituted with different metal ions (Fig. 3C and Table 3). We chose to use the commercially available substrate GlcNAc in these experiments. GlcNAc has a weakened affinity for MshB compared with GlcNAc-Ins; however, the group that undergoes hydrolysis in these two substrates is the same. (*16, 32*)

Table 2. Steady-state parameters of Me^{2+}-MshB variants with GlcNAc
Apo-MshB was incubated with stoichiometric metal for 45 min prior to activity measurement. The substrate used was GlcNAc.

	K_m	k_{cat}	k_{cat}/K_m
	mM	s^{-1}	$M^{-1}\,s^{-1}$
Apo-MshB	36 ± 7	0.13 ± 0.01	3.5 ± 0.3
Co^{2+}-MshB	34 ± 5	1.1 ± 0.08	32 ± 2
Fe^{2+}-MshB	41 ± 5	2.1 ± 0.15	52 ± 3
Fe^{3+}-MshB	56 ± 13	0.11 ± 0.01	1.8 ± 0.3
Mn^{2+}-MshB	54 ± 13	0.38 ± 0.04	7.0 ± 1.0
Ni^{2+}-MshB	53 ± 14	0.27 ± 0.03	5.3 ± 0.8
Zn^{2}-MshB[a]	38 ± 4	0.77 ± 0.04	20 ± 1

[a] Data were adapted from Ref. 32. For comparison, substrate = GlcNAc-Ins, K_m = 340 ± 80 μM, k_{cat} = 0.49 ± 0.04 s^{-1}, k_{cat}/K_m = 1440 ± 360 M^{-1} s^{-1} as reported previously (16).

The relative ability of various metal ions to activate MshB was measured. In these experiments, apo-MshB was reconstituted (stoichiometric) with the metal ion of interest, and the initial rates of product formation were measured at different substrate concentrations. Interestingly, we observed that MshB exhibited the highest activity with Fe^{2+} (Fig. 3C), with the overall trend $Fe^{2+} > Co^{2+} > Zn^{2+} > Mn^{2+}$ and Ni^{2+}. A closer examination of the steady-state parameters (Table 3) revealed that changes to the identity of the catalytic cofactor had only a minor effect on K_M (< 2-fold), with much larger effects on k_{cat} (8-fold) and k_{cat}/K_M (~10-fold).

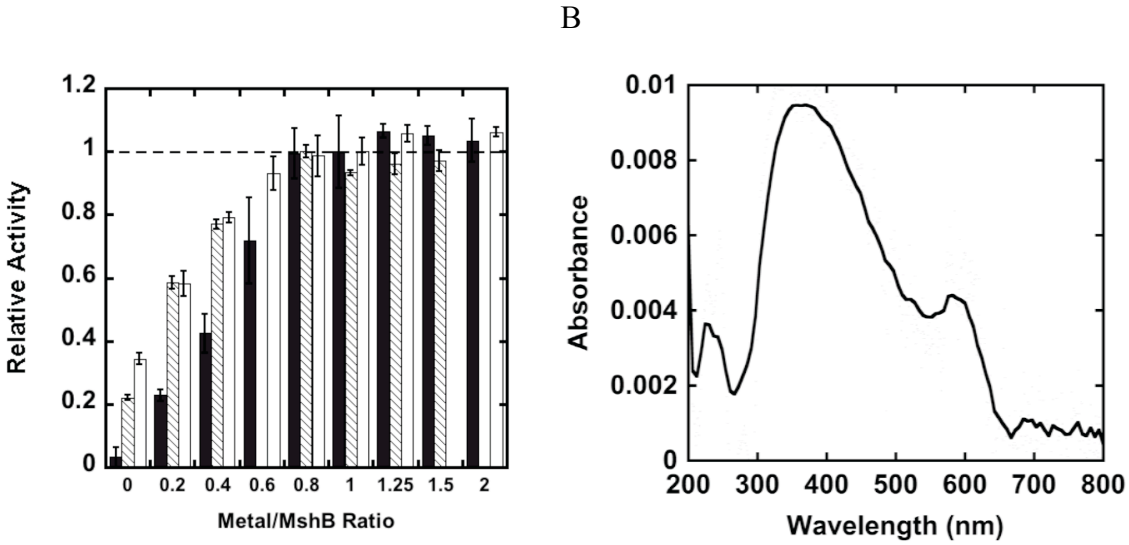

Figure 4: Characterization of Fe^{2+}-MshB. (A), Activation of apo-MshB with Zn^{2+} (black bars), Fe^{2+} (hatched bars) and Co^{2+} (white bars). Deacetylase activity was measured as a function of Me^{2+}/MshB stoichiometry. Apo-MshB was incubated with varying equivalents of Me^{2+} (0-2). After 30 minutes, the enzyme was diluted into assay buffer containing substrate GlcNAc (50 mM) and the resulting deacetylase activity was measured at 30 °C. (B) Absorbance difference spectrum of Fe^{2+}-MshB. Apo-MshB (1 μM) was reconstituted with stoichiometric concentrations of Zn^{2+} or Fe^{2+} in an aerobic chamber, the enzyme solutions transferred into sealed anaerobic cuvettes, and the UV-Vis spectrum recorded. The spectrum of the Zn^{2+}-MshB sample was subtracted from the Fe^{2+}-MshB sample to obtain the absorbance difference spectrum. The Fe^{2+}- MshB difference spectrum has a broad peak with a maximum at 362 nm (ε = 9520 $M^{-1}cm^{-1}$) and shoulder at 580 nm (ε = 4390 $M^{-1}cm^{-1}$).

3.4 Characterization of Fe^{2+}-MshB

To confirm that the activation of MshB was specific for Fe^{2+} and not Fe^{3+}, we measured the ability of Fe^{3+} to activate apo-MshB. The results in Fig. 3C indicate that the activity of Fe^{3+}-MshB was comparable with that of apo-MshB (at stoichiometric metal/enzyme), suggesting that Fe^{3+} is not an efficient catalyst. Additionally, we examined the effect of oxygen on the activity of Fe^{2+}-MshB. Results from these experiments (Fig. 3D) show that there was a time-dependent loss of activity for Fe^{2+}-MshB under aerobic conditions, whereas the activity of Fe^{2+}-MshB under anaerobic conditions was stable over a similar period of time. In contrast, the activity of Zn^{2+}-MshB was stable under aerobic conditions. We also examined the absorbance spectrum of Fe^{2+}-MshB. The Fe^{2+}-MshB difference spectrum has a broad peak at 362 nm, consistent with an iron-containing enzyme. (Fig. 4B)

3.5 The Cofactor Bound to MshB is Dependent on Environmental Conditions

Native cofactor identification is defined in large part by the metal ion that copurifies with the enzyme. (*19*) Therefore, we developed a method that would allow us to rapidly purify MshB under various conditions using the HaloTag® technology. The HaloTag does not bind metal ions, and its rapid nature should prevent re-equilibration or switching of bound cofactors during the purification process.

Because previous experiments examining the identity of the cofactor bound to MshB relied on nickel or zinc IMAC purification (*16*), which artificially introduce metal ions, we initially expressed MshB in LB medium and examined the cofactor bound to purified MshB under aerobic conditions using the HaloTag approach (Fig. 5). Under

these conditions, MshB was isolated with Zn^{2+} as the predominant bound cofactor, consistent with what has been observed following zinc IMAC purification (*16*).

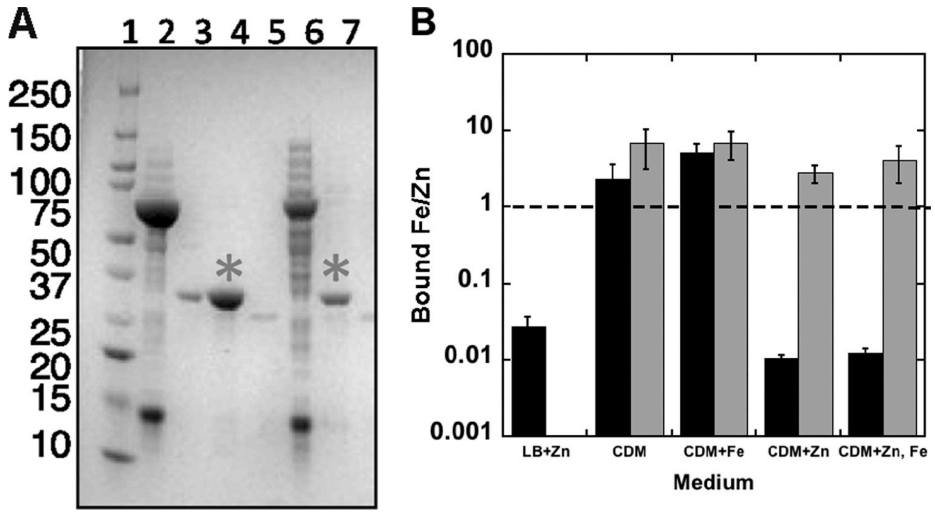

Figure 5. Metal ion content of recombinant MshB isolated from *Escherichia coli* in HaloTag pulldown experiments. pHalo-MshB-transformed *E. coli* BL21(DE3) cells were grown in LB medium or chemically defined medium (CDM) and induced with 1mM IPTG with or without iron or zinc supplementation (20 μM). MshB was purified in HaloTag pulldown experiments under aerobic and anaerobic conditions. (A), purification of MshB using HaloTag. An aliquot of protein at each step of the purification was analyzed on a 12% SDS-PAGE. Lane 1, M_r marker; lanes 2 and 6, cleared cell lysates containing HaloTag fusion proteins (MsMshB and MtMshB, respectively); lane 3, positive control (MshB); lanes 4 and 7, pulldown supernatant after TEV cleavage (*; MsMshB and MtMshB, respectively); lane 5, TEV-only control. (B), the iron/zinc ratio of metal ions bound to MshB following aerobic (black bars) and anaerobic (gray bars) purification was determined by ion chromatography.

We also probed what happened to the identity of the cofactor bound to MshB when the protein was expressed under more stringent (metal ion) conditions. In these experiments, MshB was expressed in chemically defined medium with or without zinc and/or iron supplementation to examine the effect that metal ion availability in the surrounding environment has on the identity of the bound cofactor, and MshB was purified under anaerobic and aerobic conditions to probe the effect of oxygen on the bound cofactor. Results from these experiments (Fig. 5B) clearly indicate a strong

preference for the Fe^{2+} cofactor under anaerobic conditions, regardless of the metal ion content of the medium. Additionally, these results suggest that the preferred cofactor changes between Zn^{2+} and Fe^{2+} depending on the metal ion content of the medium when MshB is purified under aerobic conditions. Because we used ion chromatography to measure the metal ions bound to MshB, we know that the iron bound to MshB is Fe^{2+} and not Fe^{3+}, as these ions elute at different retention times.

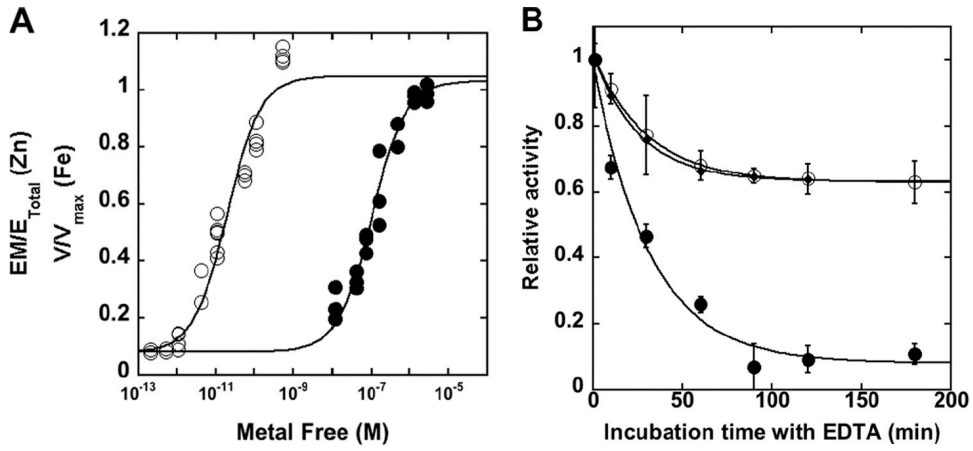

Figure 6. Properties of metal ion binding to MshB. **(**A), metal ion affinity of MshB for Zn^{2+} (○) and Fe^{2+} (●). Apo-MshB was equilibrated with buffered metal ion solutions (5 mM MOPS and 1 mM nitrilotriacetic acid (pH 7)). The fraction-bound zinc was determined by ultrafiltration and ion chromatography analysis, and the fraction-bound iron was determined by enhancement of MshB deacetylase activity using GlcNAc substrate (50 mM). A binding isotherm was fit to the resulting data to obtain $K_D^{Zn(II)}$ and $K_D^{Fe(II)}$ values (Table 2). (B), metal ion dissociation from MshB. Holo-MshB reconstituted with Zn^{2+} (○) or Fe^{2+} (●) was incubated in assay buffer (50 mM HEPES, 50 mM NaCl, and 1 mM TCEP (pH 7.5)) containing 1 mM EDTA or 5 mM EDTA (◆; Zn^{2+}). At various times, the enzyme was diluted into assay buffer containing GlcNAc (50 mM), and the deacetylase activity was measured at 30 °C. The k_{off} values (Table 2) were obtained by fitting a single exponential decay equation to these data. E_M/E_{Total}, fraction of enzyme containing a bound metal ion; E_M, enzyme-metal complex; E_{Total}, enzyme total.

3.6 Zn^{2+} Has a Higher Affinity than Fe^{2+} for MshB

To determine whether the preference we observed in the pulldown experiments could be explained by a higher affinity of iron for MshB, we measured the affinity of

Zn^{2+} and Fe^{2+} for MshB. The results from these experiments (Fig. 6 and Table 4) show that Zn^{2+} has an ~5300-fold higher affinity for MshB compared with Fe^{2+}, with K_D^{metal} values of 0.02 and 106 nM for Zn^{2+} and Fe^{2+}, respectively.

Table 3. Metal binding properties of MshB

	K_D [a]	k_{off}	k_{on} [b]
	nM	min^{-1}	$M^{-1}\,s^{-1}$
Fe^{2+}-MshB	106 ± 15	0.032 ± 0.006	5.0×10^3
Zn^{2+}-MshB	0.02 ± 0.004	0.033 ± 0.001	2.8×10^7

[a] The affinity of MshB for Zn^{2+} and Fe^{2+} was determined using ultrafiltration or activity measurements in metal ion-buffered solutions at 30 °C as described under "Materials and Methods."

[b] The association rate constants (k_{on} values) for Zn^{2+} and Fe^{2+} were calculated from the K_D and k_{off} values.

To gain insights into whether the observed differences in metal ion affinity for MshB were due to differences in metal ion association and/or dissociation, we measured the dissociation constants for Zn^{2+} and Fe^{2+} from MshB (Table 4). The results from these experiments indicate that the dissociation of Zn^{2+} and Fe^{2+} from MshB was comparable (~0.03 min^{-1}). Consequently, the differences in the K_D values are due to the faster association rate constant for Zn^{2+} compared with Fe^{2+}, which were calculated ($K_D = k_{off}/k_{on}$) to be 2.8×10^7 and 5.0×10^3 M^{-1} s^{-1}, respectively.

4. Discussion

4.1 MshB Is Most Active with the Fe^{2+} Cofactor

The data presented here indicate that MshB functions as a mononuclear metallohydrolase (Fig. 3A). The activity of MshB follows the trend $Fe^{2+} > Co^{2+} > Zn^{2+} > Mn^{2+}$ and Ni^{2+}, which is inversely related to the Lewis acidity of the metals (with the

exception of Mn^{2+}). The finding that the highest activity was with Fe^{2+}-MshB is the first evidence to suggest that MshB may not be an exclusive Zn^{2+}-dependent enzyme as previously reported and raises the possibility that Fe^{2+} may function as a biologically relevant cofactor, thereby making MshB a cambialistic enzyme. Consistent with these data, we observed that MshB copurified with Fe^{2+} and Zn^{2+} when expressed in chemically defined medium (lacking metal ion supplementation).

We measured the steady-state parameters for MshB reconstituted with various metal ions. The results from these experiments indicate that there is no significant effect on K_M, which may suggest that substrate binding is not affected by changes in the identity of the metal ion. Significantly larger effects were observed on k_{cat} and k_{cat} / K_M, suggesting that the rate of the chemical step may be altered by changes to the catalytic metal ion, as expected for a metallohydrolase.

4.2 Fe^{2+}-MshB May Be Subject to Redox Regulation

The activity observed upon activation with iron is due to Fe^{2+}, not Fe^{3+}, for the following reasons: 1) Fe^{3+} could not restore activity to apo-MshB (Fig. 3C); 2) a time-dependent decrease in activity was observed for Fe^{2+}-MshB under aerobic conditions (Fig. 3D), consistent with oxidation of Fe^{2+} to Fe^{3+}; and 3) MshB copurified with Fe^{2+}, not Fe^{3+} (Fig. 5B). These results suggest that the biological activity of Fe^{2+}-MshB may be regulated by redox changes in the surrounding environment. This possibility may have biological implications for pathogenic mycobacteria that reside inside macrophages, where they are subject to oxidative bursts upon (macrophage) activation.

4.3 Cofactor Preferences Are Determined by Metal Ion Availability

We examined the cofactor preferences of MshB for the first time by expressing the protein under conditions of varying metal ion availability and purifying the protein under anaerobic conditions using a new purification protocol that relies on the HaloTag rather than IMAC purification. We observed that MshB preferred Fe^{2+} when isolated under anaerobic conditions, regardless of the metal ion content of the medium used to grow the cells (Fig. 5B). Additionally, we found that the cofactor bound to MshB under aerobic conditions switched between Zn^{2+} and Fe^{2+} depending on the metal ion availability of the medium used during the protein expression. Similar results were observed with the metal-dependent deacetylase LpxC. (*27*) In light of the observed activity data for MshB and LpxC, these results imply that at least a subset of metallohydrolases may be cambialistic enzymes that utilize multiple cofactors in vivo and can use metal (cofactor) switching as a mechanism for regulation of enzyme activity in response to changing environmental conditions.

The affinity of MshB for Zn^{2+} was ~5300-fold greater than for Fe^{2+} (Table 4), indicating that the observed metal ion preferences are not dictated solely by metal ion affinity. Instead, the observed preference for Fe^{2+} under anaerobic conditions appears to be dictated by the greater availability of free iron versus free zinc (estimated 10 - 400 pM Zn^{2+} and 0.2– 6 μM Fe^{2+}) (*27*). Interestingly, the dissociation rate constants for Fe(II) and Zn(II) are comparable (0.03 min^{-1}), suggesting that the observed differences in affinity are attributed primarily to metal ion association with MshB. It should be pointed out that the dissociation of Zn(II) from MshB does not go to an end point of zero.

Similar findings have been reported for carboxy-peptidase A (*34, 35*), carbonic anhydrase (*36*), and, to some extent, LpxC (*27*) and may suggest that a fraction of the active site Zn(II) dissociates more rapidly. Although the association rate constant for Zn(II) with MshB approaches that of a diffusion-controlled process (2.8×10^7 M^{-1} s^{-1}), the association rate constant for Fe(II) is much slower than a diffusion-controlled process (5×10^3 M^{-1} s^{-1}) and is more consistent with a two-step binding mechanism. Two-step binding mechanisms have been used to describe Zn(II) binding to carbonic anhydrase (*37*) and Fe(II) binding to LpxC (*27*).

4.4 Significance of an Iron/Zinc Cambialistic MshB

The results suggesting that MshB may be a cambialistic enzyme that can utilize either Fe^{2+} or Zn^{2+} as a cofactor are also interesting in light of the changes in zinc and iron that occur in the mycobacterial environment (vacuoles of infected macrophages) during the course of infection. Metal imaging experiments were used to visualize changes in metal ion concentrations that occur in macrophages both following infection with mycobacteria and after activation of the infected macrophages. (*38*) Results from these experiments indicate that the vacuoles (markers for the location of mycobacteria) of macrophages infected with *M. tuberculosis* contain a much higher concentration of iron (3 mM) compared with zinc (450 μM). Furthermore, the results from these experiments indicate that zinc and iron are the only divalent metal ions that undergo significant changes in concentration during the course of infection. Activation of macrophages infected with *Mycobacterium avium* by TNF-α leads to a significant increase in zinc (from 0.12 to 1.8 mM) and decrease in iron (from 1.2 to 0.27 mM) in the vacuoles.

These dynamic changes to the iron/zinc concentrations in the mycobacterial environment during the course of infection may have a large impact on metalloenzymes whose activity is altered by changes in zinc and iron concentrations, such as MshB. Furthermore, the ability of MshB to function as an iron/zinc cambialistic enzyme would enable MshB to adapt to changing environmental conditions, such as those encountered in the macrophages, and allow the organism to continue producing MSH throughout the course of infection when large changes in iron/zinc concentrations occur. This could be one key factor that aids mycobacterial survival inside the macrophages. Additionally, these results suggest that biologically effective inhibitors will need to dually target Fe^{2+}-MshB and Zn^{2+}-MshB.

References

1. Newton, G. L., Buchmeier, N., and Fahey, R. C. (2008) Biosynthesis and functions of mycothiol, the unique protective thiol of Actinobacteria, *Microbiol Mol Biol Rev 72*, 471-494.
2. Jothivasan, V. K., and Hamilton, C. J. (2008) Mycothiol: synthesis, biosynthesis and biological functions of the major low molecular weight thiol in actinomycetes, *Nat Prod Rep 25*, 1091-1117.
3. Rawat, M., and Av-Gay, Y. (2007) Mycothiol-dependent proteins in actinomycetes, *FEMS Microbiol Rev 31*, 278-292.
4. Fan, F., Vetting, M. W., Frantom, P. A., and Blanchard, J. S. (2009) Structures and mechanisms of the mycothiol biosynthetic enzymes, *Curr Opin Chem Biol 13*, 451-459.

5. Gutierrez-Lugo, M. T., Baker, H., Shiloach, J., Boshoff, H., and Bewley, C. A. (2009) Dequalinium, a new inhibitor of Mycobacterium tuberculosis mycothiol ligase identified by high-throughput screening, *J Biomol Screen 14*, 643-652.

6. Gammon, D. W., Steenkamp, D. J., Mavumengwana, V., Marakalala, M. J., Mudzunga, T. T., Hunter, R., and Munyololo, M. (2010) Conjugates of plumbagin and phenyl-2-amino-1-thioglucoside inhibit MshB, a deacetylase involved in the biosynthesis of mycothiol, *Bioorg Med Chem 18*, 2501-2514.

7. Gutierrez-Lugo, M. T., and Bewley, C. A. (2008) Natural products, small molecules, and genetics in tuberculosis drug development, *J Med Chem 51*, 2606-2612.

8. Metaferia, B. B., Fetterolf, B. J., Shazad-Ul-Hussan, S., Moravec, M., Smith, J. A., Ray, S., Gutierrez-Lugo, M. T., and Bewley, C. A. (2007) Synthesis of natural product-inspired inhibitors of Mycobacterium tuberculosis mycothiol-associated enzymes: the first inhibitors of GlcNAc-Ins deacetylase, *J Med Chem 50*, 6326-6336.

9. Nicholas, G. M., Eckman, L. L., Newton, G. L., Fahey, R. C., Ray, S., and Bewley, C. A. (2003) Inhibition and kinetics of mycobacterium tuberculosis and mycobacterium smegmatis mycothiol-S-conjugate amidase by natural product inhibitors, *Bioorg Med Chem 11*, 601-608.

10. Bhave, D. P., Muse, W. B., 3rd, and Carroll, K. S. (2007) Drug targets in mycobacterial sulfur metabolism, *Infect Disord Drug Targets 7*, 140-158.

11. Newton, G. L., Av-Gay, Y., and Fahey, R. C. (2000) N-Acetyl-1-D-myo-inosityl-2-amino-2-deoxy-alpha-D-glucopyranoside deacetylase (MshB) is a key enzyme in mycothiol biosynthesis, *J Bacteriol 182*, 6958-6963.

12. Supuran, C. T. (2010) Carbonic anhydrase inhibitors, *Bioorg Med Chem Lett 20*, 3467-3474.

13. Lia, N. G., Shib, Z. H., Tang, Y. P., and Duan, J. A. (2009) Selective matrix metalloproteinase inhibitors for cancer, *Curr Med Chem 16*, 3805-3827.

14. Drag, M., and Salvesen, G. S. (2010) Emerging principles in protease-based drug discovery, *Nat Rev Drug Discov 9*, 690-701.

15. White, R. J., Margolis, P. S., Trias, J., and Yuan, Z. (2003) Targeting metalloenzymes: a strategy that works, *Curr Opin Pharmacol 3*, 502-507.

16. Newton, G. L., Ko, M., Ta, P., Av-Gay, Y., and Fahey, R. C. (2006) Purification and characterization of Mycobacterium tuberculosis 1D-myo-inosityl-2-acetamido-2-deoxy-alpha-D-glucopyranoside deacetylase, MshB, a mycothiol biosynthetic enzyme, *Protein Expr Purif 47*, 542-550.

17. Steffek, M., Newton, G. L., Av-Gay, Y., and Fahey, R. C. (2003) Characterization of Mycobacterium tuberculosis mycothiol S-conjugate amidase, *Biochemistry 42*, 12067-12076.

18. Nicholas, G. M., Eckman, L. L., Kovac, P., Otero-Quintero, S., and Bewley, C. A. (2003) Synthesis of 1-D- and 1-L-myo-inosityl 2-N-acetamido-2-deoxy-alpha-D-glucopyranoside establishes substrate specificity of the Mycobacterium tuberculosis enzyme AcGI deacetylase, *Bioorg Med Chem 11*, 2641-2647.

19. Hernick, M., and Fierke, C. A. (2010) Mechanisms of metal-dependent hydrolases in metabolism, In *Comprehensive Natural Products II* (Mander, L. N., and Lui, H.-W. B., Eds.), pp 547-581, Elsevier.

20. Groche, D., Becker, A., Schlichting, I., Kabsch, W., Schultz, S., and Wagner, A. F. V. (1998) Isolation and crystallization of functionally competent Escherichia coli peptide deformylase forms containing either iron or nickel in the active site, *Biochemical and Biophysical Research Communications 246*, 342-346.

21. Rajagopalan, P. T. R., Yu, X. C., and Pei, D. H. (1997) Peptide deformylase: A new type of mononuclear iron protein, *Journal of the American Chemical Society 119*, 12418-12419.

22. Rajagopalan, P. T., and Pei, D. (1998) Oxygen-mediated inactivation of peptide deformylase, *Journal of Biological Chemistry 273*, 22305-22310.

23. Ragusa, S., Blanquet, S., and Meinnel, T. (1998) Control of peptide deformylase activity by metal cations *Journal of Molecular Biology 280*, 515-523.

24. Zhu, J. G., Dizin, E., Hu, X. B., Wavreille, A. S., Park, J., and Pei, D. H. (2003) S-ribosylhomocysteinase (LuxS) is a mononuclear iron protein, *Biochemistry 42*, 4717-4726.

25. Gantt, S. L., Gattis, S. G., and Fierke, C. A. (2006) Catalytic Activity and Inhibition of Human Histone Deacetylase 8 Is Dependent on the Identity of the Active Site Metal Ion, *Biochemistry 45*, 6170-6178.

26. Hernick, M., Gattis, S. G., Penner-Hahn, J. E., and Fierke, C. A. (2010) Activation of Escherichia coli UDP-3-O-[(R)-3-hydroxymyristoyl]-N-

acetylglucosamine Deacetylase by Fe2+ Yields a More Efficient Enzyme with Altered Ligand Affinity, *Biochemistry 49*, 2246-2255.

27. Gattis, S. G., Hernick, M., and Fierke, C. A. (2010) Active site metal ion in UDP-3-O-((R)-3-hydroxymyristoyl)-N-acetylglucosamine deacetylase (LpxC) switches between Fe(II) and Zn(II) depending on cellular conditions, *J Biol Chem 285*, 33788-33796.

28. Maynes, J. T., Garen, C., Cherney, M. M., Newton, G., Arad, D., Av-Gay, Y., Fahey, R. C., and James, M. N. G. (2003) The crystal structure of 1-D-myo-inosityl-2-acetamido-2-deoxy-alpha-D-glucopyranoside deacetylase (MshB) from Mycobacterium tuberculosis reveals a zinc hydrolase with a lactate dehydrogenase fold, *Journal of Biological Chemistry 278*, 47166-47170.

29. Sobrado, P., Goren, M. A., James, D., Amundson, C. K., and Fox, B. G. (2008) A Protein Structure Initiative approach to expression, purification, and in situ delivery of human cytochrome b5 to membrane vesicles, *Protein Expression and Purification 58*, 229-241.

30. Blommel, P. G., and Fox, B. G. (2007) A combined approach to improving large-scale production of tobacco etch virus protease, *Protein Expression and Purification 55*, 53-68.

31. Andrews, P. (1964) Estimation of the molecular weights of proteins by Sephadex gel-filtration, *Biochem. J. 91*, 222-233.

32. Huang, X., and Hernick, M. (2011) A fluorescence-based assay for measuring N-acetyl-1-D-myo-inosityl-2-amino-2-deoxy-alpha-D-glucopyranoside deacetylase activity, *Anal Biochem 414*, 278-281.

33. Gattis, S. G., Hernick, M., and Fierke, C. A. (2010) The active site metal ion in UDP-3-O-(R-3-hydroxymyristoyl)-N-acetylglucosamine deacetylase (LpxC) switches between Fe(II) and Zn(II) depending on cellular conditions, *Journal of Biological Chemistry 285*, 33788-33796.

34. Chong, C. R., and Auld, D. S. (2000) Inhibition of carboxypeptidase A by D-penicillamine: mechanism and implications for drug design, *Biochemistry 39*, 7580-7588.

35. Chong, C. R., and Auld, D. S. (2007) Catalysis of zinc transfer by D-penicillamine to secondary chelators, *J Med Chem 50*, 5524-5527.

36. Huang, C. C., Lesburg, C. A., Kiefer, L. L., Fierke, C. A., and Christianson, D. W. (1996) Reversal of the hydrogen bond to zinc ligand histidine-119 dramatically diminishes catalysis and enhances metal equilibration kinetics in carbonic anhydrase II, *Biochemistry 35*, 3439-3446.

37. Kiefer, L. L., and Fierke, C. A. (1994) Functional characterization of human carbonic anhydrase II variants with altered zinc binding sites, *Biochemistry 33*, 15233-15240.

38. Wagner, D., Maser, J., Lai, B., Cai, Z., Barry, C. E., 3rd, Honer Zu Bentrup, K., Russell, D. G., and Bermudez, L. E. (2005) Elemental analysis of Mycobacterium avium-, Mycobacterium tuberculosis-, and Mycobacterium smegmatis-containing phagosomes indicates pathogen-induced microenvironments within the host cell's endosomal system, *J Immunol 174*, 1491-1500.

Chapter 6

Examination of catalytic mechanism of MshB reveals unexpected role for a dynamic tyrosine

Reproduced with permission from: Huang, X. and Hernick, M. "Examination of mechanism of *N*-acetyl-1-D-*myo*-inosityl-2-amino-2-deoxy-alpha-D-glucopyranoside deacetylase (MshB) reveals unexpected role for dynamic tyrosine." J Biol Chem, 2012. 287(13): p. 10424-34. Copyright permission from the American Society for Biochemistry and Molecular Biology.

Author Contributions
Xinyi Huang performed all the experiments and wrote the article
Marcy Hernick directed the research and wrote the article

Abstract

Actinomycetes are a group of Gram-positive bacteria that includes pathogenic mycobacterial species, such as *Mycobacterium tuberculosis*. These organisms do not have glutathione and instead utilize the small molecule mycothiol (MSH) as their primary reducing agent and for the detoxification of xenobiotics. Due to these important functions, enzymes involved in MSH biosynthesis and MSH-dependent detoxification are targets for drug development. The metal-dependent deacetylase *N*-acetyl-1-D-*myo*-inosityl-2-amino-2-deoxy-α-D-glucopyranoside deacetylase (MshB) catalyzes the hydrolysis of *N*-acetyl-1-D-*myo*-inosityl-2-amino-2-deoxy-α-D-glucopyranoside to form 1-D-*myo*-inosityl-2-amino-2-deoxy-α-D-glucopyranoside and acetate in MSH biosynthesis. Herein we examine the chemical mechanism of MshB. We demonstrate that the side chains of Asp-15, Tyr-142, His-144, and Asp-146 are important for catalytic activity. We show that NaF is an uncompetitive inhibitor of MshB, consistent with a metal-water/hydroxide functioning as the reactive nucleophile in the catalytic

mechanism. The MshB activity has a bell-shaped dependence on pH with pK_a values of 7.3 and 10.5, and mutagenesis experiments indicate that the observed pK_a values reflect ionization of Asp-15 and Tyr-142, respectively. Together, findings from our studies suggest that MshB functions through a general acid-base pair mechanism with the side chain of Asp-15 functioning as the general base catalyst and His-144 serving as the general acid catalyst, whereas the side chain of Tyr-142 probably assists in polarizing substrate/ stabilizing the oxyanion intermediate. Additionally, our results indicate that Tyr-142 is a dynamic side chain that plays key roles in catalysis, modulating substrate binding, chemistry, and product release.

1. Introduction

Actinomycetes, such as *Mycobacterium* species, are Gram-positive bacteria that contain a high GC content and a thick, hydrophobic cell wall. Pathogenic mycobacterial species are responsible for a number of infectious diseases, most notably tuberculosis and leprosy. In contrast to eukaryotes and other bacteria, these organisms do not have glutathione. Instead, they use the small molecule mycothiol (MSH) as their primary reducing agent and in xenobiotic metabolism for the detoxification of drugs and other toxins. (*1-4*) MSH is probably critical for survival of mycobacteria inside the oxidative environment of activated macrophages where they reside. Consequently, enzymes in the MSH biosynthetic and MSH-dependent detoxification pathways are targets for the development of antibiotics for the treatment of diseases, such as tuberculosis. (*5-10*)

The metalloenzyme MshB catalyzes the hydrolysis of *N*-acetyl-1-D-*myo*-inosityl-2-amino-2-deoxy-α-D-glucopyranoside (GlcNAc-Ins) to form 1-D-*myo*-inosityl-2-amino-

2-deoxy-α-D-glucopyranoside and acetate, the fourth overall step in MSH biosynthesis (Fig. 1A). MshB is an attractive drug target because it catalyzes the rate-limiting step in MSH biosynthesis (*11*), it is a metalloenzyme (*12-14*), and the three-dimensional structure is known (*15, 16*). There are past successes in targeting metalloenzymes, including inhibitors of carbonic anhydrase, matrix metalloproteases, and angiotensin-converting enzyme (*17-20*). Because inhibitors of metalloenzymes typically contain a group that binds to the catalytic metal ion, we previously examined the cofactor preferences of MshB and found that MshB is a cambialistic metalloenzyme whose *in vitro* activity follows the following trend: $Fe^{2+} > Co^{2+} > Zn^{2+} > Mn^{2+}$ and Ni^{2+} (*14*). Additionally, we found that the cofactor bound to MshB is dependent on environmental conditions (*14*). MshB prefers Fe^{2+} under anaerobic conditions regardless of the metal ion content of the medium and switches between Fe^{2+} and Zn^{2+} under aerobic conditions as the metal content of the medium is altered. MshB has a bell-shaped dependence on pH (subsaturating concentrations of substrate, *V/K*), indicating that there are two ionizations that are important for maximal catalytic activity (*14*), consistent with a reaction that proceeds through either a single bifunctional general acid-base catalyst (GABC) or GABC pair mechanism (*21*).

Herein we probe the chemical mechanism of MshB. We demonstrate that residues Asp-15, His-144, Asp-146, and Tyr-142 are important for maximal catalytic activity. Our results suggest that Asp-15 functions as a general base catalyst (GBC), whereas His-144 functions as a general acid catalyst (GAC), and the catalytic metal-water/hydroxide serves as the reactive nucleophile in the reaction. Furthermore, our results indicate that Tyr-142 is important for catalytic activity. We propose that Tyr-142

is a dynamic side chain that modulates substrate binding, chemistry (via polarization of carbonyl group /stabilization of oxyanion), and product release. These insights into the chemical mechanism indicate that MshB does not follow the prototypical metalloprotease-like mechanism but instead uses a GABC pair and a dynamics to catalyze the hydrolysis of substrate.

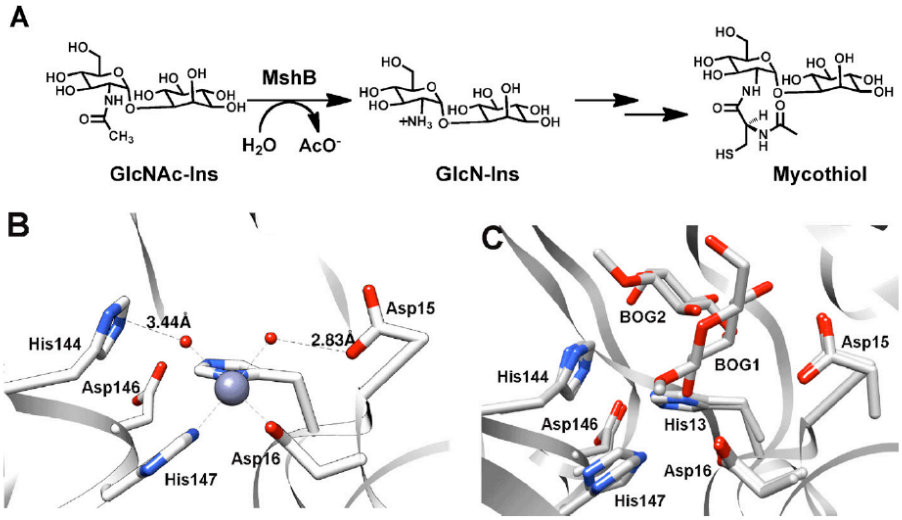

Figure 1: Overview of MshB reaction and active site. (A) Reaction catalyzed by MshB. (B) Active site of MshB (PDB 1Q74) containing a catalytic zinc ion. Only one of the four Zn^{2+}-MshB monomers is shown. (C) Active site of MshB (PDB 1Q7T) containing bound β-octyl-D-glucopyranoside (BOG). The structures of the two MshB-BOG monomers were overlaid revealing two different locations for glucose binding to MshB, BOG1 and BOG2. The octyl chains of the active site BOG molecules are not observed in either monomer.

2. Materials and Methods

2.1 General Procedures

All solutions were prepared using milliQ water. Primers were purchased from Integrated DNA Technologies. Genomic DNA was purchased from ATCC. DNA sequencing was performed at the Virginia Bioinformatics Institute DNA Sequencing Facility (Virginia Tech). All chemicals were purchased from ThermoFisher Scientific,

Sigma-Aldrich, and Gold Biotechnology. For kinetic experiments, solutions were prepared with reagents that did not contain extraneous metal ions and/or were treated with Chelex (Bio-Rad), and solutions were stored in "metal-free" plasticware. To maintain anaerobic conditions (Fe^{2+} assays), experiments were carried out in an anaerobic chamber (Coy Laboratory Products, Grass Lake, MI). Molecular graphics images were produced using the *UCSF Chimera* package (*22*).

2.2 Protein Expression and Purification

The previously reported plasmid encoding the MshB gene from *Mycobacterium smegmatis* containing an N-terminal His-MBP tag was used as the template for preparation of mutant plasmids (*14*). All mutant plasmids were prepared using the QuikChange Lightning site-directed mutagenesis kit (Stratagene). Plasmid sequences were verified by DNA sequencing. All MshB variants were expressed and purified according to published procedures (*14, 23*).

Briefly, cells were lysed using an Emulsiflex-C3 high pressure homogenizer (Avestin), and MshB variants were purified at 4 °C. Cell lysate was clarified by centrifugation (18,000 rpm, 4 °C) and loaded onto a pre-equilibrated (Buffer A; 30 mM HEPES, 150 mM NaCl, 1 mM triscarboxyethylphosphine or TCEP, 0.5 mM imidazole, pH 7.5) Co-IMAC column (50 ml of chelating Sepharose (GE Healthcare) charged with $CoCl_2$). The column was washed with 150 ml of Buffer A, and His-MBP-MshB was eluted using an imidazole step gradient (200 ml each: Buffer A + 10 mM imidazole, Buffer A + 25 mM imidazole, Buffer A + 300 mM imidazole). Fractions containing His-MBP-MshB (via SDS-PAGE) were combined, concentrated (Amicon Ultra-15

centrifugal devices, Millipore), and dialyzed (Snake-skin tubing, molecular weight cut-off 10,000; Pierce) versus 2 × 4 liters of Buffer A overnight in the presence of His-TEV protease (300 μg/ml) to remove the His-MBP tag. The resulting TEV-cleaved protein was loaded onto a pre-equilibrated (Buffer A + 25 mM imidazole) Co-IMAC column. His-MBP and His-TEV remain bound to the Co-IMAC column, whereas MshB elutes in the flow-through. Fractions containing MshB (via 12% SDS-PAGE) were combined, concentrated, and dialyzed versus 2 × 4 liters of 25 mM HEPES, 1.5 mM TCEP, pH 7.5 (Slide-a-Lyzer, molecular weight cut-off 10,000; Pierce). Protein concentration was determined using the Bradford assay (Sigma). Protein aliquots were flash frozen in liquid nitrogen and stored at -80 °C.

For the preparation of apo-MshB (*14*), purified protein (≤ 100 μM) was incubated with 10 mM HEPES, 20 mM dipicolinic acid, 250 μM EDTA, pH 7.5, on ice. After 1 h, the protein solution was concentrated; washed (diluted with buffer and then concentrated) with 3 × 15 ml of 25 mM HEPES, 1.5 mM TCEP, pH 7.5; and run over a desalting column to remove residual dipicolinic acid/EDTA. Metal ion concentrations were determined using an ICS-3000 ion chromatography system (Dionex). Apo-MshB samples contained ≤ 10% metal/protein. Prior to activity measurements, apo-MshB (≤ 10 μM) was incubated with a stoichiometric concentration of the desired metal ion ($CoCl_2$, $FeCl_2$, $FeCl_3$, $MnCl_2$, $NiCl_2$, $ZnSO_4$) and incubated on ice for 30 min.

2.3 MshB Deacetylase Activity

MshB deacetylase activity was measured with the substrate *N*-acetyl-glucosamine (GlcNAc) (Sigma) using a fluorescamine-based assay (*23*). Although the GlcNAc

substrate has a decreased affinity for MshB compared with the natural substrate GlcNAc-Ins (K_M of 38 mM versus 340 μM), the GlcNAc moiety that undergoes the chemical transformation is conserved (*12, 23*). Because our primary interest is in examining the chemical step of the reaction, the commercially available GlcNAc substrate was used in these studies. In general, assay mixtures containing 50 mM HEPES, 50 mM NaCl, 1 mM TCEP, pH 7.5, and 0–150 mM GlcNAc were pre-equilibrated at 30 °C, and reactions were initiated by the addition of enzyme (1 μM). For pH dependence experiments, the following buffers were used (all 50 mM containing 1 mM TCEP, 50 mM NaCl): MES, pH 6–6.8; Mops, pH 6.5–7.5; HEPES, pH 7.3–8.8; Bistris propane, pH 8–9; borate, pH 9–10; carbonate, pH 10–11. After incubation for various times, reactions aliquots (30 μl) were quenched by the addition of 20% TCA (10 μl), and the cleared supernatant (25 μl) was transferred into a 96-well plate, diluted with 1 M borate, pH 9 (75 μl), and reacted with fluorescamine (30 μl in CH_3CN; Invitrogen). After 10 min, the fluorescence was measured (excitation 395 nm; emission 485 nm) using a SpectraMax M5^e plate reader (Molecular Devices). Initial rates of product formation (≤ 10%) were determined from these data. Equation 1 was fit to the pH rate profile, where k_1 represents V/K at the pH optimum, and K_{a1} and K_{a2} represent dissociation constants describing the two ionizations. Equations 2 and 3 were fit to the pH rate profiles for the D15A and Y142A/F mutants, respectively, in which only a single ionization is observed. For experiments under V/K conditions, 5–50 mM GlcNAc was used as the substrate in assays. Specific concentrations of substrate used were 5 (WT, Y142F), 10 (Y142A), 20 (D15A and H144A), or 50 mM (D146A) GlcNAc.

For determination of the steady-state parameters, deacetylase activity was

measured at 6–8 different concentrations of GlcNAc (0–300 mM), and the parameters k_{cat}, K_M, and k_{cat}/K_M were obtained by fitting the Michaelis-Menten equation to the initial linear velocities using the curve-fitting program Kaleidagraph (Synergy Software), which also calculates the asymptotic S.E. values. For D146A, higher concentrations of GlcNAc (0 –375 mM) were used.

$$V/K_{obs} = \frac{k_1}{\left(1 + \frac{[H^+]}{K_{a1}} + \frac{K_{a2}}{[H^+]}\right)} \quad \text{(Eq. 1)}$$

$$V/K_{obs} = \frac{k_1}{\left(1 + \frac{K_{a2}}{[H^+]}\right)} \quad \text{(Eq. 2)}$$

$$V/K_{obs} = \frac{k_1}{\left(1 + \frac{[H^+]}{K_{a1}}\right)} \quad \text{(Eq. 3)}$$

Solvent viscosity assays were carried out using the microviscogens sucrose (0–35% (w/v)) and glycerol (0–35% (w/v)) and the macroviscogen Ficoll 400 (0–10% (w/v)) with a subsaturating concentration (5 mM) or saturating concentration (100 mM) of GlcNAc. The η_{rel} values for 0, 10, 20, 27.5, 32.5, and 35% sucrose are 1, 1.32, 1.88, 2.48, 3.06, and 3.42, respectively (*24*). The η_{rel} values for 0, 10, 20, 30, and 35% glycerol are 1, 1.3, 1.7, 2.3, and 2.9, respectively (*25*). The η_{rel} values for 0, 5, and 10% Ficoll 400 are 1, 2.2, and 4.5, respectively (*26*).

Fluoride inhibition studies were carried out with 0–200 mM NaF added to the assay mixture. There was no effect on MshB activity observed in control experiments using an additional 200 mM NaCl in the assay mixture. For solvent isotope effect experiments, initial rates at subsaturating substrate concentrations (5 (WT, Y142F), 10 (Y142A), 20 (D15A, H144A), or 50 mM (D146A) GlcNAc) in H_2O were compared with

the initial rates in ~95% D_2O. The pD values obtained for the D_2O buffers using the pH meter readings were corrected by adding 0.4 to these values.

2.4 Computational Studies

Structural alignment of the six MshB monomers in available crystal structures (Protein Data Bank entries 1Q74 and 1Q7T) (*15, 16*) was carried out using the MatchMaker program in the *UCSF Chimera* package. (*22, 27*) Potential Tyr-142 rotamers were evaluated using Chimera (*22*) with the Dunbrack backbone-dependent rotamer library (*28*). This library contains six possible Tyr rotamers that are commonly observed in proteins. A model of MshB with Tyr-142 positioned for a possible role in chemistry was prepared using *Chimera* by rotating Tyr-142 into the location of a Tyr rotamer in the Dunbrack library.

3. Results

3.1 Mutations Decrease Catalytic Activity

The crystal structure of Zn^{2+}-MshB (Fig. 1B) reveals a zinc ion in the active site bound by the side chains of three protein ligands (His-13, Asp-16, and His-147) and one to two water molecules that is surrounded by side chains typically involved in acid-base catalysis and/or stabilization of oxyanion intermediates (Asp-15, His-144, and Asp-146). Importantly, this structure reveals two potential acid-base catalysts that are in close proximity to the zinc-bound water molecules, Asp-15 and His-144; Asp-15 is located ~2.8 Å from one zinc-bound water molecule, whereas His-144 is ~3.4 Å away from the second zinc-bound water molecule. As a result of their close proximity to the catalytic

zinc ion, these side chains are best positioned to serve as GBC/GAC in the chemical reaction. Crystal structures of a MshB/β-octyl-D-glucopyranoside (BOG) complex, which lack the catalytic metal ion (Fig. 1C), also indicate that these side chains are well positioned to interact with the substrate GlcNAc moiety (*16*). Additionally, the side chain of Asp-146 is located near His-13 and His-144 (2.9–3.6 Å), suggesting a potential role for Asp-146 in catalysis. On the basis of the crystal structure of the Zn^{2+}-MshB active site (*15*) and the pH dependence of MshB deacetylase activity (*14*), the MshB-catalyzed reaction is proposed to proceed through either a single GABC or a GABC pair mechanism using the side chains of Asp-15 and/or His-144 (*21*).

Table 1. Steady-state kinetic parameters of MshB mutants

MshB[a,b]	K^m	k_{cat}	k_{cat}/K_m	WT activity
	mM	min^{-1}	$M^{-1}\,s^{-1}$	%
WT[c]	38 ± 4	46 ± 2	20 ± 1	
D15A	52 ± 11	0.29 ± 0.02	0.09 ± 0.01	0.5
Y142A	22 ± 2	1.8 ± 0.05	1.36 ± 0.10	6.8
Y142F	9 ± 0.5	0.57 ± 0.01	1.05 ± 0.05	5.3
Y142Q	17 ± 2	1.2 ± 0.04	1.17 ± 0.11	5.9
H144A	57 ± 8	0.69 ± 0.04	0.20 ± 0.02	1.0
D146A	>400	>2	~0.08[d]	<0.4

[a] Apo-MshB was incubated with stoichiometric Zn^{2+} for 30 min prior to activity measurement.
[b] Substrate used GlcNAc.
[c] Data adapted from Ref. 14.
[d] Estimated from slope of initial linear region on *V versus* [S] plot.

To distinguish between these two possible mechanisms, we used a combination of mutagenesis and kinetic experiments. We prepared a series of MshB constructs wherein active site side chains (Asp-15, His-144, and Asp-146) were mutated to Ala using site-directed mutagenesis, and the steady-state parameters for these constructs were determined using the substrate GlcNAc (Table 1). Results from these experiments indicate that removal of the Asp-15, His-144, and Asp-146 side chains lead to an overall

decrease in catalytic activity, suggesting that these side chains are important for maximal catalytic activity. Specifically, the D15A mutation leads to a modest (< 2-fold) increase in K_M, an ~80-fold decrease in k_{cat}, and a 222-fold decrease in k_{cat}/K_M. The H144A mutation leads to a modest increase in the value of K_M to ~50 mM but decreases the values of k_{cat} and k_{cat}/K_M 60- and 100- fold, respectively. The D146A mutant could not be saturated with [GlcNAc] of 375 mM; therefore, the steady-state parameters for this mutant are estimated values. The D146A mutation results in a >10-fold increase in K_M and >100-fold decrease in k_{cat}/K_M.

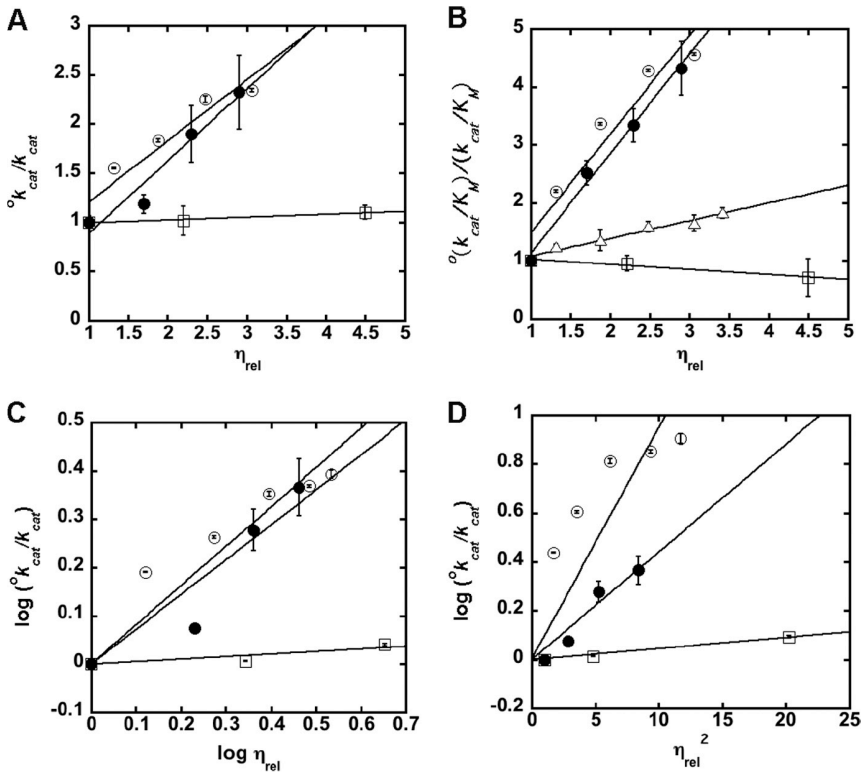

Figure 2: Effect of Solvent Viscosity on **(**A) k_{cat} and (B) k_{cat}/K_M. The effects of the microviscogens sucrose (0-35% (w/v)) and glycerol (0-35% (w/v)) on WT MshB are depicted as (○) and (●), respectively, while the macroviscogen Ficoll 400 (0-10% (w/v)) is denoted as (□). Data for the Y142F mutant in the presence of sucrose is depicted by (△). Plots (C) and (D) are used to determine if there is a conformational change associated with product release and/or substrate binding. Apo-MshB was incubated with stoichiometric Zn^{2+}. The initial rates for the deacetylation of a sub-saturating (5 mM) or saturating (100 mM) concentration of GlcNAc were measured.

3.2 Solvent Viscosity Effects on the rate of MshB-catalyzed deacetylation.

Solvent microviscosity slows the rates of steps that involve movement of small molecules, such as substrate binding and product release, as well as conformational changes in proteins (*24-26, 29-31*). In contrast, rates for internal processes, such as chemistry, proceed independent of solvent microviscosity. To control for changes in activity that arise from nonspecific interactions, we used multiple microviscogens (sucrose, glycerol) as well as the macroviscogen Ficoll 400. Macroviscogen alter solvent viscosity but do not slow the rates of diffusion of small molecules and are used to control for changes in activity that arise from nonspecific interactions (*24, 25, 29-31*).

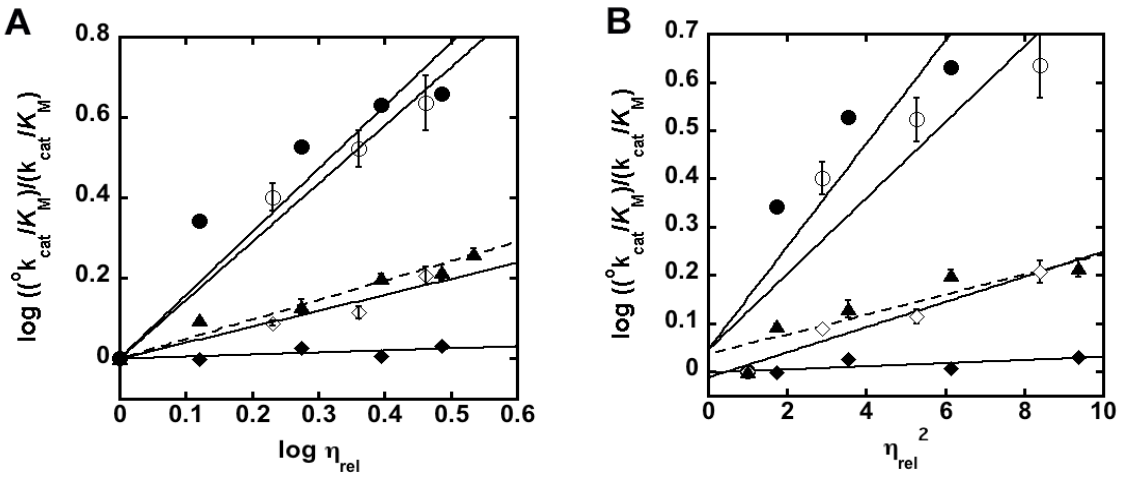

Figure 3: Effect of solvent viscosity on k_{cat}/K_M of MshB mutants. The effects of the microviscogens sucrose (0-35% (w/v)) and glycerol (0-35% (w/v)) on WT MshB are depicted as (●) and (○), respectively. The effects of the microviscogens sucrose (0-35% (w/v)) and glycerol (0-35% (w/v)) on D146A MshB are depicted as (◆) and (◇), respectively, while the effect of sucrose (0-35% (w/v)) on Y142F is depeicted as (▲). Apo-MshB was incubated with stoichiometric Zn^{2+}. After 30 minutes, the enzyme was diluted into assay buffer (50 mM HEPES, 1 mM TECP, 50 mM NaCl pH 7.5) containing substrate and the initial rates for the deacetylation of sub-saturating concentration (WT, 5 mM; D146A, 50 mM) GlcNAc.

Table 2. Effect of solvent viscosity on WT MshB

MshB variant[a]	Viscogen	Y-axis	X-axis	Slope	R^2
WT	Glycerol	$^{o}k_{cat}/k_{cat}$	η_{rel}	0.74 ± 0.13	0.945
	Sucrose			0.62 ± 0.11	0.911
	Ficoll			0.03 ± 0.006	0.956
WT	Glycerol	$(^{o}k_{cat}/K_M)/(k_{cat}/K_M)$	η_{rel}	1.72 ± 0.12	0.990
	Sucrose			1.70 ± 0.28	0.924
	Ficoll			-0.086 ± 0.02	0.958
WT	Glycerol	log ($^{o}k_{cat}/k_{cat}$)	log (η_{rel})	0.72 ± 0.09	0.889
	Sucrose			0.81 ± 0.06	0.878
	Ficoll			0.05 ± 0.01	0.810
WT	Glycerol	log ($^{o}k_{cat}/k_{cat}$)	η_{rel}^2	0.044 ± 0.005	0.923
	Sucrose			0.095 ± 0.01	0.571
	Ficoll			0.005 ± 0.0003	0.983
WT	Glycerol	log $(^{o}k_{cat}/K_M)/(k_{cat}/K_M)$	log (η_{rel})	1.45 ± 0.09	0.975
	Sucrose			1.57 ± 0.2	0.852
	Ficoll			-0.19 ± 0.05	0.890
WT	Glycerol	log $(^{o}k_{cat}/K_M)/(k_{cat}/K_M)$	η_{rel}^2	0.044 ± 0.15	0.778
	Sucrose			0.045 ± 0.13	0.822

[a] apo-MshB was incubated with stoichiometric Zn^{2+} for 30 min prior to activity measurement with a sub-saturating concentration (5 mM) or saturating concentration (100 mM) of GlcNAc as described in "Materials and Methods". A linear equation was fit to the resulting data. Select

We measured the effect of sucrose and glycerol (microviscsogens), as well as Ficoll 400 (macroviscogen), on MshB activity. Results from experiments with WT MshB (Fig. 2 and Table 2) indicate that both k_{cat} and k_{cat}/K_M are significantly slowed in the presence of the microviscogens sucrose and glycerol. For effects on k_{cat}, the slopes observed in the presence of glycerol and sucrose are 0.74 ± 0.13 and 0.62 ± 0.11, respectively. The finding that the plots for assays in the presence of glycerol and sucrose have comparable slopes suggests that the microviscogens are affecting the diffusion of small molecules and/or a conformational change in the protein and not simply having nonspecific effects on MshB (e.g. dielectric constant). For effects on k_{cat}/K_M, the slopes for assays in the presence of glycerol and sucrose are 1.72 ± 0.12 and 1.70 ± 0.28, respectively. Again, the finding that the plots for assays in the presence of glycerol and sucrose have comparable slopes suggests that the microviscogens are affecting the diffusion of small molecules and/or a conformational change in the protein and not having nonspecific effects on MshB. These initial plots of k_{cat} or k_{cat}/K_M versus η_{rel} show some deviation from linearity, and therefore, additional analyses were carried out on these data (below). As expected, the slopes of the plots examining the effect of Ficoll 400 on k_{cat} (0.03 ± 0.006) and k_{cat}/ K_M (-0.086 ± 0.02) indicate that these parameters are unaffected by the macroviscogen Ficoll 400.

Table 3. Effect of solvent viscosity on MshB mutants (k_{cat})

MshB Variant[a]	Viscogen	Y-axis	X-axis	Slope	R^2
D15A	Glycerol	$^{o}k_{cat}/k_{cat}$	η_{rel}	1.62 ± 0.18	0.975
	Sucrose			1.80 ± 0.19	0.967
Y142F	Sucrose			0.01 ± 0.02	0.075
H144A	Glycerol			0.53 ± 0.04	0.988
	Sucrose			0.14 ± 0.02	0.967
D15A	Glycerol	log ($^{o}k_{cat}/k_{cat}$)	log (η_{rel})	1.37 ± 0.07	0.973
	Sucrose			1.39 ± 0.06	0.982
Y142F	Sucrose			-0.02 ± 0.02	0.041
H144A	Glycerol			1.09 ± 0.03	0.991
	Glycerol[b]			0.92 ± 0.09	0.927
	Sucrose			0.33 ± 0.03	0.947
D15A	Glycerol	log ($^{o}k_{cat}/k_{cat}$)	η_{rel}^2	0.082 ± 0.01	0.920
	Sucrose			0.081 ± 0.005	0.980
Y142F	Sucrose			-0.001 ± 0.001	0.327
H144A	Glycerol			0.065 ± 0.006	0.950
	Sucrose			0.02 ± 0.002	0.972

[a] apo-MshB was incubated with stoichiometric Zn^{2+} for 30 min prior to activity measurement with a saturating concentration (100mM) of GlcNAc as described in "Materials and Methods". Select graphical representations of data are shown in Figures 2, 3, and S4. [b] Substrate = 300 mM GlcNAc

For rate-limiting steps where product release is associated with conformational changes in the protein, a plot of log k_{cat} versus log η_{rel} is linear, whereas for rate-limiting steps where product release occurs in the absence of a structural rearrangement, a plot of log k_{cat} versus η_{rel}^2 is linear (*29, 31*). To gain insights into whether product release in MshB is dependent on a conformational change in the protein, we examined which of these plots better describe our data (Fig. 2, C and D, and Table 2). Although both plots comparably describe data obtained using glycerol as the viscogen, the sucrose data are better described by the log k_{cat} versus log η_{rel} plot, suggesting that product release in MshB may be coupled to a conformational change in the protein. The finding that k_{cat}/K_M is also better described by log k_{cat}/K_M versus log η_{rel} (Fig. 3) may suggest that there is also a conformational change coupled with substrate binding to MshB. We examined the effect of solvent viscosity on the activity of the D15A and H144A mutants (Fig. 4 and Table 3) to determine if product release remains rate-limiting for these catalytically impaired mutants. Once again we observe that k_{cat} is significantly slowed in the presence of glycerol and sucrose. These data are clearly better described by a plot of log k_{cat} versus log η_{rel} (Fig. 4A) compared with a plot of log k_{cat} versus η_{rel}^2 (Fig. 4B), suggesting that the rate-limiting step in these mutants is a conformational change that is coupled to product release. (Note that because we are unable to reach substrate saturation with the D146A mutant, the effect of solvent viscosity could only be determined under k_{cat}/K_M conditions; Fig. 3 and Table 4).

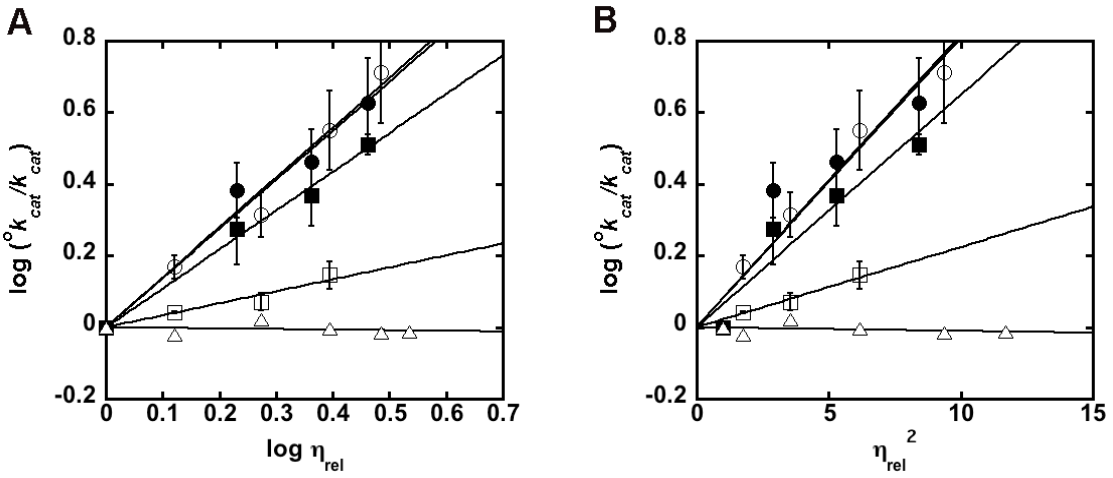

Figure 4: Effect of Solvent Viscosity on k_{cat} of MshB mutants. The effects of the microviscogens sucrose (0-35% (w/v)) and glycerol (0-35% (w/v)) on WT MshB are depicted as open and closed symbols, respectively. MshB mutants examined are: D15A (circles), H144A (squares), and Y142F (triangles). Plots (A) and (B) are used to determine if a conformational change is associated with product release/substrate binding. Apo-MshB was incubated with stoichiometric Zn^{2+}. After 30 minutes, the enzyme was diluted into assay buffer (50 mM HEPES, 1 mM TECP, 50 mM NaCl pH 7.5) containing substrate and the initial rates for the deacetylation at saturating concentrations (100 mM) of GlcNAc were measured.

Table 4. Effect of solvent viscosity on MshB mutants (k_{cat}/K_M)

MshB Variant[a]	Viscogen	Y-axis	X-axis	Slope	R^2
Y142F	Sucrose	$(^{o}k_{cat}/K_M)/(k_{cat}/K_M)$	η_{rel}	0.31 ± 0.03	0.960
D146A	Glycerol			0.30 ± 0.05	0.976
	Sucrose			0.03 ± 0.02	0.731
Y142F	Sucrose	log $(^{o}k_{cat}/K_M)/(k_{cat}/K_M)$	log η_{rel}	0.48 ± 0.03	0.957
D146A	Glycerol			0.40 ± 0.03	0.937
	Sucrose			0.05 ± 0.01	0.551
Y142F	Sucrose	log $(^{o}k_{cat}/K_M)/(k_{cat}/K_M)$	η_{rel}^2	0.04 ± 0.03	0.864
D146A	Glycerol			0.03 ± 0.003	0.957
	Sucrose			0.003 ± 0.001	0.547

[a] apo-MshB was incubated with stoichiometric Zn^{2+} for 30 min prior to activity measurement with a sub-saturating concentration of GlcNAc (5 mM, Y142F; 50 mM, D146A) as described in "Materials and Methods". A linear equation was fit to the resulting data. Select graphical

3.3 Role of Metal-Water/Hydroxide

We previously examined the ability of divalent metal ions to serve as cofactors for MshB and found that the overall activity follows the following trend: $Fe^{2+} > Co^{2+} > Zn^{2+} > Mn^{2+}$ and Ni^{2+} (*14*). Although these results confirm the importance of the metal cofactor for activity, the specific role of the metal ion in the MshB-catalyzed reaction has not been elucidated. Therefore, we set out to probe the role of the metal ion in catalysis by MshB.

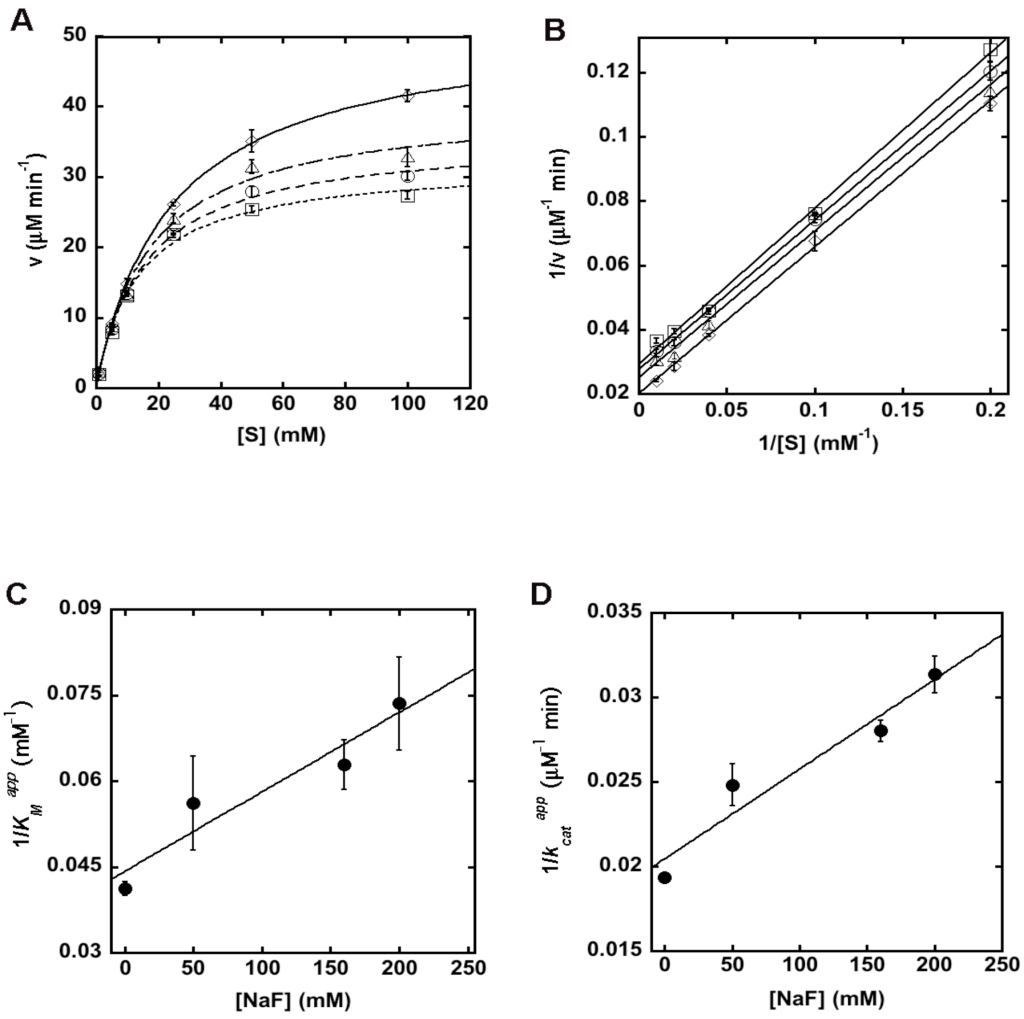

Figure 5: NaF inhibition of MshB activity. (A) Michaelis-Menten plot and (B) double-reciprocal plot of Zn^{2+}-MshB activity at various fluoride concentrations. Fluoride concentrations were 0 (◇), 50 (△), 160 (○), and 200 (□) mM. The parallel lines in panel (B) are indicative of uncompetitive inhibition. Replots showing the linear relationships between (C) $1/K_M^{app}$ and (D) $1/k_{cat}^{app}$ and fluoride concentration. Assays were performed at 30°C (50 mM HEPES, 1 mM TECP, 50mM NaCl, pH 7.5) with various concentrations of GlcNAc. The K_I values for fluoride are estimated to be 0.32 and 0.38 M for $1/K_M^{app}$ and $1/k_{cat}^{app}$, respectively.

Fluoride is often used to probe the identity of the reactive nucleophile for metallohydrolases (*32-35*). Specifically, fluoride inhibits (uncompetitive) enzymes that utilize a metal-bound water or hydroxide as the reactive nucleophile. Therefore, we measured the MshB-catalyzed deacetylation of GlcNAc in the presence of various

concentrations of NaF (0–200 mM). Results from these experiments show that NaF acts as an uncompetitive inhibitor of the deacetylation reaction consistent with the metal-water/hydroxide serving as the reactive nucleophile in the MshB-catalyzed reaction. (Fig. 5)

Table 5. Effect of metal ions on pH-dependence of wild-type MshB

Me^{2+}-MshB[a,b]	pK_{a1}	pK_{a2}	V/K at pH optimum
			$M^{-1}\,s^{-1}$
Zinc[c]	7.4 ± 0.07	10.5 ± 0.06	48 ± 1.5
Cobalt	7.2 ± 0.09	11.0 ± 0.09	56 ± 2.3
Iron	7.2 ± 0.09	10.5 ± 0.08	63 ± 2.3
Nickel	7.1 ± 0.03	11.1 ± 0.03	7.3 ± 0.1
Manganese	7.2 ± 0.12	11.0 ± 0.12	8.0 ± 0.4

[a] Apo-MshB was incubated with stoichiometric metal for 30 min prior to activity measurement.
[b] Substrate 5 mM GlcNAc.
[c] Data adapted from Ref. 14.

MshB activity (V/K) exhibits a bell-shaped dependence on pH with two ionizations having pK_a values of 7.3 (pK_{a1}) and 10.5 (pK_{a2}) (*14*). There is an increase in activity with increasing pH for the ionization described by pK_{a1}, whereas there is a decrease in activity with increasing pH for the ionization described by pK_{a2}. Because the metal-bound water could be reflected in one of these pK_a values, we examined the pH dependence of deacetylase activity for MshB reconstituted with various divalent metal ions. Results from these experiments are shown in Table 5. These results confirm that MshB activity follows the trend: $Fe^{2+} > Co^{2+} > Zn^{2+} > Mn^{2+}$ and Ni^{2+}. Furthermore, these findings indicate that the identity of the metal ion does not significantly alter pK_{a1} and has only a modest effect on pK_{a2} (0.6 pH units). These results rule out the metal-water as the source of pK_{a1}, whereas the small effect on pK_{a2} (0.6 pH units) suggests that it is unlikely that this pK_a reflects ionization of the metal-water either.

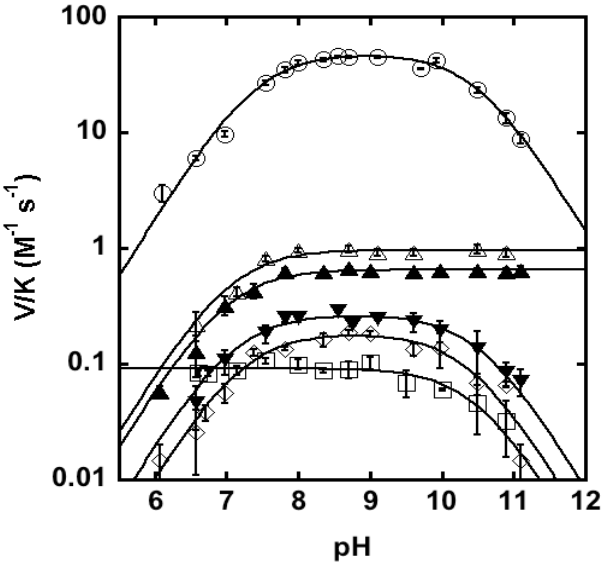

Figure 6: pH rate profiles. The effect of pH on the deacetylation of GlcNAc by MshB under sub-saturating substrate concentrations (V/K). The pH dependence of the MshB-catalyzed reaction is shown for WT (○), D15A (□), Y142A (△), Y142F (▲), H144A (▼), and D146A (◇). Assays were measured at 30°C with sub-saturating (5-50 mM) concentrations of GlcNAc. The pK_a values were determined by fitting the equation including two ionizations (Eq. 1) or one ionization (Eq. 2 or 3).

3.4 Mutations Alter pH Dependence

To gain further insights into the chemical mechanism of MshB, we probed the identities of the ionizations observed in the wild-type (WT) MshB pH profile under subsaturating concentrations of substrate (*V/K*). We chose to focus on the parameter *V/K* rather than *V* because *V/K* examines the reaction of free enzyme with free substrate through the first irreversible step, chemistry, and therefore will provide information about the chemical mechanism of the enzyme. In contrast, results from solvent viscosity experiments (Figs. 2 and 4) indicate that that the parameter k_{cat} (*V*) reflects a conformational change coupled to product release and therefore does not provide information about the chemical step of the reaction. We examined the pH dependence of the MshB Ala mutants (Asp-15, His-144, and Asp-146), and the results from these

experiments are summarized in Table 6 and Fig. 6. These results confirm that the side chains of Asp-15, His-144, and Asp-146 are important for catalytic activity because the rate at the pH optimum is decreased ~180 to 530- fold. Importantly, we observe that pK_{a1} is lost in the D15A mutant (Fig. 6), suggesting that pK_{a1} reflects ionization of Asp-15 in the WT enzyme. Although the H144A and D146Amutations decrease MshB activity, the pK_a values observed for these mutants are the same as those observed for the WT protein, suggesting that neither His-144 nor Asp-146 is responsible for the ionizations observed in the WT protein.

Table 6. pH-dependence of Zn^{2+}-MshB variants

MshB[a,b]	pK_{a1}	pK_{a2}	V/K at pH optimum	WT activity
			$M^{-1}\,s^{-1}$	
WT[c]	7.4 ± 0.07	10.5 ± 0.06	48.2 ± 1.5	%
D15A		10.5 ± 0.13	0.091 ± 0.003	0.2
Y142A	7.1 ± 0.10		0.96 ± 0.03	2.0
Y142F	7.0 ± 0.05		0.65 ± 0.01	1.3
H144A	7.1 ± 0.10	10.5 ± 0.09	0.27 ± 0.01	0.6
D146A	7.2 ± 0.10	10.4 ± 0.10	0.18 ± 0.01	0.4

[a] Apo-MshB was incubated with stoichiometric metal for 30 min prior to activity measurement.
[b] Substrate 5 (WT, Y142F), 10 (Y142A), 20 (D15A, H144A), or 50 mM (D146A) GlcNAc.
[c] Data adapted from Ref. 14.

3.5 Examination of Tyr-142

Because we could not identify the source of pK_{a2} using metal substitution or our initial mutagenesis experiments (D15A, H144A, and D146A), we examined the MshB crystal structures more closely for additional possible sources of this ionization. Importantly, the side chain of Tyr-142 appears to be a dynamic side chain, moving several Å in the Zn^{2+}-MshB and MshB-BOG complex structures. An overlay of the six

MshB monomers (four Zn^{2+}-MshB and two MshB-BOG) is shown in Fig. 7A. The Tyr-142 side chain is found in four different locations in the six monomers. The locations in red, orange, yellow, and purple are observed in the four Zn^{2+}-MshB monomers, whereas the blue and green locations are observed in MshB-BOG monomers. The locations of these side chains and rotation of Tyr-142 in chimera both indicate that the Tyr-142 side chain is unobstructed and can move freely (360°) from being on the MshB surface/solvent exposed (purple) to various locations in the active site. Additionally, we examined the Tyr rotamers using the Dunbrack database in Chimera (*22, 28*). Tyr rotamers are most commonly observed in three general locations with two orientations of the aromatic ring at each location, yielding a total of six possible rotamers (Fig. 7B). Examination of these locations reveals that two of the locations (rotamers 1– 4) are observed in the Zn^{2+}-MshB structures, whereas the third location (rotamers 5 and 6) lies between the Tyr-142 positions observed in the MshB-BOG structures. A model of MshB with Tyr-142 in this third location is shown in Fig. 7C (gray wire in Fig. 7A). In this rotamer, the hydroxyl group of Tyr-142 is within hydrogen bonding distance of the metal-water, which would be capable of participating in catalysis. Therefore, we examined the effect of the Y142A mutant on catalytic activity.

The Y142A mutation significantly alters the steady-state parameters (Table 1). This mutation leads to a ~2-fold decrease in K_M, 26-fold decrease in k_{cat}, and a 15-fold decrease in k_{cat}/K_M. To further examine the role of Tyr-142 in catalysis, we examined the Y142F (sterics, hydrophobicity) and Y142Q (hydrogen bonding) mutants. The Y142F mutation leads to a 4-fold decrease in K_M, an ~80-fold decrease in k_{cat}, and a 20-fold decrease in k_{cat}/K_M, whereas the Y142Q mutation leads to a 2-fold decrease in K_M, a ~40-

fold decrease in k_{cat}, and a 15-fold decrease in k_{cat}/K_M. Additionally, we observe that the ionization described by pK_{a2} is no longer observed in the pH profiles for the Y142A or Y142F mutants (Fig. 6). These results suggest that pK_{a2} reflects ionization of Tyr-142 in WT MshB.

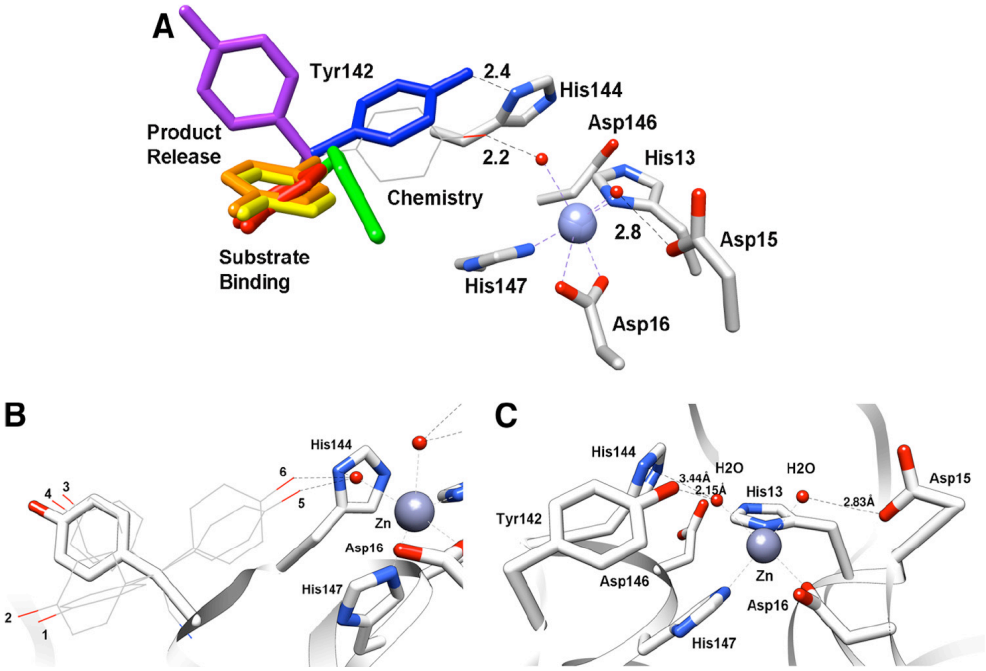

Figure 7: MshB active site. (A) Overlay of the six MshB monomers. The locations of the active site side chains (H13, D15, D16, H144, D146, H147) do not vary significantly, while the location of the Y142 side chain (rainbow colored) varies in the structures. A model of the Zn^{2+}-MshB active site with Y142 rotated into a catalytic location is represented by the gray wire. (B) Potential Tyr rotamers. The six Tyr rotamers (1-6) from the Dunbrack library are displayed as wires. The six rotamers fall into three general locations with two orientations of the phenyl ring at each location. (C) Zn^{2+}-MshB active site with Y142 rotated into a catalytic location (position of rotamer 5).

Furthermore, we find that the solvent viscosity effect under k_{cat} conditions described for MshB in WT and mutant (D15A and H144A) enzymes is lost in the Y142F mutant (Figs. 2 and 4), whereas the solvent viscosity effect under k_{cat}/K_M conditions described for WT is also significantly diminished in the Y142F mutant (Fig. 2B, Fig. 3, and Table 4).

3.6 Tyr-142 Dynamics Modulate Access to Active Site

Mutation of Tyr-142 to Ala, Phe, or Gln leads to a ≤ 4-fold decrease in K_M, suggesting that Tyr-142 plays a role in substrate binding. Because the location of Tyr-142 varies from being on the surface of the protein (purple) to inside the active site, the Tyr-142 side chain may modulate access to the active site. To probe if the side chain Tyr-142 affects access to the enzyme active site, we examined the surfaces of each overlaid monomer (Fig. 7A) with the two BOG molecules (Fig. 1C) as a model for GlcNAc-Ins binding. The results are shown in Fig. 8 and suggest that the structural changes that occur to MshB upon movement of Tyr-142 appear to alter access to the active site. A and C of Fig. 8 represent the same structures from two different viewpoints, with the side chain of Tyr-142 shown in dark gray. In the four Zn^{2+}-MshB monomers (red, orange, yellow, and purple), both sugar molecules are visible, indicating that these Tyr conformations would allow for substrate binding and product release. In the two MshB-BOG monomers (blue and green), the sugar molecules become obscured, indicating that the movement of substrate and product in/out of the active site would be hindered in these Tyr conformations. Fig. 8B is a representation of the viewpoint depicted in Fig. 8A, wherein the side chain of Tyr-142 has been truncated to Ala (dark gray) in attempts to visualize the changes that occur upon the Y142A mutation. Similarly, Fig. 8D is a representation of the viewpoint depicted in Fig. 8C, wherein the side chain of Tyr-142 has been truncated to Ala (dark gray). The information in Fig. 8, B and D, predicts that there should be better access to the active site in the Y142A mutant because the sugar molecules become more visible.

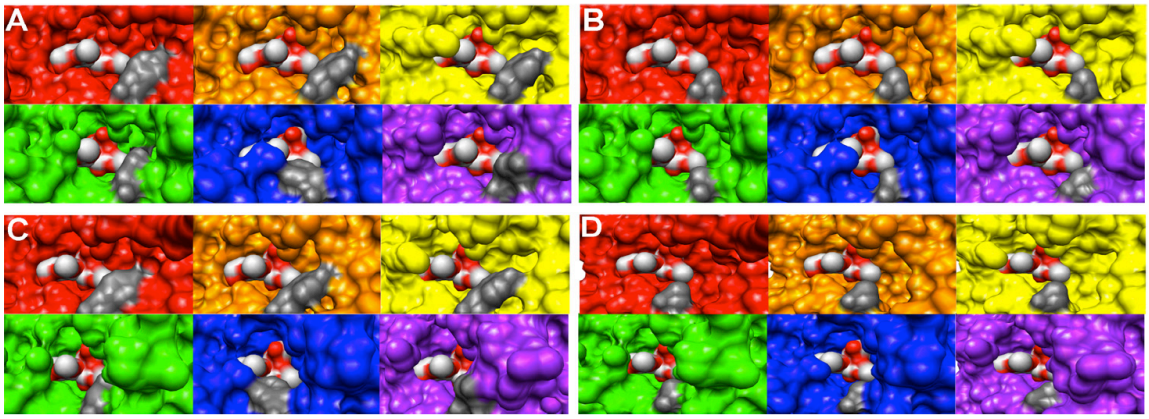

Figure 8: MshB active site accessibility. The panels show the surfaces of the six MshB monomers from the overlaid structures in Figure 6a for two different viewpoints. The surface colors correspond to locations of Y142 shown in Figure 6A and the dark gray is the Y142 side chain. The substrate GlcNAc-Ins is presumed to bind in the location of the two BOG molecules (colored in red and light gray) that are observed in the MshB-BOG structures (Figure 1C). A) Viewpoint 1 with the Y142 side chain shown in dark gray. B) Viewpoint 1 where the Y142 side chain was truncated to Ala (dark gray). C) Viewpoint 2 with the Y142 side chain shown in dark gray. D) Viewpoint 2 where the Y142 side chain was truncated to Ala (dark gray).

3.7 Solvent Isotope Effects

Because the proposed reactions involve GABC, we examined if a solvent isotope effect is observed for the MshB-catalyzed reaction. Solvent isotope effects of 2- 4 are typically observed for reactions that proceed through GBC, whereas inverse solvent isotope effects are observed for reactions that proceed through GAC (*36*). We measured the pH dependence of the solvent isotope effect for the WT protein under *V/K* conditions (Fig. 9A and Table 7). Results from these experiments reveal a small normal solvent isotope effect on *V/K* in WT MshB. This finding suggests that either 1) the chemistry step reflected in *V/K* has contributions from both GAC and GBC or 2) proton transfer is not a significant rate-determining step under these conditions.

To aid in deciphering between these two possibilities and to gain additional insights into the chemical mechanism, we also measured the pH dependence of the

solvent isotope effect for the MshB mutants D15A, Y142F, and H144A under *V/K* conditions. The results from these experiments are shown in Fig. 9 and Table 7. We observe a slight inverse solvent isotope effect of 0.8 for the D15A mutant (Fig. 9B), whereas there is no solvent isotope effect for the Y142F mutant (Fig. 9D). The most striking observation is the large solvent isotope effect for the H144A mutant (Fig. 9C) of ~5. There is no significant difference in the pK_a values observed between H_2O and D_2O for any of the mutants examined.

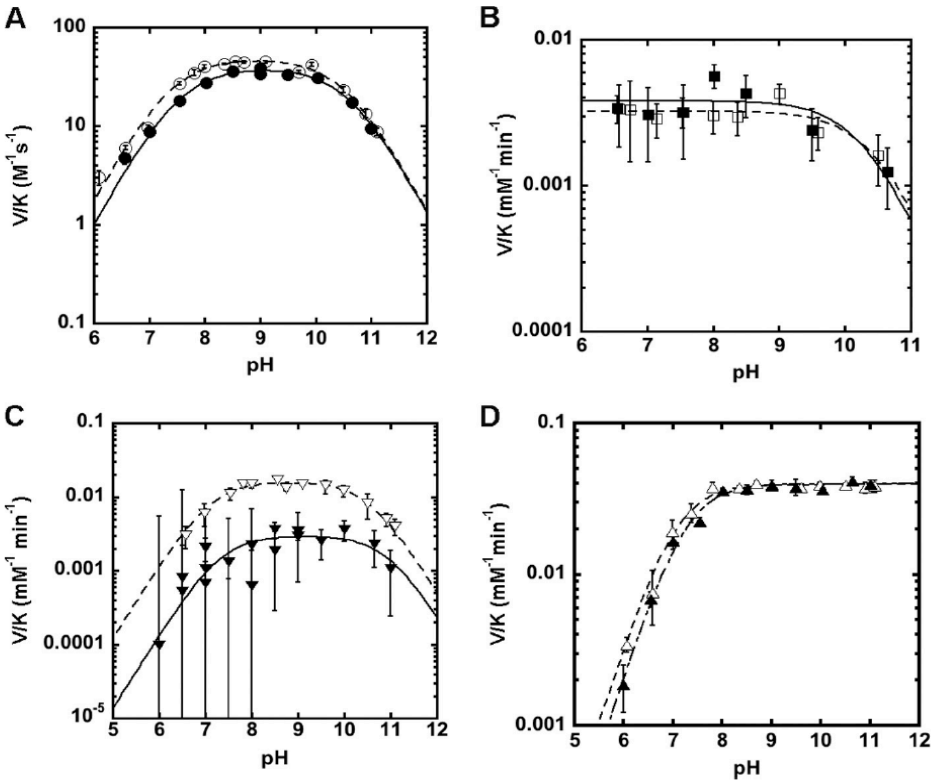

Figure 9: Solvent isotope effect of MshB variants. The solvent isotope for MshB was measured in H_2O (open symbols) and 95% D_2O (closed symbols) at 30°C. Solvent isotope effects were measured under sub-saturating substrate concentrations of GlcNAc. The values for V/K were measured using 5 or 20 mM GlcNAc. (A) WT MshB in H_2O (○) and 95% D_2O (●). (B) D15A in H_2O (□) and 95% D_2O (■). (C) H144A in H_2O (▽) and 95% D_2O (▼). (D) Y142F in H_2O (△) and 95% D_2O (▲). The pK_a values were determined by fitting an equation including one or two ionizations (Eq. 1-3) to these data and are shown in Table 4. Fits for H_2O data are represented with dashed lines and D_2O data are represented with solid lines.

4. Discussion

4.1 MshB Uses Key Protein Side Chains and Metal-Water/Hydroxide as Reactive Nucleophile

Results from mutagenesis studies (Tables 1 and 6) indicate that active site side chains Asp-15, Tyr-142, His-144, and Asp-146 are all important for catalytic activity. The locations of Asp-15 and His-144 (Fig. 1, B and C) suggest that these side chains may function as GABC in the chemical mechanism, whereas the location of Tyr-142 in the model (Fig. 7C) suggests that this side chain may play a role in polarization of substrate and/or stabilization of the oxyanion intermediate. The location of Asp-146 suggests that this side chain does not directly participate in the chemical mechanism but plays an indirect role via interaction(s) with the side chain(s) of His-13 and/or His-144 (Fig. 1, B and C). Titration of apo-D146A with Zn^{2+} (Fig. 10) suggests that the loss of activity observed for this mutant cannot be attributed to decreased binding of the catalytic Zn^{2+} ion via interaction with the zinc ligand H13 under the reaction conditions.

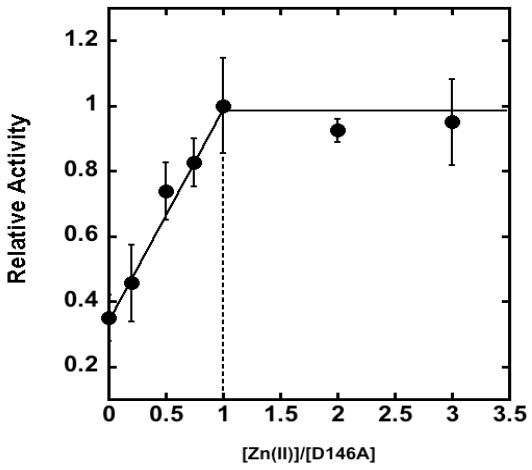

Figure 10: Activation of apo-D146A MshB with Zn^{2+}. Apo-MshB was incubated with varying equivalents of Me^{2+} (0-3). After 30 minutes, the enzyme was diluted into assay buffer containing substrate GlcNAc (50 mM) and the resulting deacetylase activity was measured at 30 °C.

Previous results have shown that the activity of MshB is dependent on the identity of the catalytic metal ion (*14*). Herein we demonstrate that NaF is an uncompetitive inhibitor of MshB (Fig. 5). These results are consistent with MshB using a metal-bound water/hydroxide as the reactive nucleophile in the reaction.

4.2 Parameter kcat Reflects Conformational Change Coupled to Product Release

Results from solvent viscosity experiments indicate that the parameter k_{cat}/K_M is inhibited by microviscogens (sucrose, glycerol), not macroviscogens (Ficoll 400). This is expected, given that the parameter k_{cat}/K_M reflects substrate binding through the first irreversible step (i.e. chemistry) and suggests that k_{cat}/K_M is partially limited by substrate association in WT MshB. The finding that the effect of solvent viscosity on k_{cat}/K_M is diminished in the Y142F mutant (Fig. 2B and Table 4) may suggest that the Tyr-142 side chain is involved in the conformational change coupled to substrate binding or that chemistry becomes more rate-limiting under k_{cat}/K_M conditions in catalytically slow mutants.

Results from solvent viscosity experiments also indicate that the parameter k_{cat} is inhibited by the microviscogens glycerol and sucrose, suggesting that k_{cat} reflects a step that involves the diffusion of small molecules (i.e. substrate binding, product release) and/or a conformational change in MshB. Because both the WT and mutant data are better described by plots of log k_{cat} versus log η_{rel} compared with plots of log k_{cat} versus η_{rel}^2, the rate-limiting step for MshB is probably a conformational change that is associated with product release or substrate binding. The finding that the value of k_{cat} is similar with the substrates GlcNAc-Ins (0.49 s^{-1}) and GlcNAc (0.77 s^{-1}), whereas K_M

values for these substrates vary significantly (340 μM and 38 mM, respectively) is consistent with the hypothesis that k_{cat} reflects a conformational change that is associated with product release in WT MshB rather than simple product dissociation (*12, 23*).

The findings that 1) mutation of Tyr-142 (Ala, Gln, Phe) results in a 15–20-fold decrease in k_{cat}, 2) the Y142F mutant is the only MshB variant examined where the value of the parameter k_{cat} is unaffected by changes in solvent viscosity, 3) the location of the Tyr-142 side chain appears to be dynamic in available crystal structures, and 4) the value of k_{cat} is identical for the D15A and Y142F mutants suggest that the Tyr-142 side chain, probably the hydroxyl group, is involved in the conformational change that is associated with product release. The slopes for log k_{cat} versus log η_{rel} plots range from 0 to 1 depending on degree of coupling of active site to solvent (*25*). The finding that the slopes for WT MshB obtained in the presence of glycerol and sucrose are 0.72 ± 0.09 and 0.81 ± 0.06, respectively, suggests that there is significant coupling between the dynamics of MshB and solvent molecules. This is expected, given the role of Tyr-142 in modulating the dynamics of MshB and its observed location(s) in the enzyme (Figs. 7 and 8). Furthermore, results from kinetics data support a role for Tyr-142 in product release because the parameter k_{cat} is significantly decreased upon mutation of Tyr-142 (Table 1). Specifically, we observe that the value of k_{cat} for the Tyr-142 mutants follows the trend Ala > Gln > Phe for substitution at position 142, suggesting that the product release becomes slower with increasing hydrophobicity of the side chain. It is likely that the rate acceleration with Tyr at this position arises from a combination of factors (i.e. hydrophobicity, hydrogen bonding interactions, and length of side chain).

4.3 Ionization of Asp-15 and Tyr-142 Is Important for Maximal Activity

Interestingly, pK_{a1} is not observed in the D15A mutant (Fig. 6), suggesting that this pK_a reflects ionization of the Asp-15 side chain in WT MshB. Because the ionization described by pK_{a1} leads to an increase in activity with increasing pH, Asp-15 most likely functions as a GBC in the reaction to deprotonate the metal-bound water, activating it for attack of the carbonyl group on substrate. Structural data available support this mechanism because the side chain of Asp-15 shares a hydrogen bond to one of the metal-waters in the MshB crystal structure (Fig. 1B). The magnitude of the decrease in activity observed for the D15A mutant (~530-fold) is smaller than that observed for side chains that are bifunctional GABC (10^3 –10^5 fold) (*37-39*), and consequently, this side chain is probably part of a GABC pair that catalyzes the deacetylation reaction. The pK_a of Asp-15 is probably elevated due to the environment of the active site, which includes an adjacent Asp-16 side chain.

Results from pH studies also reveal that the ionization described by pK_{a2} is lost in the Y142F and Y142A mutants (Fig. 6), suggesting that the side chain of Tyr-142 is responsible for pK_{a2} in WT MshB. The ionization described by pK_{a2} leads to a decrease in activity with increasing pH, indicating that the Tyr must remain protonated for maximal activity. This suggests two possible roles for Tyr-142 in the chemical reaction: 1) GAC to protonate the amine leaving group or 2) to polarize the carbonyl substrate/stabilize the oxyanion intermediate. Due to the magnitude of the decrease in activity at the pH optima (*V/K*) compared with the H144A mutant (74- versus 179-fold), the distance between the Tyr-142 hydroxyl and metal-water (2.15 Å) in the catalytic model depicted in Fig. 7C, and the orientation of Tyr-142 relative to the presumed

substrate binding site (Figs. 1C and 8), it seems most likely that Tyr-142 functions in the latter role to polarize the carbonyl group on substrate/stabilize the oxyanion intermediate. The modest change that is observed for pK_{a2} upon substitution of the active site metal ion (Table 5) may also be explained by this ionization reflecting Tyr-142 because this side chain is proposed to hydrogen-bond to the metal-water and therefore would be sensitive to the identity of the bound metal ion. The assignment of pK_{a2}, reflecting the ionization of Tyr-142, is preferred over assignment of pK_{a2} as the metal-water because 1) the pK_a is lost in the Y142A/F mutants (compared with a modest shift in pK_{a2} observed in the metal substitution experiments), and 2) it seems unlikely that substitution of Tyr-142 with Phe and Ala would both markedly increase the pK_a of the metal-water by several pH units given the differences in hydrophobicity between the active sites containing Phe versus Ala at this position.

Table 7. Solvent isotope effects of Zn^{2+}-MshB variants

MshB[a,b]	pK_{a1}	pK_{a2}	$V/K_{H2O}/V/K_{D2O}$
WT[c] (H_2O)	7.4 ± 0.1	10.5 ± 0.1	1.2
WT (D_2O)	7.6 ± 0.1	10.6 ± 0.1	
D15A (H_2O)		10.4 ± 0.3	0.8
D15A (D_2O)		10.3 ± 0.3	
Y142F (H_2O)	7.1 ± 0.05		1.0
Y142F (D_2O)	7.3 ± 0.05		
H144A (H_2O)	7.1 ± 0.1	10.5 ± 0.1	5.4
H144A (D_2O)	7.4 ± 0.4	10.9 ± 0.4	

[a] Apo-MshB was incubated with stoichiometric metal for 30 min prior to activity measurement.
[b] Substrate 5 (WT, Y142F), 10 (Y142A), or 20 mM (D15A, H144A) GlcNAc.
[c] Data adapted from Ref. 14.

The decrease in activity of H144A mutant (~180-fold) and location of the side chain (Fig. 1, B and C) are consistent with His-144 serving as the GAC in the reaction

working in concert with Asp-15 as part of a GABC pair. The magnitudes of the activity decreases for the D15A (530-fold) and H144A (180- fold) mutants are more consistent with the loss of a single GBC or GAC that functions as part of a GABC pair rather than the loss of residues that function as bifunctional GABC (10^3 –10^5 fold) (*37-39*). Additionally, results from solvent isotope effect experiments are consistent with a mechanism that uses a GABC pair. Specifically, these results suggest that there is no significant solvent isotope effect observed in the WT protein because it includes contributions from both GAC and GBC. In the D15A mutant where the proposed GBC has been removed, there is a small inverse solvent isotope effect (0.8) observed that is consistent with a reaction that proceeds via GAC. In the H144A mutant, where the proposed GAC has been removed, there is a large solvent isotope effect (5.0) observed that is consistent with a reaction that proceeds via GBC. Taken together, these results support a model in which Asp-15 and His-144 function as a GABC pair in the WT MshB-catalyzed reaction.

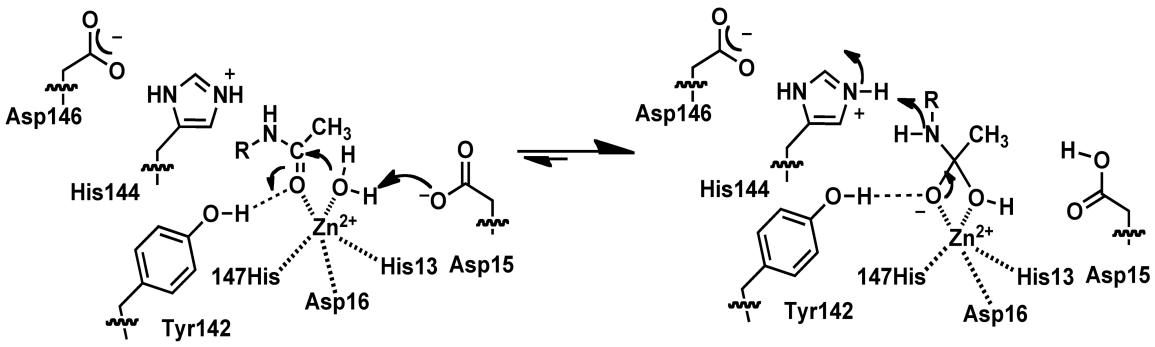

Figure 11: Proposed mechanism for MshB.

4.4 Chemical Mechanism

Together these data suggest that MshB proceeds via the chemical mechanism shown in Fig. 11. In this mechanism, the carbonyl group on substrate replaces one of the

metal-waters. Upon binding, the catalytic metal ion and the side chain of Tyr-142 polarize the substrate carbonyl group. The side chain of Asp-15 functions as a GBC to activate the metal-water for attack on the carbonyl substrate. The catalytic metal ion and Tyr-142 stabilize the resulting oxyanion tetrahedral intermediate. Finally, the side chain of His-144 functions as a GAC to facilitate breakdown of the tetrahedral intermediate. This proposed mechanism using a GABC pair is similar to the mechanism used by the metal-dependent deacetylase LpxC (UDP-3-*O*-(R-3-hydroxymyristoyl)-*N*-acetylglucosamine deacetylase) and unlike prototypical metalloprotease carboxy-peptidase A and the histone deacetylase enzymes, which use a single bifunctional GABC for catalysis (*21*).

4.5 Dynamics of Tyr-142 Play Critical Role in Catalysis

The changes in K_M that are observed in the Tyr-142 mutants, solvent viscosity effects, and the overlay of structures with BOG molecules (Fig. 8) are consistent with Tyr-142 playing a role in substrate binding and product release, whereas the activity data indicate that Tyr-142 plays a role in the chemical mechanism. These different roles for MshB in catalysis can be described using the structures in Fig. 8. We hypothesize that when Tyr-142 is located in the red and orange positions, the active site is open and allows for substrate binding. Movement of Tyr-142 (counterclockwise) toward the catalytic metal ion blocks access to the active site and allows for participation of Tyr-142 in catalysis (model lies between blue and green positions). Following participation in chemistry, Tyr-142 continues moving counter-clockwise to the purple and then red locations, allowing for product release. Results from solvent viscosity experiments are

consistent with a role for Tyr-142 assisting in substrate binding and product release, whereas effects on k_{cat}/K_M and V/K support a role for Tyr-142 in chemistry. Together, our findings suggest that the dynamic Tyr-142 plays a critical role in catalysis by modulating substrate binding, chemistry, and product release.

References

1. Newton, G. L., Buchmeier, N., and Fahey, R. C. (2008) Biosynthesis and functions of mycothiol, the unique protective thiol of Actinobacteria, *Microbiol Mol Biol Rev 72*, 471-494.
2. Jothivasan, V. K., and Hamilton, C. J. (2008) Mycothiol: synthesis, biosynthesis and biological functions of the major low molecular weight thiol in actinomycetes, *Nat Prod Rep 25*, 1091-1117.
3. Rawat, M., and Av-Gay, Y. (2007) Mycothiol-dependent proteins in actinomycetes, *FEMS Microbiol Rev 31*, 278-292.
4. Fan, F., Vetting, M. W., Frantom, P. A., and Blanchard, J. S. (2009) Structures and mechanisms of the mycothiol biosynthetic enzymes, *Curr Opin Chem Biol 13*, 451-459.
5. Gutierrez-Lugo, M. T., Baker, H., Shiloach, J., Boshoff, H., and Bewley, C. A. (2009) Dequalinium, a new inhibitor of Mycobacterium tuberculosis mycothiol ligase identified by high-throughput screening, *J Biomol Screen 14*, 643-652.
6. Gammon, D. W., Steenkamp, D. J., Mavumengwana, V., Marakalala, M. J., Mudzunga, T. T., Hunter, R., and Munyololo, M. (2010) Conjugates of plumbagin

and phenyl-2-amino-1-thioglucoside inhibit MshB, a deacetylase involved in the biosynthesis of mycothiol, *Bioorg Med Chem 18*, 2501-2514.

7. Gutierrez-Lugo, M. T., and Bewley, C. A. (2008) Natural products, small molecules, and genetics in tuberculosis drug development, *J Med Chem 51*, 2606-2612.

8. Metaferia, B. B., Fetterolf, B. J., Shazad-Ul-Hussan, S., Moravec, M., Smith, J. A., Ray, S., Gutierrez-Lugo, M. T., and Bewley, C. A. (2007) Synthesis of natural product-inspired inhibitors of Mycobacterium tuberculosis mycothiol-associated enzymes: the first inhibitors of GlcNAc-Ins deacetylase, *J Med Chem 50*, 6326-6336.

9. Nicholas, G. M., Eckman, L. L., Newton, G. L., Fahey, R. C., Ray, S., and Bewley, C. A. (2003) Inhibition and kinetics of mycobacterium tuberculosis and mycobacterium smegmatis mycothiol-S-conjugate amidase by natural product inhibitors, *Bioorg Med Chem 11*, 601-608.

10. Bhave, D. P., Muse, W. B., 3rd, and Carroll, K. S. (2007) Drug targets in mycobacterial sulfur metabolism, *Infect Disord Drug Targets 7*, 140-158.

11. Newton, G. L., Av-Gay, Y., and Fahey, R. C. (2000) N-Acetyl-1-D-myo-inosityl-2-amino-2-deoxy-alpha-D-glucopyranoside deacetylase (MshB) is a key enzyme in mycothiol biosynthesis, *J Bacteriol 182*, 6958-6963.

12. Newton, G. L., Ko, M., Ta, P., Av-Gay, Y., and Fahey, R. C. (2006) Purification and characterization of Mycobacterium tuberculosis 1D-myo-inosityl-2-acetamido-2-deoxy-alpha-D-glucopyranoside deacetylase, MshB, a mycothiol biosynthetic enzyme, *Protein Expr Purif 47*, 542-550.

13. Nicholas, G. M., Eckman, L. L., Kovac, P., Otero-Quintero, S., and Bewley, C. A. (2003) Synthesis of 1-D- and 1-L-myo-inosityl 2-N-acetamido-2-deoxy-alpha-D-glucopyranoside establishes substrate specificity of the Mycobacterium tuberculosis enzyme AcGI deacetylase, *Bioorg Med Chem 11*, 2641-2647.

14. Huang, X., Kocabas, E., and Hernick, M. (2011) The activity and cofactor preferences of N-acetyl-1-D-myo-inosityl-2-amino-2-deoxy-alpha-D-glucopyranoside deacetylase (MshB) change depending on environmental conditions, *J Biol Chem 286*, 20275-20282.

15. Maynes, J. T., Garen, C., Cherney, M. M., Newton, G., Arad, D., Av-Gay, Y., Fahey, R. C., and James, M. N. (2003) The crystal structure of 1-D-myo-inosityl 2-acetamido-2-deoxy-alpha-D-glucopyranoside deacetylase (MshB) from Mycobacterium tuberculosis reveals a zinc hydrolase with a lactate dehydrogenase fold, *J Biol Chem 278*, 47166-47170.

16. McCarthy, A. A., Peterson, N. A., Knijff, R., and Baker, E. N. (2004) Crystal structure of MshB from Mycobacterium tuberculosis, a deacetylase involved in mycothiol biosynthesis, *J Mol Biol 335*, 1131-1141.

17. Supuran, C. T. (2010) Carbonic anhydrase inhibitors, *Bioorg Med Chem Lett 20*, 3467-3474.

18. Lia, N. G., Shib, Z. H., Tang, Y. P., and Duan, J. A. (2009) Selective matrix metalloproteinase inhibitors for cancer, *Curr Med Chem 16*, 3805-3827.

19. Drag, M., and Salvesen, G. S. (2010) Emerging principles in protease-based drug discovery, *Nat Rev Drug Discov 9*, 690-701.

20. White, R. J., Margolis, P. S., Trias, J., and Yuan, Z. (2003) Targeting metalloenzymes: a strategy that works, *Curr Opin Pharmacol 3*, 502-507.

21. Hernick, M., and Fierke, C. A. (2010) Mechanisms of metal-dependent hydrolases in metabolism, In *Comprehensive Natural Products II* (Mander, L. N., and Lui, H.-W. B., Eds.), pp 547-581, Elsevier.

22. Pettersen, E. F., Goddard, T. D., Huang, C. C., Couch, G. S., Greenblatt, D. M., Meng, E. C., and Ferrin, T. E. (2004) UCSF Chimera--a visualization system for exploratory research and analysis, *J Comput Chem 25*, 1605-1612.

23. Huang, X., and Hernick, M. (2011) A fluorescence-based assay for measuring N-acetyl-1-D-myo-inosityl-2-amino-2-deoxy-alpha-D-glucopyranoside deacetylase activity, *Anal Biochem 414*, 278-281.

24. Hall, R. S., Xiang, D. F., Xu, C., and Raushel, F. M. (2007) N-Acetyl-D-glucosamine-6-phosphate deacetylase: substrate activation via a single divalent metal ion, *Biochemistry 46*, 7942-7952.

25. Raber, M. L., Freeman, M. F., and Townsend, C. A. (2009) Dissection of the stepwise mechanism to beta-lactam formation and elucidation of a rate-determining conformational change in beta-lactam synthetase, *J Biol Chem 284*, 207-217.

26. Schneck, J. L., Briand, J., Chen, S., Lehr, R., McDevitt, P., Zhao, B., Smallwood, A., Concha, N., Oza, K., Kirkpatrick, R., Yan, K., Villa, J. P., Meek, T. D., and Thrall, S. H. (2010) Kinetic mechanism and rate-limiting steps of focal adhesion kinase-1, *Biochemistry 49*, 7151-7163.

27. Meng, E. C., Pettersen, E. F., Couch, G. S., Huang, C. C., and Ferrin, T. E. (2006) Tools for integrated sequence-structure analysis with UCSF Chimera, *BMC Bioinformatics 7*, 339.

28. Dunbrack, R. L., Jr. (2002) Rotamer libraries in the 21st century, *Curr Opin Struct Biol 12*, 431-440.

29. Arnett, S. O., Gerratana, B., and Townsend, C. A. (2007) Rate-limiting steps and role of active site Lys443 in the mechanism of carbapenam synthetase, *Biochemistry 46*, 9337-9345.

30. Ricci, G., Caccuri, A. M., Lo Bello, M., Rosato, N., Mei, G., Nicotra, M., Chiessi, E., Mazzetti, A. P., and Federici, G. (1996) Structural flexibility modulates the activity of human glutathione transferase P1-1. Role of helix 2 flexibility in the catalytic mechanism, *J Biol Chem 271*, 16187-16192.

31. Raber, M. L., Arnett, S. O., and Townsend, C. A. (2009) A conserved tyrosyl-glutamyl catalytic dyad in evolutionarily linked enzymes: carbapenam synthetase and beta-lactam synthetase, *Biochemistry 48*, 4959-4971.

32. Chen, G., Edwards, T., D'Souza V, M., and Holz, R. C. (1997) Mechanistic studies on the aminopeptidase from Aeromonas proteolytica: a two-metal ion mechanism for peptide hydrolysis, *Biochemistry 36*, 4278-4286.

33. Javid-Majd, F., and Blanchard, J. S. (2000) Mechanistic analysis of the argE-encoded N-acetylornithine deacetylase, *Biochemistry 39*, 1285-1293.

34. Harris, M. N., and Ming, L. J. (1999) Different phosphate binding modes of Streptomyces griseus aminopeptidase between crystal and solution states and the status of zinc-bound water, *FEBS Lett 455*, 321-324.

35. Todd, M. J., and Hausinger, R. P. (2000) Fluoride inhibition of Klebsiella aerogenes urease: mechanistic implications of a pseudo-uncompetitive, slow-binding inhibitor, *Biochemistry 39*, 5389-5396.

36. Schowen, K. B., and Schowen, R. L. (1982) Solvent isotope effects of enzyme systems, *Methods Enzymol 87*, 551-606.

37. Hernick, M., Gennadios, H. A., Whittington, D. A., Rusche, K. M., Christianson, D. W., and Fierke, C. A. (2005) UDP-3-O-((R)-3-hydroxymyristoyl)-N-acetylglucosamine deacetylase functions through a general acid-base catalyst pair mechanism, *J Biol Chem 280*, 16969-16978.

38. Cha, J., and Auld, D. S. (1997) Site-directed mutagenesis of the active site glutamate in human matrilysin: investigation of its role in catalysis, *Biochemistry 36*, 16019-16024.

39. Wetterholm, A., Medina, J. F., Radmark, O., Shapiro, R., Haeggstrom, J. Z., Vallee, B. L., and Samuelsson, B. (1992) Leukotriene A4 hydrolase: abrogation of the peptidase activity by mutation of glutamic acid-296, *Proc Natl Acad Sci U S A 89*, 9141-9145.

Chapter 7

Molecular Recognition of Substrates by MshB

Abstract

Mycothiol (MSH) is a unique thiol found in Actinobacteria such as *Mycobacterium* species that contain pathogens known to cause serious human diseases including tuberculosis (TB). MSH serves a protective role, functioning as the primary reducing agent and aiding in the detoxification of xenobiotics. The metal-dependent deacetylase MshB catalyzes the deacetylation of *N*-acetyl-1-D-*myo*-inosityl-2-amino-2-deoxy-α-D-glucopyranoside (GlcNAc-Ins), the committed step in MSH biosynthesis. Herein we examine the molecular recognition properties of MshB using a combination of automated docking, site-directed mutagenesis, and kinetics approaches. A model of MshB with the native substrate GlcNAc-Ins bound to the cleft-like active site of MshB was generated using Autodock 4.2. The resulting model predicts that the *N*-acetyl-glucosamine (GlcNAc) moiety binds to the active site via hydrogen bonding interactions with the side chains of Arg68, Asp95, and His144. Experimental examination reveals that the R68A and D95A mutants are completely inactive with the GlcNAc substrate, while the H144A mutant exhibits a 100-fold decrease in the k_{cat}/K_M value. Furthermore, this model predicts that the carbonyl O atom on the substrate coordinates to the catalytic Zn^{2+} and the side chain of Tyr142, thereby polarizing the carbonyl C atom and facilitating nucleophilic attack by a metal-water nucleophile (Chapter 6). The *myo*-inositol moiety is predicted to bind at the entrance of active site through hydrogen bonding interactions with the side chains of Glu47, Ser260, and Asn261, and hydrophobic packing with Met98. In addition, computational data suggest that Met98 is located on a surface loop that is highly flexible in the absence of bound

ligand, but is stabilized upon substrate binding. Kinetic results for the M98A mutant suggest a possible role for Met98 in preventing ligand dissociation from the active site. MshB also possesses an amidase activity and is able to catalyze the hydrolysis of larger amide substrates. Docking of CySmB-GlcN-Ins (bimane derivative of 1-D-*myo*-inosityl-2-(L-cysteinyl)amido-2-deoxy-α-D-glucopyranoside) to MshB reveals a hydrophobic cavity adjacent to the GlcNAc binding site that consists of the side chains of Leu19, Leu185, Ile124, Phe216, and Leu259. The additional hydrophobic interaction may contribute to the high reactivity of CySmB-GlcN-Ins to MshB, which displays 2.5-fold decrease and 19-fold increase in K_M and k_{cat}/K_M, respectively, from that of GlcNAc-Ins (Newton *et al*, (2006) Protein Expr Purif, 47(2): p. 542-50.); therefore the presence of this hydrophobic cavity is advantageous for structural based rational design of inhibitors as potential TB drugs with high affinity and specificity against MshB.

1. Introduction

Mycobacterium tuberculosis is the causative agent of human TB and infects one-third of the world's population with 8.7 million new cases and 1.4 million deaths worldwide each year. (*1*) The presence of persistent *M. tuberculosis* and emergence of drug-resistant TB pose significant challenges to current TB therapies.(*2*) Consequently, new therapeutic agents that can be effective against these types of TB are needed. *Mycobacterium* species produce a unique thiol, mycothiol (MSH), that functions as their primary cellular reducing agent to protect against damaging effects from reactive oxygen species, similar to glutathione in mammalian cells.(*3*) MSH is also used to detoxify xenobiotics; MSH mutants display increased sensitivity to antibiotics such as streptomycin, ethionamide, rifampin, and alkylating toxins.(*4, 5*) Due to these protective effects that MSH provides, *M. tuberculosis* mutants with decreased levels of MSH fail

to grow in primary murine macrophages.(*6*) The half-life for loss of MSH is 50 hours during the stationary phase in *Mycobacterium smegmatis*, indicating the turnover of MSH remains active during dormancy.(*7*) In light of its importance for TB infection and persistence, and its absence in humans, MSH is a potential drug target for TB treatment.

There are six enzymes involved in MSH biosynthesis. The metalloenzyme MshB catalyzes the fourth step in this pathway - the deacetylation of GlcNAc-Ins to form 1-D-*myo*-inosityl-2-amino-2-deoxy-α-D-glucopyranoside (GlcN-Ins) and acetate. MshB is considered an attractive drug target because it catalyzes the rate-limiting step in MSH biosynthesis.(*8*) Information about MshB protein structure and function will be useful for the development of potent and specific enzyme inhibitors. The three-dimensional structure of MshB was first resolved as a tetramer containing a bound zinc ion coordinated in the active site by His13, His147 and Asp16, and two water molecules (Zn-MshB; PDB 1Q74).(*9*) One of the water molecules is located ~3Å away from the conserved Asp15, which is proposed to function as a general base catalyst in the MshB-catalyzed reaction.(*9, 10*) The structure of MshB with β-octylglucoside (BOG-MshB; PDB 1Q7T) co-crystallized near the zinc-binding site was solved as a dimer with two asymmetric units (A and B).(*11*) The glycosyl ring of the BOG molecule in each unit occupies similar positions with different orientations. In unit A, the octyl tail is projected out of the active site through an entrance with hydrophobic stacking with side-chain of Met98 and exposed to solvent, while in unit B the octyl tail of the BOG is buried inside a hydrophobic cavity.(*11*) The most recent structural study on MshB reveals a molecule of acetate coordinated to the active-site zinc ion (Act-MshB; PDB 4EWL) with the carboxylate O atoms replacing the two water molecules observed in Zn-MshB.(*12*) A molecule of glycerol is also observed in the active site and shares hydrogen bonds with the side chains of Arg68 and

Asp95.(*12*) Since inhibitors of metalloenzymes typically contain a group that binds to the catalytic metal ion, (*13-16*) we previously examined the metal cofactor preferences of MshB. Our results indicate that MshB is a cambialistic metalloenzyme that likely uses Fe^{2+} and Zn^{2+} *in vivo* and that the cofactor preferences MshB are dependent on environmental oxidative status and metal availability.(*17*) Additionally, we probed the chemical mechanism of MshB using site-directed mutagenesis and kinetic studies, and identified that the side chains of Asp15, His144, and Tyr142 are important for MshB activity.(*10*) Interestingly, Tyr142 appears to be a dynamic side chain that participates throughout the catalytic cycle, participating in substrate binding, chemistry, and product release.

Herein we examine the molecular recognition properties of MshB using a combination of docking simulations, site-directed mutagenesis, and kinetic studies. Results from docking experiments predict that the GlcNAc moiety of the GlcNAc-Ins substrate shares hydrogen bonds with the side chains of Arg68, Asp95, and His144. Additionally, the docked structure suggests that the carbonyl group on the substrate is polarized by coordination to a catalytic metal ion and hydrogen bonding interaction with the hydroxyl group on Tyr142, as predicted in our former study.(*10*) These predictions from the docking studies are supported by results from kinetic studies on the R68A, D95A, and H144A mutants. Docking results with GlcNAc-Ins also predict that the Met98 and Glu47 side chains may regulate access to the MshB active site via rotation of their side-chains. Results from kinetic studies on the M98A and E47A mutants confirm the importance of the Met98 and Glu47 side chains in the deacetylation of GlcNAc. Additionally, the *myo*-inositol ring is located at the entrance of active site and is stabilized by parallel stacking of its cyclohexyl ring with the side-chain of Met98. Since MshB has also been shown to possess amidase activity, we repeated the automated docking studies with larger amidase substrates.

Automated docking of CySmB-GlcN-Ins into MshB predicts a binding mode that is reasonably expected to allow for chemistry. The conformation of GlcN-Ins moiety is similar to GlcNAc-Ins and the bimane group is buried inside a hydrophobic cavity in the vicinity of active site. The additional hydrophobic interaction may contribute to the high reactivity of CySmB-GlcN-Ins to MshB, which displays 2.5-fold increase and 19-fold increase in K_M and k_{cat}/K_M, respectively, compared to the native substrate GlcNAc-Ins.(*18*) Thus the presence of this hydrophobic cavity may be advantageous for structural based design of inhibitors with high affinity and specificity against MshB.

2. Materials and Methods

2.1 General Procedures

All solutions were prepared using milliQ water. Primers were purchased from Integrated DNA Technologies. Genomic DNA was purchased from ATCC. DNA sequencing was performed at the Virginia Bioinformatics Institute DNA Sequencing Facility (Virginia Tech). All chemicals were purchased from ThermoFisher Scientific, Sigma-Aldrich and Gold Biotechnology. For kinetic experiments, solutions were prepared with reagents that did not contain extraneous metal ions and/or were treated with Chelex (Biorad), and solutions were stored in "metal-free" plasticware. Automatic docking calculations were performed with AutoDock4.2.(*19, 20*) Molecular graphic images were produced using the *UCSF Chimera* package (*21*).

2.2 Docking of ligands to MshB using AutoDock 4.2

Automated docking calculations were performed in AutoDock 4.2.(*19, 20*) The coordinate files of GlcNAc-Ins, CySmB-GlcN-Ins, fCySmB-GlcN-Ins, and MSmB were prepared in AutoDockTool (ADT) to add hydrogen, compute Gasteiger charges and merge the non-polar hydrogen.(*20*) Flexibility was limited to 10 torsional degrees of freedom for each ligand, allowing the fewest number of atoms to move. The crystal structure of Act-MshB (PDB 4EWL) was chosen as the receptor, and was prepared in ADT by removing solvent and the bound acetate and glycerol. Although a charge of +2 for zinc was reported to dock Zn-hydrolases, our experiments show that the charge of zero gives a better binding model for MshB. A grid centered on the acetate-binding site was defined using AutoGrid. The grid size was set to 70x70x70 points with a grid point spacing of 0.375Å. The Lamarckian genetic algorithm (LGA) was used to simulate the docking, and docking experiment for GlcNAc-Ins, CySmB-GlcN-Ins, fCySmB-GlcN-Ins, and MSmB, respectively, was derived from 10, 15, 20 and 50 independent runs, each yielding 15 to 50 docked conformations. For each independent run, searching started from random position and conformation, and a maximum number of 27,000 LGA operations were generated on a single population of 50 individuals. Step sizes of 1 Å for translation and 50 degree for rotation were chosen. The maximum number of energy evaluation was set to 250,000. Operator weights for crossover, mutation, and elitism were set to 0.80, 0.02, and 1, respectively. The results were clustered using a tolerance of 1 Å. Manual docking of MSmB was performed in *UCSF Chimera* by superimposing the molecule onto the corresponding atoms of the automated docking result of fCySmB-GlcN-Ins. (*21, 22*)

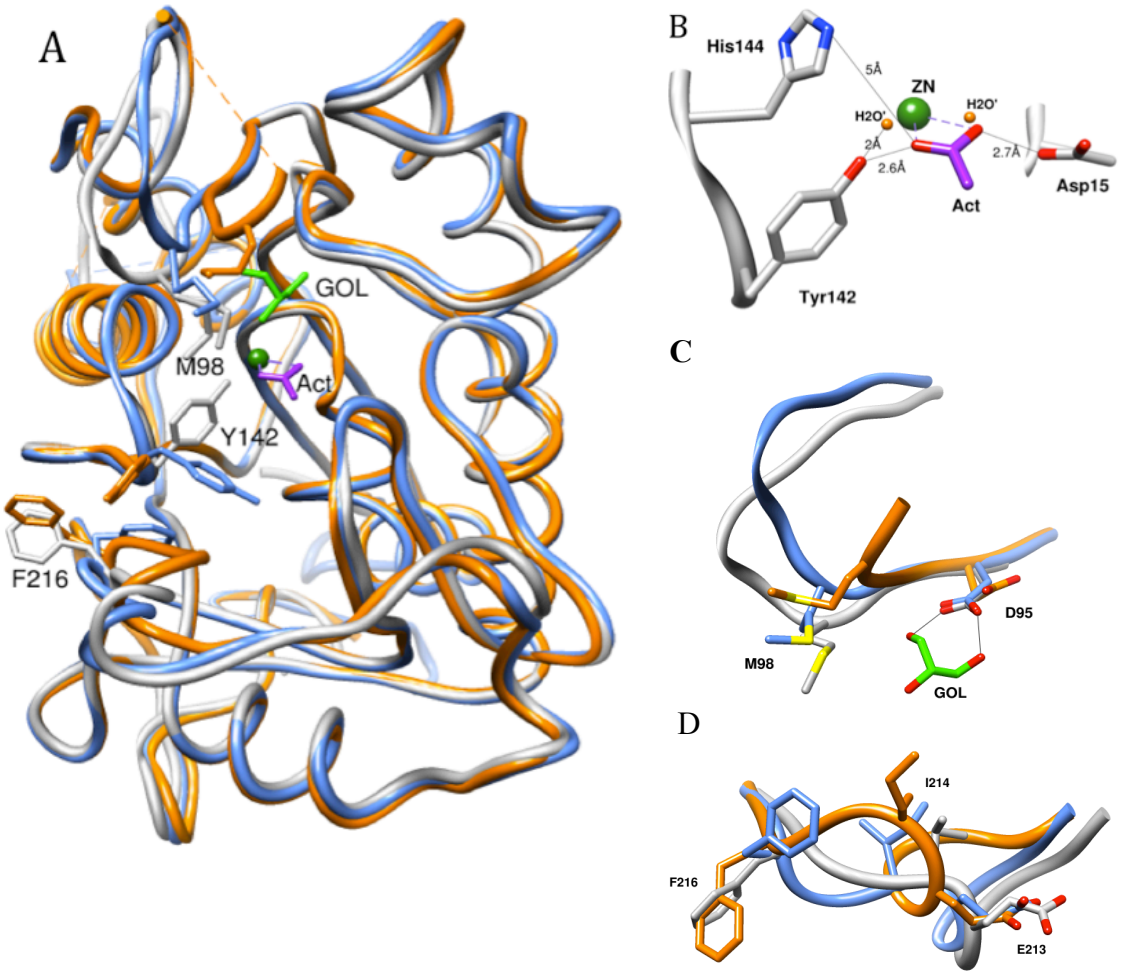

Figure 1. *Mycobacterium smegmatis* MshB structure. (A) Alignment of the MshB monomers from three crystal structures: Zn-MshB (PDB 1Q74, orange), BOG-MshB (PDB 1Q7T, blue), and Act-MshB (PDB 4EWL, gray). The catalytic zinc is shown in dark green, and the glycerol and acetate observed in Act-MshB is colored with light green and purple, respectively. The overall conformation of the protein and the active site do not vary significantly, whereas the surface loops contain dynamic Met98, Tyr142, and Phe216 side chains that vary in the structures. (B) Active site of Act-MshB. The phenolic hydroxyl of Tyr142 points toward the catalytic zinc (dark green) and is 2.6 Å away from the O atom on bound acetate. The distance between O^{η} of Tyr142 in Act-MshB and the metal-bound water observed in Zn-MshB (orange) is 2 Å as predicted by Huang, *et al*. (*10*). (C) and (D) display the flexible loops in MshB identified by overlay of the MshB monomers from three crystal structures. (C) Overlay of loop (residues 95-104) (only residues 95-99 are visible in Zn-MshB). The side-chains of Asp95 and Met98 are shown in stick and colored by heteroatom. The acetate co-crystallized in Act-MshB is shown in purple and is hydrogen bonded to Asp95. The BOG molecule in BOG-MshB locates at the same position as the acetate and interacts with Asp95 in a similar manner (not shown). The Zn-MshB does not contain a ligand in this site. (D) Overlay of loop (residues 211-217). The side-chains of Glc213, Ile214, and Phe216 are shown in stick and colored by heteroatom.

2.3 Protein Expression and Purification

The previously reported plasmid encoding the MshB gene from *Mycobacterium smegmatis* containing an N-terminal His-MBP tag was used as the template for preparation of mutant plasmids. (*17*) All mutant plasmids were prepared using the QuikChange Lightning site-directed mutagenesis kit (Stratagene). Plasmid sequences were verified by DNA sequencing. All MshB variants were expressed and purified according to published procedures (*10, 17, 23*).

Briefly, cells were lysed using an Emulsiflex-C3 high pressure homogenizer (Avestin) and MshB variants were purified at 4 °C. Cell lysate was clarified by centrifugation (18,000 rpm, 4 °C) and loaded onto a pre-equilibrated (Buffer A; 30 mM HEPES, 150 mM NaCl, 1 mM TCEP, 0.5 mM imidazole, pH 7.5) Co-IMAC column (50 ml of chelating Sepharose (GE Healthcare) charged with $CoCl_2$). The column was washed with 150 ml of Buffer A, and His-MBP-MshB was eluted using an imidazole step gradient (200 ml each: Buffer A + 10 mM imidazole, Buffer A + 25 mM imidazole, Buffer A + 300 mM imidazole). Fractions containing His-MBP-MshB (via SDS-PAGE) were combined, concentrated (Amicon Ultra-15 centrifugal devices, Millipore), and dialyzed (Snake-skin tubing, molecular weight cut-off 10,000; Pierce) against 2 × 4 liters of Buffer A overnight at 4°C in the presence of His-TEV protease (300 μg/ml) to remove the His-MBP tag. The resulting TEV-cleaved protein was loaded onto a pre-equilibrated (Buffer A + 25 mM imidazole) Co-IMAC column. His-MBP and His-TEV remain bound to the Co-IMAC column, whereas MshB elutes in the flow-through. Fractions containing MshB (via 12% SDS-PAGE) were combined, concentrated, and dialyzed against 2 × 4 liters of 25 mM HEPES, 1.5 mM TCEP, pH 7.5 (Slide-a-Lyzer, molecular weight cut-off 10,000; Pierce). Protein concentration was determined using the Bradford assay (Sigma). Protein aliquots were flash frozen in liquid nitrogen and stored at -80 °C.

For the preparation of apo-MshB (*17*), purified protein (≤ 100 μM) was incubated with 10 mM HEPES, 20 mM dipicolinic acid, 250 μM EDTA, pH 7.5, on ice. After 1 h, the protein solution was concentrated, washed (diluted with buffer and then concentrated) with 3 × 15 ml of 25 mM HEPES, 1.5 mM TCEP, pH 7.5, and run over a desalting column to remove residual dipicolinic acid/EDTA. Metal ion concentrations were determined using an ICS-3000 ion chromatography system (Dionex). Apo-MshB samples contained ≤ 10% metal/protein. Prior to activity measurements, apo-MshB (≤ 10 μM) was incubated with a stoichiometric concentration of $ZnSO_4$ and incubated on ice for 30 min.

2.4 MshB Deacetylase Activity

MshB deacetylase activity was measured with the substrate *N*-acetyl-glucosamine (GlcNAc, Sigma) using a fluorescamine (FSA)-based assay (*24*). Although the GlcNAc substrate has a decreased affinity for MshB compared with the natural substrate GlcNAc-Ins (K_M of 38 mM versus 340 μM), the GlcNAc moiety that undergoes the chemical transformation is conserved.(*18, 23*) In general, assay mixtures containing 50 mM HEPES, 50 mM NaCl, 1 mM TECP, pH 7.5 and 0-150 mM GlcNAc were pre-equilibrated at 30 °C, and reactions were initiated by the addition of enzyme (1 μM). After incubation for various times, reaction aliquots (30 μL) were quenched by the addition of 20% trichloroacetic acid (TCA, 10 μL), and the cleared supernatant (25 μL) was transferred into a 96-well plate, diluted with 1 M borate pH 9 (75 μL) and reacted with FSA (30 μL in CH_3CN, Invitrogen). After 10 minutes, the fluorescence was measured (Ex. 395 nm, Em. 485 nm) using a SpectraMax M5^e platereader (Molecular Devices). Initial rates of product formation (< 10%) were determined from these data. For determination of the steady-state parameters, the parameters k_{cat}, K_M, and k_{cat}/K_M were

obtained by fitting the Michaelis-Menten equation to the initial linear velocities using the curve-fitting program Kaleidagraph (Synergy Software), which also calculates the asymptotic S.E. values.

3. Results

3.1 Docking of GlcNAc-Ins with MshB predicts several key binding interactions between various side chains and substrate

Molecular automated docking is an efficient method to probe and predict protein-ligand interactions.(*25*) It has been reported that re-docking of zinc metalloproteinases with their ligands was capable to regenerate the binding interactions observed in the crystal structures. (*26*) Docking simulations include two parts: a search algorithm to explore the conformational space and a scoring function to evaluate each conformation.(*25*) In this study, docking calculations were performed in Autodock 4.2, which utilizes a Lamarckian Genetic algorithm (LGA) to sample the ligand conformations (*19*) and a grid-based technique for energy evaluation at each step of simulation (*20*). Docking simulations for native substrate (GlcNAc-Ins) binding were performed in AutoDock4.2 using Act-MshB as the receptor. The active site of Act-MshB contains a molecule of acetate, the product of deacetylation reaction, and glycerol, the structure component of glycoside ring (Fig. 1); therefore, it gives rise to a reliable model of the true substrate GlcNAc-Ins bound to MshB. Starting from random initial positions and orientations, the docking calculations produced 10 independent conformations that were ranked according to binding energy and grouped into 7 clusters (1.0 Å cutoffs). (Table 1) The docking results were evaluated by comparison to the co-crystallized glycerol and acetate in active site of Act-MshB. The most reliable result displays a conformation in which the atoms of the glucosamine ring

superimpose onto the corresponding atoms of glycerol and the carbonyl group of the amide bond overlays with the carbonyl group of acetate. (Fig. 2A) This result exhibits the lowest binding energy and is identified in the first and most highly populated cluster that contains four conformations. (Table 1)

Table 1. Results of Automated Docking of ligands to MshB

Ligand	Number of Cluster [a]	Rank [b]	Binding Energy (kcal mol^{-1})		Intermolecular energy [c] (kcal mol^{-1})	Torsional energy [c] (kcal mol^{-1})
			Lowest [d]	Reliable result [c]		
GlcNAc-Ins [e]	7	1	-8.05	-8.05	-9.24	1.19
CySmB-GlcN-Ins [e]	15	6	-11.60	-10.38	-13.36	2.98
fCySmB-GlcN-Ins [e]	20	2	-9.96	-9.74	-13.02	3.28
MSmB [e, f]	50	—	-10.43	—	—	—

[a] The results were clustered using a tolerance of 1 Å
[b] The docking results are ranked according to binding energy.
[c] Docking results are evaluated by superimposing onto the corresponding atoms of glycerol and acetate co-crystallized in active site of Act-MshB. the most reliable results (superimposible to co-crystallized ligands) are shown in Fig. 4 and Fig. 3, and corresponding parameters are presented here.
[d] The docking conformations with lowest energy may or may not be the reliable docking results.
[e] Docking of GlcNAc-Ins, CySmB-GlcN-Ins, fCySmB-GlcN-Ins, and MSmB were performed with 10, 15, 20, and 50 independent runs, respectively
[f] Docking experiment for MSmB was derived from 50 runs and replicated twice. None of the resulting conformations can either superimpose with co-crystallized ligands in Act-MshB or ligate the amide oxygen to the catalytic zinc.

Additionally, the docking result with GlcNAc-Ins has the glucosamine ring tethered to the active site through extensive hydrogen bonding interactions with its 3-OH to Arg68 $N^{\eta 2}$, 4-OH to Arg68 $N^{\eta 1}$ and Asp95 $O^{\delta 2}$, and 6-OH to Asp95 $O^{\delta 1}$ and His144 $N^{\varepsilon 2}$. (Fig. 2B) Additional stabilization is provided by interactions between the amide O atom with Tyr142 O^{η} and the

catalytic zinc, with distances of 3.4 Å and 3.0 Å, respectively. (Fig. 4) The amide bond on GlcNAc-Ins occupies the acetate-binding site in Act-MshB, with the carbonyl C atom located ~2 Å away from the zinc-bound water observed in Zn-MshB.

Docking result with GlcNAc-Ins also indicates potential role for His144 in substrate binding. The side chain of His144 is located ~6 Å from carbonyl amide, while the $N^{\varepsilon 2}$ on the imidazole of H144 is within the hydrogen bonding distance to 6-OH on GlcNAc (2.5 Å). The carboxylate O atom of Asp15 is located ~3.8 Å away from the amide N atom on substrate. (Fig. 4) The side chain of Asp146 is too buried to directly interact with substrate, as the closest distance between the carboxylate oxygen to the glucosamine hydroxyl is ~5 Å. (Fig. 2D) As for the possibility of Asp146 interacting with other active site side chains, the distance between carboxylate O atom on Asp146 and imidazole N atom on His144 is larger than 4 Å, while the distance of Asp 146 $O^{\delta 1}$ and His13 $N^{\varepsilon 2}$ is only 3 Å. (Fig. 2D)

The *myo*-inositol moiety is known to provide important substrate binding interactions as the value of K_M is increased from 0.34 mM with GlcNAc-Ins (*18*) to 38 mM with GlcNAc (*10*), whereas the values of k_{cat} for both substrates are comparable. The *myo*-inositol moiety on GlcNAc-Ins is accommodated at the entrance of the active site surrounded by Met98, Glu47, Ser260, and Asn261. (Fig. 2C) This space is occupied by the octyl tail of BOG in unit A of the BOG-MshB complex (*11*). The inositol ring is stabilized by possible hydrogen bonds between the 2'-OH and Ser260 O^{γ}, 3'-OH and Glu47 $O^{\varepsilon 2}$, and 5'-OH and Asn261 $O^{\delta 1}$ (Fig. 4). In addition, parallel stacking of the Met98 side-chain and the cyclohexyl ring of inositol with average distance of ~4 Å is observed. (Fig. 2C) Met98 is located on the surface loop (residues 95-104) and partially covers the entrance of active site. (Fig. 1A) The interaction from

hydrophobic packing may contribute to stabilization of the inositol moiety as well as the flexible loop.

Table 2. Available X-ray structures of MshB

	PDB ID	Resolution	Ligand(s) in active site	Oligomeric state	Chain ID	Residues visible	Ref.
Zn-MshB	1Q74	1.7Å	Zn^{2+}	Tetramer	A	3-99, 104-163, 170-299	(*11*)
					B	2-97, 104-163, 168-206, 216-298	
					C	2-96, 104-162, 168-210, 217-298	
					D	2-99, 103-163, 168-204, 217-298	
BOG-MshB	1Q7T	1.9 Å	BOG[§], Hg	Dimer	A	12-164, 171-303	(*9*)
					B	2-164, 171-299	
Act-MshB	4EWL	1.85 Å	Zn^{2+}, GOL[§], Act[§]	Dimer	A	1-299	(*12*)
					B	1-164, 173-298	

[§]Abbreviations: BOG, β-octylglucoside; GOL: Glycerol; Act: Acetate.

3.2 Docking of larger amidase substrates with MshB reveals a hydrophobic cavity located adjacent to the active site

MshB shows broad substrate specificity and displays amidase activity with mycothiol S-conjugates and related derivatives.(*18*) (Fig. 3) Among all the substrates that have been tested,

the bimane derivative of desacetylmycothiol, termed CySmB-GlcN-Ins, exhibits the highest reactivity with MshB. MshB can hydrolyze this compound to generate CySmB and GlcN-Ins, with a specific rate 5-fold higher than the native substrate GlcNAc-Ins.(*18*) Further elaboration of the amine on the cysteine moiety of CySmB-GlcN-Ins by formylation (fCySmB-GlcN-Ins) or acetylation (bimane derivative of MSH, MSmB) reduces the chemical reactivity by 100- and 200-fold, respectively. (*18*)

CySmB-GlcN-Ins was docked into MshB and the results from these studies predict that the carbonyl O on the reactive amide bond is coordinated to the zinc and the *myo*-inositol moiety is packed against the side chain of Met98, with an overall geometric conformation of the GlcN-Ins moiety similar to GlcNAc-Ins. (Fig. 6) The binding conformations of CySmB-GlcN-Ins generated from the docking calculations are highly variable and cannot be clustered at 1Å rmsd. (Table 1) Although the most reliable docking result from 15 independent runs did not exhibit the lowest binding energy, it is the one that targeted the amide bond to the active site and coordinated it to the catalytic zinc. (Table 1 and Fig. 6) Interestingly, the bimane group is buried into an adjacent hydrophobic groove consisting of Leu19, Leu185, Phe216, Ile 214, and Leu259. (Fig. 6A) This same hydrophobic cavity is occupied by the octyl tail of β-octylglucoside in unit B of the BOG-MshB complex. (*11*)

Docking of fCySmB-GlcN-Ins to MshB generates the same binding conformation as observed for CySmB-GlcN-Ins. (Fig. 6B) However, automated docking of MSmB was not successful, with no result displaying a distance within 5 Å between the amide O and the catalytic zinc. (Table 1) Manual docking of MSmB into MshB by superimposing MSmB onto the corresponding atoms of fCySmB-GlcN-Ins reveals a clash between the acetyl methyl group and the side-chains of Asp15.

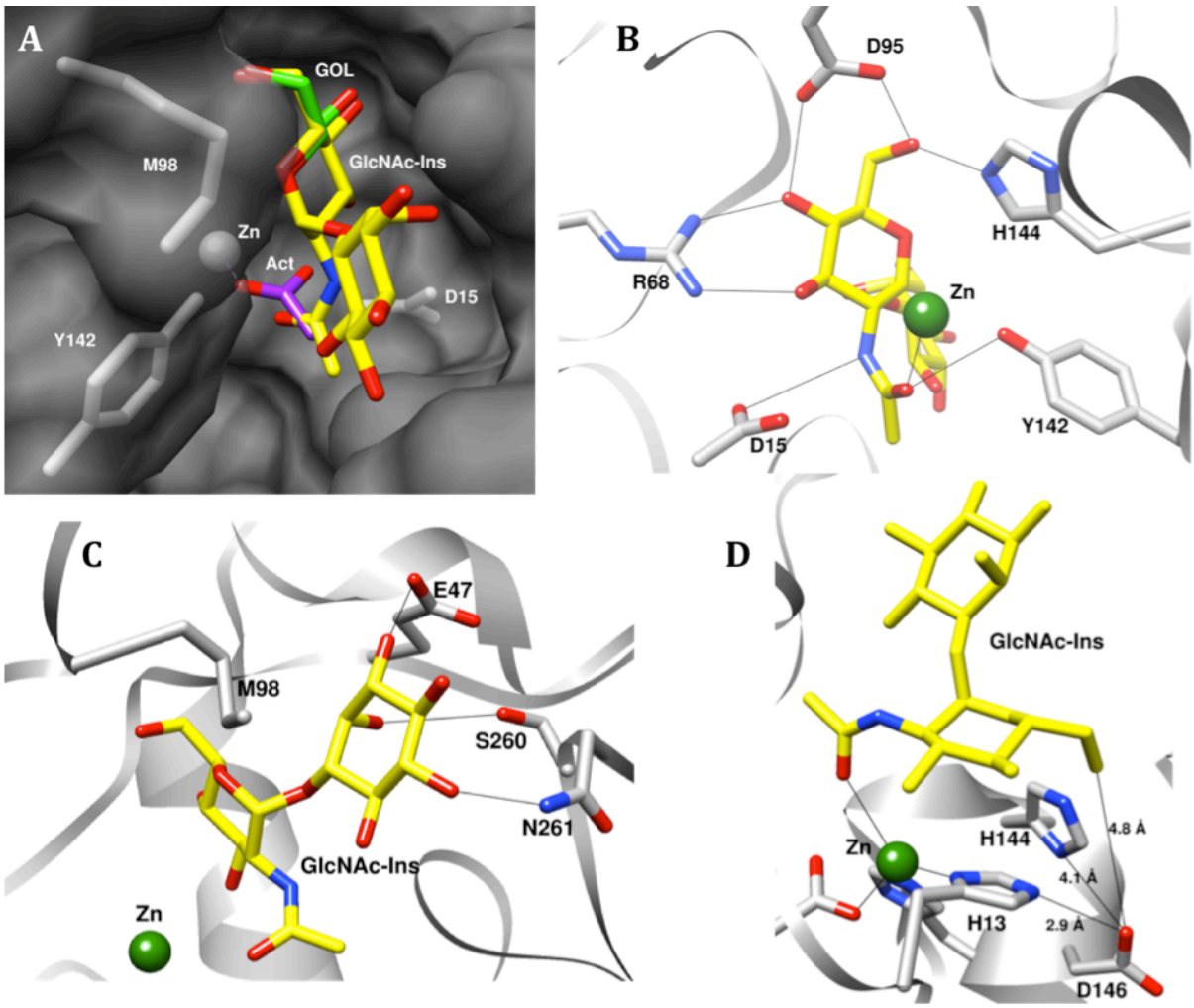

Figure 2. Results of docking GlcNAc-Ins to Act-MshB (PDB 4EWL). (A) GlcNAc-Ins is bound to the cleft-like active site with atoms of glucosamine ring superimposed onto the corresponding atoms of glycerol and the carbonyl group of the amide bond onto the acetate. The carbons on GlcNAc-Ins, glycerol, and acetate are colored with yellow, light green, and purple, respectively. The protein residues and their surfaces are shown in gray. (B) Hydrogen bonding interactions between the hydroxyl groups on the GlcNAc moiety with the active site residues Arg68, Asp95, and His144. The amide O atom is coordinated to the catalytic zinc (green) and phenolic O atom of Tyr142. The distance between the amide N atom and carboxylate O on Asp15 is 3.8 Å. (C) Stabilization of the *myo*-inositol moiety at the entrance of active site provided by hydrogen bonding interactions between the hydroxyl groups and Glu47, Ser260, and Asn261 and the cyclohexyl ring parallel stacking with Met98. (D) Asp146 forms part of the second metal binding shell by interacting with His13, while the distance of $O^{\delta 1}$ of Asp146 to His144 and 6-OH on GlcNAc moiety (glucosamine ring is colored with yellow and the amide bond is colored by heteroatoms) are larger than 4 Å.

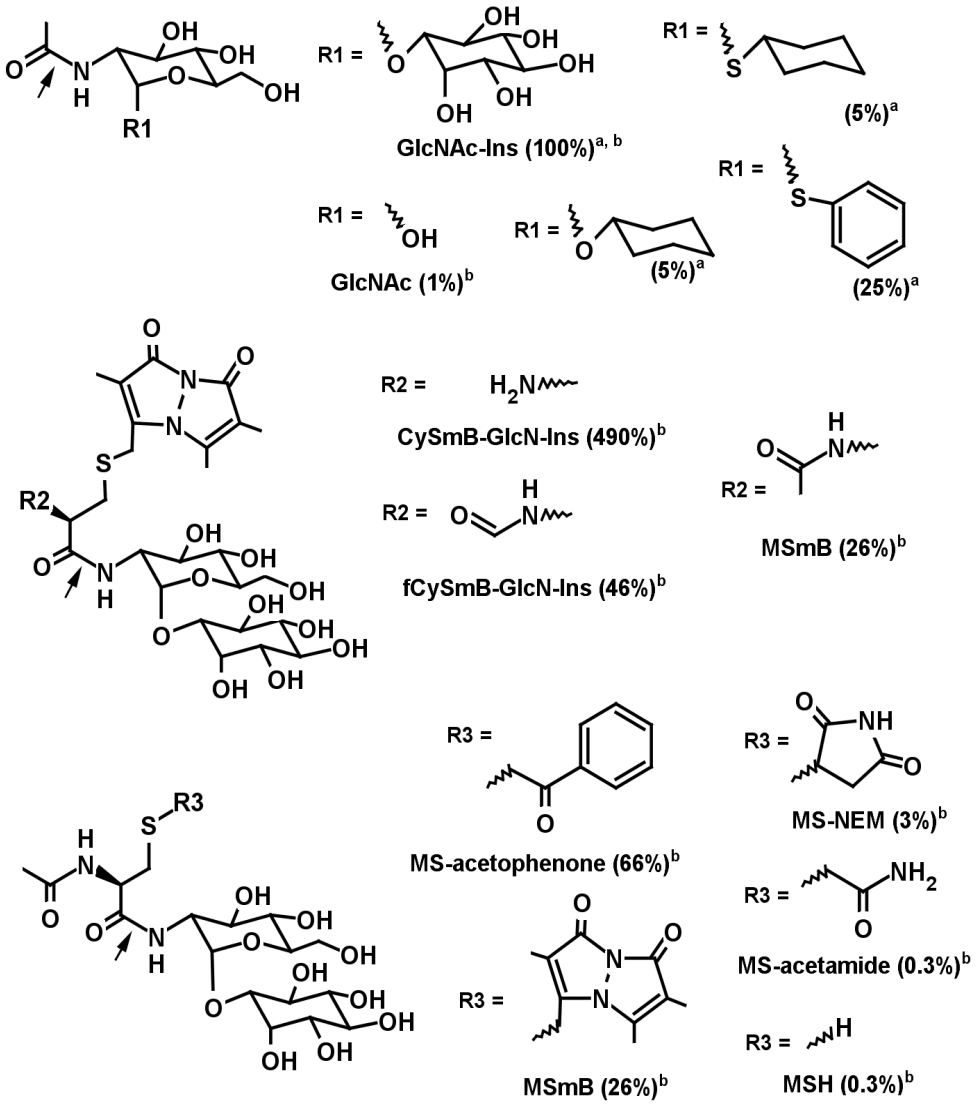

Figure 3. MshB substrates. Bonds potentially cleaved in deacetylase and amidase reactions with each substrate are indicated by arrows. The rate of natural substrate GlcNAc-Ins is set at 100% as a reference. Relative rates of MshB cleavage of amide are indicated in parenthesis as percentage of GlcNAc-Ins activity. [a], data adapted from (*27*); [b], data adapted from (*28*).

3.3 Mutagenesis and Kinetic Studies Support Proposed Substrate Binding Modes

We have initiated efforts to test the binding interactions predicted by the automated docking studies using a combination of site-directed mutagenesis and enzyme kinetics with the substrate GlcNAc. Arg68 and Asp95 share hydrogen bonds with the bound glycerol in the Act-

MshB structure. (*12*) Removal of either of these side chains with either the R68A or D95A mutant results in an inactive enzyme with no measurable activity using the GlcNAc substrate. (Table 3) These results indicate that the side chains of Arg68 and Asp95 are essential for catalysis, mostly likely via substrate binding interactions with the hydroxyl group on substrate. The docking results also suggest a hydrogen bonding interaction between the glucosamine hydroxyl and the side chain of His144. Mutation on His144 to Ala results in a significant effect on k_{cat} and $(k_{cat}/K_M)^{GlcNAc}$, which are decreased 60- and 100-fold, respectively. There is a < 2-fold increase in K_M^{GlcNAc} observed for the H144A mutant. (Table 3)

An overlay of available MshB structures (Table 2) suggests dynamic movements of the Tyr142 side chain. (Fig. 1A) While the side chain of Tyr142 is unobstructed and can move freely (360°), the phenyl hydroxyl points to the catalytic metal ion in Act-MshB with a distance of 2.6 Å from the carboxylate O atom on acetate. (Fig.1B) We have shown that mutations to this side chain significantly alter the steady-state parameters.(*10*) Mutation on Tyr142 by removal of the side-chain (Ala), or substitution with hydrophobic (Phe) or hydrophilic (Gln) residues leads to a 2 to 4-fold decrease in K_M^{GlcNAc} and 15 to 20-fold decrease in $(k_{cat}/K_M)^{GlcNAc}$, (Table 3) suggesting that both the sterics and hydrogen-bonding potential of Tyr are important for ligand-protein interaction.

We previously reported the importance of Asp146 in catalysis of MshB with the substrate GlcNAc.(*10*) The D146A mutant exhibits a 10-fold increase and 250-fold decrease on K_M^{GlcNAc} and $(k_{cat}/K_M)^{GlcNAc}$, respectively. (Table 3) In this study, when the side chain of Asp146 is mutated to Asn, the K_M^{GlcNAc} value is 2-fold higher than the value observed with WT. However, a 27-fold decrease in the $(k_{cat}/K_M)^{GlcNAc}$ value is still observed for D146N mutant, indicating that the side chain of Asp146 is important for binding GlcNAc and/or stabilizing the intermediate.

Table 3. Steady-state parameters of Zn^{2+}-MshB variants with GlcNAc

MshB[a,b]	K_M (mM)	k_{cat} (min^{-1})	k_{cat}/K_M (M^{-1} s^{-1})	% WT activity
WT[c]	38 ± 4	46 ± 2	20 ± 1	--
D15A[d]	52 ± 11	0.29 ± 0.02	0.09 ± 0.01	0.5
Y142A[d]	22 ± 2	1.8 ± 0.05	1.36 ± 0.10	6.8
Y142F[d]	9 ± 0.5	0.57 ± 0.01	1.05 ± 0.05	5.3
Y142Q[d]	17 ± 2	1.2 ± 0.04	1.17 ± 0.11	5.9
H144A[d]	57 ± 8	0.69 ± 0.04	0.20 ± 0.02	1.0
D146A[d]	> 400	> 2	~0.08[d]	< 0.4
D146N	63 ± 8	2.8 ± 0.10	0.74 ± 0.07	3.7
D95A			No detectable	
R68A			No detectable	
E47A	17.5 ± 1.0	63 ± 0.9	60 ± 2.7	300
M98A	114 ± 11	20 ± 0.8	2.9 ± 0.2	15
L19A	31± 2.2	43 ± 1.0	23 ± 1.2	115
F216A	27 ± 1.4	36 ± 0.7	22 ± 0.8	110

[a] apo-MshB was incubated with stoichiometric Zn^{2+} for 30 min prior to activity measurement; [b] Substrate used GlcNAc (0-150 mM); [c] Data adapted from (*17*); [d] Data adapted from (*10*).

Results from structure overlays and automated docking studies also indicate that there are three loops on MshB that are important for ligand recognition. The surface loop (95-104) contains Met98, which is located at the entrance to the active site. (Fig. 1A) Loop (95-104) is mobile and may be partially stabilized upon binding of either BOG (*11*) or glycerol (*12*). (Fig. 1C) The side-chain of Met98 blocks access to the active site in the Act-MshB and BOG-MshB structures; however, movement of this loop and Met98 opens the active site as observed in the

ligand-free MshB structure (Zn-MshB). Mutation to M98A results in 3-fold increase in K_M^{GlcNAc} and 7-fold decrease in $(k_{cat}/K_M)^{GlcNAc}$, (Table 3) further supporting a role of Met98 in ligand binding.

Glu47 is located on the surface of active site with at least 8 Å away from the substrate-binding site in the Act-MshB structure, which is too far away to form direct interaction with GlcNAc. However, this side chain is rotated ~ 5 Å in the Zn-MshB structure suggesting that the side chain may block access to the active site. The E47A mutation has a modest effect on catalysis with a 2-fold decrease in K_M^{GlcNAc} and 3-fold increase in $(k_{cat}/K_M)^{GlcNAc}$ observed. (Table 3)

Alignment of three MshB structures reveals a Phe216 located on a third loop (residues 211-217) and its side chain moves several Å in three MshB structures. (Fig. 1D) The close spatial distance between Tyr142 and Phe216 led to the hypothesis that a π-π interaction may regulate movement of Tyr142. (Fig. 1A) However, mutation of Phe216 to Ala doesn't alter the kinetic parameters of MshB with the GlcNAc substrate (Table 3), suggesting that these two residues are not working synergistically in ligand binding.

4. Discussion

4.1 Three flexible loops regulate the molecular binding of ligands to MshB

Alignment of the three available crystal structures reveals a relatively rigid overall structure of MshB and active site residues. (Fig. 1A) However, significant movements of three glycine rich surface loops occur upon substrate binding. (*29*) Surface loop (95-104) is highly flexible. (Fig. 1C) Residues 100 –103 had untraceable electron density in the Zn-MshB structure (*9*), while the missing peptide is partially ordered in the ligand bound BOG-MshB (*11*) and Act-

MshB (*12*) structures, suggesting that the loop becomes disordered in the ligand-free form. (Fig. 1C and Table 2) Upon ligand binding to the active site, Met98 moves ~6 Å to seal the active site. This movement may be a consequence of hydrogen bonding between Asp95 and glucosamine hydroxyl. Catalysis takes place in this closed conformation to prevent dissociation of substrate/intermediate, and following catalysis the loops move to allow for release of products and access to the active site. Similar loop movement cycles to regulate ligand binding have been observed for enzymes such as triosephosphate isomerase (TIM) (*30*) and UDP-GlcNAc enolpyruvyl transferase (EPT) (*31*). A potential role for Met98 in ligand recognition is supported by the finding that the M98A mutant exhibits a 4-fold increase in the K_M^{GlcNAc} value (Table 3) and ~2- and 7-fold decrease in k_{cat} and k_{cat}/K_M, respectively.

The second loop (residues 138-143) contains the dynamic Tyr142 that is proposed to regulate access to the active site. (*10*) The phenolic hydroxyl of Tyr142 projects out of the active site in one of the ligand-free MshB structures (Zn-MshB), and orients back toward the active site upon binding of glucoside (BOG-MshB). (*9, 11*) (Fig. 1A) Based on this observation, we proposed in previous study that Tyr142 participates in the chemical step of the reaction by rotating its side-chain into a position in which O^{η} is ~2 Å away from one of the metal-bound water molecules, where it could polarize the substrate carbonyl group and/or stabilize the oxyanion intermediate. In the new MshB structure (Act-MshB) that was cocrystallized with acetate (*12*), the distance between O^{η} and the metal-bound water molecules is 2.2 Å (Fig. 1B), consistent with our above hypothesis that Tyr142 polarizes the carbonyl bond on substrate and/or stabilizes the resulting oxyanion intermediate.

The third mobile surface loop (residues 211-217) is part of the putative hydrophobic cavity adjacent to active side. (Fig. 1A and Fig. 6A) The side chains of Glu213, Ile214, and

Phe216 are highly flexible (Fig 1D) and residues 211–216 were missing in three units of Zn-MshB tetramer (*9*) (Table 2). In addition, the side chains of these residues adopt different orientations in three MshB structures (Fig. 1D). Broad substrate specificity of MshB (deacetylase and amidase activity) suggests that the protein can tolerate groups with different sizes and hydrophobicities on the GlcN-Ins moiety. (*18*) Our docking results suggest that loop (211-217) forms the outside wall of the hydrophobic cavity that accommodates bimane group on CySmB-GlcN-Ins. Thus flexibility of the loop and dynamics of the individual side chains may play a role in adjusting the size of this cavity to accommodate substrates with different sizes.

4.2 GlcNAc core is stabilized by hydrogen bonding to active site residues and electrostatic interaction with catalytic metal cofactor

Hydrogen bonding interactions between the GlcNAc hydroxyl groups with Asp95 and Arg68 are observed in available crystal structures and automated docking studies with various substrates. The importance of these side chains in ligand recognition have been confirmed biochemically using site-directed mutagenesis and enzyme kinetics. Removal of either side chain in the D95A and R68A mutants results in a complete loss of activity (GlcNAc substrate), suggesting that the hydrogen bonding interactions are essential for molecular recognition of the glucosamine moiety. (Table 3) Docking calculations indicate that two hydrogen bonds are provided by each of these residues to orient the glucosamine in a conformation suitable for catalysis. (Fig. 2B) Asp95 is located on the surface loop (95-104) and may play an important role in stabilizing this flexible loop upon substrate binding. (Fig. 1C) In BOG-MshB and Act-MshB, the side-chain of Asp95 is rotated ~ 1 Å from the position observed in Zn-MshB and forms direct interactions with the corresponding hydroxyl groups on the ligands. Additionally,

the conformational change of loop (95-104) moves the side chain of Met98 into a position that closes access to the active site as discussed above. In contrast, Arg68 is located on helix α2 and its side chain appears to be relatively rigid in the available structures.

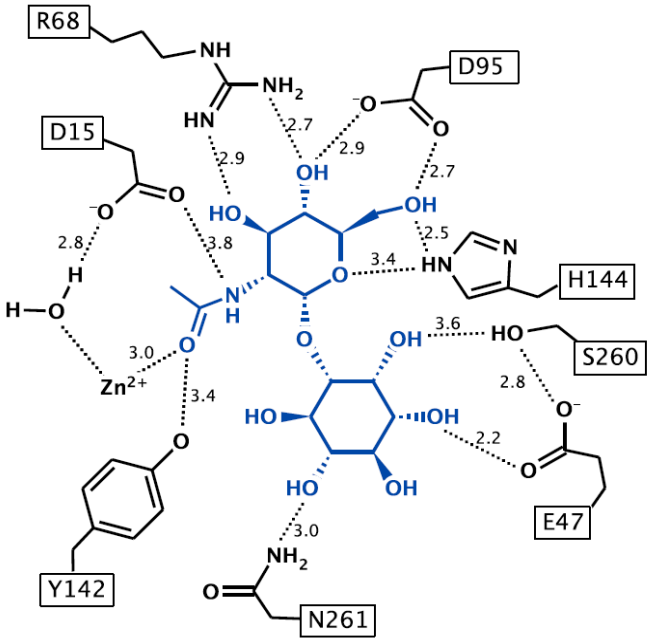

Figure 4. Two-dimensional diagram of MshB contacts with GlcNAc-Ins docked to the active site. The interatomic distances are given in angstroms over dashed lines.

Site-directed mutagenesis studies indicate a role of Asp146 in ligand binding. The value of K_M^{GlcNAc} increases 10-fold in D146A mutant and reverses back to WT levels in D146N mutant (Table 3), implying the importance of the steric and/or electrostatic role of the side-chain of Asp146 in enhancing GlcNAc affinity and/or stabilizing the catalytic transition state. Careful examination of the active site reveals a distance of 2.7 Å between Asp146 $O^{\delta 1}$ and the metal ligand His13 $N^{\varepsilon 2}$ (Fig. 2D), suggesting that Asp146 may be a second shell metal ligand. Since the catalytic metal ion directly binds to the carbonyl O on substrate and stabilizes the oxyanion intermediate, this interaction likely influences ligand affinity for MshB. Our previous studies

indicate that metal affinity isn't significantly altered in the D146A mutant (*10*). Therefore, it is possible that the D146A mutation increases the flexibility of the metal binding site without affecting metal affinity and results in a shifted location of the bound metal that prevents an interaction between the amide O atom and the metal. An alternative explanation for the significant decrease on ligand binding affinity may be that the microenvironment electrostatics or hydrophobicity is altered in the D146A mutant and, therefore, the glucosamine substate is not longer favored in active site. Further substitution with Asn at this position results in a 6-fold decrease on K_M (Table 3) compared to D146A, suggesting that the N146-H13 interaction positions the metal in a position that is favorable for ligand binding or that Asn reverses the hydrophilic microenvironment in active site. The k_{cat}/K_M of D146N is 27-fold lower than WT (Table 3), suggesting that Asn cannot fully substitute for Asp, thus impairing the catalytic efficiency.

4.3 Docking results imply an alternative GABC mechanism

We previously examined the MshB mechanism using a combination of mutagenesis and kinetics experiments, and proposed the GABC pair mechanism shown in Figure 4A wherein Asp15 serves as GBC to activate the metal-water and His144 functions a GAC to protonate the amine leaving group, with Tyr142 and the metal ion polarizing the carbonyl substrate and/or stabilizing the tetrahedral intermediate. (*10*) Unexpectedly, His144 $N^{\varepsilon 2}$ is located ~6 Å away from the GlcNAc amide N atom in the docking model, which is too far to directly protonate the amine leaving group. Additionally, His144 $N^{\varepsilon 2}$ is 4.1 Å away from Asp146 $O^{\delta 1}$ (Fig. 2D), and therefore unlikely to form a charge-relay with Asp146 as proposed by Maynes *et al* (*9*). These

results suggest that His144 does not play a direct role in chemistry, but instead participates in the catalytic cycle by providing favorable substrate binding interactions.

Asp15 $O^{\delta 1}$ is 2.2 Å away from the metal bound water, while $O^{\delta 2}$ is 3.8 Å away from the amide N on GlcNAc in the docking model. (Fig. 4) This observation appears to be more consistent with a single GABC mechanism in which Asp15 serves as a general base to activate the metal-bound water in the first step and as a general acid in the second step (Fig. 5B) (*9*). However, the magnitude of the decrease in activity observed for the D15A mutant (530-fold) (*10*) is much smaller than that observed for side chains that are bifunctional GABC (10^3 –10^5 - fold) (*32-34*), suggesting Asp15 is more likely part of a GABC pair. Close examination of the structure of active site indicates that only the side-chains of Asp15, His144, and Tyr142 are within 5 Å to the catalytic zinc. Tyr142 is likely acting as the GAC with the following reasons: 1) mutation on Tyr142 to Ala, Phe, or Glu, respectively, exhibited 15 to 20-fold decrease on k_{cat}/K_M (Table 3); 2) ionization of the phenolic group is the origin of pK_{a2} observed in the WT pH-profile (*10*); 3) the phenolate ion form of Tyr142 is inactive for MshB activity(*10*). It is also possible that the second proton-transfer step is mediated by a water molecule in the active site. (Fig. 5C)

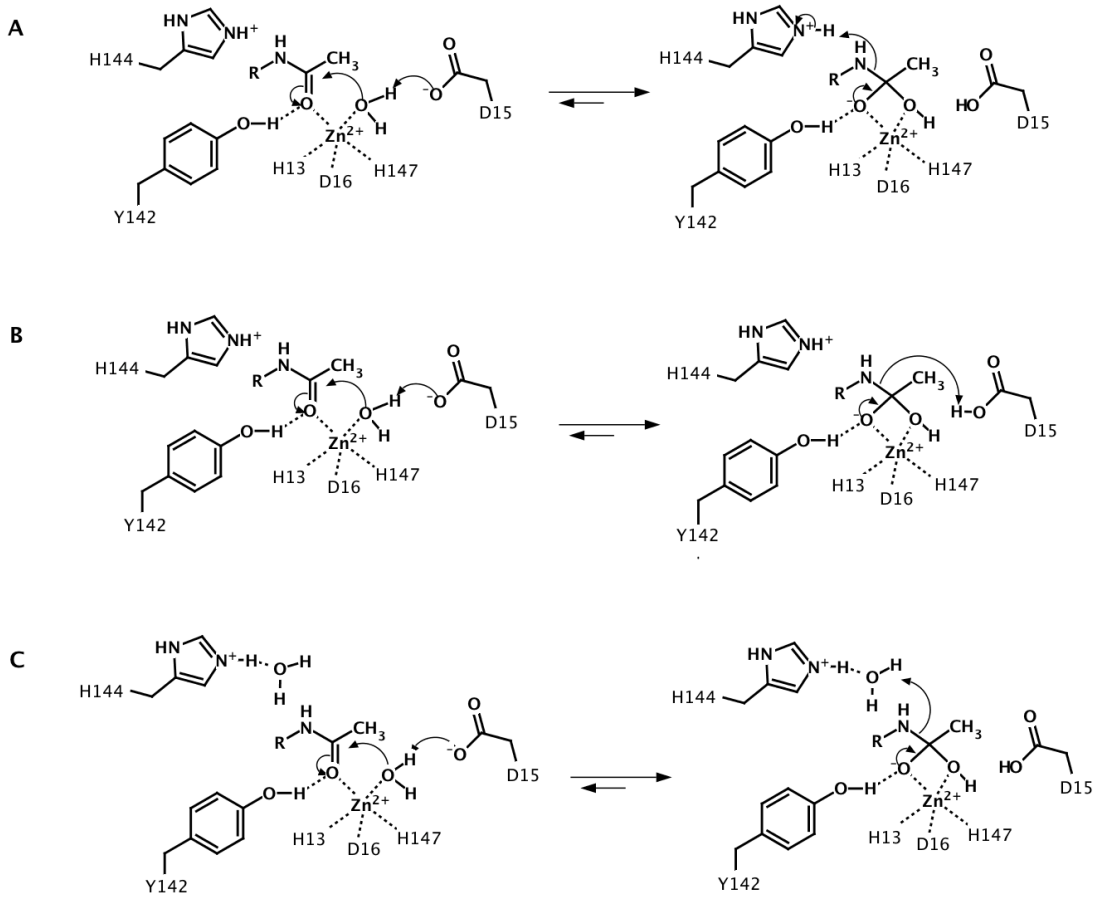

Figure 5. Proposed mechanisms for MshB. A, GABC pair mechanism. Asp15 acts as the base to activate the metal-bound water and His144 serves as the acid to protonate the leaving group. B, single bifunctional GABC mechanism. Asp15 activates a water molecule in the first step and protonates the leaving group in the second step. C, GABC pair mechanism. A metal-bound water is activated by Asp15 to attack the substrate in the first step and a second water (probably mediated by His144) protonates the leaving group.

4.4 Hydrophobic packing of *myo*-inositol against Met98 is important for ligand affinity

In the docking simulations, the inositol ring is tethered at the cleft-like active site entrance with its hydroxyl groups hydrogen bonding to side-chains of Glu47, Ser260, and Asn261 and the cyclohexyl ring of inositol interacting with side-chain of Met98 via hydrophobic contacts. (Fig. 2C) Examination of substrate specificity (Fig. 3) results suggests that the importance of hydrogen bonds on binding of inositol moiety on substrate may be limited.

Replacement of the inositol moiety with an O- or S- linked cyclohexyl group results in a 20-fold decrease in specific activity, (*27*) while complete loss the inositol moiety causes a 100-fold reduction in activity (*18*). In addition, phenyl-2-amino-1-thioglucoside containing a S-linked phenyl as an inositol surrogate shows only 4-fold decrease in specific activity of MshB.(*27*) These results may suggest that the stacking between the side-chain of Met98 and the cyclohexyl ring of inositol observed in the docking result is a more important interaction than the observed hydrogen bondings. The hydrophobic packing of the aliphatic carbon ring may stabilize the inositol moiety and optimize the binding conformation of GlcNAc-Ins to facilitate catalysis. In addition, the binding interaction between Met98 and the inositol group may stabilize loop (95-104) in the closed active site conformation to prevent the dissociation of substrate/intermediate during catalysis. Recent studies have applied the importance of this hydrophobic interaction in ligand binding to the design and screening of potential MshB inhibitors, as compounds containing S-linked cyclohexyl or phenyl rings as 'space-filling' substitutes for the inositol moiety exhibit IC_{50} values in sub to low micro molar range. (*27, 28*)

4.5 A putative hydrophobic cavity adjacent to active site is advantage for inhibitor design

CySmB-GlcN-Ins (Fig. 3) has been shown to be a better substrate for MshB *in vitro.* The specific activity of MshB is 5-fold higher with CySmB-GlcN-Ins compared to the natural substrate GlcNAc-Ins, while the values of K_M and k_{cat}/K_M are decreased 2.5-fold and increased 19-fold, respectively (*18*). Docking calculations predicts that the backbone of the cysteine moiety extends the molecule to allow desolvation of the bimane group in an adjacent cavity consisting of Leu19, Val184, Leu185, Phe216, Ile 214, and Leu259, while the carbonyl group of the cleavable amide bond is positioned to interact with the catalytic zinc. (Fig. 6A) The

additional hydrophobic interactions provided by this cavity on MshB may contribute to the enhanced affinity of CySmB-GlcN-Ins compared to GlcNAcIns. Furthermore, the specific activity of MshB with amidase substrates follows the trend: MS-acetophenone > MSmB > MS-NEM > MS-acetamide (*18*) (Fig. 3), suggesting that increases in the size and hydrophobicity of the group appended to the amine on the GlcN-Ins moiety improve substrate affinity to facilitate amidase activity.

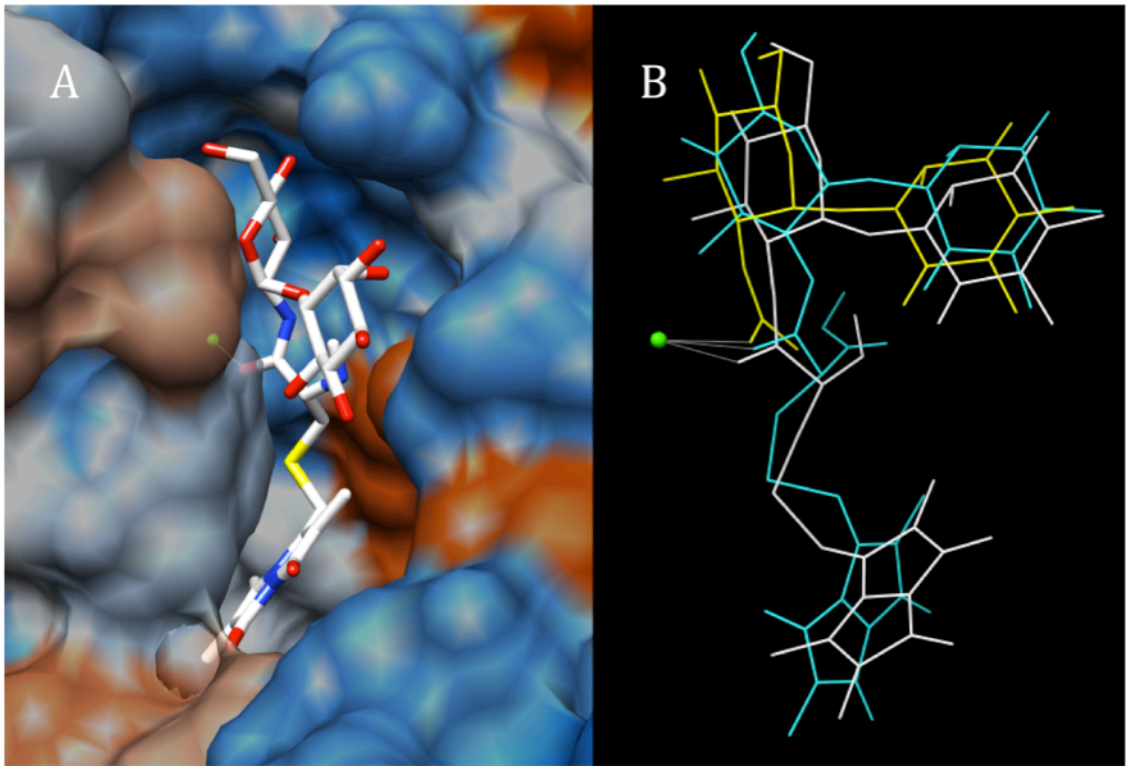

Figure 6. Results of docking amidase substrates to Act-MshB (PDB 4EWL). (A) CySmB-GlcN-Ins (white stick) is bound to MshB with GlcN moiety located in the active site with the carbonyl O atom coordinated to the catalytic zinc (green ball), inositol moiety is accommodated at the entrance of active site, and the bimane group buried into an adjacent hydrophobic cavity. The hydrophobic and hydrophilic residues and their surfaces are colored respectively with orange and blue. (B) Overlay of the docking result for GlcNAc-Ins (yellow), CySmB-GlcN-Ins (white), and fCySmB-GlcN-Ins (cyan). The carbonyl O atom on the cleavable amide bond is coordinated to the catalytic zinc (green) in all substrates.

Docking of fCySmB-GlcN-Ins to MshB generates a binding conformation similar to that observed for CySmB-GlcN-Ins, in which the GlcN-Ins moiety is superimposed onto GlcNAc-Ins, while the bimane moiety is buried into the hydrophobic cavity. (Fig. 6) Although the specific activity of MSmB is only 50% lower than that observed with fCySmB-GlcN-Ins (Fig. 3), manual docking of MSmB reveals a clash between the acetyl methyl group and the side-chains of Asp15 in MshB, indicating that a slight conformational change in the active site may be required to avoid the significant clash. This suggests that automated docking with MshB as a rigid receptor might not be suitable for predicting the binding of large substrates as MSmB to MshB.

The presence of a hydrophobic cavity adjacent to the active site may be an advantage for structural based design of MshB inhibitors. Inhibitors designed to exploit interactions with a hydrophobic cavity adjacent to the active site have been reported for HIV 1-integrase (*35*) and 5-Lipoxygenase (*36*). Recently, a library of MshB inhibitors was constructed that incorporated features of amidase substrates bearing oxazole, oxazine (*28*), or plumbagin (*27*) moieties on the amino group of the GlcN-Ins moiety. Variations in the structure of this aromatic substituent significantly impacted inhibitory potency and several compounds with sub- to low micromolar IC_{50} values were reported. Therefore, further characterization of this adjacent hydrophobic pocket may provide valuable information for the future design of efficient MshB inhibitors as potential TB drugs.

References

1. WHO. (2012) Global Tuberculosis Control.
2. Zhang, Y. (2005) The magic bullets and tuberculosis drug targets, *Annu Rev Pharmacol Toxicol 45*, 529-564.

3. Spies, H. S., and Steenkamp, D. J. (1994) Thiols of intracellular pathogens. Identification of ovothiol A in Leishmania donovani and structural analysis of a novel thiol from Mycobacterium bovis, *Eur J Biochem 224*, 203-213.

4. Rawat, M., Newton, G. L., Ko, M., Martinez, G. J., Fahey, R. C., and Av-Gay, Y. (2002) Mycothiol-deficient Mycobacterium smegmatis mutants are hypersensitive to alkylating agents, free radicals, and antibiotics, *Antimicrob Agents Chemother 46*, 3348-3355.

5. Rawat, M., Johnson, C., Cadiz, V., and Av-Gay, Y. (2007) Comparative analysis of mutants in the mycothiol biosynthesis pathway in Mycobacterium smegmatis, *Biochem Biophys Res Commun 363*, 71-76.

6. Rengarajan, J., Bloom, B. R., and Rubin, E. J. (2005) Genome-wide requirements for Mycobacterium tuberculosis adaptation and survival in macrophages, *Proc Natl Acad Sci U S A 102*, 8327-8332.

7. Bzymek, K. P., Newton, G. L., Ta, P., and Fahey, R. C. (2007) Mycothiol import by Mycobacterium smegmatis and function as a resource for metabolic precursors and energy production, *J Bacteriol 189*, 6796-6805.

8. Newton, G. L., Av-Gay, Y., and Fahey, R. C. (2000) N-Acetyl-1-D-myo-inosityl-2-amino-2-deoxy-alpha-D-glucopyranoside deacetylase (MshB) is a key enzyme in mycothiol biosynthesis, *J Bacteriol 182*, 6958-6963.

9. Maynes, J. T., Garen, C., Cherney, M. M., Newton, G., Arad, D., Av-Gay, Y., Fahey, R. C., and James, M. N. (2003) The crystal structure of 1-D-myo-inosityl 2-acetamido-2-deoxy-alpha-D-glucopyranoside deacetylase (MshB) from Mycobacterium tuberculosis reveals a zinc hydrolase with a lactate dehydrogenase fold, *J Biol Chem 278*, 47166-47170.

10. Huang, X., and Hernick, M. (2012) Examination of mechanism of N-acetyl-1-D-myo-inosityl-2-amino-2-deoxy-alpha-D-glucopyranoside deacetylase (MshB) reveals unexpected role for dynamic tyrosine, *J Biol Chem 287*, 10424-10434.

11. McCarthy, A. A., Peterson, N. A., Knijff, R., and Baker, E. N. (2004) Crystal structure of MshB from Mycobacterium tuberculosis, a deacetylase involved in mycothiol biosynthesis, *J Mol Biol 335*, 1131-1141.

12. Broadley, S. G., Gumbart, J. C., Weber, B. W., Marakalala, M. J., Steenkamp, D. J., and Sewell, B. T. (2012) A new crystal form of MshB from Mycobacterium tuberculosis with glycerol and acetate in the active site suggests the catalytic mechanism, *Acta Crystallogr D Biol Crystallogr 68*, 1450-1459.

13. Supuran, C. T. (2010) Carbonic anhydrase inhibitors, *Bioorg Med Chem Lett 20*, 3467-3474.

14. Lia, N. G., Shib, Z. H., Tang, Y. P., and Duan, J. A. (2009) Selective matrix metalloproteinase inhibitors for cancer, *Curr Med Chem 16*, 3805-3827.

15. Drag, M., and Salvesen, G. S. (2010) Emerging principles in protease-based drug discovery, *Nat Rev Drug Discov 9*, 690-701.

16. White, R. J., Margolis, P. S., Trias, J., and Yuan, Z. (2003) Targeting metalloenzymes: a strategy that works, *Curr Opin Pharmacol 3*, 502-507.

17. Huang, X., Kocabas, E., and Hernick, M. (2011) The activity and cofactor preferences of N-acetyl-1-D-myo-inosityl-2-amino-2-deoxy-alpha-D-glucopyranoside deacetylase (MshB) change depending on environmental conditions, *J Biol Chem 286*, 20275-20282.

18. Newton, G. L., Ko, M., Ta, P., Av-Gay, Y., and Fahey, R. C. (2006) Purification and characterization of Mycobacterium tuberculosis 1D-myo-inosityl-2-acetamido-2-deoxy-

alpha-D-glucopyranoside deacetylase, MshB, a mycothiol biosynthetic enzyme, *Protein Expr Purif 47*, 542-550.

19. Morris, G. M., Goodsell, D. S., Halliday, R. S., Huey, R., Hart, W. E., Belew, R. K., and Olson, A. J. (1998) Automated docking using a Lamarckian genetic algorithm and an empirical binding free energy function, *Journal of Computational Chemistry 19*, 1639-1662.

20. Huey, R., Morris, G. M., Olson, A. J., and Goodsell, D. S. (2007) A semiempirical free energy force field with charge-based desolvation, *Journal of Computational Chemistry 28*, 1145-1152.

21. Pettersen, E. F., Goddard, T. D., Huang, C. C., Couch, G. S., Greenblatt, D. M., Meng, E. C., and Ferrin, T. E. (2004) UCSF Chimera—A visualization system for exploratory research and analysis, *Journal of Computational Chemistry 25*, 1605-1612.

22. Meng, E., Pettersen, E., Couch, G., Huang, C., and Ferrin, T. (2006) Tools for integrated sequence-structure analysis with UCSF Chimera, *BMC Bioinformatics 7*, 339.

23. Huang, X., and Hernick, M. (2011) A fluorescence-based assay for measuring N-acetyl-1-D-myo-inosityl-2-amino-2-deoxy-alpha-D-glucopyranoside deacetylase activity, *Anal Biochem 414*, 278-281.

24. Huang, X., and Hernick, M. (2011) A fluorescence-based assay for measuring N-acetyl-1-D-myo-inosityl-2-amino-2-deoxy-α-D-glucopyranoside deacetylase (MshB) activity, *Anal. Biochem. 414*, 278-281.

25. Sousa, S. F., Fernandes, P. A., and Ramos, M. J. (2006) Protein-ligand docking: current status and future challenges, *Proteins 65*, 15-26.

26. Hu, X., Balaz, S., and Shelver, W. H. (2004) A practical approach to docking of zinc metalloproteinase inhibitors, *J Mol Graph Model 22*, 293-307.

27. Gammon, D. W., Steenkamp, D. J., Mavumengwana, V., Marakalala, M. J., Mudzunga, T. T., Hunter, R., and Munyololo, M. (2010) Conjugates of plumbagin and phenyl-2-amino-1-thioglucoside inhibit MshB, a deacetylase involved in the biosynthesis of mycothiol, *Bioorg Med Chem 18*, 2501-2514.

28. Metaferia, B. B., Fetterolf, B. J., Shazad-Ul-Hussan, S., Moravec, M., Smith, J. A., Ray, S., Gutierrez-Lugo, M. T., and Bewley, C. A. (2007) Synthesis of natural product-inspired inhibitors of Mycobacterium tuberculosis mycothiol-associated enzymes: the first inhibitors of GlcNAc-Ins deacetylase, *J Med Chem 50*, 6326-6336.

29. Gutteridge, A., and Thornton, J. (2004) Conformational change in substrate binding, catalysis and product release: an open and shut case?, *FEBS Lett 567*, 67-73.

30. Joseph, D., Petsko, G. A., and Karplus, M. (1990) Anatomy of a conformational change: hinged "lid" motion of the triosephosphate isomerase loop, *Science 249*, 1425-1428.

31. Eschenburg, S., and Schonbrunn, E. (2000) Comparative X-ray analysis of the un-liganded fosfomycin-target murA, *Proteins 40*, 290-298.

32. Hernick, M., Gennadios, H. A., Whittington, D. A., Rusche, K. M., Christianson, D. W., and Fierke, C. A. (2005) UDP-3-O-((R)-3-hydroxymyristoyl)-N-acetylglucosamine deacetylase functions through a general acid-base catalyst pair mechanism, *J Biol Chem 280*, 16969-16978.

33. Cha, J., and Auld, D. S. (1997) Site-directed mutagenesis of the active site glutamate in human matrilysin: investigation of its role in catalysis, *Biochemistry 36*, 16019-16024.

34. Wetterholm, A., Medina, J. F., Radmark, O., Shapiro, R., Haeggstrom, J. Z., Vallee, B. L., and Samuelsson, B. (1992) Leukotriene A4 hydrolase: abrogation of the peptidase activity by mutation of glutamic acid-296, *Proc Natl Acad Sci U S A 89*, 9141-9145.

35. Huang, M., Grant, G. H., and Richards, W. G. (2011) Binding modes of diketo-acid inhibitors of HIV-1 integrase: a comparative molecular dynamics simulation study, *J Mol Graph Model 29*, 956-964.

36. Reddy, N. P., Chandramohan Reddy, T., Aparoy, P., Achari, C., Sridhar, P. R., and Reddanna, P. (2012) Structure based drug design, synthesis and evaluation of 4-(benzyloxy)-1-phenylbut-2-yn-1-ol derivatives as 5-lipoxygenase inhibitors, *Eur J Med Chem 47*, 351-359.

Chapter 8

Conclusion

One unique feature of mycobacteria is the presence of inositol metabolism that is ubiquitously found in eukaryotes but is restricted to certain class of bacteria and archae. Mycobacteria utilize inositol in two unique pathways, namely, the production of phosphatidylinositol (PI) and the biosynthesis of mycothiol (MSH). MSH is a thiol exclusively found in *Mycobacterium* species that contain pathogens known to cause tuberculosis (TB). MSH plays critical roles in TB infection and persistence in the host. MshB catalyzes the deacetylation of GlcNAc-Ins, the committed step in MSH synthesis, and is one of the potential inhibitor targets for MSH biosynthesis.

My dissertation aims to understand the relationship between structure and function of MshB, including the cofactor preferences, chemical mechanism, and ligand recognition. A fluorescamine (FSA)-based assay for measuring MshB activity with the substrate GlcNAc was developed in this study, which aids in further biochemical characterization of this enzyme. FSA reacts with primary amines in the product GlcN to form a fluorescent product (excitation 395 nm, emission 485 nm). Although the observed K_M value for GlcNAc is significantly larger (~110-fold) than the K_M of native substrate GlcNAc–Ins, less than a 2-fold change in k_{cat} for GlcNAc versus GlcNAc–Ins was observed. Therefore, while GlcNAc is not the natural substrate and has a weakened affinity for MshB, the GlcNAc moiety undergoes same chemical transformation as GlcNAc-Ins by MshB in MSH biosynthesis.

MshB has a mononuclear metal binding site in which a divalent metal ion is 5-coordinate with three protein ligands (His13, Asp16, and His147), one water molecule and the carbonyl oxygen from the substrate. The activity of MshB is absolutely dependent on the presence of this

metal ion and follows the trend: $Fe^{2+} > Co^{2+} > Zn^{2+} > Mn^{2+}, Ni^{2+}$. The metal cofactor bound to MshB is highly dependent on the expression and purification conditions. MshB strongly prefers Fe^{2+} under anaerobic conditions regardless of the metal ion content of the medium, and switches between Fe^{2+} and Zn^{2+} under aerobic conditions as the metal content of the medium is altered. These results suggest that MshB is a cambialistic metallohydrolase with a dynamic cofactor that is dependent on metal availability and oxidative status *in vivo*.

The chemical reaction catalyzed by MshB involves a general acid-base catalyst mechanism and is examined in detail in this study. MshB activity displays a bell-shaped dependence on pH with pK_a values of ~ 7.3 and 10.5, which are originated from the ionization of the side chain of Asp15 and Tyr142, respectively. The side chain of Asp15 serves as the general base catalyst that activates the metal-water/hydroxide for nucleophilic attack on carbonyl carbon in GlcNAc. Significant solvent isotope effect observed in H144A mutant indicates a role of His144 in hydrogen transfer step, probably via functioning as the general acid catalyst. The Tyr142 assists in polarizing substrate/stabilizing the oxyanion intermediate. Detailed structural analyses indicate that Tyr142 is a dynamic side chain that plays key roles in catalysis via modulating substrate binding, chemistry, and product release.

A molecular model of the binding interaction between the native substrate GlcNAc-Ins and MshB was built by automated docking simulation and examined by site-directed mutagenesis in this study. The *N*-acetyl-glucosamine moiety is stabilized in active site by hydrogen bonding to Asp95, Arg68, and His144, and the importance of the side-chain of these residues is experimentally confirmed. The previous proposed GABC pair mechanism is challenged by the observation that the side-chain of His144 is located too far away from the amide bond to act as GAC. The *myo*-inositol ring is stabilized by hydrogen bonding to Glu47,

Ser260 and Asn261 as well as by hydrophobic stacking with Met98. In addition, automated docking of CySmB-Glc-Ins to MshB reveals the presence of a hydrophobic pocket adjacent to the GlcNAc binding site. The additional hydrophobic interactions may contribute to the high reactivity of CySmB-GlcN-Ins to MshB, which displays 2.5-fold increase and 19-fold increase in K_M and k_{cat}/K_M, respectively, from that of GlcNAc-Ins; therefore the presence of this hydrophobic cavity is advantageous for structural based design of inhibitors as potential TB drugs that exhibit high affinity and specificity against MshB.

This dissertation presents an examination of mycobacterial MshB that provides insight into the cofactor preference, chemical mechanism, and molecular recognition, and presents the groundwork for developing specific inhibitors against MshB. Future efforts are needed to identify the cofactor that binds to MshB in the mycobacterial cytosol during growth *in vitro* and during infection in macrophage. Additionally, the proposed chemical mechanism and molecular recognition properties of MshB require further examination using the native substrate GlcNAc-Ins. Lastly, structural and thermodynamic characterization of the nearby hydrophobic cavity identified in the docking simulation is necessary for structure-based design and synthesis of MshB inhibitors, which will lead to the development of novel drugs for TB treatment.

Appendix A

A continuous spectrophotometric assay for measuring MIPS activity

Author Contributions
Xinyi Huang performed all the experiments and wrote the article.
Marcy Hernick directed the research and wrote the article.

Abstract

Myo-inositol-1-phosphate synthase (MIPS) catalyzes the conversion of glucose-6-phosphate to *myo*-inositol 1-phosphate. The reaction catalyzed by MIPS is the first step in the biosynthesis of inositol and inositol-containing molecules that serve important roles in both eukaryotes and prokaryotes. Consequently, MIPS is a target for the development of therapeutic agents for the treatment of infectious diseases and bipolar disorder. We recently reported a continuous spectrophotometric method for measuring MIPS activity using a coupled assay that allows the rapid characterization of MIPS in a multiwell plate format. Here we validate the continuous assay as a high-throughput alternative for measuring MIPS activity and report on one limitation of this assay — the inability to examine the effect of divalent metal ions (at high concentrations) on MIPS activity. In addition, we demonstrate that the activity of MIPS from *Arabidopsis thaliana* is moderately enhanced by the addition Mg^{2+} and is not enhanced by other divalent metal ions (Zn^{2+} and Mn^{2+}), consistent with what has been observed for other eukaryotic MIPS enzymes. Our findings suggest that the continuous assay is better suited for characterizing eukaryotic MIPS enzymes that require monovalent cations as cofactors than for characterizing bacterial or archeal MIPS enzymes that require divalent metal ions as cofactors.

1. Introduction

Myo-inositol-1-phosphate synthase (MIPS) catalyzes the conversion of glucose-6-phosphate to form L-*myo*-inositol-1-phosphate (Fig. 1A). The reaction catalyzed by MIPS is the first step in the biosynthesis of inositol and inositol-containing molecules (e.g., inositol hexakisphosphate, mycothiol, phosphatidylinositol) that serve important roles in both eukaryotes and prokaryotes as signaling molecules, components of cellular membranes, and protectors against cellular damage (e.g., redox, toxins) (*1-3*). Consequently, enzymes involved in the biosynthesis of inositol-containing molecules are of biological interest.

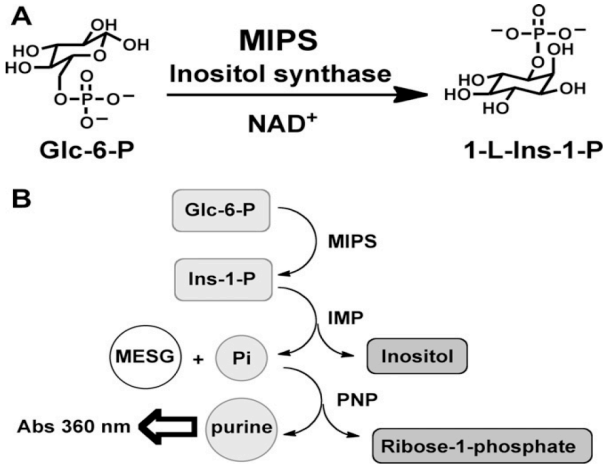

Figure1. (A) Reaction catalyzed by MIPS. (B) Overview of IMP-coupled assay.

MIPS catalyzes the formation of L-*myo*-inositol-1-phospate (Ins-1-P) from glucose-6-phosphate (Glc-6-P) using NAD^+ and belongs to the aldolase family of enzymes. Eukaryotic MIPS are larger molecular weight proteins that require monovalent cation cofactors (often NH_4^+) and are class III aldolase enzymes, whereas bacterial and archeal MIPS are smaller molecular weight proteins that require divalent metal ions for maximal activity and are class II aldolase enzymes (*4-6*). There is some structural evidence to suggest that eukaryotic MIPS enzymes may

contain a bound metal ion (proposed to be Zn^{2+}); however, the addition of Zn^{2+} is not essential for catalytic activity (*4, 6*). Because no net NAD^+ is consumed in the overall reaction catalyzed by MIPS, enzyme activity cannot be measured by monitoring changes in NAD^+/NADH absorbance. Consequently, traditional activity-based assays either use stopped-point assays to measure phosphate release (*7, 8*) or measure product formation using nuclear magnetic resonance (NMR) (*9*). Neither of these approaches is amenable to high-throughput analysis. Consequently, we developed a continuous *myo*-inositol monophosphatase (IMP)-coupled spectrophotometric assay to measure MIPS activity and used this assay to characterize MIPS from *Arabidopsis thaliana* (AtMIPS) (*10*). Whereas the continuous IMP-coupled assay requires only absorbance measurements to determine MIPS activity, the traditional periodate-based assay (*7, 8*) requires approximately 3 h of sample processing prior to absorbance measurements for determination of MIPS activity. Thus, the continuous IMP-coupled assay is much more rapid and convenient than traditional assays.

The continuous spectrophotometric assay (*10*) monitors MIPS activity via the detection of inorganic phosphate (Pi) released from *myo*-inositol 1-phosphate by IMP using 2-amino-6-mercapto-7-methylpurine riboside (MESG) and purine nucleoside phosphorylase (PNP) with an increase in absorbance at 360 nm (Fig. 1B). The enzyme IMP selectively removes the phosphate from Ins-1-P and not Glc-6-P, as illustrated in Fig. 2A. However, one concern about the continuous spectrophotometric assay is that IMP is a metalloenzyme whose activity is affected by divalent metal ions (*11*). Consequently, changes in the observed activity in the presence of divalent metal ions could be attributed to changes in IMP, and not MIPS, activity. If true, this would suggest that the continuous assay is not suitable for the characterization of bacterial or archeal MIPS enzymes that require divalent metal ion cofactors.

Here we address this question by measuring AtMIPS activity in the absence and presence of divalent metal ions (Mg^{2+}, Zn^{2+}, and Mn^{2+}) with two different methods: the continuous IMP-coupled assay (*10*) and the periodate stopped-point assay (*8*). Because At-MIPS is a eukaryotic enzyme, it is expected to primarily use monovalent cations (e.g., NH_4^+). Consequently, the observed activity for AtMIPS should not be altered by the presence of divalent metal ions. Results from our experiments confirm that AtMIPS is moderately enhanced by Mg^{2+} and is not activated by the addition of Zn^{2+} or Mn^{2+}, as expected for eukaryotic MIPS enzymes. Furthermore, our results indicate that the steady-state parameters are artificially altered in the presence of Mn^{2+} and Zn^{2+} using the continuous assay, suggesting that the IMP-coupled continuous assay is better suited for characterizing eukaryotic MIPS enzymes that require monovalent cations as cofactors than for characterizing bacterial MIPS enzymes that require divalent metal ions as cofactors.

2. Materials and Methods

2.1 Materials

All solutions were prepared using MilliQ water. All chemicals were purchased from ThermoFisher Scientific, Sigma–Aldrich, and Gold Biotechnology except where otherwise noted. IMP from bovine brain was purchased from Sigma. D-*myo*-inositol-3-phosphate sodium salt (equivalent to L-*myo*-inositol-1-phosphate) was purchased from Cayman Chemical. MESG, PNP, and phosphate standard (50 mM) for the IMP-coupled assay were purchased from Invitrogen (EnzChek Phosphate Assay Kit). Phosphate standard (HPLC [high-performance liquid chromatography] grade, 1000 mg/L) for the periodate assay was purchased from Dionex. Two different phosphate standards were needed because the EnzChek assay buffer is

incompatible with the periodate assay. MIPS1 from *A. thaliana* was expressed and purified as described previously (*10*). All enzyme assays were carried out in 96-well plates (UV [ultraviolet] half area, Corning).

2.2 Enzyme activity assay–continuous spectrophotometric assay

For the IMP-coupled reactions, assay mixtures (50 mM Tris–HCl, pH 7.5; 1, 4, or 10 mM $MgCl_2$; 20 mM NH_4Cl; 0, 5, or 50 μM $ZnSO_4$ or $MnCl_2$; 0.5–1 μM MIPS; 300 μM NAD^+; 0.6 mg IMP; 0.2 mM MESG; and 4 U/ml PNP) were pre-incubated at 30 °C, and the reactions were initiated with the addition of Glc-6-P (0–50 mM) (*10*). The time course for Pi production was monitored by measuring the absorbance at 360 nm at various time points using a SpectraMax $5M^e$ plate reader. The amount of Pi production was calculated from a standard curve (Fig. 2B). The steady-state parameters (k_{cat}, K_M, and k_{cat}/K_M) shown in Tables 1 and 2 were obtained by fitting the Michaelis–Menten equation to the initial linear velocities measured at the various substrate concentrations using the curve-fitting program Kaleidagraph (Synergy Software), which also calculates the asymptotic standard errors. The steady-state parameters reported here are within error of the reported values obtained when the [NAD^+] was held constant at 20 μM (*10*).

2.3 Enzyme activity assay–periodate assay

The periodate assay was carried out as described previously. (*8*) In this approach, the $NaIO_4$ oxidizes and releases phosphate from Ins-1-P and not Glc-6-P. Assay mixtures (100 mM Tris-acetate and 2 mM dithiothreitol [DTT], pH 7.5; 0 or 1 mM $MgCl_2$; 20 mM NH_4Cl; 0 or 50 μM $ZnSO_4$ or $MnCl_2$; 0.5–1 μM MIPS; and 300 μM NAD^+) were pre-incubated at 30 °C (1.7-ml

microfuge tubes), and the reactions were initiated with the addition of Glc-6-P (0–10 mM). After various times, aliquots of the reaction mixture (30 µl) were quenched with 20% trichloroacetic acid (TCA, 10 µl), and precipitated protein was removed by centrifugation. The cleared supernatant was incubated with an equal volume of 0.2 M $NaIO_4$ at 37 °C for 1 h to release the Pi from the Ins-1-P, and excess periodate was removed by the addition of an equal volume of 1 M Na_2SO_3 to the reaction. An aliquot (50 µl) of the reaction mixture was incubated with 6 M sulfuric acid (10 µl) for 10 min at room temperature, followed by the addition of distilled water (dH_2O, 20 µl) and 2.5% ammonium molybdate (10 µl). After 10 min, 10% ascorbic acid (10 µl) was added and the mixture was incubated at 37 °C for 1.5 h. The absorbance at 820 nm was measured (SpectraMax 5M[e]), and the amount of Pi was calculated from a Pi standard curve (Fig. 2C). The steady-state parameters (k_{cat}, K_M, and k_{cat}/K_M) shown in Tables 1 and 2 were obtained by fitting the Michaelis–Menten equation to the initial linear velocities measured at the various substrate concentrations.

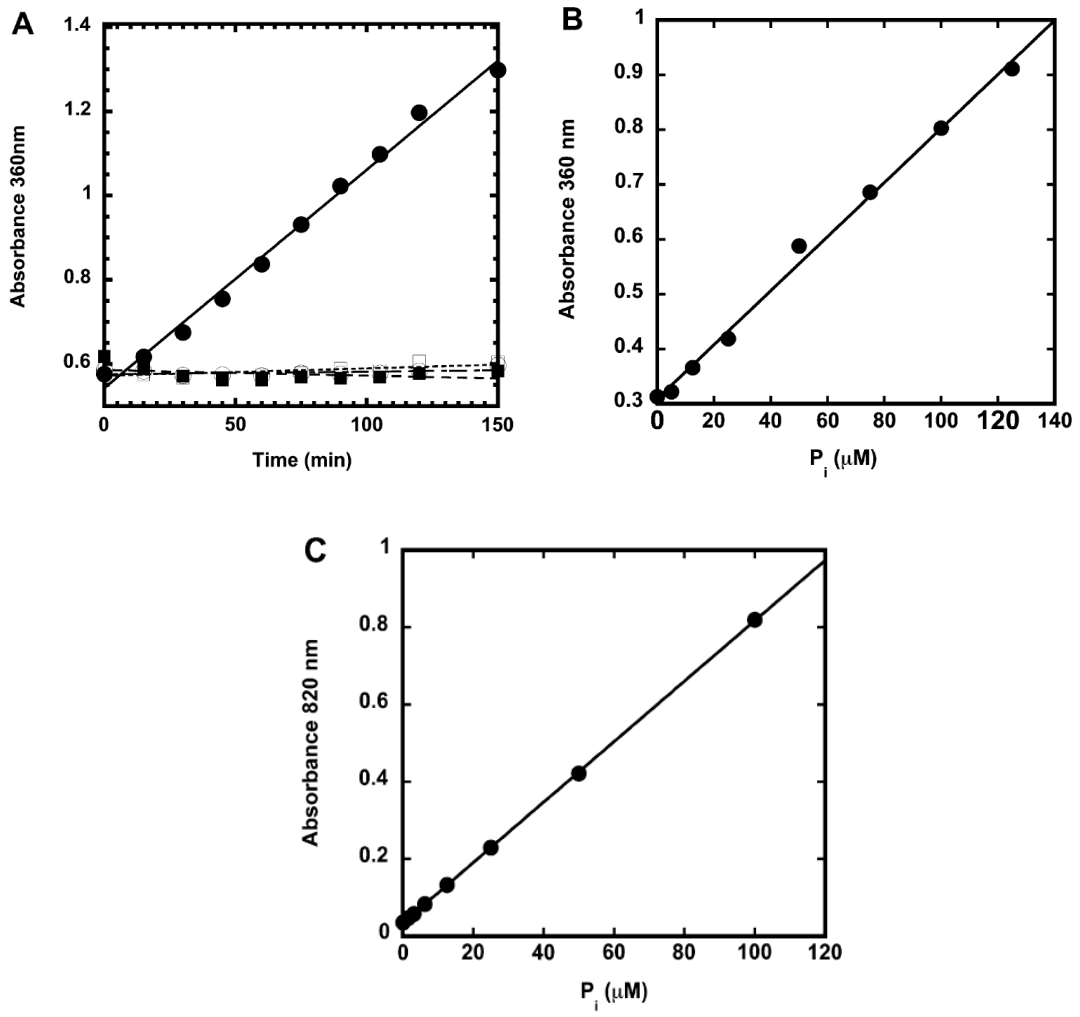

Figure.2. Detection of inositol-1-phosphate formation. (A) IMP-catalyzed reaction. Reaction was initiated by the addition of Ins-1-P (1 mM) or Glc-6-P (5 mM), and the resulting absorbance at 360 nm was measured. ●, Ins-1-P and IMP; ○, Ins-1-P only (no IMP); ■, Glc-6-P and IMP; □, Glc-6-P only (no IMP); ▲, IMP only (no substrate). (B) Phosphate standard curve determined using PNP/MESG. Phosphate (0–120 μM) was detected in the continuous spectrophotometric assay, and the resulting increase in absorbance (360 nm) was plotted against phosphate concentration to yield the standard curve. A linear equation was fit to these data. (C) Phosphate standard curve determined using molybdate/ascorbic acid. Phosphate (0–100 μM) was detected in the periodate assay as described in Materials and Methods, and the resulting increase in absorbance (820 nm) was plotted against phosphate concentration to yield the standard curve. A linear equation was fit to these data.

3. Results and Discussion

We examined the steady-state turnover of Glc-6-P by AtMIPS1 in the absence and presence of divalent metal ions (Mg^{2+}, Zn^{2+}, and Mn^{2+}) using the continuous IMP-coupled assay and traditional periodate assay. Sample plots showing the initial rates of reactions catalyzed by MIPS are shown in Fig. 3. If we compare the steady-state parameters for AtMIPS in the presence of 1 mM $MgCl_2$, we observe that the values of K_M (~0.7 mM), k_{cat} (~6–7 min^{-1}), and k_{cat}/K_M (~8–10 mM^{-1} min^{-1}) obtained using the two different assays are within the margin of error (Table 1). The finding that there is no significant difference in the steady-state parameters for AtMIPS1 observed using the two different assays validates the continuous IMP-coupled assay as a more rapid and convenient alternative for measuring MIPS activity. For experiments examining the effects of Mg^{2+}, we used concentrations of 1–10 mM $MgCl_2$ based on results obtained with the human MIPS (hMIPS) (*8*). For experiments examining the effects of the divalent metal ions Zn^{2+} and Mn^{2+}, concentrations of 5 or 50 μM Zn^{2+} or Mn^{2+} were used based on information for the MIPS from *Archaeoglobus fulgidus* (AfMIPS) (*12*). To date, AfMIPS is the only archeal MIPS that has been well characterized in terms of its activity and the effect of divalent metal ions on activity. AfMIPS requires divalent metal ions for catalytic activity, and the K_D of Zn^{2+} and Mn^{2+} for AfMIPS is estimated to be 1 μM using activity measurements (*12*). Other bacterial and archeal MIPS enzymes are expected to have comparable binding affinity for divalent metal ions. Consequently, it is expected that a concentration of 5–50 μM Zn^{2+} or Mn^{2+} would be sufficient for activation of other MIPS enzymes that use divalent metal ion cofactors.

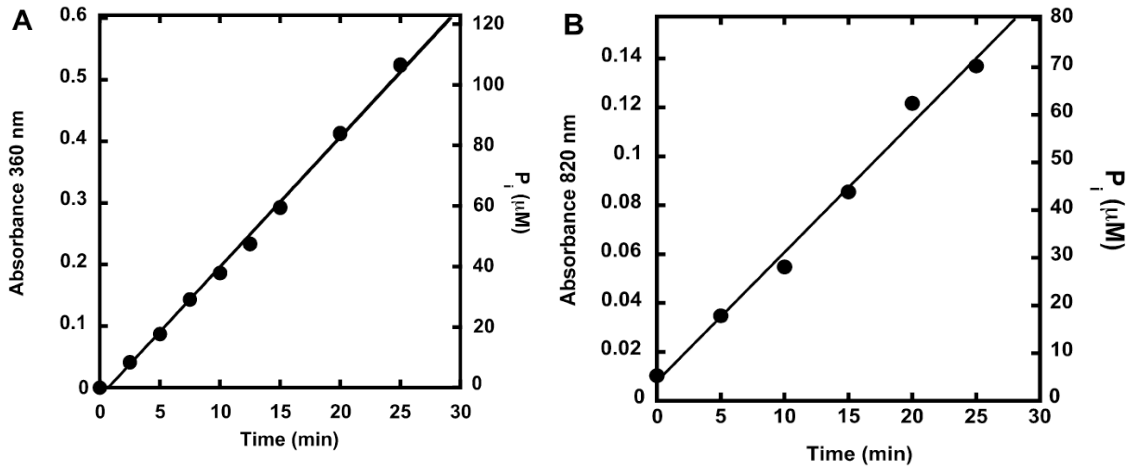

Figure 3. Catalytic activity of AtMIPS1. (A) AtMIPS-catalyzed reaction detected using the IMP-coupled assay. The assay mixture (50 mM Tris–HCl and 1 mM $MgCl_2$, pH 7.5; 20 mM NH_4Cl; 1 μM MIPS; 300 μM NAD^+; 0.6 mg IMP; 0.2 mM MESG; and 4 U/ ml PNP) was pre-equilibrated at 30 °C, the reaction was initiated by the addition of Glc-6-P (0.8 mM) to this mixture, and the resulting absorbance at 360 nm was measured. Data shown are background corrected (zero substrate). The phosphate standard curve (Fig. 2B) was used to convert the observed rate of the reaction into μM/min. The observed rate is 4.2 ± 0.01 μM/min. (B) AtMIPS-catalyzed reaction detected using the periodate assay. The assay mixture (100 mM Tris–acetate and 2 mM DTT, pH 7.5; 20 mM NH_4Cl; 0.5–1 μM MIPS; and 300 μM NAD^+) was pre-incubated at 30 °C, and the reactions were initiated with the addition of Glc-6-P (0.8 mM). Data shown are background corrected (zero substrate). The phosphate standard curve (Fig. 2C) was used to convert the observed rate of the reaction into μM/min. The observed rate is 2.78 ± 0.04 μM/min.

We examined the effect of Mg^{2+} on AtMIPS activity by determining the steady-state parameters for AtMIPS at different concentrations of Mg^{2+} using the periodate and IMP-coupled assays (Table 1). The IMP-coupled assay requires $MgCl_2$; therefore, the activity of AtMIPS could not be determined in the absence of $MgCl_2$ using this assay (*13, 14*). Comparison of the data obtained with 0 and 1 mM $MgCl_2$ using the periodate assay indicates that the values of k_{cat} and k_{cat}/K_M are modestly increased (~15-25%) in the presence of Mg^{2+}. Similarly, we observe an increase in the steady-state parameters with increasing [$MgCl_2$] using the IMP-coupled assay. These results suggest that AtMIPS activity is modestly enhanced in the presence of Mg^{2+}, as is observed with hMIPS (*8*). Although eukaryotic MIPS enzymes are class III aldolases, the

enzymes may use Mg^{2+} to (i) enhance substrate binding (Mg^{2+} is commonly used by enzymes to enhance the binding affinity of phosphate-containing substrates or (ii) provide additional stabilization of negatively charged reaction intermediates. The finding that the magnitude of the enhancement in activity is greater with the IMP-coupled assay than with the periodate assay suggests that the Mg^{2+} must also be affecting the rates of the IMP- and/or PNP-catalyzed reactions. In light of the finding that $[Mg^{2+}] > 1$ mM increases the K_M of Glc-6-P and the fact that Mg^{2+} is known to alter IMP activity at high $[Mg^{2+}]$ (*13*), we chose to examine the effects of Zn^{2+} and Mn^{2+} on AtMIPS using 1 mM $MgCl_2$—the standard concentration of $MgCl_2$ used in PNP assays (*14*).

If we compare the data for AtMIPS activity obtained using the periodate assay (Tables 1 and 2), we observe that the values of K_M (0.7 mM), k_{cat} (5 min^{-1}), and k_{cat}/K_M (7mM^{-1} min^{-1}) in the absence and presence of 50 μM Zn^{2+} or Mn^{2+} are all within error of one another (at 0 mM $MgCl_2$). In addition, no significant change in AtMIPS activity is observed with 50 μM Zn^{2+} or Mn^{2+} using the periodate assay (Fig. 4) in the presence of 1 mM $MgCl_2$. These results suggest that Zn^{2+} or Mn^{2+} does not affect the activity of AtMIPS, as expected. These findings support the hypothesis that AtMIPS is primarily activated by monovalent cations, not divalent metal ions, consistent with results for other eukaryotic MIPS enzymes.

Table 1
Effect of Mg^{2+} on *At*MIPS1 activity.

Assay[a]	$MgCl_2$ (mM)	$K_M^{Glc\text{-}6\text{-}P}$ (mM)	$k_{cat}^{Glc\text{-}6\text{-}P}$ (min^{-1})	k_{cat}/K_M (mM^{-1} min^{-1})
Periodate	0	0.69 ± 0.10	4.9 ± 0.2	7.2 ± 0.8
	1	0.72 ± 0.11	6.1 ± 0.3	8.4 ± 1.0
IMP-coupled	0	ND[b]	ND[b]	ND[b]
	1	0.68 ± 0.08[c]	6.4 ± 0.2[c]	9.4 ± 0.9[c]
		0.67 ± 0.13	6.9 ± 0.4	10.2 ± 1.6
	4	1.2 ± 0.15	13.0 ± 0.6	11.3 ± 1.1
	10	1.3 ± 0.20	18.0 ± 1.0	14.0 ± 1.7

[a] All assays were conducted at pH 7.5 with 20 mM NH_4Cl. The concentration of NAD^+ was held at 300 μM (the K_M for NAD^+ is 0.46 μM [10]), and the concentration of Glc-6-P was varied (0–50 mM).
[b] Not determined. The IMP-coupled assay requires $MgCl_2$.
[c] Data adapted from Ref. [10] included for comparison purposes. Value determined with the concentration of NAD^+ held constant at 20 μM.

Table 2
Effect of Zn^{2+} and Mn^{2+} on *At*MIPS1 activity.

Assay[a]	Me^{2+} (μM)	$K_M^{Glc\text{-}6\text{-}P}$ (mM)	$k_{cat}^{Glc\text{-}6\text{-}P}$ (min^{-1})	k_{cat}/K_M (mM^{-1} min^{-1})
Periodate	50 (Zn)	0.65 ± 0.19	4.6 ± 0.4	7.2 ± 1.6
	50 (Mn)	0.69 ± 0.08	4.8 ± 0.2	7.0 ± 0.6
IMP-coupled	5 (Zn)[b]	0.65 ± 0.04	5.5 ± 0.1	8.5 ± 0.4
	50 (Zn)[b]	0.59 ± 0.06	6.2 ± 0.2	10.6 ± 0.4
	50 (Zn)[c]	2.1 ± 0.8	6.6 ± 0.9	3.2 ± 0.8
	5 (Mn)[b]	0.68 ± 0.14	5.6 ± 0.3	8.3 ± 1.4
	50 (Mn)[b]	1.30 ± 0.06	13.8 ± 0.2	10.6 ± 1.4
	50 (Mn)[c]	0.62 ± 0.14	15.0 ± 1.0	25.0 ± 4.0

[a] All assays were conducted at pH 7.5 with 20 mM NH_4Cl. The concentration of NAD^+ was held at 300 μM (the K_M for NAD^+ is 0.46 μM [10]), and the concentration of Glc-6-P was varied (0–50 mM).
[b] Assay buffer contained 1 mM $MgCl_2$.
[c] Assay buffer contained 4 mM $MgCl_2$.

The steady-state parameters (Table 2) obtained using the IMP coupled assay are not significantly altered in the presence of low concentrations of divalent metal ions (5 μM Zn^{2+} or Mn^{2+}). At higher concentrations of Zn^{2+} (50 μM), the k_{cat} and K_M values obtained for AtMIPS with 1 mM $MgCl_2$ are comparable using the periodate and IMP-coupled assays (Table 2), whereas the value of k_{cat}/K_M is modestly increased when measured using the IMP-coupled assay. In addition, we observe that all of the steady-state parameters are altered in the presence of 50 μM Zn^{2+} at 4 mM $MgCl_2$. Examination of the steady-state parameters obtained for AtMIPS at the higher concentration of Mn^{2+} (50 μM) reveals that the values of K_M, k_{cat}, and k_{cat}/K_M are significantly increased approximately 2- to 3-fold when measured using the IMP-coupled assay (Table 2 and Fig. 4) at both 1 and 4 mM $MgCl_2$. Because the steady-state parameters are not significantly altered in the presence of 50 μM Zn^{2+} or Mn^{2+} when assayed using the periodate assay, these observed changes in activity with Zn^{2+} and Mn^{2+} must be attributed to changes in the IMP and/or PNP enzymes in the coupled assay. These results suggest that the IMP-coupled assay is sensitive to extent Zn^{2+}, at higher concentrations (i.e., > 5 μM), thereby confirming the inability to examine the effects of divalent metal ions on MIPS activity at these concentrations as a limitation of the IMP-coupled assay.

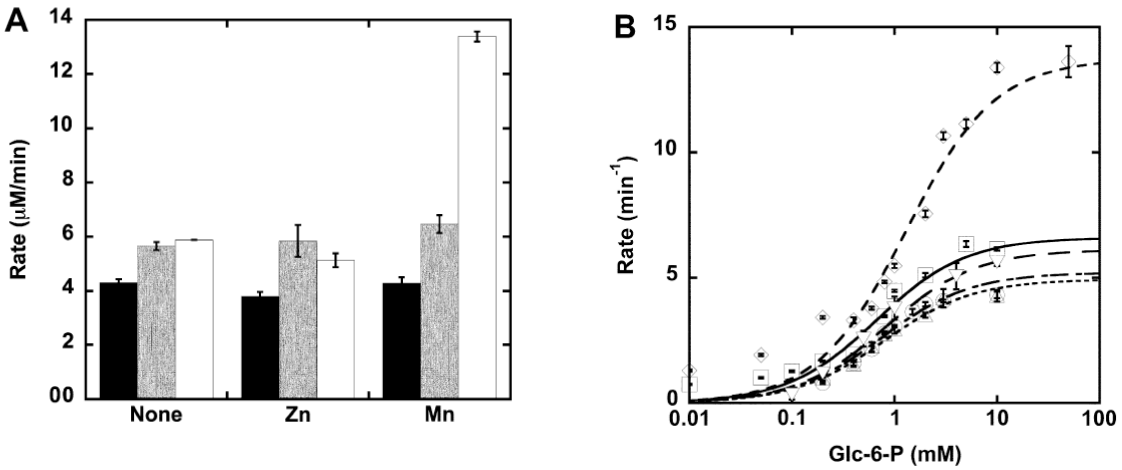

Figure 4. Effect of metal ions on AtMIPS1 activity. **(A)** Effect of Zn^{2+} and Mn^{2+} on AtMIPS. The rates for the conversion of Glc-6-P (10 mM) were measured at 30 °C using the IMP-coupled or periodate assay in the absence and presence of 50 μM Zn^{2+} and Mn^{2+}, as described in Materials and methods. Black bars: periodate assay, 0 mM $MgCl_2$; gray bars: periodate assay, 1 mM $MgCl_2$; white bars: IMP-coupled assay, 1 mM $MgCl_2$. **(B)** Michaelis–Menten plot for AtMIPS. The initial rates for the conversion of Glc-6-P (0–50 mM) were measured at 30 °C using the IMP-coupled or periodate assay in the absence and presence of 50 μM Mn^{2+} at 1 mM $MgCl_2$ unless otherwise noted. □, IMP-coupled assay, 0 μM Mn^{2+}; ○, periodate assay, 0 μM Mn^{2+} (0 mM $MgCl_2$); ▽, periodate assay, 0 μM Mn^{2+}; ◇, IMP-coupled assay, 50 μM Mn^{2+}; △, periodate assay, 50 μM Mn^{2+} (0 mM $MgCl_2$). The steady-state parameters k_{cat}, K_M, and k_{cat}/K_M were obtained by fitting the Michaelis–Menten equation to the initial rates (Tables 1 and 2).

In conclusion, we have validated the continuous IMP-coupled assay as a viable rapid, high-throughput alternative for measuring MIPS activity by comparing the steady-state parameters obtained using the traditional periodate assay with the IMP-coupled assay. Our results confirm that AtMIPS is similar to other characterized eukaryotic MIPS enzymes in that it is primarily activated by monovalent cations over divalent metal ions, with a modest enhancement by Mg^{2+} observed. Finally, our results highlight one limitation of the IMP-coupled assay—the inability of the assay to be used to examine the effects of divalent metal ions on MIPS activity at higher concentrations (> 5 μM). These results suggest that the IMP-coupled

assay is better suited for examining the activity of eukaryotic MIPS enzymes than for examining the activity of bacterial or archeal MIPS enzymes that require divalent metal ion cofactors.

References

1. Roberts, M. (2006) Inositol in Bacteria and Archaea, In *Biology of Inositols and Phosphoinositides* (Majumder, A. L., and Biswas, B. B., Eds.), pp 103-133, Springer US.
2. Shi, Y., Azab, A., Thompson, M., and Greenberg, M. (2006) Inositol Phosphates and Phosphoinositides in Health and Disease, In *Biology of Inositols and Phosphoinositides* (Majumder, A. L., and Biswas, B. B., Eds.), pp 265-292, Springer US.
3. Parthasarathy, L. K., Ratnam, L., Seelan, S., Tobias, C., Casanova, M. F., and Parthasarathy, R. N. (2006) Mammalian Inositol 3-phosphate Synthase: Its Role in the Biosynthesis of Brain Inositol and its Clinical Use as a Psychoactive Agent, In *Biology of Inositols and Phosphoinositides* (Majumder, A. L., and Biswas, B. B., Eds.), pp 293-314, Springer US.
4. Geiger, J. H., and Jin, X. (2006) The Structure and Mechanism of myo -Inositol-1-Phosphate Synthase, In *Biology of Inositols and Phosphoinositides* (Majumder, A. L., and Biswas, B. B., Eds.), pp 157-180, Springer US.
5. Dastidar, K. G., Chatterjee, A., Chatterjee, A., and Majumder, A. L. (2006) Evolutionary Divergence of L-myo-Inositol 1-Phosphate Synthase: Significance of a "Core Catalytic Structure", In *Biology of Inositols and Phosphoinositides* (Majumder, A. L., and Biswas, B. B., Eds.), pp 315-340, Springer US.
6. Stieglitz, K. A., Yang, H., Roberts, M. F., and Stec, B. (2005) Reaching for Mechanistic Consensus Across Life Kingdoms: Structure and Insights into Catalysis of the myo-

Inositol-1-phosphate Synthase (mIPS) from Archaeoglobus fulgidus, *Biochemistry 44*, 213-224.

7. Barnett, J. E., Brice, R. E., and Corina, D. L. (1970) A colorimetric determination of inositol monophosphates as an assay for D-glucose 6-phosphate-1L-myoinositol 1-phosphate cyclase, *Biochem J 119*, 183-186.
8. Ju, S., Shaltiel, G., Shamir, A., Agam, G., and Greenberg, M. L. (2004) Human 1-D-myo-inositol-3-phosphate synthase is functional in yeast, *J Biol Chem 279*, 21759-21765.
9. Chen, L., Spiliotis, E. T., and Roberts, M. F. (1998) Biosynthesis of Di-myo-inositol-1,1'-phosphate, a novel osmolyte in hyperthermophilic archaea, *J Bacteriol 180*, 3785-3792.
10. Donahue, J. L., Alford, S. R., Torabinejad, J., Kerwin, R. E., Nourbakhsh, A., Ray, W. K., Hernick, M., Huang, X., Lyons, B. M., Hein, P. P., and Gillaspy, G. E. (2010) The Arabidopsis thaliana Myo-inositol 1-phosphate synthase1 gene is required for Myo-inositol synthesis and suppression of cell death, *Plant Cell 22*, 888-903.
11. Chen, L., and Roberts, M. F. (2000) Overexpression, purification, and analysis of complementation behavior of E. coli SuhB protein: comparison with bacterial and archaeal inositol monophosphatases, *Biochemistry 39*, 4145-4153.
12. Chen, L., Zhou, C., Yang, H., and Roberts, M. F. (2000) Inositol-1-phosphate synthase from Archaeoglobus fulgidus is a class II aldolase, *Biochemistry 39*, 12415-12423.
13. Hallcher, L. M., and Sherman, W. R. (1980) The effects of lithium ion and other agents on the activity of myo-inositol-1-phosphatase from bovine brain, *J Biol Chem 255*, 10896-10901.

14. Webb, M. R. (1992) A continuous spectrophotometric assay for inorganic phosphate and for measuring phosphate release kinetics in biological systems, *Proc Natl Acad Sci U S A 89*, 4884-4887.

Appendix B

Expression of mycobacterial MIPS from *Mycobacterium smegmatis*

Abstract

Myo-inositol 1-phosphate synthase (MIPS, E.C. 5.5.1.4) catalyzes the first step in inositol production by converting glucose-6-phosphate (Glc-6P) to *myo*-inositol 1-phosphate (Ins-1P) using NAD^+ as the oxidizing/reducing agent. The three dimensional structure of MIPS from *Mycobacterium tuberculosis* with a co-crystallized NAD^+ has been solved in which the mycobacterial protein was prepared as recombinant protein from *E. coli*. However, the *in vitro* activity of recombinant MIPS has not been reported yet. In our lab, the mycobacterial MIPS protein expressed from *E. coli* is capable of binding the cofactor NAD^+ but shows no detectable MIPS activity. Therefore we chose to use *Mycobacterium smegmatis* mc^24517 as the host for recombinant expression. The *E.coli-Mycobacterium* shuttle plasmid pHALOsmg was constructed in this study and used as the expression vector for mycobacterial MIPS. This plasmid retains the *lac* operon and T7 promoter on the pYUB1049, contains the cloning site from pFN18K that is compatible with Flexi® cloning technology, and yields recombinant proteins that can be prepared via HaloLink™ purification system, as well as metal affinity chromatography. The recombinant proteins of MIPS from *M. bovis* BOG or *M. smegmatis* prepared from mycobacterial host exhibit low but significant activity on Glc-6P, while *E. coli* cannot produce active mycobacterial MIPS. Gel filtration analysis of the purified mycobacteria expressed protein reveals multiple peaks, implying that only a small portion of the purified protein is active. Further separation of the active form of MIPS and detailed structure/mechanism analyses are needed to identify the key factors for the enzymatic activity.

1. Introduction

All members *Mycobacterium* species, which contains the causative agents for tuberculosis (TB), perform the *myo*-inositol metabolisms that are rarely found in bacteria. (*1*) In mycobacteria, *myo*-inositol is utilized as precursor for the production of the phosphatidyl-*myo*-inositol (PI) and mycothiol (MSH). PI is further elaborated to phosphatidyl-*myo*-inositol mannosides (PIMs), lipomannan (LM), and lipoarabinomannan (LAM), which are unique glycolipids found in the membrane of cell envelop of mycobacteria. (*2*) PIMs and LAM play important role in interference of the phagosome maturation during TB infection, resulting in adaptation to the host and less inflammatory immune response. (*3*) MSH is the primary reducing agent that is exclusively found in actinobacteria, and is involved in the drug detoxification and TB persistence. (*4*) Therefore, inositol pathways have been considered as attractive drug targets for TB treatment. Inositol can be obtained either from environment by an active inositol-transport system or from *de novo* synthesis through a conserved pathway that requires two enzymatic reactions. (*2, 5, 6*) *Myo*-inositol 1-phosphate synthase (MIPS) converts the glucose-6-phosphate (Glc-6P) to *myo*-inositol 1-phosphate (Ins-1P), which is further hydrolyzed by Ins-1P phosphatase (IMP) to generate *myo*-inositol.

MIPS has been clustered into two distinct phylogenetic branches, the bacterial and archaeal enzymes (~40 kDa) and the larger (~60 kDa) eukaryotic orthologs. (*7*) *Rv0046c (ino1)* from the genome of *Mycobacterium tuberculosis* encodes an MIPS (tMIPS). (*8, 9*) Sequence analyses suggest that mycobacteria recruited the *ino1* gene from archaea. (*10*) The expression level of *ino1* in *M. tuberculosis* is 0.98 to *sigA*, the major sigma factor that is moderately highly expressed in mycobacteria. (*6*) Inhibition of mRNA expression of tMIPS results in enhanced

susceptibility of mycobacterial pathogens to antibiotics. (*11*) A *M. tuberculosis* mutant lacking the functional *ino1* can only be isolated with the supplement of exogenous inositol (77mM), indicating that tMIPS is an essential enzyme for inositol synthesis. (*6*) The virulence of the *ino1* mutant is severely attenuated and the *M. tuberculosis* mutants are easily cleared from the macrophages during infection and incapable of developing disease in SCID mouse model. (*12, 13*) Rapid killing of the mutants may result from a reduced level of mycothiol, leaving the bacteria susceptible to oxidative stress in macrophages. (*6*)

MIPS from *M. tuberculosis* has been expressed as recombinant protein from *E. coli* and the crystal structure with a bound NAD^+ has been solved. (*14*) This MIPS contains a zinc ion in the active site, leading to the question that if it functions as a type III aldolase as eukaryotic MIPSs that are activated by ammonium ions, or follows the mechanism of type II aldolase as archaeal MIPS that involves a divalent cation such as zinc or manganese as a Lewis acid. (*15-17*) In order to illuminate the mechanism, mycobacterial MIPS needs be prepared for biochemical and enzymatic study *in vitro*.

In this study, a mycobacteria expression vector pHALOsmg that is derived from the *E.coli-Mycobacterium* shuttle plasmid pYUB1049 and Flexi® vector pFN18K has been constructed. The expression of aim protein from *Mycobacterium smegmatis* mc^24517 can be induced by IPTG and recombinant proteins produced from this vector contain a N-terminal His_6-HaloTag that can be removed by TEV protease after purification to generate the native-like proteins. In this study, mycobacterial MIPS enzymes are recombinantly expressed from *E. coli* as well as from *Mycobacterium smegmatis* expression system. The recombinant MIPS proteins expressed from *M. smegmatis* exhibit low but significant activity on Glc-6P, while *E. coli* cannot produce the active proteins.

2. Materials and Methods

2.1 Cloning

The open reading frame (ORF) encoding MIPS from the genomics of *M. bovis* BCG (*Rv0046c*) or *M. smegmatis* (*MSMEG_6904*) is cloned to the expression vectors pVP55A and pFN18K using Flexi® technology (Promega) to generate pVP55A/MIPS and pFN18K/MIPS. Briefly, the PCR fragment containing PmeI and SgfI restriction site at 5' and 3' end is digested by Flexi blend (containing PmeI and SgfI) and ligated to expression vector by T4 ligase. The resulting expression vectors yield the recombinant proteins with a N-terminal His_8 tag (pVP55A) or N-terminal HaloTag (pFN18K) with a TEV protease site between the tag and MIPS. The *ino1* proteins from *M. bovis* BCG and *M. smegmatis* are termed as tMIPS and msMIPS, respectively, in this chapter.

To apply the mycobacterial expression system, the primer pair of Halo_1 (CATGCCATGGCAGAAATCGGTACTGGCTTTCCAT) and Halo_2 (CGATAAGCTTGGTACCGAGCCCGAATTCGTTTAAAC) is used to amplify the ORF of Halo-TEV-MIPS from the vector pFN18K/MIPS. The PCR fragment contains NcoI and HindIII restriction site at 5' and 3' end. The NcoI/HindIII digested PCR product is cloned to the *E. coli* - *Mycobacterium* shuttle vector pYUB1049 (provided by Dr. Jacobs, Albert Einstein College of Medicine) to produce the pHALOsmg/MIPS. The resulted expression vector pHALOsmg contains the replication origin of *E. coli* (*ori* E) and *M. smegmatis* (*ori* M), a copy of hygromycin resistant gene, the inducible *lac* operon, and the T7 promoter (from pYUB1049) and yields a recombinant protein with a N-terminal His_6-HaloTag that can be removed by TEV protease (from pFN18K). The PmeI and SgfI restriction sites are cloned to the pYUB1049 plasmid along with the msMIPS ORF; therefore the resulting *E. coli-Mycobacterium* shuttle vector pHALOsmg

is also a Flexi vector. (Fig. 1) The MIPS ORF from *M. bovis* BOG is cloned to the pHALOsmg by using the Flexi® technology as described above.

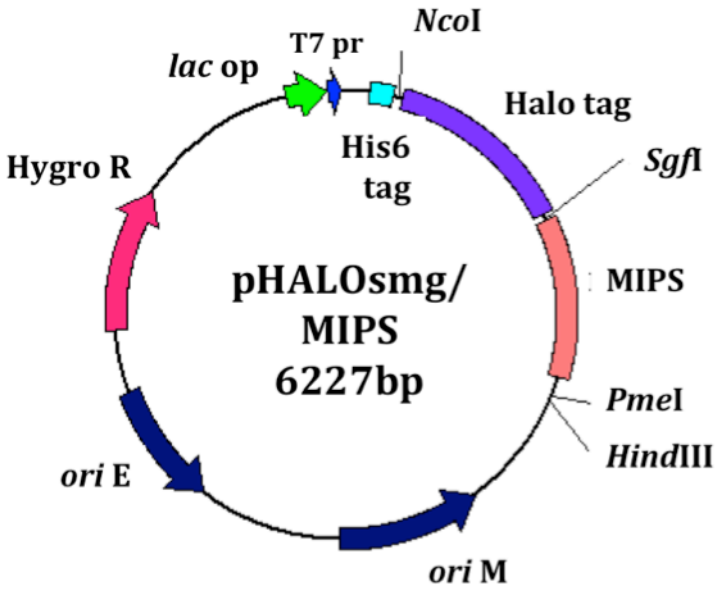

Figure 1. The arrangement of genetic elements in expression vector pHALOsmg/MIPS.

2.2 Expression and purification from *E. coli*

Expression and purification of MIPS from *E. coli* is conducted in large scale, in which the pVP56K-MIPS is transformed into *E. coli* BL21(DE3) pLysS cells and grow on LB agar supplied with 50 µg/mL kanamycin. A single colony is picked and inoculated to LB broth/Kan. The 2 L of cell culture is growing at 37 °C with shaking (250 rpm) until $A_{600} \sim 0.6$. Then 0.8 mM IPTG is added to induce the protein expression. The cells are harvested after shaking at 25 °C for 4 - 6 hours and lysed by high-pressure homogenization. The cell lysate is loaded to a pre-equilibrated Ni-IMAC column (Buffer A: 30 mM HEPES, 150 mM NaCl, 1 mM TCEPS, 0.5 mM imidazole, pH 7.5). The His-MBP-MIPS is eluted with an imidazole gradient step by Buffer A + 10 mM imidazole, Buffer A + 25 mM imidazole, and Buffer A + 250 mM imidazole.

Fractions containing aim protein (via 12% SDS-PAGE) are combined, concentrated and dialyzed against 4 L of buffer A overnight at 4 °C with the presence of His-TEV protease (Slide-a-Lyzer, molecular weight cut-off 10,000; Pierce). The resulting protein is loaded to a second pre-equilibrated Ni-IMAC column, to which the His-MBP, His-TEV, and un-cleaved His-MBP-MIPS bind, whereas MIPS is eluted in the flow-through. Fractions containing MIPS (via 12% SDS-PAGE) are combined, concentrated, and dialyzed versus 4 L of buffer A. Protein concentration is determined using the Bradford assay (Sigma). Protein aliquots are flash frozen in liquid nitrogen and stored at -80 °C.

2.3 Expression and purification from *M. smegmatis*

To express MIPS from mycobacterial system, the expression vectors pHALOsmg/MIPS is transformed into *M. smegmatis* competent cell by electroporation as previously described. (*18*) Briefly, to prepare the competent cell, the *M. smegmatis* $mc^2$4517 is grown in 7H9/ADC/Tween supplied with 50 μg/mL kanamycin at 37 °C. The cells are harvested when A_{600} reached 0.6, followed by 1.5 hours chilling on ice. The cell pellet is washed by ice-cold 10% glycerol for 3 times, resuspended in 0.5 mL 10% glycerol, aliquoted to 40 μL and stored in -80 °C. Single aliquot of the competent cell (40 μL) is transferred with 1μL pHALOsmg/MIPS and additional 260 μL 10% glycerol to a 2 cm cuvette. Electroporation is performed with the parameters of: R = 1000 Ω, Q = 25 μF, and V = 2.5 kV. After one pulse, cells are transferred to 1 mL 7H9/ADC/Tween and recovered at 37 °C for 3 hours. Positive transformants are selected after 3-4 days growing on 7H10 agar supplied with 50 μg/mL kanamycin and 50 μg/mL hygromycin.

A single colony is used to inoculate 10 mL 7H9/ADC/Tween. After 36 hours growth at 37 °C, the start culture is transformed to 1 L ZYP-5052 medium for auto-induced expression.

(*18-20*) The harvested cells are lysed by high-pressure homogenization and the lysates are clarified by centrifugation.

For small-scale purification, the supernant is added to 500 μL HaloLink^{TM} Resin (125 μL in settled) pre-equilibrated with buffer B (30 mM HEPES, 150 mM NaCl, and 1 mM TCEPS, pH7.5) in a 1.7-mL Eppendorf tube. After incubating for 1 hour, the resin is washed three times by buffer B. The His-TEV protease is added and incubated with the resin for another 1 hour. The un-tagged MIPS is harvested from the resin by centrifugation. (Fig. 2) The Ni-IMAC is used for large-scale purification by following the procedure described above.

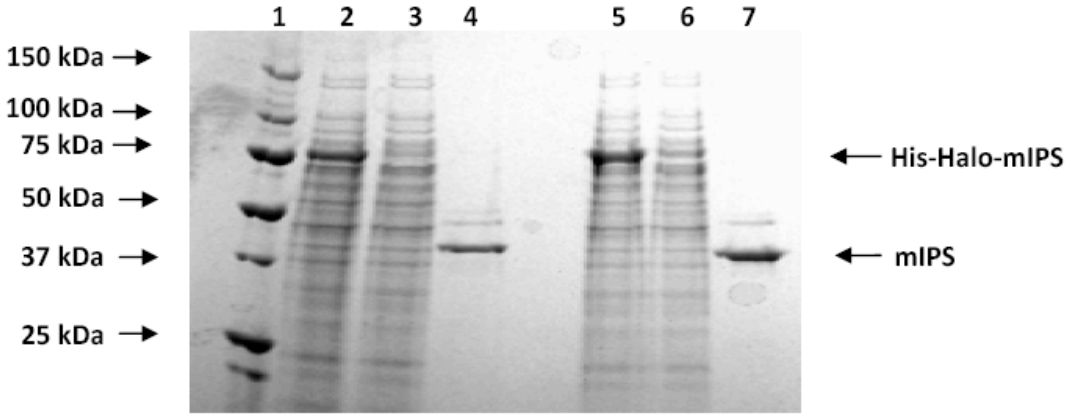

Figure 2. SDS-PAGE of small-scale purification of MIPS by HaloLink^{TM} Resin. Lane 1, protein ladder. Lane 2 and 5, the cell lysates of HisHalo-MIPS (msMIPS and tMIPS, respectively). Lane 3 and 6, the supernant after incubating cell lysates with halo resin (msMIPS and tMIPS, respectively). Lane 4 and 7, the purified msMIPS and tMIPS, respectively.

2.4 NAD^+ binding assay

The NAD^+ binding is quantified by measuring the decrease of fluorescence intensity. 0 - 1 mM NAD^+ is incubated with 40 μM msMIPS (100 mM HEPES, 400 μM EDTA, pH 7.5) at room temperature for 5 minutes at dark. Then the fluorescence signal of 100 μL mixtures is recorded by SpectraMax 5M^e plate reader at room temperature with the excitation wavelength of

280 nm and emission wavelength of 334 nm. The addition of NAD^+ causes a decrease in MIPS intrinsic fluorescence, which is plotted as $\Delta I_{fl} = I_0 - I$ (ΔI_{fl}, decrease in MIPS intrinsic fluorescence; I_0, fluorescence of MIPS before adding NAD^+; I, fluorescence of MIPS after adding NAD^+). The concentration of NAD^+ for 50% of the maximum fluorescence change is used to determine the apparent K_D for NAD^+.

2.5 Activity measurement

Two assays are used to test the activities of MIPS proteins. (*21, 22*) Briefly, in periodate assay, the MIPS enzymes are assayed with 300 μM NAD^+ and various amount of Glc-6P at 30 °C (100 mM Tris–acetate and 2 mM dithiothreitol (DTT), pH 7.5). The reaction is quenched at various times by adding 10 μL 20% trichloroacetic acid (TCA) to 30 μL reaction mixture, and precipitated protein is removed by centrifugation. The phosphate group is released from Ins-1P by reacting with an equal volume of 0.2 M sodium peroxide at 37°C for 1 hour. Excess peroxide is removed by adding an equal volume of 1 M Sodium Sulfite. 50 μL of the reaction mixture is then incubated with 10 μL 3 M Sulfuric acid for 10 min, followed by adding 20 μL H_2O and 10 μL ammonium molybdate (2.5%) and sitting for another 10 min. Then 10 μL of 10% ascorbic acid is added to the mixture, and incubated at 37°C for 1.5 hours. The absorbance value at 820 nm is recorded, and amount of phosphate production (μM min^{-1}) is calculated from the phosphate standard curve (Appendix A).

For IMP-coupled assay, the activity of converting Glc-6P to Ins-1P by MIPS proteins is continuously measured by sensing phosphate formation following reaction with IMP from bovine brain (Sigma). (*22*) The inorganic phosphate released by IMP is measured by coupling with reaction of 2-amino-6-mercapto-7-methylpurine riboside (MESG) and purine nucleoside

phosphorylase (PNP), which leads to an increase in absorbance at 360 nm. The assay mixtures (MIPS with 300 μM NAD^+, 20 mM NH_4Cl, 0.6 mg IMP, 0.2 mM MESG, 4 U/mL PNP in buffer of 50 mM Tris, 1 mM $MgCl_2$, pH 7.5) are pre-incubated at 30 °C, then Glc-6-P is added to initiate the reaction. The time course for phosphate production is monitored by recording UV spectrum at various times and the phosphate standard curve (Appendix A) is used to convert the observed rate of the reaction to μM min^{-1}.

2.6 Gel filtration

The oligomeric states of MIPS proteins are determined by size exclusion chromatography. Purified proteins are mixed with Blue Dextran 2000 and loaded onto Superdex 200 10/300 GL column pre-equilibrated with 50 mM sodium phosphate and 150 mM NaCl (pH 7.5). The elution volumes are used to calculate the K_{av} values ($K_{av} = (V_e-V_0)/(V_t-V_0)$, where V_0 is the void volume of the column, V_t is the total volume of the column, and V_e is the elution volume of the protein). A standard curve is prepared by plotting log (Molecular Weight) vs. K_{av} using the following protein standards (GE Healthcare): aprotinin, 6.5 kDa; ribonuclease A, 13.7 kDa; carbonic anhydrase, 29 kDa; ovalbumin, 44 kDa; and conalbumin, 75 kDa.

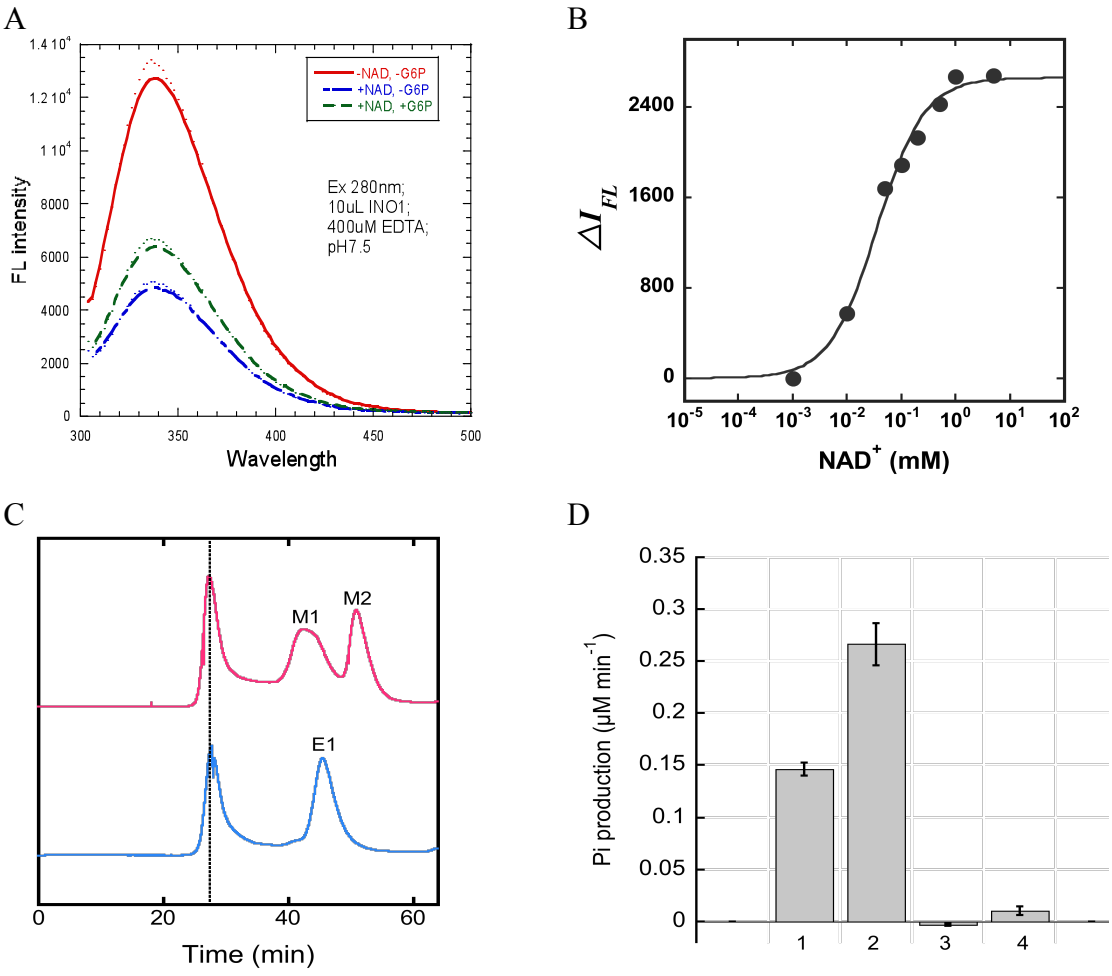

Figure 3. Activity of mycobacterial MIPS. (A) Fluorescence spectrum of NAD^+ binding to mIPS. Red line, MIPS only; blue line, addition of NAD^+ to mIPS; green line, addition of Glc-6P to the NAD^+/MIPS mixture. (B) Plot of NAD^+ binding to MIPS. (C) Elution profile of MIPS expressed from *E. coli* (lower blue line) and *M. smegmatis* (upper red line) in gel-filtration. The dash crossing the first peak in two elution profiles represents the Dextran 2000. (D) Reaction rate of msMIPS (expressed from *M. smegmatis*), tMIPS (expressed from *M. smegmatis*), MshB (control, expressed from *M. smegmatis*), and msMIPS (expressed from *E. coli*) by periodate assay are shown in column 1, 2, 3, and 4, respectively.

3. Results and Discussion

The mycobacterial MIPS expressed from *E. coli* exhibits no detectable activity. (Fig. 3D) However, NAD^+ binding assay indicates that msMIPS is capable of binding the cofactor NAD^+ as being observed in the crystal structure (*14*). The MIPS uses NAD^+ as the cofactor to oxidize the C5 on glucose ring to form the keto intermediate, and the resulting NADH is consumed in a later internal reduction reaction without dissociation from the active site. (*23*) Binding of NAD^+ will diminish the intrinsic fluorescence intensity of MIPS due to altered characteristics of two tryptophans near the active site. (*15*) The fluorescence spectrum of tMIPS shows a maximum emission at 334 nm when excited at 280 nm. (Red line, Fig. 3A) Addition of 300 μM NAD^+ decreases the intrinsic fluorescence intensity of MIPS but not the maximum emission. (Blue line, Fig. 3A) The K_D^{NAD+} measured in this assay is 0.036 ± 0.004 mM (Fig. 3B). Subsequent addition of 50 mM Glc-6P to the tMIPS/NAD^+ mixture does not change the fluorescence spectrum. (Green line, Fig. 3A)

In order to understand the reason of the absence of activity, the *Mycobacterium smegmatis* expression system is used for mycobacterial MIPS preparation. The activities of MIPS enzymes purified by HaloLink™ Resin (Fig. 2) are first tested by using the periodate assay with a single Glc-6P concentration of 100 mM. Both tMIPS and msMIPS expressed from *M. smegmatis* show significant activities compared to MIPS expressed from *E. coli*. (Fig. 3D) The control protein MshB (expressed from *M. smegmatis* and purified by HaloLink™ Resin) is also tested under the same condition and lack of phosphate production indicates that the observed MIPS activities are not from the contamination of native mycobacterial enzymes. (Fig. 3D) The value of $K_M^{Glc\text{-}6P}$ and apparent specific activity are determined by periodate assay and IMP coupled assay. (Table 1) The slightly lower $K_M^{Glc\text{-}6P}$ observed in IMP-coupled assay might result from the presence of 1mM $MgCl_2$, which is required for the IMP activity. (*22*)

The specific activity of 10^{-5} μmol/min/mg observed for tMIPS in this study is too low compared to MIPS from other organisms such as *Arabidopsis thaliana* (11.8 μmol/min/mg (*15*)) and *Archaeoglobus fulgidus* (0.24 μmol/min/mg (*24*)). This extremely low specific activity may due to a large portion of inactive enzymes in the protein purified via affinity chromatography. The gel-filtration result shows that a single peak is observed in the elution profile of the inactive MIPS expressed from *E. coli* (peak E1, Fig. 3C), which corresponds to a trimer. On the other hand, recombinant MIPS produced from *M. smegmatis* displays multiple and broad peaks in the elution profile of gel-filtration (peak M1 and M2, Fig. 3C). M2 corresponds to a monomer, whereas M1 is relatively board and covers the range from tetramer to hexamer. Generally, the MIPS proteins from different species present as tetramers in solution, therefore it is possible the tetramer is the active form of tMIPS. (*10, 14, 25*) We did not separate peaks observed in the gel-filtration result and test the activity of each oligometic form in this study. Hence, further purification steps are necessary to get the pure tMIPS for future discovering the key factor for activity and investigating the catalytic mechanism.

Table 1. Activity of tMIPS expressed from *M. smegmatis*

Assay[a]	$K_m^{Glc\text{-}6P}$ (mM)	Specific activity (μmol/min/mg)
Periodate	11.4 ± 3.0	4.0×10^{-5}
IMP-coupled [b]	6.0 ± 2.5	3.4×10^{-5}

[a] All assays are conducted at pH 7.5 with 20 mM NH_4Cl. The concentration of NAD^+ is held at 300 μM and the concentration of Glc-6-P is varied (0 – 40 mM).
[b] IMP-coupled assay requires 1 mM $MgCl_2$

A zinc ion is observed in the crystal structure of tMIPS, which is tetrahedral bonded to NO7 and NO2 atoms on the nicotinamide of NAD^+, S310 hydroxyl, and a water molecule. (*14*) This metal ion is also observed at the same location in the crystal structures of *Saccharomyces cerevisiae* MIPS (yMIPS) and *Archaeoglobus fulgidus* MIPS (aMIPS), which bridges the amide and the posphodiester on NAD^+. (*23, 25*) Interestingly, the activity of yMIPS is unaffected by the presence of EDTA, whereas aMIPS is absolutely divalent metal dependent. (*15-17*) Therefore, the zinc observed in tMIPS most likely has a structural role of stabilizing the NAD^+ cofactor, as being proposed for yMIPS. (*25, 26*) A second metal site that binds the catalytic divalent metal has been proposed in the active site of aMIPS, which occupies the same position for the putative ammonium ion in the yMIPS. (*25*) The putative divalent metal site contains five metal ligands, including two hydroxyl O atoms (O1 and O2) from Glc-6P, one D304 bridged water molecule, two hydroxyl oxygen atoms from D261 and D332. (*25*) Interestingly, the three Asp residues are conserved in tMIPS (D282/D235/D310) and yMIPS (D410/D356/D438). (*25*) Therefore, further biochemical and structure studies are needed to clarify whether tMIPS catalyzes the reaction through an aldolase type II or type III mechanism.

Acknowledgement

The plasmid pYUB1049 and strain *Mycobacterium smegmatis* $mc^2$4517 is kindly provided by Dr. William *Jacobs*, Albert Einstein College of Medicine.

References

1. Michell, R. H. (2008) Inositol derivatives: evolution and functions, *Nat Rev Mol Cell Biol 9*, 151-161.

2. Morita, Y. S., Fukuda, T., Sena, C. B., Yamaryo-Botte, Y., McConville, M. J., and Kinoshita, T. (2011) Inositol lipid metabolism in mycobacteria: biosynthesis and regulatory mechanisms, *Biochim Biophys Acta 1810*, 630-641.

3. Mishra, A. K., Driessen, N. N., Appelmelk, B. J., and Besra, G. S. (2011) Lipoarabinomannan and related glycoconjugates: structure, biogenesis and role in Mycobacterium tuberculosis physiology and host-pathogen interaction, *FEMS Microbiol Rev 35*, 1126-1157.

4. Newton, G. L., Buchmeier, N., and Fahey, R. C. (2008) Biosynthesis and functions of mycothiol, the unique protective thiol of Actinobacteria, *Microbiol Mol Biol Rev 72*, 471-494.

5. Bettaney, K. E., Sukumar, P., Hussain, R., Siligardi, G., Henderson, P. J., and Patching, S. G. (2012) A systematic approach to the amplified expression, functional characterization and purification of inositol transporters from Bacillus subtilis, *Mol Membr Biol*.

6. Movahedzadeh, F., Smith, D. A., Norman, R. A., Dinadayala, P., Murray-Rust, J., Russell, D. G., Kendall, S. L., Rison, S. C., McAlister, M. S., Bancroft, G. J., McDonald, N. Q., Daffe, M., Av-Gay, Y., and Stoker, N. G. (2004) The Mycobacterium tuberculosis ino1 gene is essential for growth and virulence, *Mol Microbiol 51*, 1003-1014.

7. Bachhawat, N., and Mande, S. C. (2000) Complex evolution of the inositol-1-phosphate synthase gene among archaea and eubacteria, *Trends Genet 16*, 111-113.

8. Cole, S. T., Brosch, R., Parkhill, J., Garnier, T., Churcher, C., Harris, D., Gordon, S. V., Eiglmeier, K., Gas, S., Barry, C. E., 3rd, Tekaia, F., Badcock, K., Basham, D., Brown, D., Chillingworth, T., Connor, R., Davies, R., Devlin, K., Feltwell, T., Gentles, S.,

Hamlin, N., Holroyd, S., Hornsby, T., Jagels, K., Krogh, A., McLean, J., Moule, S., Murphy, L., Oliver, K., Osborne, J., Quail, M. A., Rajandream, M. A., Rogers, J., Rutter, S., Seeger, K., Skelton, J., Squares, R., Squares, S., Sulston, J. E., Taylor, K., Whitehead, S., and Barrell, B. G. (1998) Deciphering the biology of Mycobacterium tuberculosis from the complete genome sequence, *Nature 393*, 537-544.

9. Bachhawat, N., and Mande, S. C. (1999) Identification of the INO1 gene of Mycobacterium tuberculosis H37Rv reveals a novel class of inositol-1-phosphate synthase enzyme, *J Mol Biol 291*, 531-536.

10. Majumder, A. L., Chatterjee, A., Ghosh Dastidar, K., and Majee, M. (2003) Diversification and evolution of L-myo-inositol 1-phosphate synthase, *FEBS Lett 553*, 3-10.

11. Li, Y., Chen, Z., Li, X., Zhang, H., Huang, Q., Zhang, Y., and Xu, S. (2007) Inositol-1-phosphate synthetase mRNA as a new target for antisense inhibition of Mycobacterium tuberculosis, *J Biotechnol 128*, 726-734.

12. Smith, D., Hansch, H., Bancroft, G., and Ehlers, S. (1997) T-cell-independent granuloma formation in response to Mycobacterium avium: role of tumour necrosis factor-alpha and interferon-gamma, *Immunology 92*, 413-421.

13. Hansch, H. C., Smith, D. A., Mielke, M. E., Hahn, H., Bancroft, G. J., and Ehlers, S. (1996) Mechanisms of granuloma formation in murine Mycobacterium avium infection: the contribution of CD4+ T cells, *Int Immunol 8*, 1299-1310.

14. Norman, R. A., McAlister, M. S., Murray-Rust, J., Movahedzadeh, F., Stoker, N. G., and McDonald, N. Q. (2002) Crystal structure of inositol 1-phosphate synthase from

Mycobacterium tuberculosis, a key enzyme in phosphatidylinositol synthesis, *Structure 10*, 393-402.

15. Chen, L., Zhou, C., Yang, H., and Roberts, M. F. (2000) Inositol-1-phosphate synthase from Archaeoglobus fulgidus is a class II aldolase, *Biochemistry 39*, 12415-12423.

16. Escamilla, J. E., Contreras, M., Martinez, A., and Zentella-Pina, M. (1982) L-myoinositol-1-phosphate synthase from Neurospora crassa: purification to homogeneity and partial characterization, *Arch Biochem Biophys 218*, 275-285.

17. Neelon, K., Wang, Y., Stec, B., and Roberts, M. F. (2005) Probing the mechanism of the Archaeoglobus fulgidus inositol-1-phosphate synthase, *J Biol Chem 280*, 11475-11482.

18. Bashiri, G., Squire, C. J., Baker, E. N., and Moreland, N. J. (2007) Expression, purification and crystallization of native and selenomethionine labeled Mycobacterium tuberculosis FGD1 (Rv0407) using a Mycobacterium smegmatis expression system, *Protein Expr Purif 54*, 38-44.

19. Studier, F. W. (2005) Protein production by auto-induction in high density shaking cultures, *Protein Expr Purif 41*, 207-234.

20. Goldstone, R. M., Moreland, N. J., Bashiri, G., Baker, E. N., and Shaun Lott, J. (2008) A new Gateway vector and expression protocol for fast and efficient recombinant protein expression in Mycobacterium smegmatis, *Protein Expr Purif 57*, 81-87.

21. Barnett, J. E., Brice, R. E., and Corina, D. L. (1970) A colorimetric determination of inositol monophosphates as an assay for D-glucose 6-phosphate-1L-myoinositol 1-phosphate cyclase, *Biochem J 119*, 183-186.

22. Huang, X., and Hernick, M. (2011) A limitation of the continuous spectrophotometric assay for the measurement of myo-inositol-1-phosphate synthase activity, *Anal Biochem 417*, 228-232.

23. Jin, X., and Geiger, J. H. (2003) Structures of NAD(+)- and NADH-bound 1-l-myo-inositol 1-phosphate synthase, *Acta Crystallogr D Biol Crystallogr 59*, 1154-1164.

24. Donahue, J. L., Alford, S. R., Torabinejad, J., Kerwin, R. E., Nourbakhsh, A., Ray, W. K., Hernick, M., Huang, X., Lyons, B. M., Hein, P. P., and Gillaspy, G. E. (2010) The Arabidopsis thaliana Myo-inositol 1-phosphate synthase1 gene is required for Myo-inositol synthesis and suppression of cell death, *Plant Cell 22*, 888-903.

25. Stieglitz, K. A., Yang, H., Roberts, M. F., and Stec, B. (2005) Reaching for mechanistic consensus across life kingdoms: structure and insights into catalysis of the myo-inositol-1-phosphate synthase (mIPS) from Archaeoglobus fulgidus, *Biochemistry 44*, 213-224.

26. Jin, X., Foley, K. M., and Geiger, J. H. (2004) The structure of the 1L-myo-inositol-1-phosphate synthase-NAD+-2-deoxy-D-glucitol 6-(E)-vinylhomophosphonate complex demands a revision of the enzyme mechanism, *J Biol Chem 279*, 13889-13895.